CRUDE SHIPPING PROJECT, WHANGAREI HARBOUR

Predicted physical environmental effects from channel deepening and offshore disposal

Report prepared for
Chancery Green for Refining NZ

MetOcean Solutions

Specialists in Oceanography and Meteorology

MetOcean Solutions Ltd: Report P0297-02

July 2017

Report status

Version	Date	Status	Approved by
RevA	19/06/2016	Draft for internal review	Monetti
RevB	21/06/2016	Draft for internal review	McComb
RevC	24/06/2016	Draft for client review	Gardiner
RevD	12/08/2016	Updated draft for internal review	Monetti
RevE	16/08/2016	Updated draft for internal review	McComb
RevF	23/08/2016	Updated draft for client review	Gardiner
RevG	20/10/2016	Updated draft for client review	Monetti
RevH	19/01/2017	Updated draft for client review	Monetti
Rev0	07/02/2017	Draft for public consultation	Monetti
Rev1	25/07/2017	Final version	Monetti

It is the responsibility of the reader to verify the currency of the version number of this report.

Acknowledgements

Thanks to Ross Sneddon from the Cawthron Institute for ADCP deployment and data collection.

Thanks to Ricky Eyre from Northland Regional Council for supplying LIDAR and single-beam data for Whangarei Harbour, Stuart Caie from LINZ for supplying offshore multi-beam data and historic survey data of Mair Bank and Jae Staite from Northport Ltd for supplying multi-beam survey data for main channel and multiple historic surveys of Mair Bank.

EXECUTIVE SUMMARY

Refining NZ is investigating options for the deepening and realignment of the shipping channel leading to the Marsden Point Refinery at the entrance to Whangarei Harbour.

Given the emphasis on preserving or enhancing the environment, one of the most critical aspects affecting the regulatory approval of such a project is the assessment of its impacts on the existing environment. MetOcean Solutions participation in the impact assessment for the project has involved an evaluation of the physical effects of the channel deepening on the wave, current and sediment dynamics of the harbour entrance, the effects of dredging and disposal on water quality, and the effects of sediment disposal on the receiving environment. This has been undertaken through the use of a suite of numerical model investigations supported by empirical data, observations and historical / contemporary measurements.

The study investigations are presented in two reports. The first report (MSL Report P0297-01) is a technical reference document that provides details on the establishment of numerical models for wind, wave, current and sediment dynamics, and the data collection programme that was undertaken to support the model establishment and to validate the numerical schemes. The present report (MSL Report P0297-02) summarises the existing physical environment and outlines the likely effects of the Crude Shipping Project on the wave, hydrodynamic and short- and long-term sediment dynamics. This is also a technical reference document.

The dominant physical processes at both regional and local scales have been replicated through the application of industry-standard numerical models based on published scientific methodologies and the background knowledge acquired from numerous previous numerical modelling studies. Several models were investigated and the most appropriate ones chosen for the domain of application. Wherever possible, models were validated using historical and contemporary oceanographic data sets. The models chosen are considered suitable for characterising the dominant physical processes in the region and also for identifying the potential physical effects arising from the Crude Shipping Project.

Bathymetry and sediment character

The surficial sediments within the main channel of Whangarei Harbour are a mix of sands and coarser material (likely to be shell) in varying proportions. Coring has shown that a minor fraction of silty material is also found at depth. The subtidal regions of the ebb tidal shoal are mainly made up of sandy material. This is true for the region south of Mair Bank as well as the edge of Mair Bank adjacent to the channel. The intertidal region of Mair Bank is covered with a shell substrate, mostly consisting of pipi shells, with deposits of fine sands in the lee of shell ridges. With increasing water depth the amount of sand interspersed with the shells increases down the edge of the bank. The results presented here support the assertions in previous literature that sediment reworking and biological activity are important processes on Mair Bank that govern its morphology. However, as a large scale ebb tide delta, it is relatively stable in position.

Based on the characterisation of the existing environment and extensive modelling of the wave, hydrodynamic and sediment dynamics, a summary of the predicted effects of the Crude Shipping Project is as follows.

Wave climate

The proposed channel modifications are not expected to fundamentally change the wave climate in the vicinity of the harbour entrance. However, there are areas where the wave climate will change slightly as a result of deepening the channel, with a different degree of significance depending on the location.

Outside the harbour entrance, the overall changes in the mean significant wave height fields are very subtle and do not exceed 2 cm. During infrequent storm events associated with offshore significant wave height of more than 5 m, the significant wave height may increase by 5 to 10% outside the harbour entrance, corresponding to a small increase of few centimetres (< 15 cm) of the significant wave height. The western edge of the channel entrance near Busby Head may occasionally experience an increase of the significant wave height up to 20% (~20 cm) during extreme events due to enhanced refraction. Such changes in the wave height fields are expected to be constrained to a limited area of the tidal delta shoal where bottom friction processes dissipate a large fraction of the incident wave energy. The increase of the wave energy during extreme storm events due to the dredging are thus predicted to be inconsequential for the adjacent beaches, sand banks, Marine 1 Management Areas or Marine Reserves.

The offshore extent of the deepened channel slightly modifies the refraction pattern of waves at the delta entrance. Enhanced refraction occurring along the eastern margin of the deepened channel is predicted to increase wave height at Busby Head and Smugglers Bay up to a maximum of 15 cm when offshore wave heights are around 5 m during storm events. Conversely, a minor decrease of wave height (-1 cm on average) is expected along sections of Ruakaka Beach. Note that modifications of the wave refraction at the distal margin of the channel may generate a zone to the north of the Ruakaka River mouth characterised by a slight increase in wave height (up to a 5 cm maximum during storms). Changes in wave height over Mair Bank are not expected to exceed 1 cm on average and 5 cm during extreme wave events. No consequences for recreational surfing activities along Ruakaka Beach are therefore expected.

Tidal hydrodynamics

The proposed channel modifications are not expected to change the overall tidal hydrodynamics of the harbour entrance, and the existing complex asymmetries induced by the ebb and flood tidal flows will be maintained after deepening. However, there are areas where the tidal hydrodynamics of Whangarei Harbour will be changed as a result of deepening the channel, with a different degree of significance depending on the location.

There will be a reduction in the peak tidal speed by up to 0.10 $m.s^{-1}$ in the main channel and an acceleration of up to 0.10 $m.s^{-1}$ in some areas adjacent to the channel. Removal of the lobe in the central channel (north of Mair Bank) is predicted to result in a localised decrease of up to 0.15 $m.s^{-1}$ (from 0.5 to 0.35 $m.s^{-1}$) while the current speed is expected to increase from 0.05 to 0.09$m.s^{-1}$ along the northern flank of the inlet channel between Motukaroro Island and High Island. The subtle realignment of the channel by removal of the toe on some of the bends has a localised influence on the tidal flows in the channel for both the ebb and the flood tidal stages. Both ebb and flood flows on the delta margin will be slightly reoriented by the dredged channel and exhibit areas of flow acceleration and deceleration - up to 0.02 ms^{-1}. The deepening is predicted to reduce the peak bed shear stress in the main channel by up to 20% in the area adjacent to Marsden Point and cause small

localised increases and decreases up to 30% over areas of the delta during the flood tidal stage. The percentage of time the bed shear stress exceeds the critical threshold for entrainment of 200 µm sand is predicted to increase by approximately 10% over the eastern margin of the channel close to Busby Head at flood tides. This area currently features a slight bathymetric indentation, and it may be an area of active (and asymmetric) sediment transport.

Sediment transport

The proposed channel modifications are not expected to significantly change the governing sediment dynamics of the harbour entrance, and the existing complex asymmetries induced by the ebb and flood tidal flows will be maintained after deepening.

The morphodynamics of Mair Bank are largely influenced by the bio-stabilisation provided by live shellfish and their residual shell fragments. This bio-stabilisation is expected to play a more significant role on future evolution of the Bank than the effect of the proposed channel deepening. The studies undertaken here do not indicate that channel deepening will materially change the sedimentary outcomes on the Mair Bank.

The sedimentary stability of Ruakaka Beach is not expected to be influenced by the slight variation in the wave conditions caused by channel deepening. However, enhanced wave refraction along the eastern ridge of the channel on the delta may increase the bed shear stress around Busby Head somewhat and Smugglers Bay in a lesser extent, although this not anticipated to disturb the stability of the sea bed, which is largely composed of sandy and shelly gravel and already occasionally subjected to 4 m wave height during storms.

Sedimentation is expected to occur immediately adjacent to the Marsden Point jetty. Here, the tidal flows reduce and the tidal asymmetry is expected to promote infilling of the deepened areas over time at a relatively constant rate. While a reliable volumetric estimate is difficult to make with confidence, the likely evolution pattern will be of accretion from the southern shore. A degree of infilling at the toe of Mair Bank may occur where the channel has been realigned. These areas of sedimentation will require regular maintenance dredging to ensure on-going navigability.

Infilling of the main channel south of Busby Head toward the distal margin is expected, and a programme of maintenance dredging will also be required here for ongoing navigability. The deepened channel is exposed to diffusive infilling from wave action and there is a predicted change to the location and width of the ebb tide jet along with an increase in the sediment flux from the adjacent channel margins. The source of infilling material to the channel is the adjacent delta and the rate of accretion is expected to decrease over time until equilibrium is reached. The initial infilling of this part of the channel is calculated to be 86,000 m^3 per year, with a margin of error of ±36,000 m^3.

Dredging plumes

The plume dispersion associated with two different (large and small) trailing suction hopper dredgers (TSHD), one cutter suction dredger (CSD) and one Backhoe Dredger (BHD) was simulated in the present study. The sediment plumes associated with dredging, caused by the action of the drag head, are constrained within the lower water column, with negligible expression at mid-water and surface

levels. In contrast, the sediment plumes associated with the overflow phase are spread across the entire water column. The resultant plumes from either source are predicted to follow the general channel alignment, consistent with the tidal currents. A SSC threshold of 12 mg/L was selected. This corresponds to the difference between the 15 NTU level Response Limit and the 3 NTU existing background level (Brian T. Coffey and Associates Limited, 2016a) considering a 1:1 relationship between SSC and Turbidity. This linear relationship was established by Stewart (2017) analysing vibro-core samples from the dredging footprint. The maximum excursion of any plume modelled did not exceed 1200 m with the maximum extension evident near the bottom of the channel. All plumes were confined to the channel. There is no evidence of the plume dispersing to the adjacent beaches, sand banks, Marine 1 Management Areas and Marine Reserves. The sensitivity analysis carried out based on more conservative configurations of the sediment release did not show any fundamental changes in the plume dispersion.

Of the two dredge vessels considered for this study, the large dredge vessel generates more extended and concentrated plumes than the smaller vessel. The overflow duration has a notable effect on the magnitude and extent of the plumes. Comparisons between plumes generated for the existing channel and the post-dredging scenario indicates that the plume excursions will decrease slightly as the channel becomes deeper due to the slightly reduced tidal velocities.

The SSC plumes associated with dredging operations using the CSD or the BHD at the Refining New Zealand (RNZ) jetty pocket were characterised by a lower horizontal extension, with no evidence of plume dispersion to the adjacent beaches, sand banks, Marine 1 Management Areas and Marine Reserves. In the case of the CSD, the sediment release was caused by the effect of the rotating cutter head and therefore constrained to the bottom water layer. The discharge of sediments using floating pipelines avoids any sediment discharges over the extent of the water column by overflow. The anticipated plume dispersion associated with the use of the CSD for the dredging operations is predicted to be within the plume range associated with the use of the TSHD. For this reason, the CSD plume modelling was not repeated at all the dredging locations over the proposed channel.

Simulations of dredging with the proposed BHD led to sediment discharges over the entire water column due to the excavation, hoisting and slewing phases. The relative low production rate of the BHD associated to the bucket limits the release of a large amount of sediment per hour and thus the SSC.

Disposal ground dynamics

Numerical testing of the proposed offshore disposal ground (Area 3.2) at 40-45 m depth in Bream Bay shows that the wave and current regime can occasionally mobilise sediments in this area. This will only occur during more energetic storm conditions, when sediments can be transported in suspension or by bedload processes. Following the outcomes from the consultations involving RNZ and the relevant experts, the study considered a conservative estimate of a 4 m high disposal mound over the 2 km^2 area of Disposal site 3.2, and area that can contain the capital dredge volume plus the placement of maintenance dredge volumes over 35 years. For this scenario, the percentage of erosion of the disposal mound after 1 year is not expected to exceed 5% (i.e. 400,000 m^3) of the total volume based on an 8 million m^3 disposal mound (conservative approach). The predicted rate of movement of sediment from the site is very low and essentially omni-directional, however there is a slight bias towards transport to the south. After one year, the

extent of movement of sediment was predicted to be very limited, and modelled sediments did not reach any of the sensitive areas identified such as beaches, Marine Reserves, Marine 1 Management Areas or 3 Mile Reef. The predicted maximum changes to the nearshore wave climate caused by the presence of a disposal mound will be very minor and are not expected to exceed +/- 5 cm under the larger wave conditions. This is not expected to have any consequence for the beach or nearshore processes, including surf activities at any areas (including proximate to Ruakaka River).

The location of Disposal Site 1.2 on the flank of the ebb tidal delta for the disposal of 2.5 – 5% of the capital dredge volume and up to 100% of the maintenance dredge volume favours the replenishment of the delta and adjacent beach over years. The net transport from the disposal ground is directed onshore and recirculation back into the channel is not predicted. For an example mound of 0.6 m height, approximately 8% of the volume would be moved out of the site over the course of one year, from which it would contribute positively to the nourishment of the adjacent beach areas. The Disposal mound 1.2 is predicted to cause changes in the significant wave height fields which do not exceed a maximum of 5 cm and 10 cm (< 5%) along the shoreline and near the mound, respectively. These estimations are based on a highly conservative approach which includes the placement of the maintenance dredge volumes over 10 years without considering the reduction of the disposal mound due to erosion over years. In this context, surf conditions along Ruakaka Beach are not expected to be affected by the placement of dredge material at Disposal sites 1.2 and 3.2.

Disposal plumes

The plumes caused by the offshore disposal are short lived and not highly dispersive. They typically extend along a northeast – southwest axis, preserving the adjacent reef from settlement, and 99% of the plume material is predicted to settle to the seabed within 14 hours. The disposal plumes calculated from the measured current profiles have a lesser excursion than those determined from the long term environmental hindcast, and do not show incursion towards the adjacent 3 Mile Reef to the west of the proposed disposal ground.

TABLE OF CONTENTS

Executive summary ii
1. Introduction 2
    1.1. Report structure 2
    1.2. Study Area 4
    1.3. Proposed channel deepening design 5
    1.4. Proposed disposal ground designs 7
2. Bathymetry and seabed character 8
    2.1. Bathymetry 8
    2.2. Sediment characteristics 8
        2.2.1. Sediment sampling 8
        2.2.2. Mair Bank 17
3. Wind climate 20
    3.1. Characterising the wind climate 20
4. Wave climate 23
    4.1. Characterising the wave climate 23
    4.2. Effects of channel deepening on the wave climate 28
    4.3. Summary of predicted effects of channel deepening on the wave climate 34
5. Regional scale hydrodynamics 35
    5.1. Characterising the regional hydrodynamics 35
6. Nearshore tidal hydrodynamics 38
    6.1. Characterising the tidal dynamics 38
    6.2. Effects of channel deepening on tidal hydrodynamics 43
    6.3. Summary of effects on the nearshore tidal hydrodynamics 52
7. Sediment transport 54
    7.1. Conceptual modelling – tide only transport scenarios 54
    7.2. Conceptual modelling – wave and tide scenarios 57
        7.2.1. Existing environment 57
        7.2.2. Predicted changes to the sediment flux due to channel deepening 63
    7.3. Sediment dynamics 68
        7.3.1. Bed composition generation (BCG) simulation 68
        7.3.1. Predicted changes in the spatial distribution of sediment fractions 73
    7.4. Predicted morphological changes 75
    7.5. Estimates of channel infilling 83
    7.6. Summary of effects on sediment transport 84
8. Dredging plumes 86
    8.1. Dredging plume modelling results 86
    8.2. Summary of dredging plumes 102
9. Disposal ground dynamics 104
    9.1. Wave climate 104
    9.2. Hydrodynamics 110
    9.3. Sediment dynamics for disposal ground 3.2 112
    9.4. Sediment dynamics for Disposal ground 1.2 113
    9.5. Effects of disposal grounds on the wave climate 114

9.6. Summary of effects of the disposal grounds 120
10. Disposal plumes 121
10.1. Disposal plume modelling results 121
10.2. Disposal plume summary 122
References 134
Appendix A – Wind statistics 135
Appendix B – Wave statistics 138
Appendix C – Tidal and Non-Tidal time series 143
Appendix D – Additional dredging plume results 144
Appendix E – Additional dredging plume results 154
Appendix F – Plume modelling at different tide stages 159
Appendix G – Overflow mode at different tide stages 176
Appendix H – Sensitivity analysis of the plume model 193

LIST OF FIGURES

Figure 1.1 Flow chart showing the numerical modelling process for the study. Red lines indicate hydrodynamics; blue indicate waves; green indicate wind, brown indicate bathymetry and yellow lines indicate sediments / grain size. 3

Figure 1.2 Maps of Whangarei Harbour (top) and its entrance (bottom) with the locations used in the present study for the establishment of the numerical models and the description of the effect of the channel deepening on the coastal dynamics. 4

Figure 1.3 Depths (upper plot) and depth differences (lower plot) between the Option 4.2 channel design and the existing channel configuration. Positive amplitudes indicate a deepening of the channel. 6

Figure 1.4 Location of sites 1.2, and 3.2 (indicated by coloured diagonal cross-hatch polygons) for the disposal of capital and maintenance volumes. 3 Mile Reef, indicated by a green polygon, is a sensitive reef because of its benthic encrusting communities. 7

Figure 2.1 Sources of bathymetry data used in the study. 8

Figure 2.2 Folk classification system for sediments (Folk, 1954). 9

Figure 2.3 Whangarei Harbour inner channel sediment samples (sediment class according to the Folk scale). 10

Figure 2.4 Whangarei Harbour mid channel sediment samples (sediment class according to the Folk scale). 10

Figure 2.5 Whangarei Harbour outer channel and ebb tidal shoal sediment samples (sediment class according to the Folk scale). 11

Figure 2.6 Wider Bream Bay sediment samples (sediment class according to the Folk scale). 11

Figure 2.7 Whangarei Harbour inner channel vibrocore locations. 12

Figure 2.8 Whangarei Harbour outer channel vibrocore locations. 12

Figure 2.9 Vibrocore samples for site v10. 13

Figure 2.10 Vibrocore samples for site v10a. 13

Figure 2.11 Vibrocore samples for site v10b. 14

Figure 2.12 Vibrocore samples for site v11. 14

Figure 2.13 Results from channel edge diver survey carried out by Vince Kerr (Figure 2.15 in Kerr, 2016). Areas ranked qualitatively according to the amount of shell component. 15

Figure 2.14 Selection of photos and locations from diver survey, illustrating the varied spatial nature of sediments and bedforms on the edge of Mair Bank. From Kerr (2016). 16

Figure 2.15 Pipi shell bank. 17

Figure 2.16 Shell structure of pipi bank. 18

Figure 2.17 Mussel colony on Mair Bank. 18

Figure 2.18 Fine sand deposited to the lee (northern side) of the shell ridges. 19

Figure 2.19 More advanced stage of sand deposition with a greater proportion of sand overlaying the shell substrate. 19

Figure 3.1 Locations of the WRB site used to extract the wind climate from the 36-year hindcast data. 20

Figure 3.2 Annual wind rose plot at WRB. Sectors indicate the direction from which the wind is coming. 21

Figure 3.3 Monthly wind rose plots at WRB. Sectors indicate the direction from which the wind is coming. 22
Figure 4.1 Locations of the wave gauges (red circles) along Ruakaka Beach and offshore of the harbour entrance. 24
Figure 4.2 Annual mean and snapshots of modelled significant wave height over the regional SWAN parent domain for different weather events. The wave height annual mean was calculated for 2015. 25
Figure 4.3 Annual mean and snapshots of modelled significant wave height over the local SWAN domain for different weather events. The wave height annual mean was calculated for 2015. 26
Figure 4.4 Annual wave rose plot for the total significant wave height at WRB. Sectors indicate the direction from which waves approach. 26
Figure 4.5 Monthly wave rose plots for the total significant wave height at WRB. Sectors indicate the direction from which waves approach. 27
Figure 4.6 Average annual change in significant wave height due to the deepened channel. Positive amplitudes indicate areas with a predicted increase, negative areas a decrease. 29
Figure 4.7 Significant wave height changes for wave classes 1 – 4 due to the deepened channel. Positive amplitudes indicate areas with a predicted increase, negative values a decrease. 29
Figure 4.8 Significant wave height changes for wave classes 5 – 8 due to the deepened channel. Positive amplitudes indicate areas with a predicted increase, negative values a decrease. 30
Figure 4.9 Significant wave height changes for wave classes 9 – 12 due to the deepened channel. Positive amplitudes indicate areas with a predicted increase, negative values a decrease. 31
Figure 4.10 Significant wave height changes for wave classes 13 – 16 due to the deepened channel. Positive amplitudes indicate areas with a predicted increase, negative values a decrease. 32
Figure 4.11 Locations used to calculate statistics of the difference in wave height due to channel deepening 32
Figure 5.1 Climatological flow patterns offshore Whangarei Harbour based on mean current speeds computed off a 10 year (2000-2010) ROMS hindcast. Current speeds in red shades ($m.s^{-1}$). 36
Figure 5.2 Long term current rose at the proposed offshore disposal ground. Current directions are represented as “going to”. 36
Figure 5.3 Monthly averaged flow for March 2005 as an example of the regional circulation. Note the interaction of the southward flow and the coastline geometry between Bream Bay and the offshore islands, generating coastal eddies and bifurcations. 37
Figure 5.4 Monthly climatology of alongshore current at the proposed offshore disposal ground (site WRB). 37
Figure 6.1 Modelled peak ebb flows during spring tide at Whangarei Harbour entrance. 39
Figure 6.2 Modelled peak ebb flows during neap tide at Whangarei Harbour entrance. 40
Figure 6.3 Modelled peak flood flows during spring tide at Whangarei Harbour entrance. 41
Figure 6.4 Modelled peak flood flows during neap tide at Whangarei Harbour entrance. 42

Figure 6.5 Absolute (top) and relative (bottom) difference in tidal flows post-deepening during the peak spring ebb flows. Plots on the right show a zoomed in view of the entrance region. Positive values indicate a predicted increase in flow (red scale), while the negative values indicate a decrease (blue scale). 45

Figure 6.6 Absolute (top) and relative (bottom) difference in tidal flows post-deepening during the peak spring flood flows. Plots on the right show a zoomed in view of the entrance region. Positive values indicate a predicted increase in flow (red scale), while the negative values indicate a decrease (blue scale). 46

Figure 6.7 Location of the cross-sections used to evaluate the tidal flow differences following channel deepening. 47

Figure 6.8 Ebb tidal flow differences during spring tide along sections A, B and C shown in Figure 6.7. The dotted line indicates the 0-m.s^{-1} velocity threshold....47

Figure 6.9 Flood tidal flow differences during spring tide along transects A, B and C shown in Figure 6.7. The dotted line indicates the 0-m.s^{-1} velocity threshold....48

Figure 6.10 Percentage of change in the bed shear stress fields during peak spring ebb (left) and flood stages (right) between the existing and the deepened channel bathymetry....48

Figure 6.11 Percentage of time the bed shear stress exceeds the critical shear stress threshold for 200 µm sand at ebb tide. Calculated from a 28-day simulation of the existing harbour (left) and the deepened channel (right)....49

Figure 6.12 Percentage of time the bed shear stress exceeds the critical shear stress threshold for 200 µm sand at flood tide. Calculated from a 28-day simulation of the existing harbour (left) and the deepened channel (right)....50

Figure 6.13 Difference of percentage of time the bed shear stress exceeds the critical shear stress threshold for 200 µm sand at ebb (left) and flood (right) tidal stages, calculated from a 28-day simulation of the existing harbour and the deepened channel. Noise in the difference fields was cleaned using an arbitrary minimum threshold of 5% to highlight the areas of significant changes. 51

Figure 7.1 Modelled current speed fields over the whole domain (left) and over Mair Bank (right) for the tide-only scenario during spring ebb (top) and flood (bottom) tides....55

Figure 7.2 Modelled net transport fluxes over Mair Bank for the tide-only scenario during ebb (left) and flood (right) tides. 55

Figure 7.3 Diagram showing the range of average current speeds at which sediment particles of different sizes are eroded, i.e. set in motion. The curve for sediments finer than about 0.1 mm is for relatively uncompact silts and muds (from Wright et al. (1999))....56

Figure 7.4 Diagram showing the range of average current speeds at which sediment particles of different sizes are transported, in suspension or as bedload, and below which they are deposited. The broken line indicates the transition between bedload and suspension transport (from Wright et al. (1999))....56

Figure 7.5 Modelled mean bed shear stress calculated over one tidal cycle for the tide-only scenario....57

Figure 7.6 Modelled net transport fluxes calculated over one tidal cycle for the tide-only scenario. 57
Figure 7.7 Wave height fields for Classes 1 to 8. Black arrows indicate the peak direction. 59
Figure 7.8 Wave height fields for Classes 9 to 16. Black arrows indicate the peak direction. 60
Figure 7.9 Mean net transport fluxes calculated over one tidal cycle for Classes 1 to 8. 61
Figure 7.10 Mean net transport fluxes calculated over one tidal cycle for Classes 9 to 16. 62
Figure 7.11 Mean net transport fluxes (left) and mean net transport differences (right) between pre- and post-dredge scenarios over one tidal cycle for Classes 1 to 4. A positive magnitude represents an increase. 64
Figure 7.12 Mean net transport fluxes (left) and mean net transport differences (right) between pre- and post-dredge scenarios over one tidal cycle for Classes 5 to 8. A positive magnitude represents an increase. 65
Figure 7.13 Mean net transport fluxes (left) and mean net transport differences (right) between pre- and post-dredge scenarios over one tidal cycle for Classes 9 to 12. A positive magnitude represents an increase. 66
Figure 7.14 Mean net transport fluxes (left) and mean net transport differences (right) between pre- and post-dredge scenarios over one tidal cycle for Classes 13 to 16. A positive magnitude represents an increase. 67
Figure 7.15 Distribution of 100 µm grain size sediments in the active layer generated by the BCG run for a 6-month fair-weather period. 70
Figure 7.16 Distribution of 150 µm grain size sediments in the active layer generated by the BCG run for a 6-month fair-weather period. 70
Figure 7.17 Distribution of 200 µm grain size sediments in the active layer generated by the BCG run for a 6-month fair-weather period. 71
Figure 7.18 Distribution of 300 µm grain size sediments in the active layer generated by the BCG run for a 6-month fair-weather period. 71
Figure 7.19 Distribution of 500 µm grain size sediments in the active layer generated by the BCG run for a 6-month fair-weather period. 72
Figure 7.20 Distribution of 1 mm grain size sediments in the active layer generated by the BCG run for a 6-month fair-weather period. 72
Figure 7.21 Distribution of 10 mm grain size sediments in the active layer generated by the BCG run for a 6-month fair-weather period. 73
Figure 7.22 Differences in spatial sediment fraction distributions. Positive amplitude indicates an increase of the given sediment fraction in the post-deepening configuration. 74
Figure 7.23 Wave height fields during storm event. Black arrows indicate the peak direction. 77
Figure 7.24 Mean total transport calculated during the 5-day storm period. Note that sediment transport was calculated over a complete number of tidal cycles (peak to peak). 77
Figure 7.25 Simulated depth changes after 5 days of storm conditions. Positive and negative magnitudes indicate sedimentation and erosion patterns, respectively. 78
Figure 7.26 Simulated depth changes after 16-day simulation of low energy waves. Positive and negative magnitudes indicate sedimentation and erosion patterns, respectively. 79

Figure 7.27 Changes in sedimentation and erosion patterns over the study area between the existing and post-deepening configurations over a 5-day storm event. 80
Figure 7.28 Changes in sedimentation and erosion patterns over the entrance to Whangarei Harbour between the existing and post-deepening configurations over a 5-day storm event. Zoom. 80
Figure 7.29 Changes in sedimentation and erosion patterns over the study area between the existing and post-deepening configurations over a 16-day fair weather event. 81
Figure 7.30 Changes in sedimentation and erosion patterns over the entrance to Whangarei Harbour between the existing and post-deepening configurations over a 16-day fair weather event. 81
Figure 7.31 Changes in sedimentation and erosion patterns over the study area between the existing and post-deepening configurations over a 21-day sequence of storm and fair weather conditions. 82
Figure 7.32 Changes in sedimentation and erosion patterns over the entrance to Whangarei Harbour between the existing and post-deepening configurations over a 21-day sequence of storm and fair weather conditions. 82
Figure 7.33 Predicted infilling in the outermost section of the channel between Busby Head and the distal margin to the delta estimated from a 1-year simulation including the post-dredging bathymetry. 84
Figure 8.1 Location of the sensitive areas considered for the investigation of the dredging plume dispersion. The blue, yellow and green polygons depict Marine Reserves, Marine 1 (Protection) Management Areas and sensitive areas, respectively, used for the mapping of the dredging plume modelling results. 88
Figure 8.2 Probabilistic *SSC* plumes during dredging phase (large trailing suction hopper dredger, TSHD) at sites R0, R1, R6 and R5 at three levels of the water column presented in MSL Report P0297-01. The drag head source rate used is 3% and the minimum threshold of SSC is 12 mg/L (black line). The grey contours indicate the 10 and 20 m isobaths delimiting the channel. The green polygons show the area of interest in terms of environment impact. 90
Figure 8.3 Probabilistic *SSC* plumes during dredging phase (small trailing suction hopper dredger, TSHD) at sites R0, R1, R6 and R5 at three levels of the water column presented in MSL Report P0297-01. The drag head source rate used is 3% and the minimum threshold of SSC is 12 mg/L (black line). The grey contours indicate the 10 and 20 m isobaths delimiting the channel. The green polygons show the areas of interest in terms of environment impact. 91
Figure 8.4 Probabilistic *SSC* plumes during overflow phase (large trailing suction hopper dredger, TSHD) at sites R0, R1, R6 and R5 at three levels of the water column presented in MSL Report P0297-01. SSC plumes are illustrated for a 79 min period. The minimum threshold of SSC is 12 mg/L (black line). The grey contours indicate the 10 and 20 m isobaths delimiting the channel. The green polygons show the areas of interest in terms of environment impact. 92
Figure 8.5 Probabilistic *SSC* plumes during overflow phase (small trailing suction hopper dredger, TSHD) at sites R0, R1, R6 and R5 at three levels of the water column presented in MSL Report P0297-01. SSC plumes are illustrated for a 95 min period. The minimum threshold of SSC is

12 mg/L (black line). The grey contours indicate the 10 and 20 m isobaths delimiting the channel. The green polygons show the areas of interest in terms of environment impact. 93

Figure 8.6 Probabilistic *SSC* plumes during overflow phase (large trailing suction hopper dredger, TSHD) at site R0 at three levels of the water column presented in MSL Report P0297-01. SSC plumes are illustrated for a 10, 30, 50 and 79 min period of overflow. The minimum threshold of SSC is 12 mg/L (black line). The grey contours indicate the 10 and 20 m isobaths delimiting the channel. The green polygons show the areas of interest in terms of environment impact..... 94

Figure 8.7 Probabilistic *SSC* plumes during overflow phase (small trailing suction hopper dredger, TSHD) at site R0 at three levels of the water column presented in MSL Report P0297-01. SSC plumes are illustrated for a 10, 30, 50 and 95 min period of overflow. The minimum threshold of SSC is 12 mg/L (black line). The grey contours indicate the 10 and 20 m isobaths delimiting the channel. The green polygons show the areas of interest in terms of environment impact..... 95

Figure 8.8 Probabilistic *SSC* plumes during overflow phase (large trailing suction hopper dredger, TSHD) at site R1 at three levels of the water column presented in MSL Report P0297-01. SSC plumes are illustrated for a 10, 30, 50 and 79 min period of overflow. The minimum threshold of SSC is 12 mg/L (black line). The grey contours indicate the 10 and 20 m isobaths delimiting the channel. The green polygons show the areas of interest in terms of environment impact..... 96

Figure 8.9 Probabilistic *SSC* plumes during overflow phase (small trailing suction hopper dredger, TSHD) at site R1 at three levels of the water column. SSC plumes are illustrated for a 10, 30, 50 and 95 min period of overflow. The minimum threshold of SSC is 12 mg/L (black line). The grey contours indicate the 10 and 20 m isobaths delimiting the channel. The green polygons show the areas of interest in terms of environment impact. 97

Figure 8.10 Probabilistic *SSC* plumes during dredging phase at site R2 for both the large (top) and the small (bottom) trailing suction hopper dredger (TSHD) considering the existing and the post-dredging configurations. The minimum threshold of SSC is 12 mg/L (black line). The grey contours indicate the 10 and 20 m isobaths delimiting the channel. The green polygons show the areas of interest in terms of environment impact. 98

Figure 8.11 Probabilistic *SSC* plumes during overflow phase at site R2 for both large (top) and small (bottom) trailing suction hopper dredger (TSHD) considering the existing and the post-dredging configurations. SSC plumes are illustrated for a 79 min and 95 min period of overflow depending on the barge. The minimum threshold of SSC is 12 mg/L (black line). The grey contours indicate the 10 and 20 m isobaths delimiting the channel. The green polygons show the areas of interest in terms of environment impact..... 99

Figure 8.12 Probabilistic *SSC* plumes during dredging phase at site R3 for both the large (top) and the small (bottom) trailing suction hopper dredger (TSHD) considering the existing and the post-dredging configurations. The minimum threshold of SSC is 12 mg/L (black line). The grey contours indicate the 10 and 20 m isobaths delimiting the channel. The green polygons show the areas of interest in terms of environment impact. 100

Figure 8.13 Probabilistic *SSC* plumes during overflow phase at site R3 for both large (top) and small (bottom) trailing suction hopper dredger (TSHD) considering the existing and the post-dredging configurations. SSC plumes are illustrated for a 79 min and 95 min period of overflow depending on the barge. 101
Figure 8.14 Probabilistic *SSC* plumes during dredging at site R0 for cutter suction dredger (CSD) considering the existing configuration. 102
Figure 8.15 Probabilistic *SSC* plumes during dredging at site R0 for backhoe dredger (BHD) considering the existing configuration. 102
Figure 9.1 Wave rose for the proposed disposal ground from 10-year wave hindcast (2005 – 2014). Wave directions are in the ‘‘coming from’’ convention. 104
Figure 9.2 Time series (2005 – 2014) of modelled significant wave height (Hs) within the proposed disposal ground. 105
Figure 9.3 Wave height fields over Bream Bay for wave classes 1 to 8. Hs, Tp, Dp and Occ (% Occurrence) presented in the upper left corner indicate the wave conditions at the offshore position BND (see MSL Report P0297-01). 106
Figure 9.4 Wave height fields over Bream Bay for wave classes 9 to 16. Hs, Tp, Dp and Occ (% Occurrence) presented in the upper left corner indicate the wave conditions at the offshore position BND (see MSL Report P0297-01). 107
Figure 9.5 Near bottom orbital velocity fields over the disposal ground for wave scenarios 1 to 9. Hs, Tp, Dp and Occ (% Occurrence) presented in the upper left corner indicate the wave conditions at the offshore position BND (see MSL Report P0297-01). 108
Figure 9.6 Near bottom orbital velocity fields over the disposal ground for wave scenarios 9 to 16. Hs, Tp, Dp and Occ (% Occurrence) presented in the upper left corner indicate the wave conditions at the offshore position BND (see MSL Report P0297-01). 109
Figure 9.7 Current roses showing total current speed at 0, 15 and 30 m below sea surface (bss) from ROMS hindcast data for the period 2000 – 2010 in the proposed disposal ground. Current directions are in the “going to” convention. 111
Figure 9.8 Disposal ground 3.2 dynamics simulated for a 1 year period. 113
Figure 9.9 Disposal ground 1.2 dynamics simulated for a 1 year period. 114
Figure 9.10 Difference in wave height fields caused by the disposal mound 3.2 over Bream Bay for wave scenarios 1 to 8. Hs, Tp, Dp and Occ (% Occurrence) presented in the upper left corner indicate the wave conditions at the offshore position BND (MSL Report P0297-01). 116
Figure 9.11 Difference in wave height fields caused by the disposal mound 3.2 over Bream Bay for wave scenarios 9 to 16. Hs, Tp, Dp and Occ (% Occurrence) presented in the upper left corner indicate the wave conditions at the offshore position BND (MSL Report P0297-01). 117
Figure 9.12 Difference in wave height fields caused by the disposal mound 1.2 near Ruakaka Beach for wave scenarios 1 to 8. Hs, Tp, Dp and Occ (% Occurrence) presented in the upper left corner indicate the wave conditions at the offshore position BND (MSL Report P0297-01). 118
Figure 9.13 Difference in wave height fields caused by the disposal mound 1.2 near Ruakaka Beach for wave scenarios 9 to 16. Hs, Tp, Dp and Occ

(% Occurrence) presented in the upper left corner indicate the wave conditions at the offshore position BND (MSL Report P0297-01). 119

Figure 10.1 Predicted suspended sediment concentrations (SSC) after 24h at bottom, mid water and surface levels for a release at sites PW, PN, PE, PS and ADCP. Note that a large TSHD is considered here for the amount of released sediments. The green polygon indicates the contour of 3 Mile Reef. The black and grey lines indicate the 12- and 20- mg/L SSC threshold corresponding to the critical threshold for rocky reef systems and to the highest background concentration recorded near the entrance to Whangarei Harbour. 123

Figure 10.2 Predicted suspended sediment concentrations (SSC) after 24h at bottom, mid water and surface levels for a release at sites PW, PN, PE, PS and ADCP. Note that a small TSHD is considered here for the amount of released sediments. The green polygon indicates the contour of the adjacent reef. The black and grey lines indicate the 12- and 20- mg/L SSC threshold corresponding to the critical threshold for rocky reef systems and to the highest background concentration recorded near the entrance to Whangarei Harbour. 124

Figure 10.3 Overview of the predicted suspended sediment concentrations (SSC) after 24h at sites PW, PN, PE, PS and ADCP, for both the large and the small TSHD. 125

Figure 10.4 Predicted suspended sediment concentrations (SSC) after 24h at bottom, mid water and surface levels for a release at site ADCP forced by measured current data. 125

Figure 10.5 Percentage of time *SSC* thresholds of 12, 50, 100 $mg.L^{-1}$ are exceeded between 10/12/1995 12:00 and 12/12/1995 12:00, assuming disposal at site PW with the large TSHD. The green polygon indicates an adjacent reef classified as sensitive. 126

Figure 10.6 Percentage of time *SSC* thresholds of 12, 50, 100 $mg.L^{-1}$ are exceeded between 10/12/1995 12:00 and 12/12/1995 12:00, assuming disposal at site PW with the small TSHD. The green polygon indicates an adjacent reef classified as sensitive. 127

Figure 10.7 Percentage of time *SSC* thresholds of 12, 50, 100 $mg.L^{-1}$ are exceeded between 06/02/1995 12:00 and 08/02/1995 12:00, assuming disposal at site PW with the large TSHD. The green polygon indicates an adjacent reef classified as sensitive. 128

Figure 10.8 Percentage of time *SSC* thresholds of 12, 50, 100 $mg.L^{-1}$ are exceeded between 06/02/1995 12:00 and 08/02/1995 12:00, assuming disposal at site PW with the small TSHD. The green polygon indicates an adjacent reef classified as sensitive. 129

Figure 10.9 Percentage of time *SSC* thresholds of 12, 50, 100 $mg.L^{-1}$ are exceeded during the summer month of January, assuming disposal at site PW with the large TSHD. The green polygon indicates an adjacent reef classified as sensitive. 130

Figure 10.10 Percentage of time *SSC* thresholds of 12, 50, 100 $mg.L^{-1}$ are exceeded during the summer month of January, assuming disposal at site PW with the small TSHD. The green polygon indicates an adjacent reef classified as sensitive. 131

Figure 10.11 Percentage of time *SSC* thresholds of 12, 50, 100 $mg.L^{-1}$ are exceeded during the winter month of August, assuming disposal at site PW with the large TSHD. The green polygon indicates an adjacent reef classified as sensitive. 132

Figure 10.12 Percentage of time *SSC* thresholds of 102, 50, 100 mg.L^{-1} are exceeded during the winter month of August, assuming disposal at site PW with the small TSHD. The green polygon indicates an adjacent reef classified as sensitive. 133

LIST OF TABLES

Table 4.1 Changes in mean and maximum significant wave height at positions 1 to 10 from 16 wave scenarios between the dredged channel and the existing configurations. Positive magnitude indicates a predicted increase of wave height due to the dredging.....33

1. INTRODUCTION

Refining NZ (RNZ) is investigating options for the deepening and realignment of the shipping channel leading to the Marsden Point Refinery at the entrance to Whangarei Harbour. Increasing the navigable depth is necessary to allow vessels with increased draft to safely transit to the refinery. MetOcean Solutions Ltd (MSL) have been contracted to provide coastal oceanographic expertise and investigate the potential effects of channel deepening on the physical environment. The scope of work includes i) an evaluation of the wave, hydrodynamic and sediment dynamic regime throughout the Whangarei Harbour entrance region, ii) consideration of the effects of capital and maintenance dredging on this environment, iii) potential effects on the coastal sediment budgets, iv) the stability of the adjacent beaches and the sub-tidal delta, and v) the effects of dredging and disposal on water quality in the receiving environment. A flow chart of the study processes is shown in Figure 1.1, and a map of Whangarei Harbour with the different locations referred to in the study is presented in Figure 1.2. A map showing the proposed deepening is presented in Figure 1.3. The location of the proposed disposal grounds for the placement of capital and maintenance volumes is shown in Figure 1.4.

The study investigations are presented in two reports:

- The first report (MSL Report P0297-01) is a technical reference document that provides details on the establishment of numerical models for wind, wave, current and sediment dynamics, and the data collection programme that was undertaken to support the model establishment and to validate the numerical schemes.

- The present report (MSL Report P0297-02) first characterises the existing environment and then investigates the likely physical effects of the Crude Shipping Project. This is also a technical reference document.

1.1. Report structure

This report is structured as follows. The bathymetry sources and sediment sampling results used for the present study are presented in Section 2. The wind and wave climate is described in Sections 3 and 4, respectively. Section 4 also includes the predicted effects of the channel deepening on the wave climate. The regional hydrodynamic regime is described in Section 5. The nearshore hydrodynamic regime and the expected changes caused by the channel deepening are presented in Section 6. The existing sediment dynamics and predicted effects of the channel deepening are provided in Section 7. Results of the dredging plume modelling are provided in Section 8, while predictions of the disposal ground dynamics and the disposal plume dispersion are provided and discussed in Sections 9 and 10. The executive summary is presented at the beginning of the report.

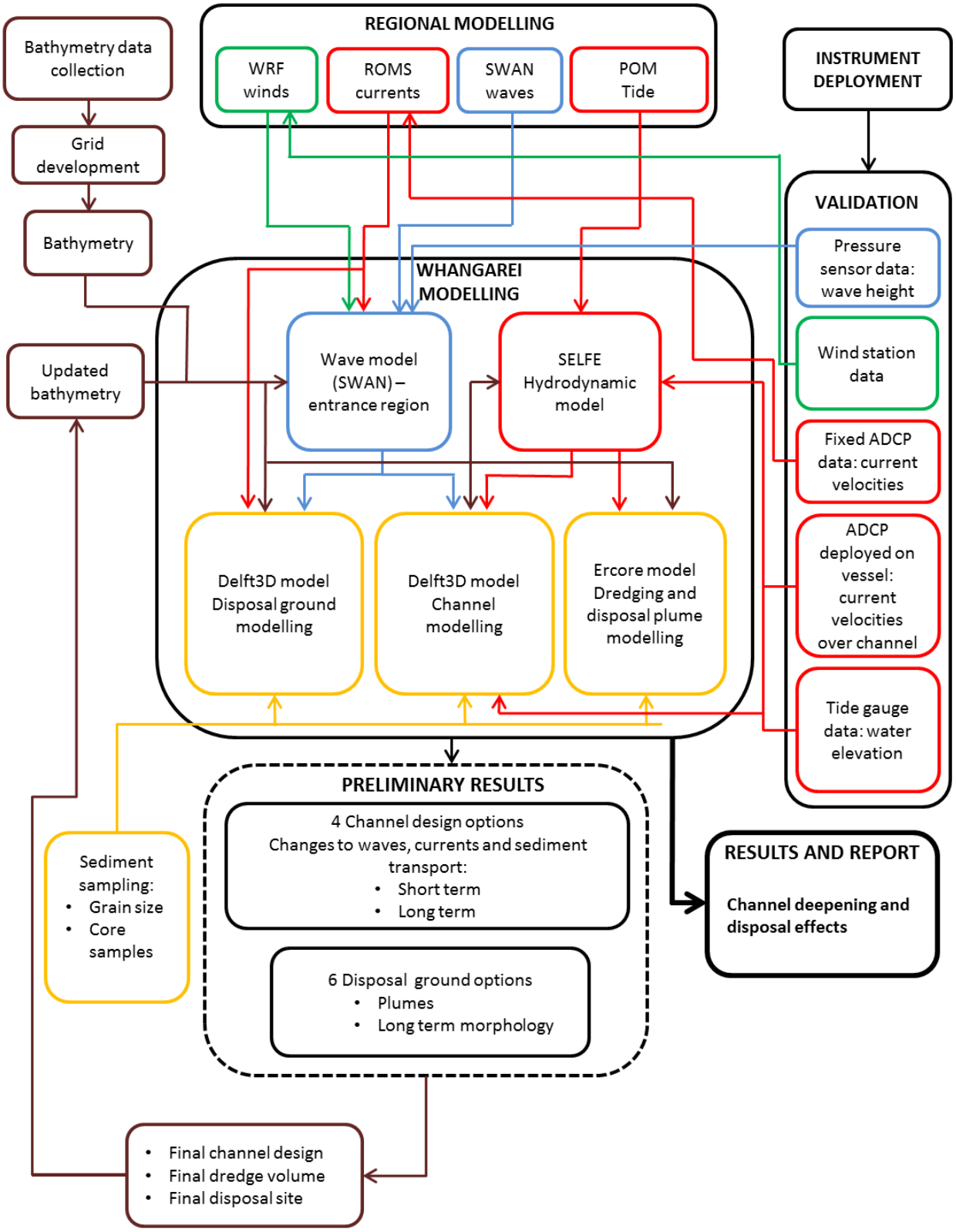

Figure 1.1 Flow chart showing the numerical modelling process for the study. Red lines indicate hydrodynamics; blue indicate waves; green indicate wind, brown indicate bathymetry and yellow lines indicate sediments / grain size.

1.2. Study Area

The different locations referred in the present report for the description of the effect of the deepening channel on the coastal dynamics at Whangarei Harbour are summarised in Figure 1.2.

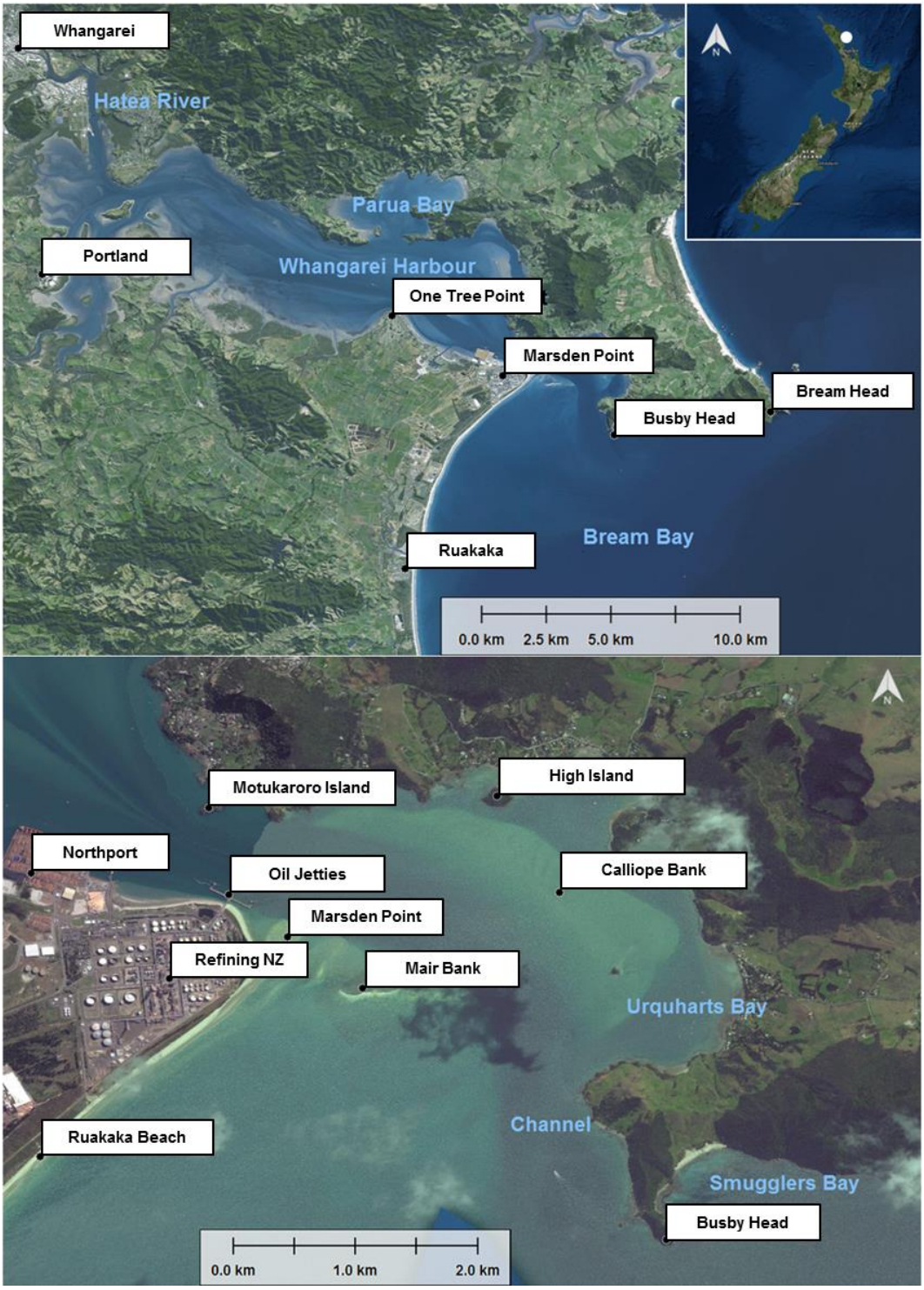

Figure 1.2 Maps of Whangarei Harbour (top) and its entrance (bottom) with the locations used in the present study for the establishment of the numerical models and the description of the effect of the channel deepening on the coastal dynamics.

1.3. Proposed channel deepening design

As part of the Crude Shipping Project, RNZ commissioned Royal Haskoning DHV (RHDHV) to define an optimal navigation channel design, including the associated dredging requirements, in order to provide high water access for vessels with increased draft to safely transit to the Crude Jetty.

Different options for the channel design (RHDHV Shipping Channel - Concept Design Report, Royal HaskoningDHV, 2016a) were provided and discussed with RNZ. An Under Keel Clearance study was completed by OMC in the OMC International (2016) - Marsden Point Channel Optimisation report, based on the channel designs provided by RHDHV and the long period wave analysis performed by MSL. Further assessment of the channel was undertaken from a navigation perspective (RHDHV Report - Desktop Simulation Study, Royal HaskoningDHV, 2015). The Option 4.2 was the stated preferred option from a channel design perspective and was confirmed via the alternatives assessment work presented in Tonkin and Taylor (2016a).

For the present study, Option 4.2 has been adopted as the design case for the numerical modelling. Details about the characteristics of the proposed channel and corresponding dredging requirements are described in Royal HaskoningDHV, 2016b, as part of the dredging methodology assessment provided by RHDHV to RNZ.

An overview of the proposed channel design (Option 4.2) and the resultant differences between existing and post-dredging bathymetries are shown in Figure 1.3 based on the depth datasets used by MSL to setup the model water depth.

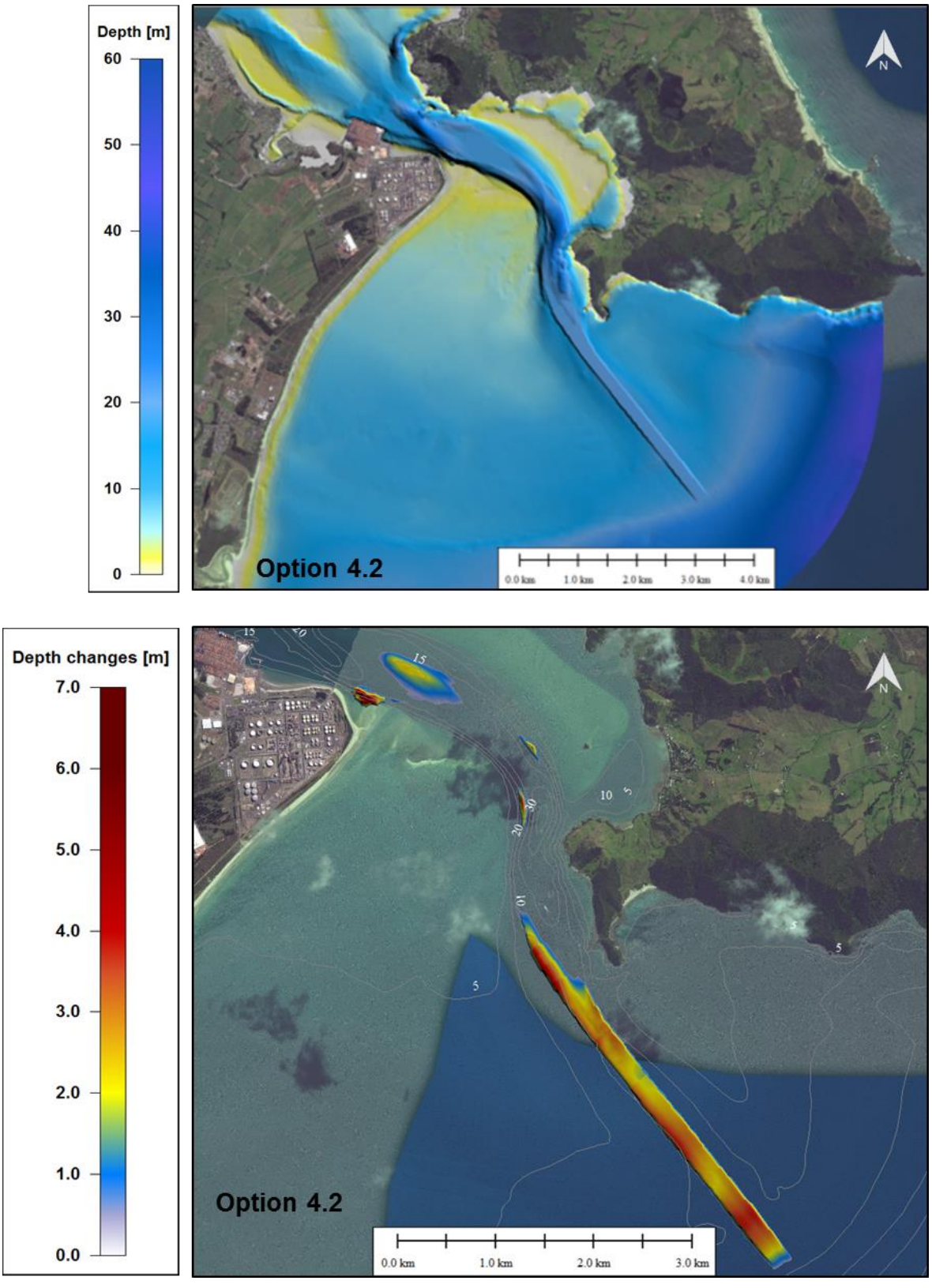

Figure 1.3 Depths (upper plot) and depth differences (lower plot) between the Option 4.2 channel design and the existing channel configuration. Positive amplitudes indicate a deepening of the channel.

1.4. Proposed disposal ground designs

A selection process was adopted to identify the preferred location to dispose the capital and maintenance volumes from the Crude Shipping Project. Two disposal sites are currently considered by RNZ (Tonkin and Taylor, 2016a) as potential options for the disposal of capital and maintenance dredge spoils volumes (see Figure 1.4):

- Disposal Site 1.2 (yellow polygon) is located over the south-western flank of the tidal delta where depths range between 2 and 10 m. Its distance from Ruakaka Beach and Busby Head is approximately 2 km and 1.6 km, respectively. This disposal site is considered by RNZ as an option for the placement of maintenance volume and up to 5% of the capital dredging volume and the site has therefore been investigated in the present study.

- Disposal Site 3.2 (red polygon) is an area measuring approximately 2 km^2, which ranges in depth from 41 to 48 m. This option for the disposal of capital volumes is located approximately 3.5 km south of Bream Head and 700 m east of 3 Mile Reef. Its distance from Busby Head and the inlet entrance is approximately 7 km. This disposal site is considered the preferred option for the placement of up to 95% of the capital volume and from up to 100% of the maintenance volume by RNZ and the area was therefore investigated in the present study.

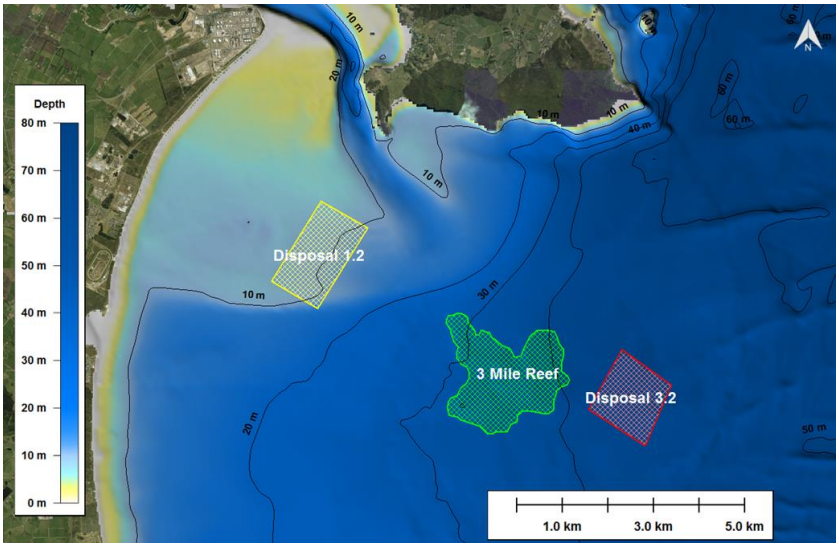

Figure 1.4 Location of sites 1.2, and 3.2 (indicated by coloured diagonal cross-hatch polygons) for the disposal of capital and maintenance volumes. 3 Mile Reef, indicated by a green polygon, is a sensitive reef because of its benthic encrusting communities.

2. BATHYMETRY AND SEABED CHARACTER

This section provides details on the bathymetry of Whangarei Harbour, and outlines the seabed analysis used as fundamental inputs to the numerical models.

2.1. Bathymetry

Bathymetry is an essential requirement for modelling. MSL has compiled an extensive national and regional bathymetric dataset from various sources, which have been used and validated in previous hydrodynamic studies. These datasets were updated with the latest Whangarei Harbour, main channel and offshore surveys. Specialist data manipulation tools have been developed in-house to allow the merging, interpolation and QA of raw bathymetric data when establishing numerical model domains. The bathymetry data and sources are shown in Figure 2.1.

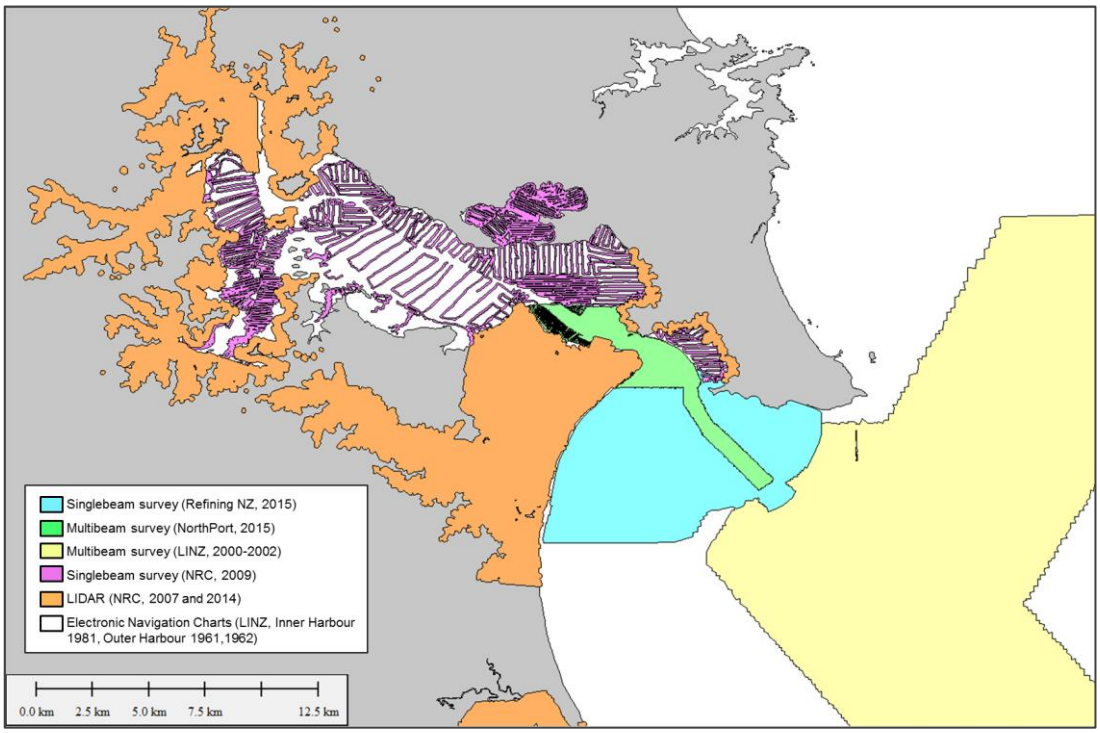

Figure 2.1 Sources of bathymetry data used in the study.

2.2. Sediment characteristics

2.2.1. Sediment sampling

A series of sediment sampling programmes were undertaken in the study area (Tonkin and Taylor, 2010) to provide information on the sediment grain size of the proposed dredge and disposal areas. This information was used as an input to both the morphological and plume models with representative sediment compositions in order to realistically predict the short- and long-term morphodynamics of the seabed pre- and post-dredging. Sediments were classed according to the Folk scale (Figure 2.2).

The sediment sampling programmes are described in detail in other reports, but in summary were as follows:

Firstly, surficial sediment sampling was undertaken, the sites and sediment class of which are shown in Figure 2.3 - Figure 2.6 . Sample sites were confined to the regions to be dredged within the main channel and areas identified initially as potential disposal areas. Limited fines (silts and clays) were identified in these surficial samples, with most sites exhibiting varying proportions of sand and gravel/coarse material.

Secondly, a total of 26 vibrocores were collected in 2016 for geotechnical and environmental testing (Tonkin and Taylor, 2016b). The core locations are shown in Figure 2.7 and Figure 2.8. Of particular interest are the cores at sites v10a,b,c and v11 at the edge of Mair Bank (Figure 2.9 to Figure 2.12, which indicate that this region is predominantly sandy and show no indication of shell armouring with depth.

Thirdly a diver survey was undertaken (Kerr, 2016) in order to visually inspect the subtidal habitat and sediment composition of Mair Bank. Photos were taken at locations along transects at the edge of Mair Bank, with amount of shell hash, bed composition and bed form noted (Figure 2.13 and Figure 2.14). A gradation of shell hash to sand was observed from the top of the Bank down into the subtidal on the channel walls, finally grading back to shell hash in the channel bed. In areas of sand on the channel edge, sand waves were observed, indicating active sediment transport in this region.

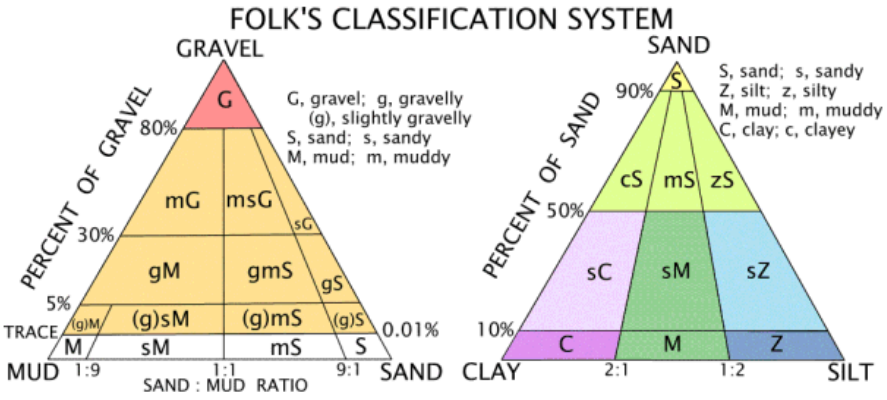

Figure 2.2 Folk classification system for sediments (Folk, 1954).

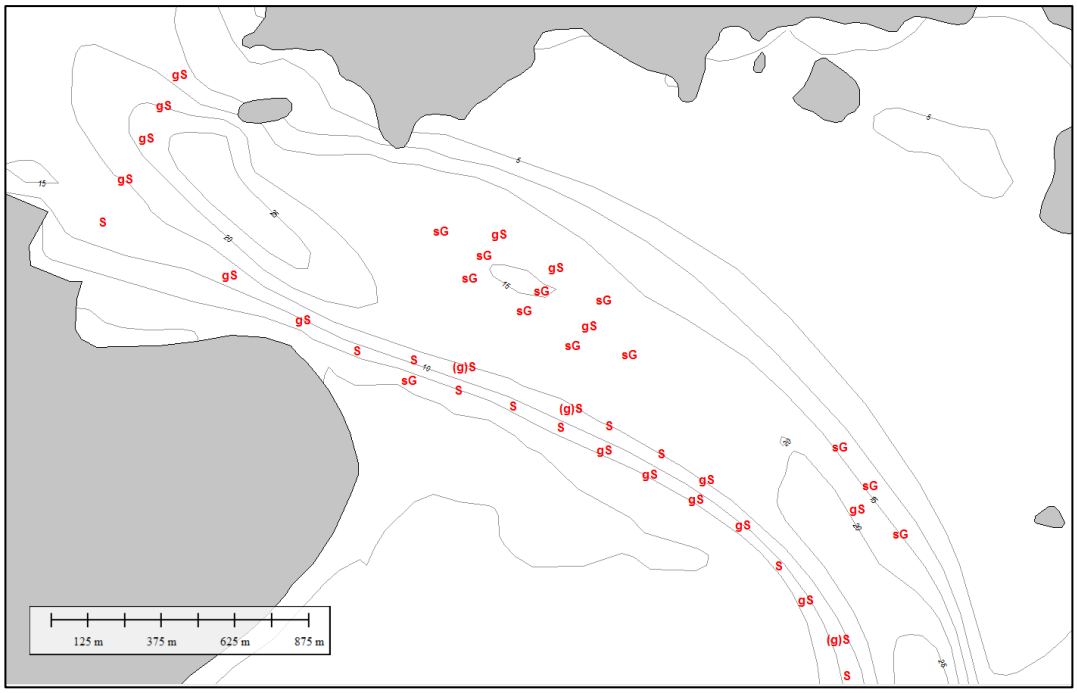

Figure 2.3 Whangarei Harbour inner channel sediment samples (sediment class according to the Folk scale).

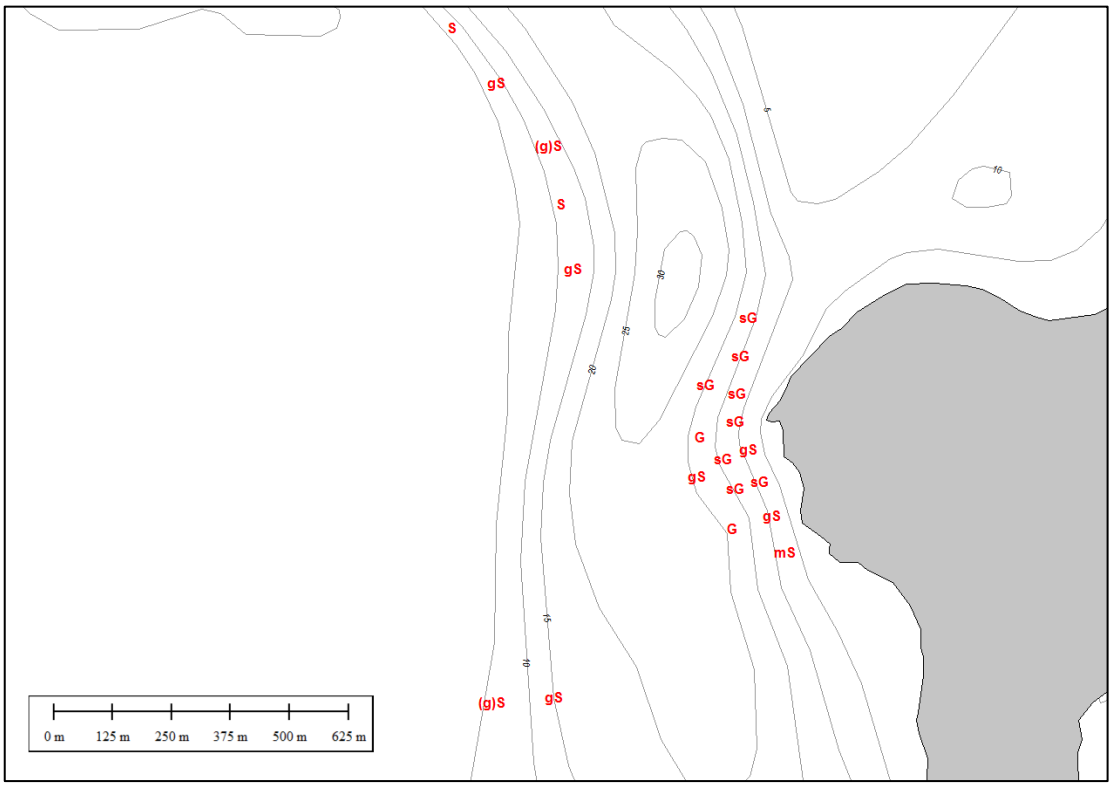

Figure 2.4 Whangarei Harbour mid channel sediment samples (sediment class according to the Folk scale).

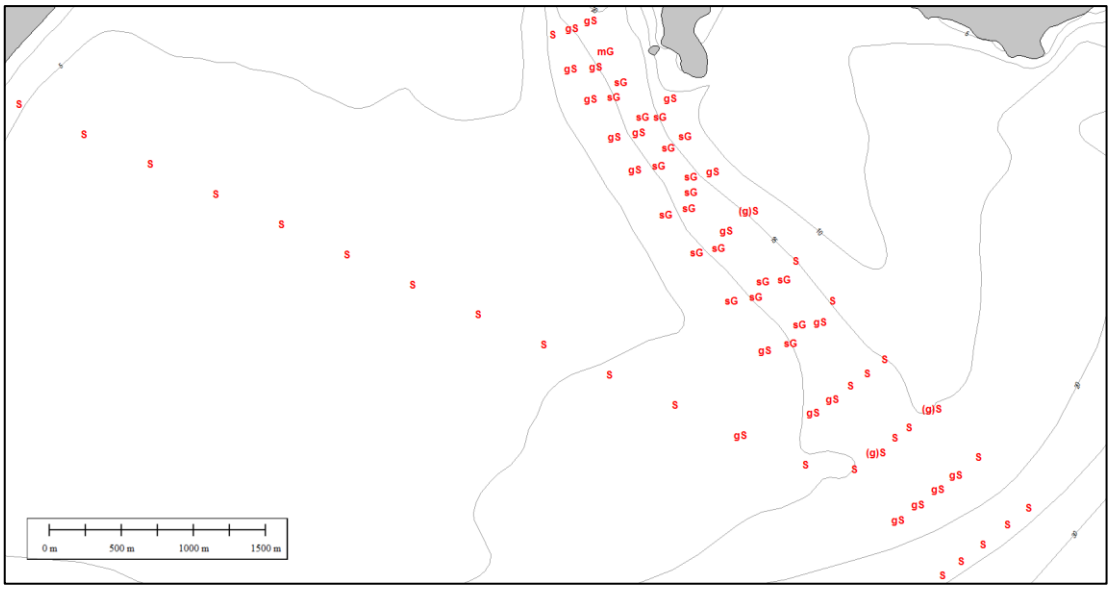

Figure 2.5 Whangarei Harbour outer channel and ebb tidal shoal sediment samples (sediment class according to the Folk scale).

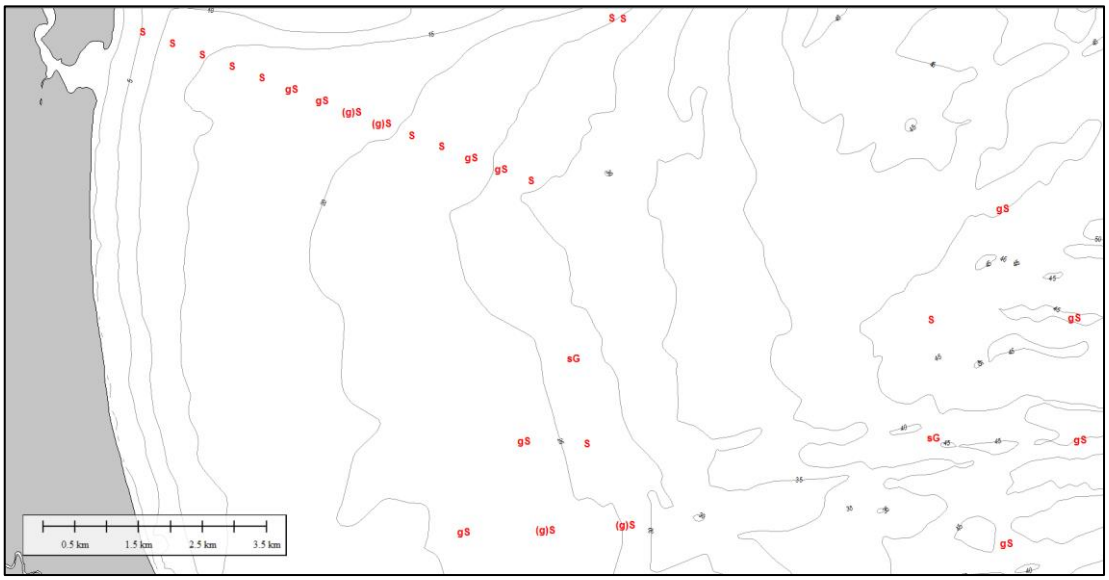

Figure 2.6 Wider Bream Bay sediment samples (sediment class according to the Folk scale).

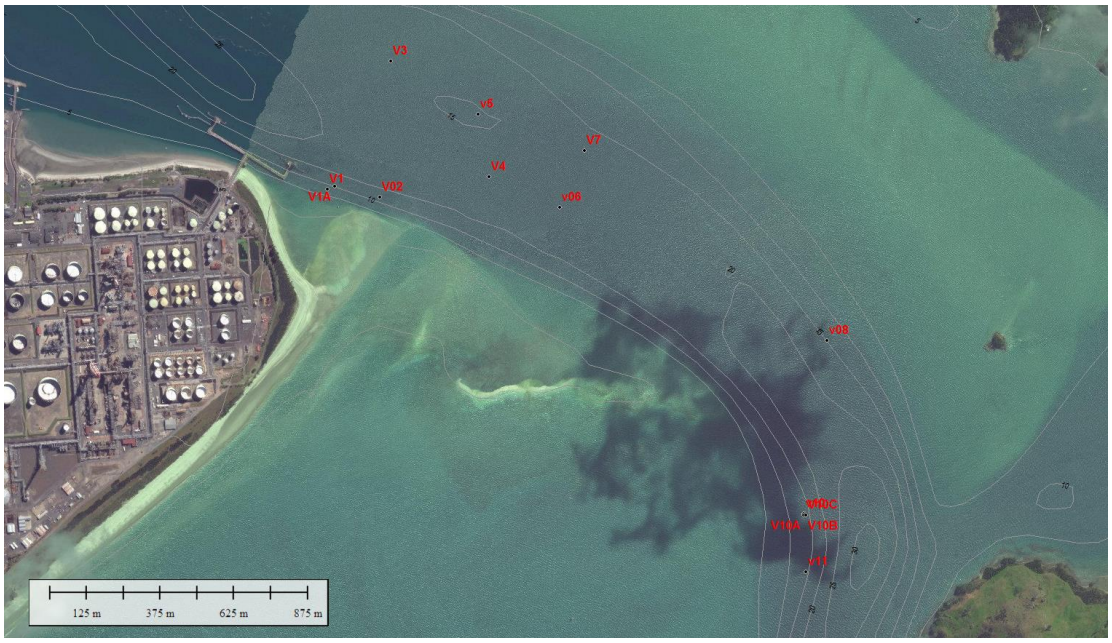

Figure 2.7 Whangarei Harbour inner channel vibrocore locations.

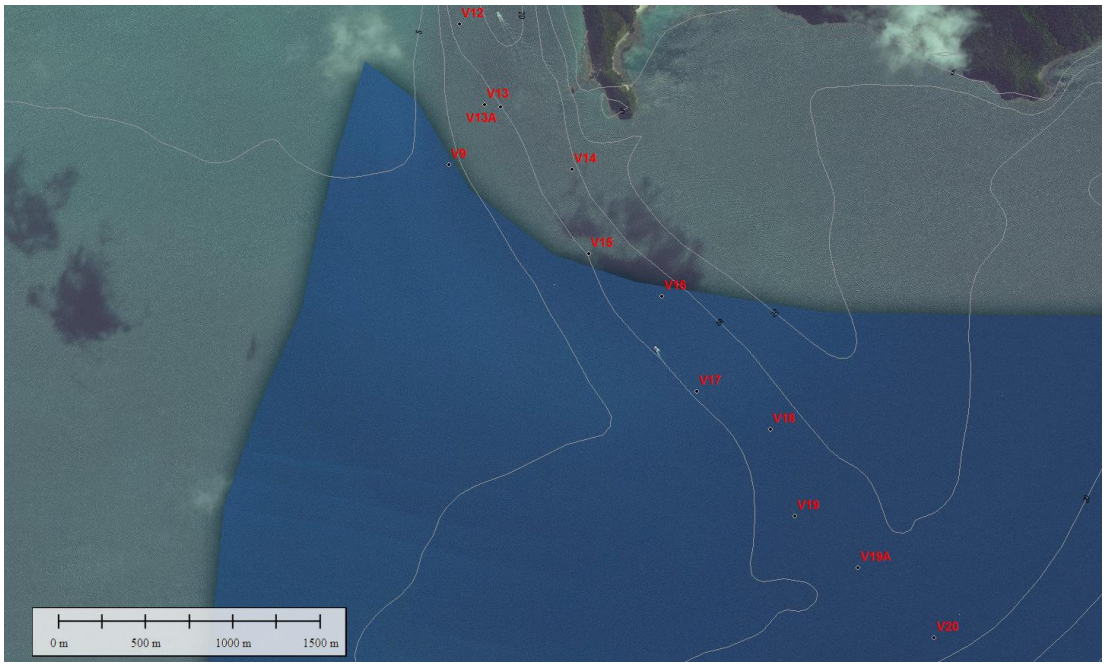

Figure 2.8 Whangarei Harbour outer channel vibrocore locations.

Figure 2.9 Vibrocore samples for site v10.

Figure 2.10 Vibrocore samples for site v10a.

Figure 2.11 Vibrocore samples for site v10b.

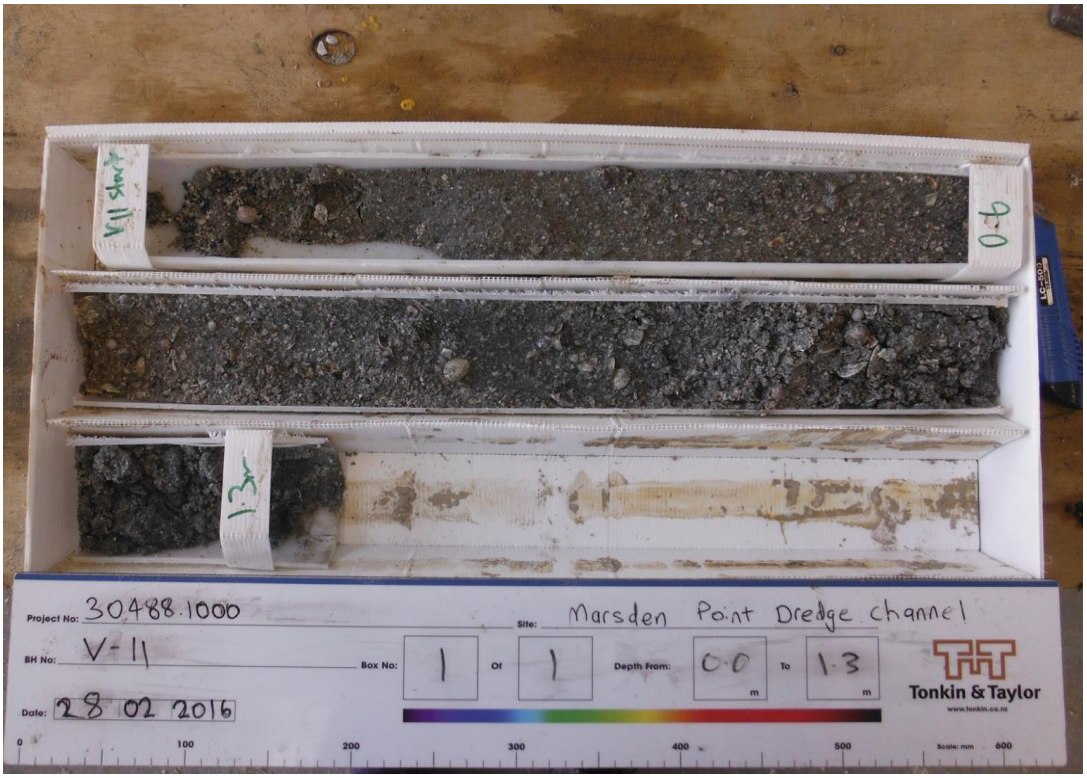

Figure 2.12 Vibrocore samples for site v11.

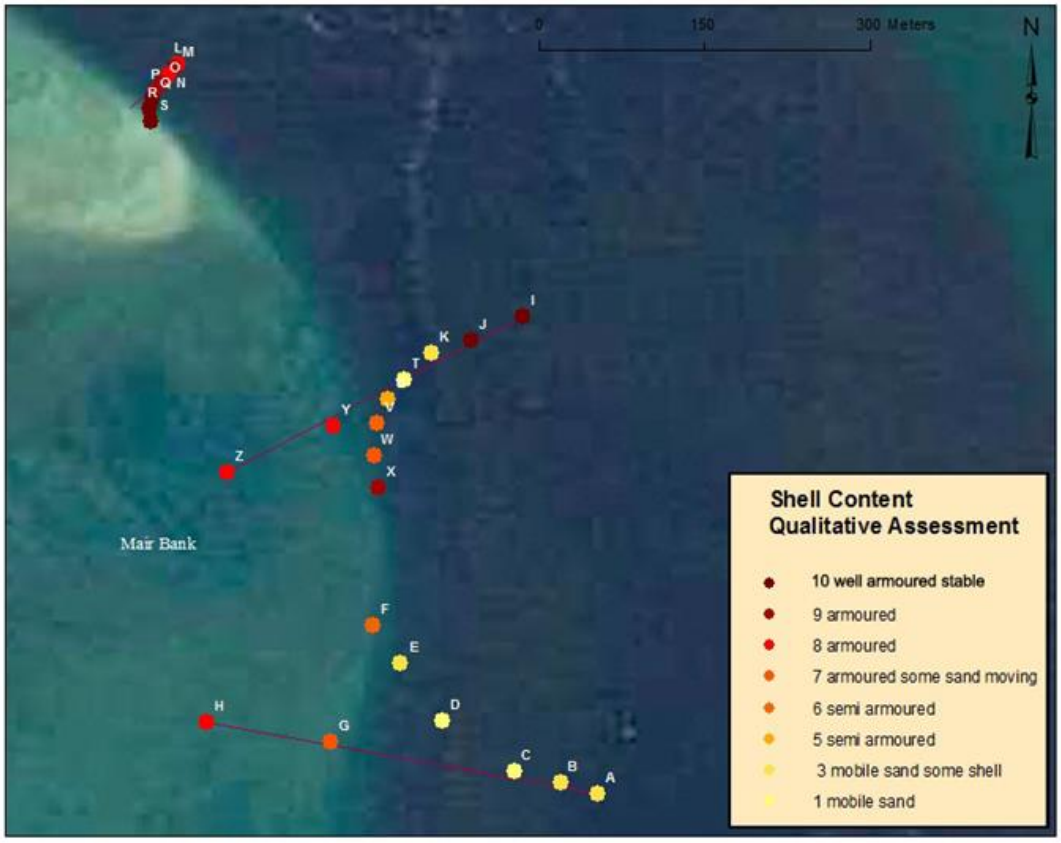

Figure 2.13 Results from channel edge diver survey carried out by Vince Kerr (Figure 2.15 in Kerr, 2016). Areas ranked qualitatively according to the amount of shell component.

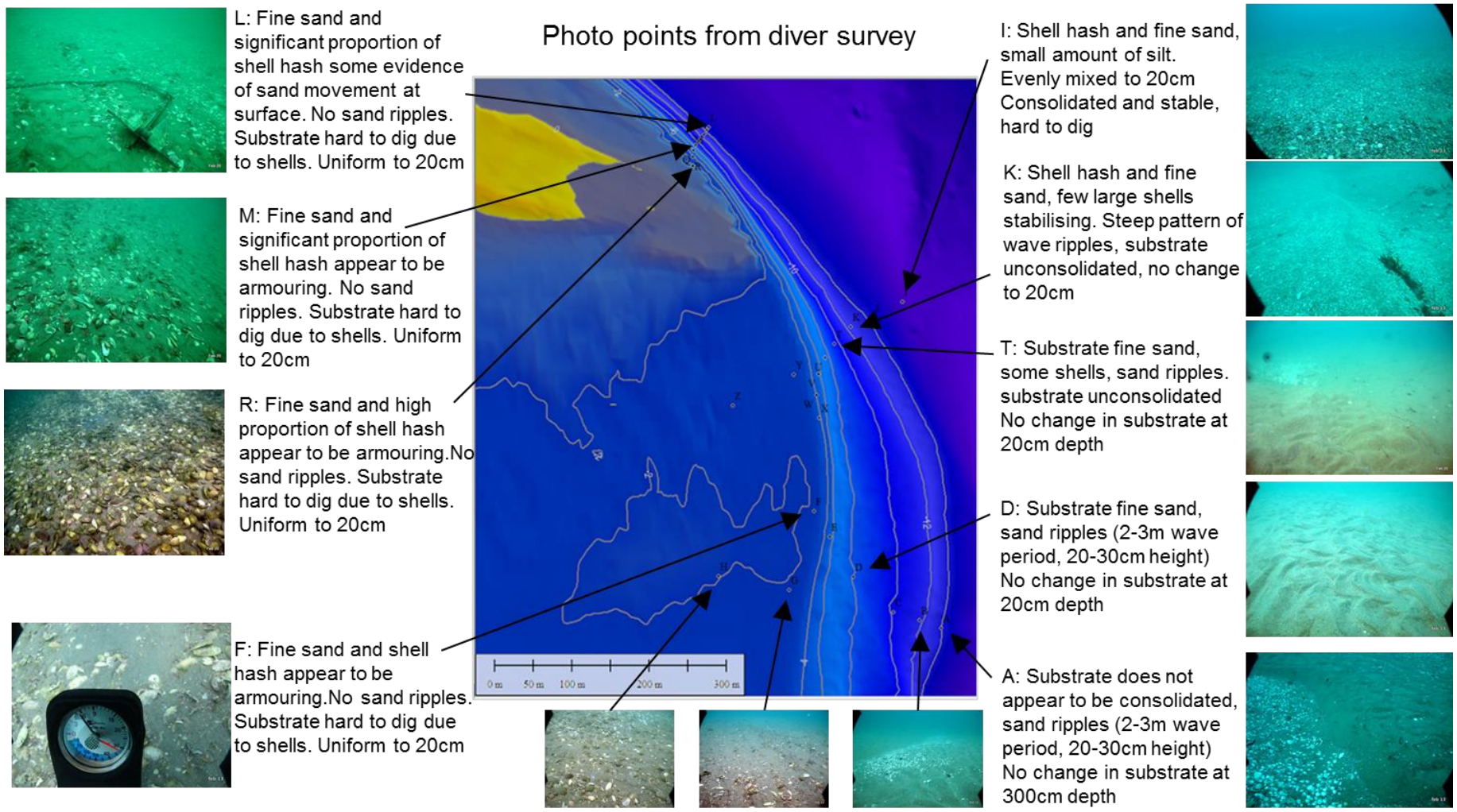

Figure 2.14 Selection of photos and locations from diver survey, illustrating the varied spatial nature of sediments and bedforms on the edge of Mair Bank. From Kerr (2016).

2.2.2. Mair Bank

A field trip to Mair Bank was undertaken on 23rd of January 2016 by MSL to observe sediment composition and structure of shell armouring in the intertidal.

Mair Bank consists of significant amounts of shell material, in the past this has mostly consisted of pipi and their shells (Figure 2.15 and Figure 2.16), however mussel colonies were also observed; contributing to the general consolidation of surficial sediments (Figure 2.17). To the lee of the shell ridges, fine sediment had been deposited. This suggests that sediment transport actively occurs across the bank as shown in Figure 2.18 and Figure 2.19. Such process may be due to the duration of submersion and positioning within the tidal stage as well as sand deposits in response to storm events.

Figure 2.15 Pipi shell bank.

Figure 2.16 Shell structure of pipi bank.

Figure 2.17 Mussel colony on Mair Bank.

Figure 2.18 Fine sand deposited to the lee (northern side) of the shell ridges.

Figure 2.19 More advanced stage of sand deposition with a greater proportion of sand overlaying the shell substrate.

3. WIND CLIMATE

The long-term wind climate at Whangarei required as inputs for the wave and hydrodynamic models was prepared using the regional scale WRF atmospheric numerical model. The model was validated using measured data provided by a local wind station (MSL Report P0297-01). Wind-wave and wind-driven circulation predictions depend upon the accuracy of the predicted wind field and the techniques used for hindcasting. The results of the validation process showed that the wind hindcast was suitable for providing wind forcing to the wave and hydrodynamic numerical models.

This section summarises the regional wind conditions in the vicinity of Whangarei extracted from the 36-year regional atmospheric hindcast carried out by MSL. These data are used, along with outputs from the ROMS hydrodynamic model (described in Section 5) to provide boundary conditions for the local wave modelling carried out for the study.

3.1. Characterising the wind climate

The wind rose calculated at the wave rider buoy (WRB) site (Figure 3.1) and presented in Figure 3.2 shows that the wind regime is dominated by south-westerly winds in frequency of occurrence (approximately 30%). However, the strongest wind intensities occur during easterly and north-easterly events related to local storms and extra-tropical cyclones.

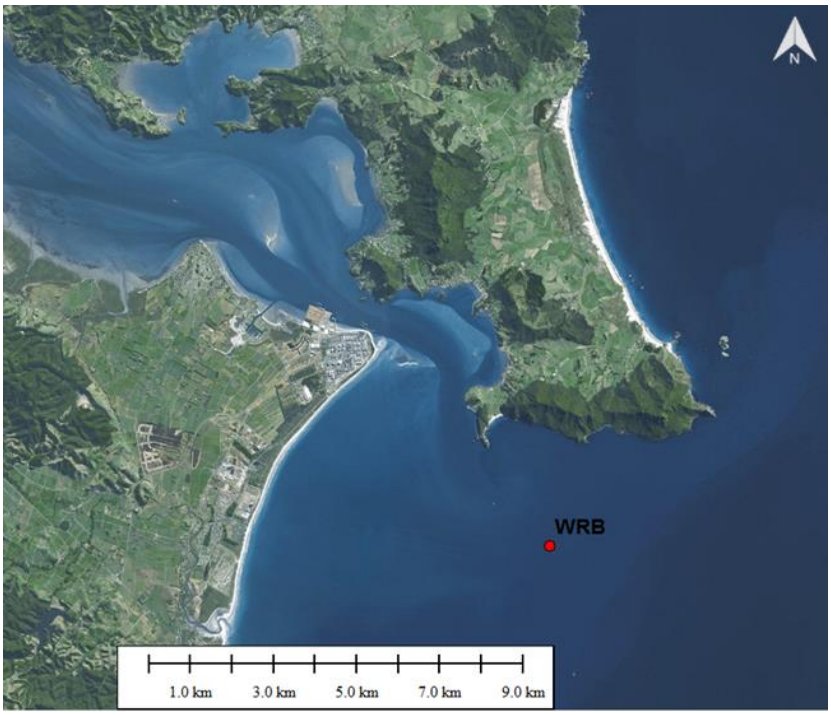

Figure 3.1 Locations of the WRB site used to extract the wind climate from the 36-year hindcast data.

The summary of the wind speed statistics (Appendix A – Wind statistics) indicates a mean speed of ~6 $m.s^{-1}$. The mean wind speed variability between winter and summer conditions is approximately 1 $m.s^{-1}$. The maximum wind speed observed over the hindcast period was 23.7 $m.s^{-1}$ corresponding to cyclone Bola in 1988. July and December are typically the months with the highest and lowest occurrence

of strong wind events, respectively. The occurrence of easterly winds increases in summer and decreases in winter (Figure 3.3).

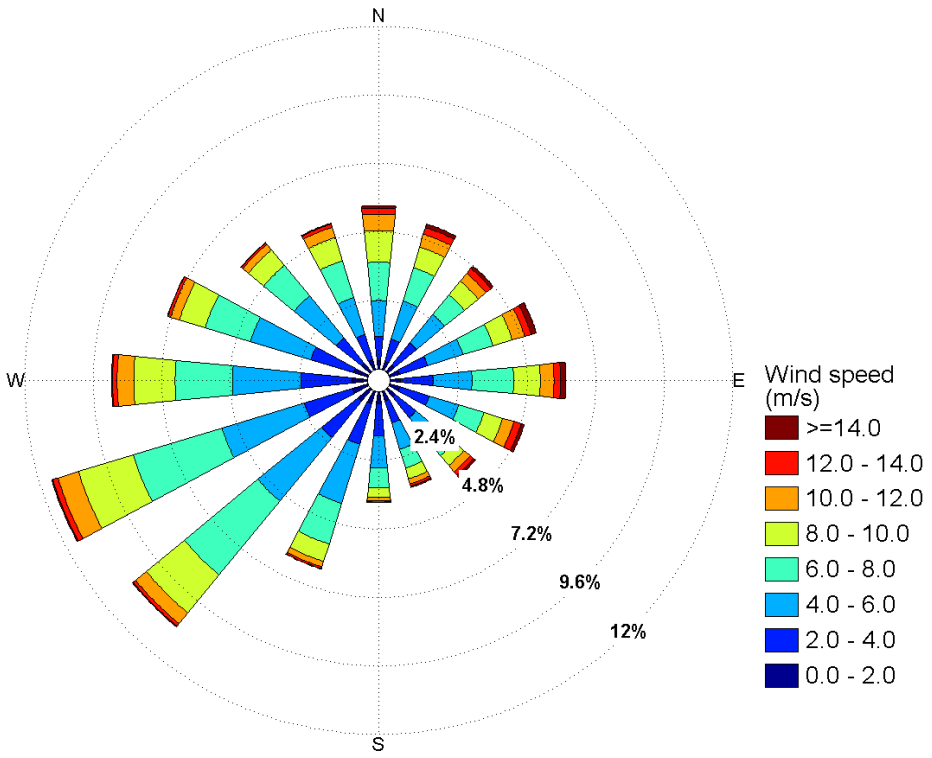

Figure 3.2 Annual wind rose plot at WRB. Sectors indicate the direction from which the wind is coming.

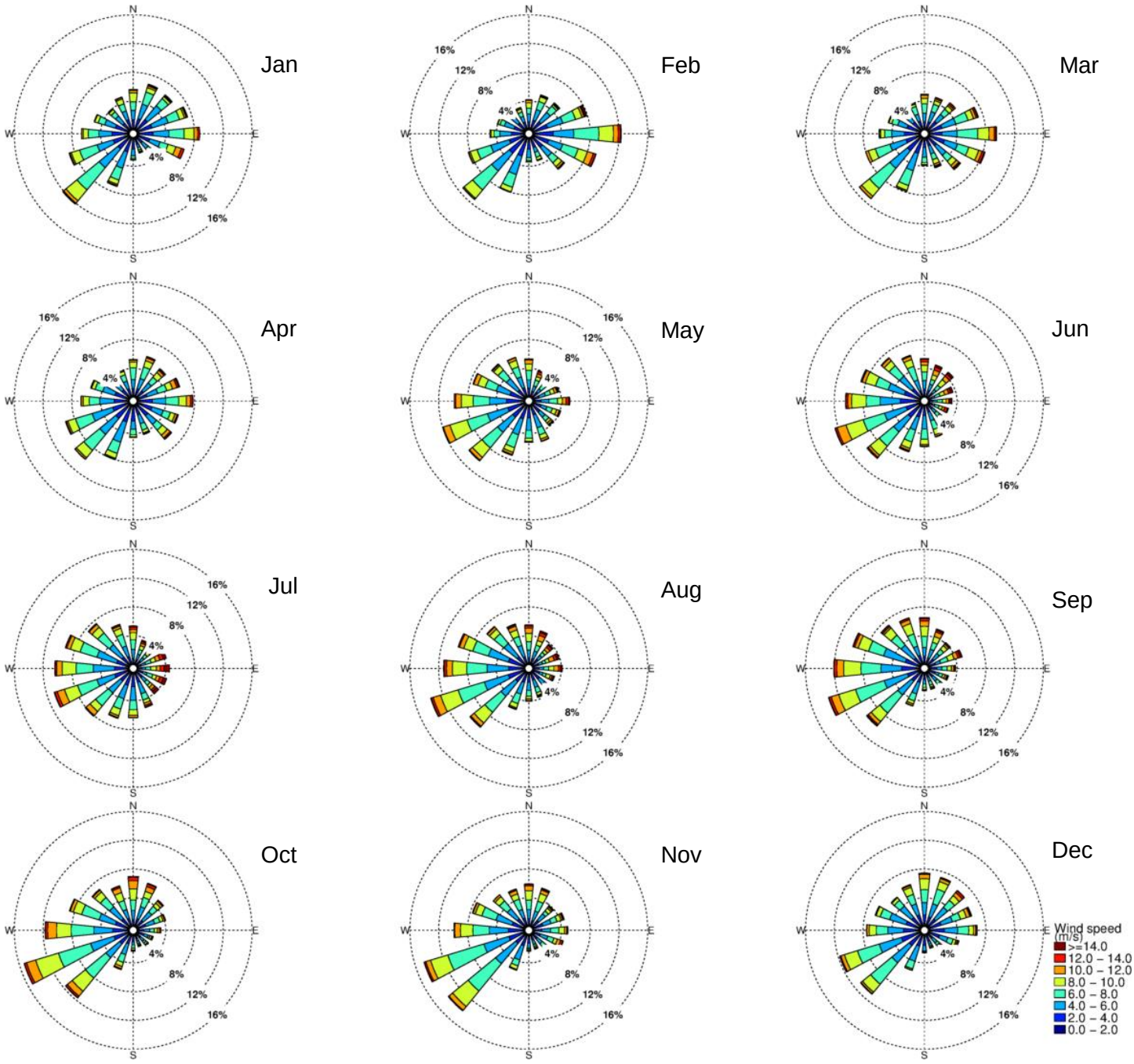

Figure 3.3 Monthly wind rose plots at WRB. Sectors indicate the direction from which the wind is coming.

4. WAVE CLIMATE

The SWAN model was used to hindcast the wave climate and further examines the wave transformation across the ebb tide delta based on a 3-level nested domain. This approach allowed the replication of the spectral wave transformations from offshore to the nearshore region occurring at different spatial scales. This model was validated with measurements from 5 locations (see MSL Report P0297-01 for details), and was shown to represent the wave climate at the entrance to Whangarei Harbour and along Ruakaka beach well, except for one site near the Ruakaka river mouth where wave heights were over-predicted by the model. The wave model did not fully capture the redistribution of wave energy to the south of the tidal delta largely controlled by refraction processes. The relative good agreement between the model and the measured data at the other locations close to Whangarei Harbour entrance confirms the model is suitable for the impact assessment over Whangarei Harbour entrance and the surroundings.

This section presents a detailed characterisation of the wave climate at the entrance to Whangarei Harbour and Bream Bay and the predicted effects of the channel deepening on the nearshore wave transformation processes. Potential changes in the wave field in coastal waters are of importance given that wave forcing is a significant contributor to both the morphodynamic and the navigability conditions through the access channel.

4.1. Characterising the wave climate

The wave climate in the northern region of Bream Bay at position WRB, shown in Figure 4.1, is characterised by a mean annual significant wave height of 0.80 m. The largest significant wave height modelled over the hindcast period was 5.86 m (cyclone Bola, 1988), while the annual 99th percentile non-exceedance level (P99) was 2.85 m (i.e. on an annual basis, for 99% of the time the total significant wave height is less than 2.85 m). On average the total significant wave heights are less than 1.0 m for durations of 36 hours and greater for some 73 % of the time. These statistics indicate a typically low energy wave environment that is occasionally affected by strong storms and cyclonic systems. Wave height maps for a range of wave conditions are provided in Figure 4.2 and Figure 4.3. Easterly sea states predominate (see Figure 4.4) and the monthly wave roses (Figure 4.5) do not suggest any strong seasonality in the wave height distribution.

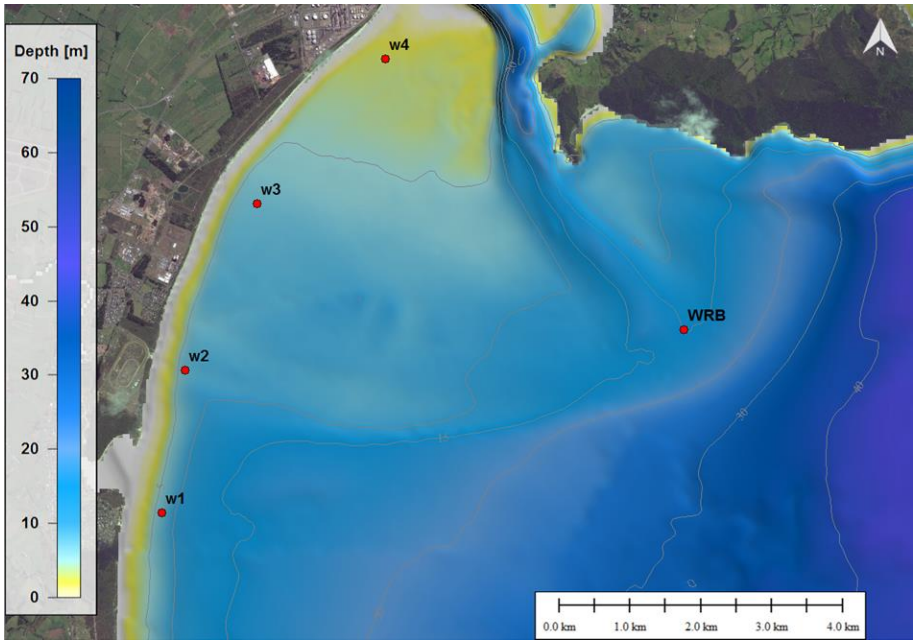

Figure 4.1 Locations of the wave gauges (red circles) along Ruakaka Beach and offshore of the harbour entrance.

A summary of the significant wave statistics for swell, wind-sea and total frequency bands at position WRB is provided in Appendix B – Wave statistics. This includes the monthly and annual significant wave height exceedance probabilities, the annual joint probability distribution of total significant wave height and mean wave direction at peak energy, the annual joint probability distribution of total significant wave height and peak spectral wave period, and the annual persistence non-exceedance probabilities for total significant wave height.

The seabed morphology of the ebb tide delta and adjacent headland plays an important role in the wave climate along Ruakaka Beach and at the harbour entrance (Figure 4.3), particularly in dictating the along shore variability of the wave field. Strong wave refraction patterns develop over the delta and near Busby Head. This typically leads to a shift in the wave direction from northeast to east at WRB and southeast, causing wave focusing along the eastern edge of the delta entrance toward Busby Head and the penetration of a fraction of wave energy through the entrance channel. Moreover, this mechanism of refraction increases the exposure of the southwestern flank of Mair Bank to waves during strong storm events. The extended and gradual bed slope of the western flank of the ebb-tidal delta largely dissipates the amount of refracted wave energy through bottom friction and wave breaking, which reduces the wave energy reaching Mair Bank, thereby contributing to its relative stability. During extreme wave events (e.g. cyclonic conditions), wave breaking and overwash can occur over Mair Bank, potentially leading to the formation of a non-permanent marginal channel between Marsden Bank and Mair Bank(. Note, however, that overwash mechanisms are not resolved by the SWAN model.

The configuration of the Whangarei Harbour entrance, which is characterised by an S-shaped access channel and sheltered by an extended cross-shore sandy/shelly bank, decreases the amount of wave energy propagating within the tidal inlet. For example, during ebb tide the opposing current induces a steepening of waves which decreases the wavelength and the apparent wave period and causes an increase of the whitecapping dissipation. Variations of tidal water elevation near

Mair Bank also result in a tidal modulation of wave height and period as observed at position W4 (see Figure 4.1). This tidal modulation effect is typically caused by variations in the vertical profile of roughness according to the water depth.

Effects of waves on currents is further discussed in Section 8 (Sediment Transport Modelling), in which a two-way fully coupled model was used to replicate the effect of wave-current interactions on the morphological dynamics at the entrance to Whangarei Harbour.

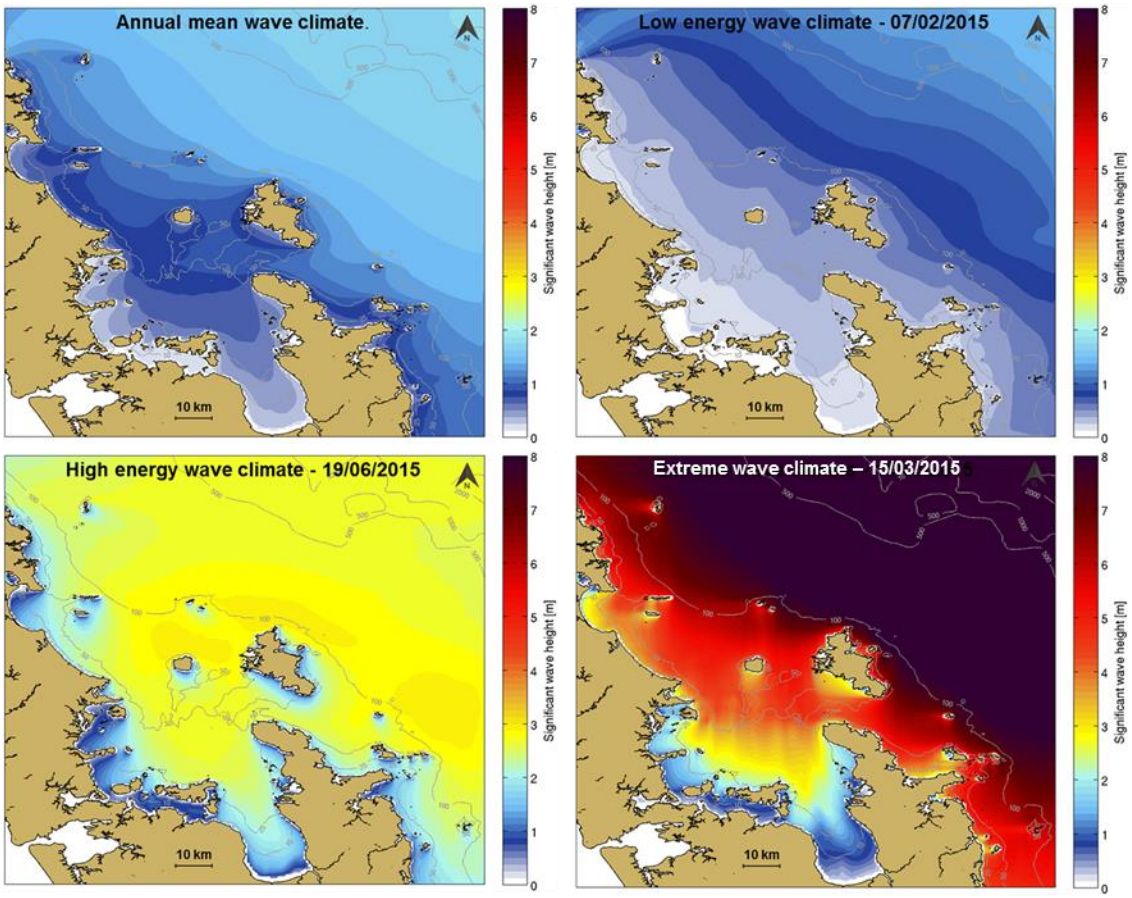

Figure 4.2 Annual mean and snapshots of modelled significant wave height over the regional SWAN parent domain for different weather events. The wave height annual mean was calculated for 2015.

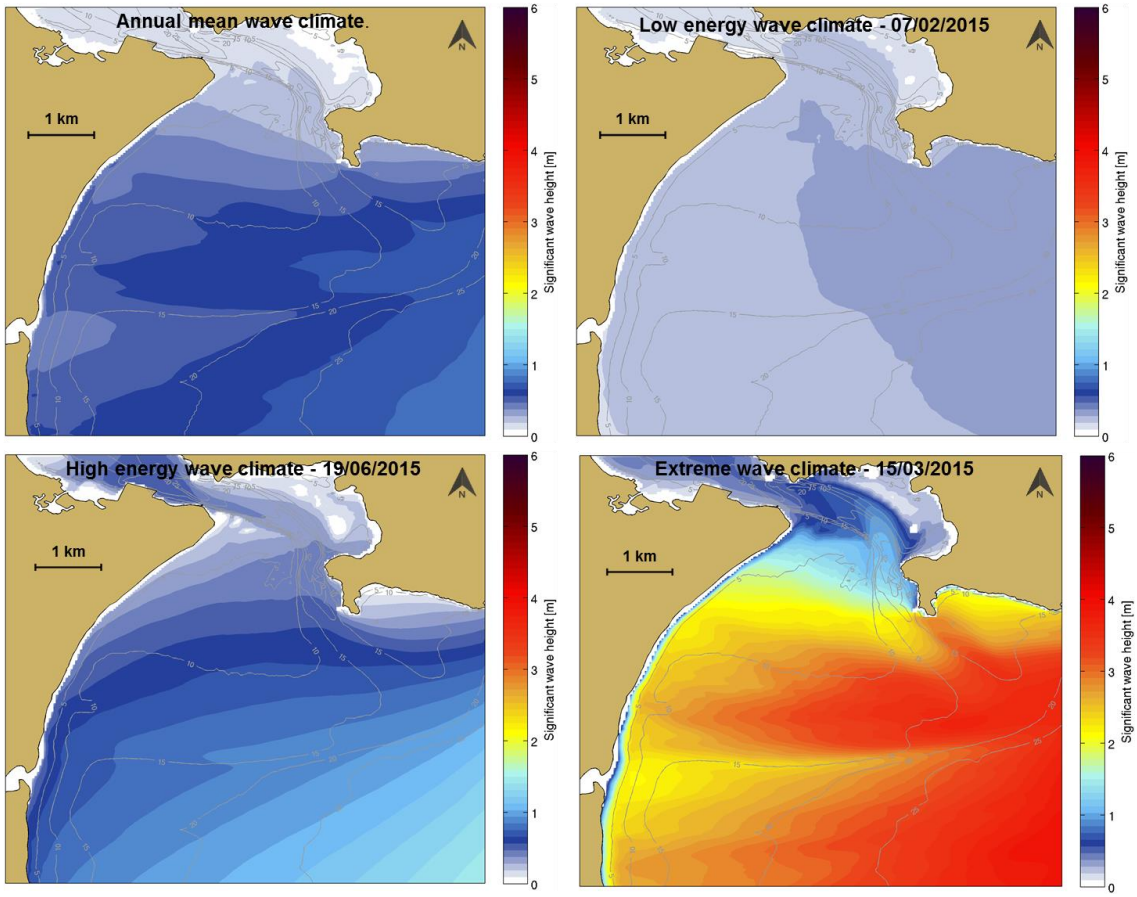

Figure 4.3 Annual mean and snapshots of modelled significant wave height over the local SWAN domain for different weather events. The wave height annual mean was calculated for 2015.

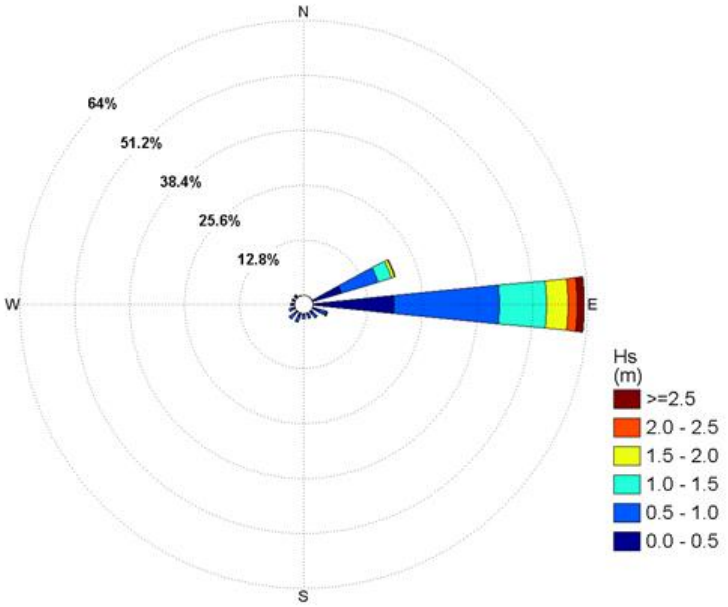

Figure 4.4 Annual wave rose plot for the total significant wave height at WRB. Sectors indicate the direction from which waves approach.

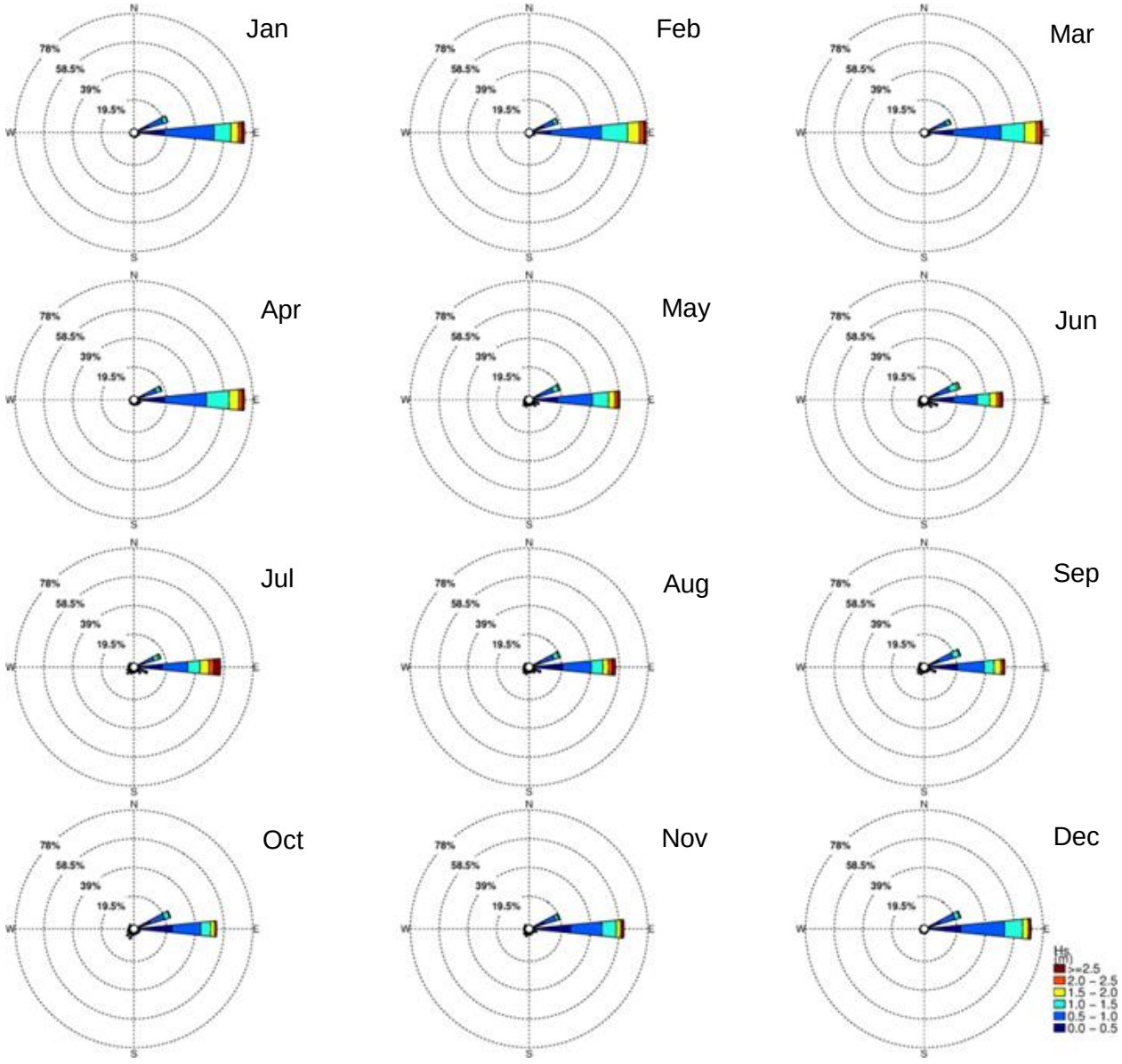

Figure 4.5 Monthly wave rose plots for the total significant wave height at WRB. Sectors indicate the direction from which waves approach.

4.2. Effects of channel deepening on the wave climate

The spectral wave model (SWAN) was applied to simulate the propagation of waves across the ebb tide delta and consider the effects of the channel deepening. These effects were assessed by modelling the existing harbour and a scenario with a deepened channel, in order to evaluate the changes in the wave climate through direct comparison of modelled outcomes. The wave modelling technique employed in this assessment is fully described in MSL Report P0297-01.

A one-year period (2015) covering the measuring periods was used to assess the changes, being duration sufficient to capture the full range of likely conditions. The wave model produced the spatial distribution of wave heights over the entire delta at hourly intervals. The mean absolute change to the significant wave height is presented in Figure 4.6. The predicted changes are very subtle; a slight increase (1 cm) east of the channel and zones of increase and decrease (~1 – 2 cm) west of the channel. The offshore extent of the deepened channel induces slight changes to the speed of the incoming swell waves, which results in a change to the wave refraction outcomes. The absolute magnitude of the changes is further illustrated with a series of 16 wave classes that represent the wave climate range (Figure 4.7 to Figure 4.10). Note that during a highly energetic storm (significant wave height of more than 5 m) the changes in significant wave height are predicted to be in the order of 20 cm.

Enhanced refraction occurs along the eastern margin of the dredged channel, directing energy toward the rocky point of Busby Head and Smugglers Bay. This leads to a slight increase in the mean and maximum wave height by 2 and 10 cm (~5%) at Busby Head and by 2 and 15 cm (~10%) at Smugglers Bay (Figure 4.7 to Figure 4.10), respectively. The limited impact of such changes in the wave propagation in terms of sediment dynamics for both Busby Head and Smugglers Bay are discussed in Section 7.4.

Conversely, there is a minor decrease in wave energy over a wide zone along Ruakaka Beach. Here, the reduction of wave height during storms will be as much as 10 cm. However modification of the wave refraction at the distal margin of the channel is expected to give rise to a zone of slightly increased values along the beach just north of the Ruakaka River, the increase predicted to be in the order of - up to maximum of around 5 cm in storm conditions. Over Mair Bank, the model results suggest a slight overall increase in wave heights (less than 1 cm on average).

The range of predicted changes to the significant wave height at the sites shown in Figure 4.11 are presented in Table 4.1.

The validation process of the wave model (detailed in MSL Report P0297-01) highlighted some disparities between modelled and measured data at sites W1 to W4, which suggest that the model cannot fully resolve the redistribution of wave energy along Ruakaka Beach. Thus, the effect of the channel deepening on the existing wave climate described previously may be slightly over-predicted at some locations and under-predicted at others. Based on the relative low effect of the channel deepening on the wave climate along Ruakaka Beach we consider that this poses no fundamental change the outcomes of the wave modelling stage along Ruakaka Beach and should not affect the recreational surfing activities over this area.

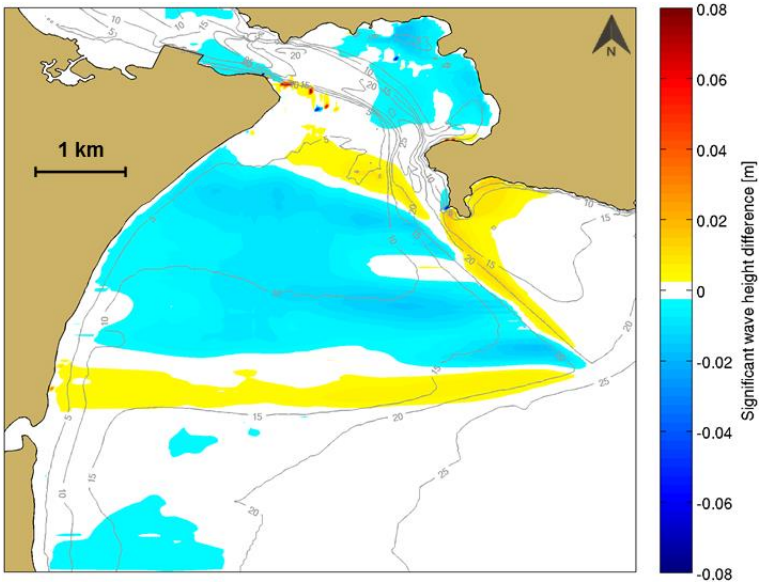

Figure 4.6 Average annual change in significant wave height due to the deepened channel. Positive amplitudes indicate areas with a predicted increase, negative areas a decrease.

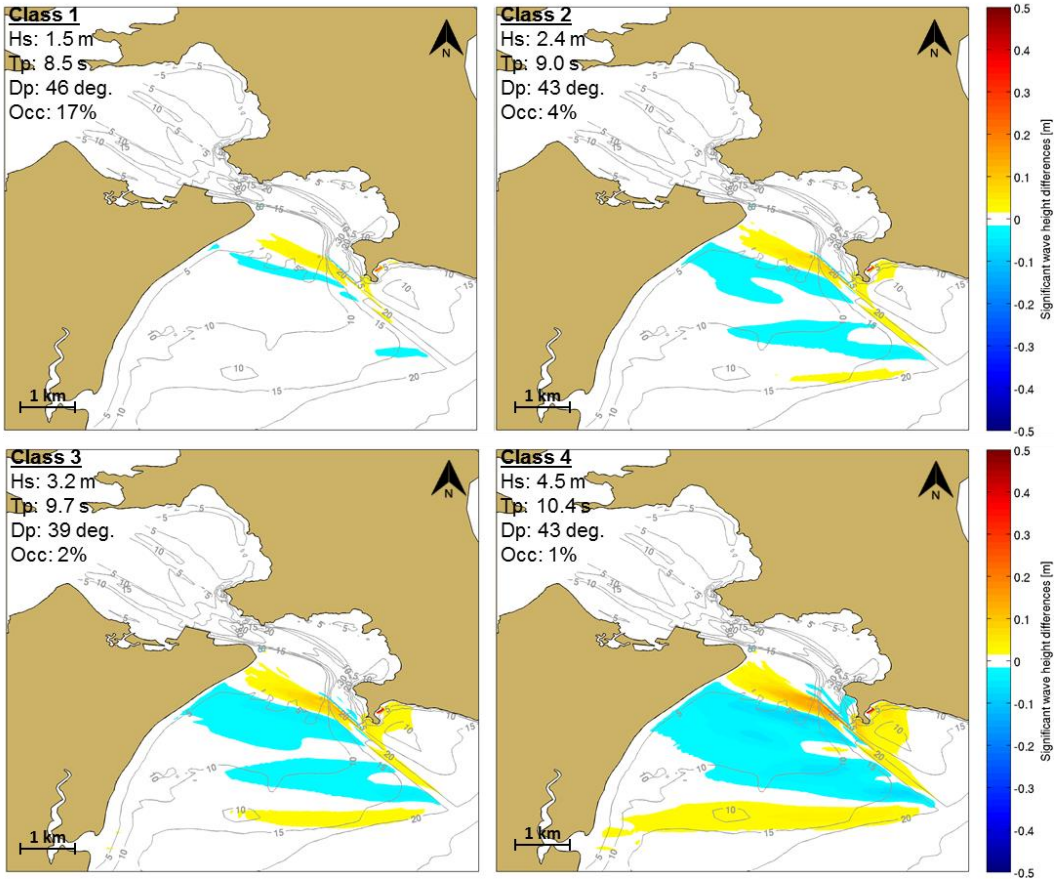

Figure 4.7 Significant wave height changes for wave classes 1 – 4 due to the deepened channel. Positive amplitudes indicate areas with a predicted increase, negative values a decrease.

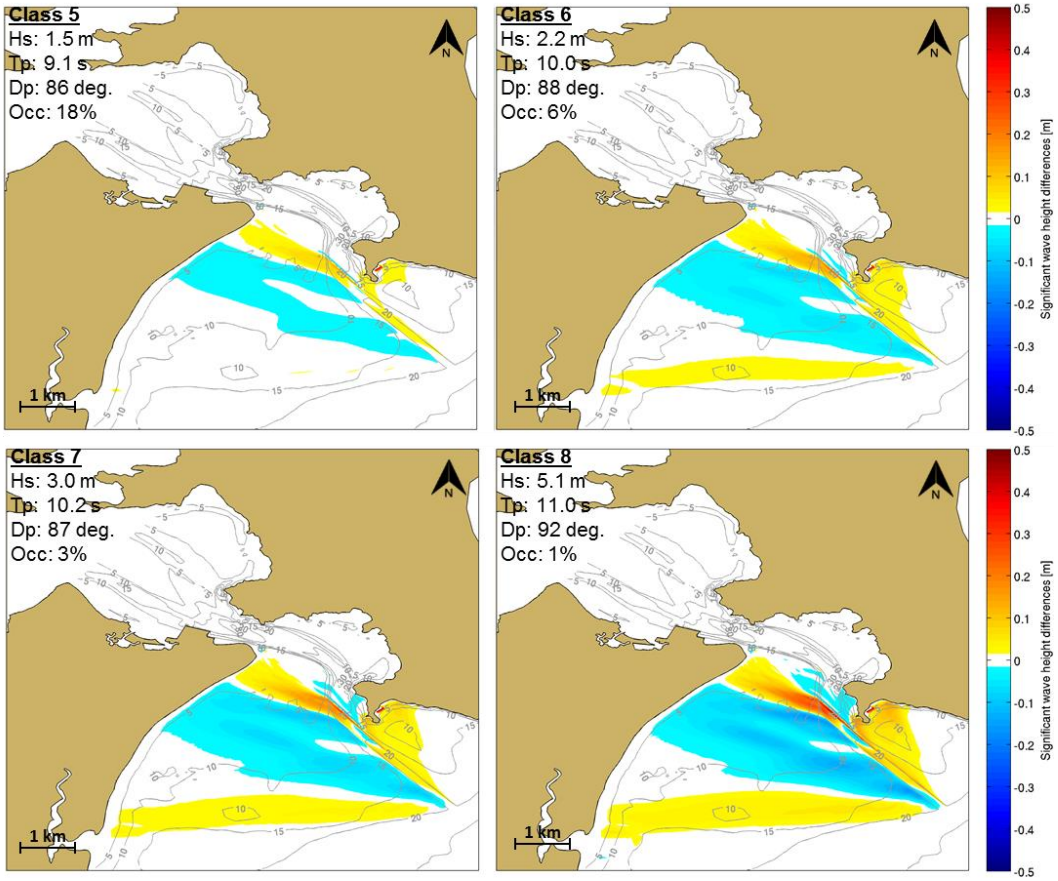

Figure 4.8 Significant wave height changes for wave classes 5 – 8 due to the deepened channel. Positive amplitudes indicate areas with a predicted increase, negative values a decrease.

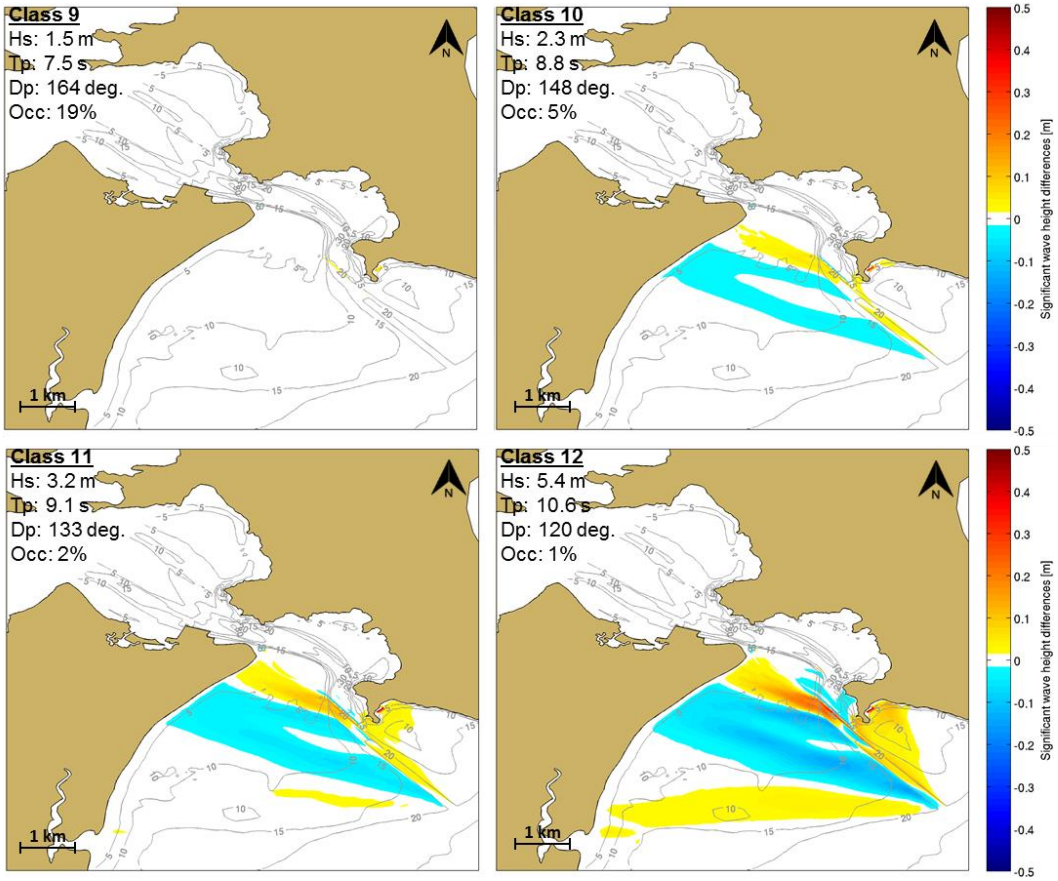

Figure 4.9 Significant wave height changes for wave classes 9 – 12 due to the deepened channel. Positive amplitudes indicate areas with a predicted increase, negative values a decrease.

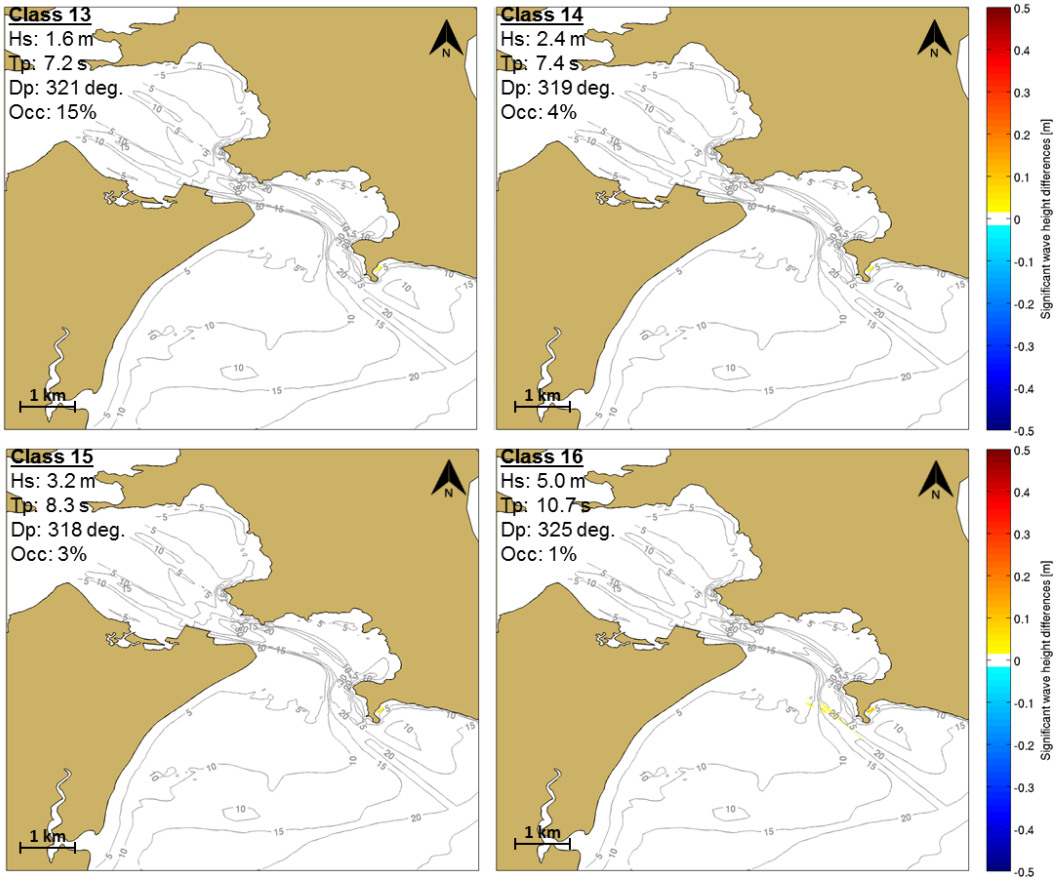

Figure 4.10 Significant wave height changes for wave classes 13 – 16 due to the deepened channel. Positive amplitudes indicate areas with a predicted increase, negative values a decrease.

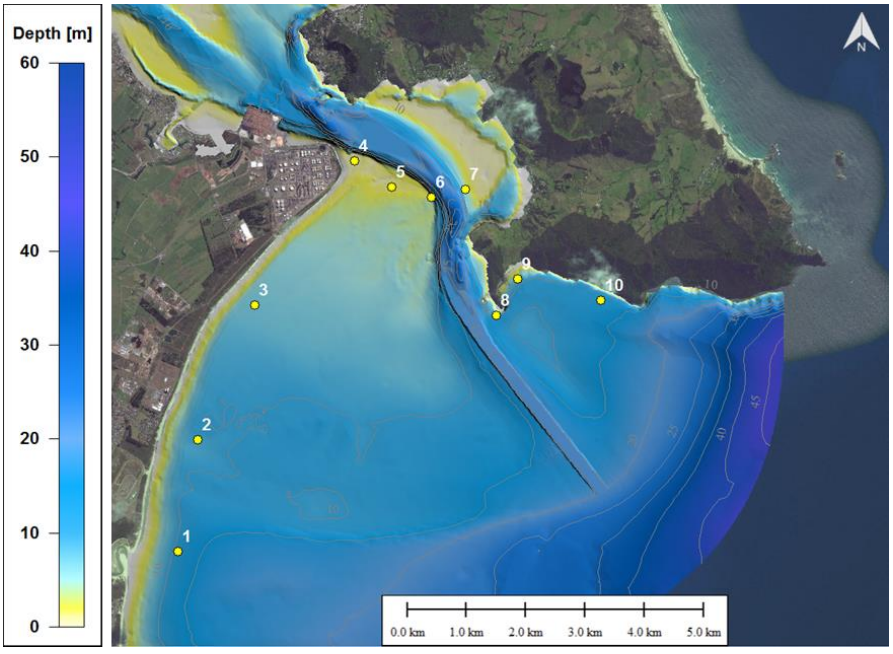

Figure 4.11 Locations used to calculate statistics of the difference in wave height due to channel deepening.

Table 4.1 Changes in mean and maximum significant wave height at positions 1 to 10 from 16 wave scenarios between the dredged channel and the existing configurations. Positive magnitude indicates a predicted increase of wave height due to the dredging.

Positions		Existing mean wave height* (m)	Changes in mean wave height* (cm)	Existing maximum wave height (m)	Changes in maximum wave height (cm)
1	Ruakaka Beach - river mouth	0.43	No changes	1.75	+2 cm
2	Ruakaka Beach	0.55	No changes	2.04	+1 cm
3	Ruakaka Beach – northern area	0.45	-1 cm	1.71	- 5 cm
4	Marsden - Mair Bank	0.11	+1 cm	0.29	+2 cm
5	Mair Bank - middle area	0.08	No changes	0.32	-1 cm
6	Mair Bank - eastern edge	0.03	No changes	0.11	-1 cm
7	Calliope Bank	0.02	No changes	0.06	No changes
8	Busby Head	0.42	+2 cm	1.92	+ 10 cm
9	Smugglers Bay – western area	0.26	+3 cm	1.23	+ 15 cm
10	Smugglers Bay – eastern area	0.27	No changes	1.21	No changes

* The mean wave height calculation included the percentage of occurrence of each wave event.

4.3. Summary of predicted effects of channel deepening on the wave climate

The methodology used to characterise the existing wave climate at Whangarei and to examine the effect of channel deepening is detailed in MSL Report P0297-01, including the validation of the model at 5 locations. The anticipated effects of the channel deepening on the wave climate are as follows:

- The effect on the mean significant wave height fields is likely to be very subtle and generally not exceed 2 cm. During storm events where offshore waves can reach more than 5 m, changes in the significant wave height fields generally should not exceed 10 cm (less than 10% changes), except over a limited area to the west of Busby Head where the significant wave height may increase by 20 cm (~20%) during extreme wave events.

- The offshore extent of the deepened channel modifies the refraction pattern of waves at the delta entrance. Enhanced refraction occurring along the eastern margin of the deepened channel is predicted to increase wave height at Busby Head and offshore of Smugglers Bay up to a maximum of 10 and 15 cm during storm conditions, respectively.

- Conversely, a minor increase of wave height (1 – 2 cm on average) is expected along sections of Ruakaka Beach. Note that modifications of the wave refraction at the distal margin of the channel may generate a zone to the north of the river mouth characterised by a slight increase of the wave height (up to a 5 cm maximum).

- Changes in wave height over Mair Bank are not expected to exceed 2 cm.

5. REGIONAL SCALE HYDRODYNAMICS

The characterisation of the circulation in the continental shelf waters adjacent to Whangarei Harbour is important when considering the local scale hydrodynamic and sediment transport processes, as they prescribe the boundary conditions for the nearshore and harbour entrance numerical modelling. The presence of strong along-shelf winds and offshore oceanic boundary currents year round can all play a role in forcing the circulation near the coast. A careful modelling strategy is required to reproduce the different spatial and temporal scales and circulation phenomena at the shelf and deep ocean environments and adequately feed the local scale models. This section describes the results of the modelling studies that were undertaken to characterise regional hydrodynamics. The modelling methodology is detailed in MSL Report P0297-01.

5.1. Characterising the regional hydrodynamics

The results from the regional scale modelling show that the mean flow patterns in the northern Hauraki Gulf area are oriented in the along-shore direction, due to open ocean currents and the predominant wind forcing (Figure 5.1). Offshore of Whangarei Harbour, channelling effects between the coast and the offshore islands intensify and steer the flow to a quasi-meridional orientation (Figure 5.1 and Figure 5.3).

The long term (10-year) net flow is oriented from north to south, and most of the strength and variability of the currents is observed in the along-shore direction (Figure 5.2). The high order hydrodynamics at the inner shelf and in the vicinity of Whangarei Harbour are mainly controlled by the tides and the interaction between the offshore flows and the local bathymetry (Figure 5.3). The residual circulation at Bream Bay is complex but normally responds to the shelf flow to the east of the bay (Figure 5.3).

The monthly analysis of hindcast current data at position WRB highlights a relative weak seasonal variability (Figure 5.4), with late winter and early spring showing the stronger current flows. Current fields exhibit much more strength and variability in the along-shore direction and the predominant flow direction is from north to south year round.

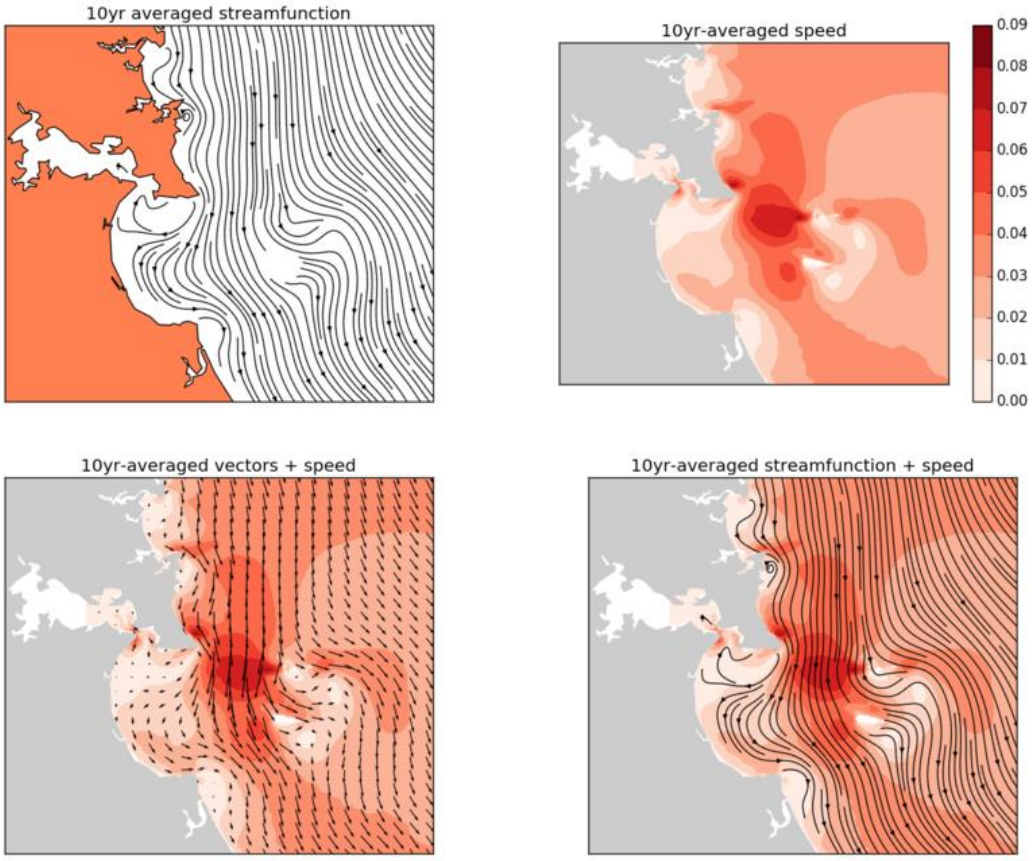

Figure 5.1 Climatological flow patterns offshore Whangarei Harbour based on mean current speeds computed off a 10 year (2000-2010) ROMS hindcast. Current speeds in red shades ($m.s^{-1}$).

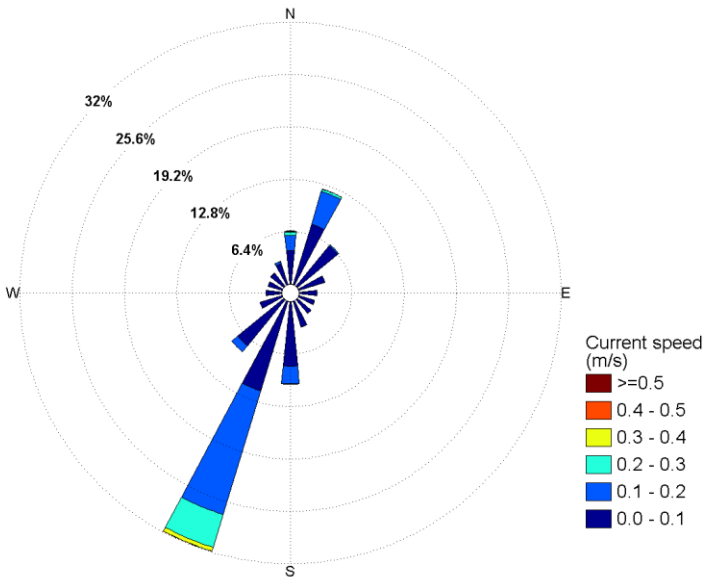

Figure 5.2 Long term current rose at the proposed offshore disposal ground. Current directions are represented as “going to”.

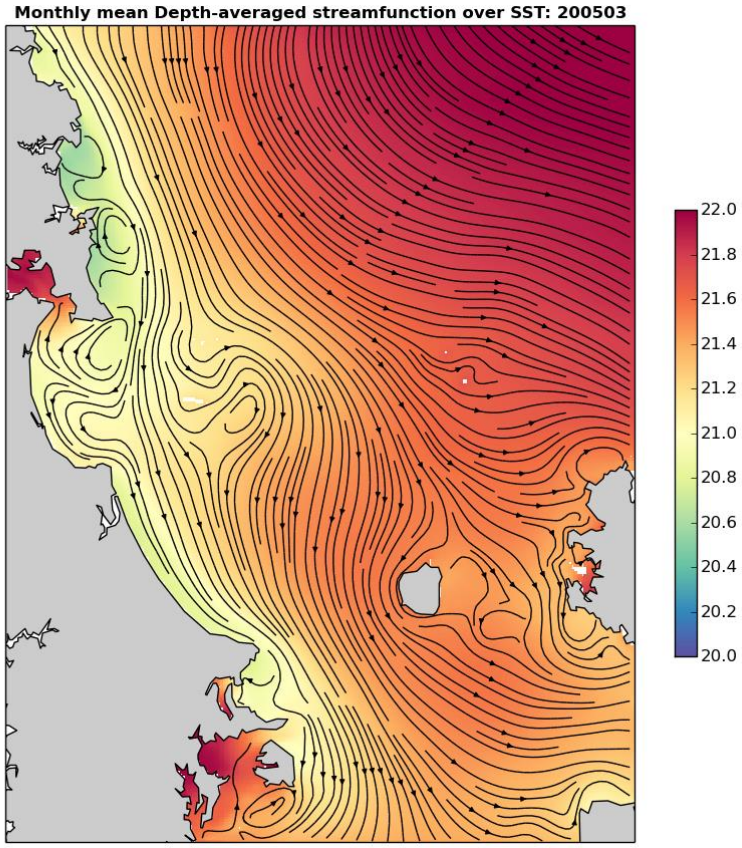

Figure 5.3 Monthly averaged flow for March 2005 as an example of the regional circulation. Note the interaction of the southward flow and the coastline geometry between Bream Bay and the offshore islands, generating coastal eddies and bifurcations.

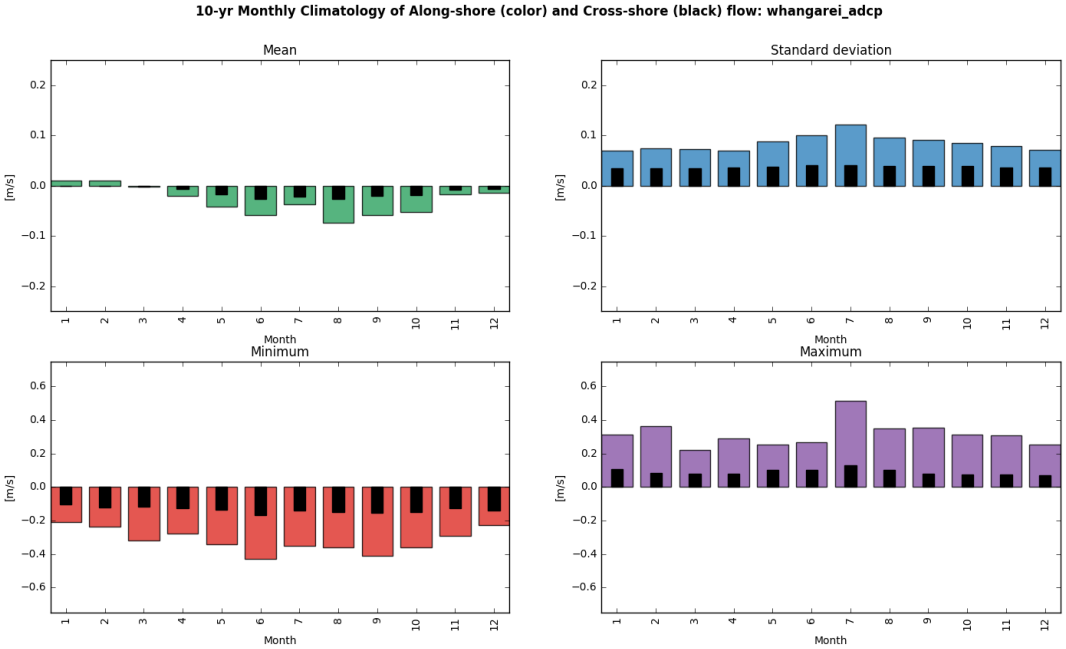

Figure 5.4 Monthly climatology of alongshore current at the proposed offshore disposal ground (site WRB).

6. NEARSHORE TIDAL HYDRODYNAMICS

The SELFE model was used to simulate the 2D tidal flows through the entire Whangarei Harbour to accurately replicate the tidal hydrodynamic in a very complex environment characterised by the presence of marginal channels, sand banks and small islands. The model was validated against water levels measured at four locations and current profiles measured over regions of the outer channel where dredging is proposed (see validation results in MSL Report P0297-01). The model was shown to replicate the governing hydrodynamic of the harbour, including the phase and amplitude of the tidal elevations and the spatially complex flows along the main shipping channel.

This section describes the existing tidal hydrodynamics of the Whangarei Harbour and examines the predicted effects of the channel deepening on the ebb and flood tidal flows. Changes in the bed shear stress fields are also presented and discussed.

6.1. Characterising the tidal dynamics

The modelled ebb and flood tidal flow patterns are shown in Figure 6.1 to Figure 6.4 for the spring and neap tidal regimes. Ebb flows gradually accelerate through the inlet with velocities ranging between 0.8 $m.s^{-1}$ near One Tree Point and increasing to 1.3 $m.s^{-1}$ through the narrow constriction of the channel during spring tides. During neap tide, ebb flow velocities range between 0.3 and 0.8 ms^{-1}. The south-southeast directed ebb-jet drives a velocity field on the ebb-tidal delta that extends up to 3.5 km into Bream Bay. On the western flank of the delta, the ebb-jet contributes to a clockwise tidal circulation along Ruakaka Beach and Mair Bank, with current velocities up to 0.35 $m.s^{-1}$ during the spring tide. The northern subtidal area of Mair Bank adjacent to the channel presents the highest exposure to strong currents (up to 1.4 $m.s^{-1}$). Interactions of the tidal flow and Mair Bank bathymetry result in accelerated and diverted flow velocities toward the inlet entrance. Between Marsden Point and Mair Bank, this acceleration occurs particularly over the southern edge of the channel where the depth exhibits steeper bed slopes. On the opposite flank, ebb flows do not exceed 0.8 $m.s^{-1}$ along Calliope Bank.

The hydrodynamic model results show that an approximate 0.5 to 1 hour phase lag in transition from flood to ebb flow between inlet and the open sea occurs, and it takes approximately 1 hour from the beginning of the ebb-tide to a complete current reversal.

At peak flood, the strongest velocities are located near Motukaroro Island and Marsden Point where the constriction of the channel accelerates the flows. Mair Bank is dominated by large uni-directional flood flow velocities ranging from1.2 $m.s^{-1}$ over the subtidal areas to 1.6 $m.s^{-1}$ over the intertidal area, which are directed from southwest to northeast. A weak counter current develops along Mair Bank to the southern flank of the channel. Within the harbour, segregation of flows due to marginal channels and bottom friction tends to reduce the flow velocities for both flood and neap tides leading to current speeds which do not exceed 0.9 $m.s^{-1}$.

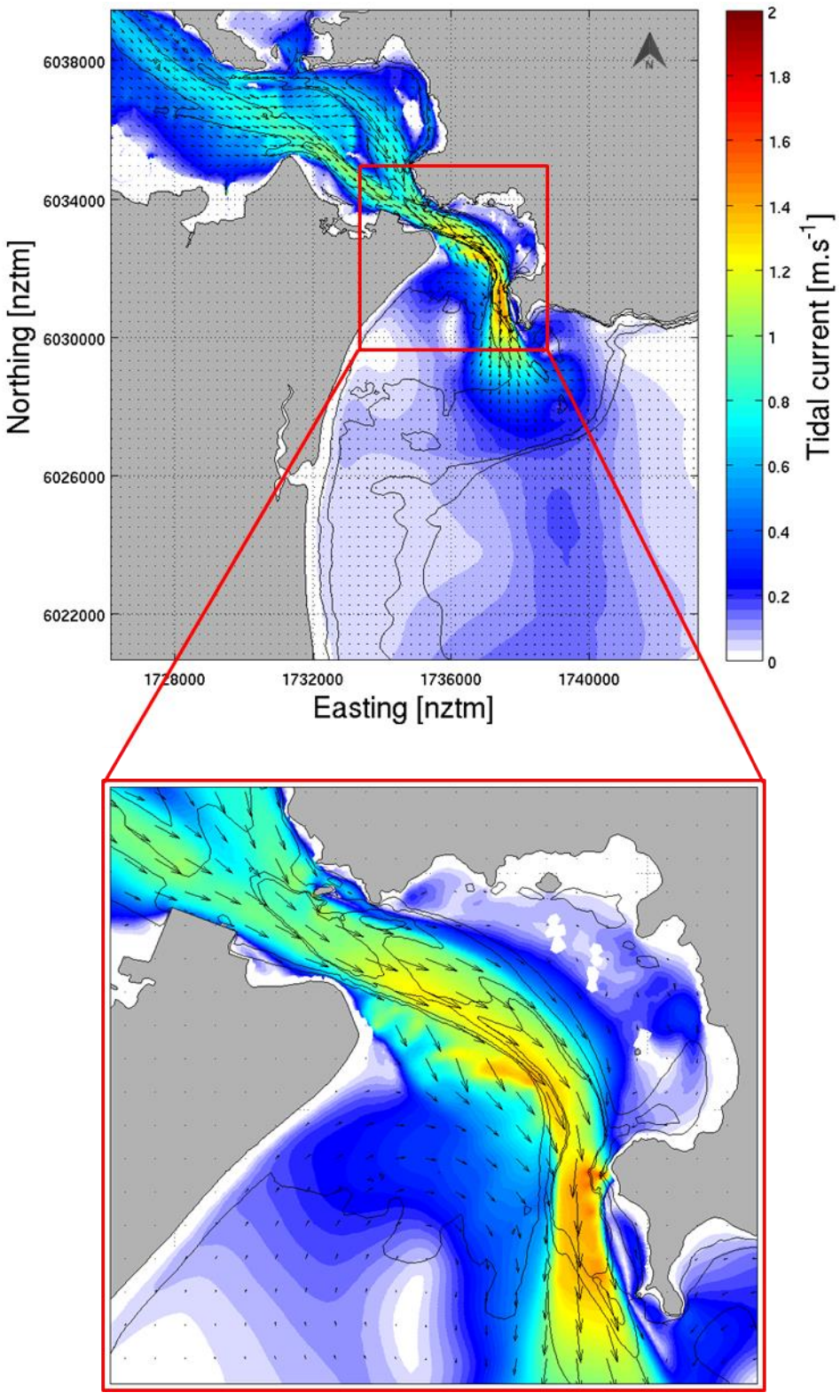

Figure 6.1 Modelled peak ebb flows during spring tide at Whangarei Harbour entrance.

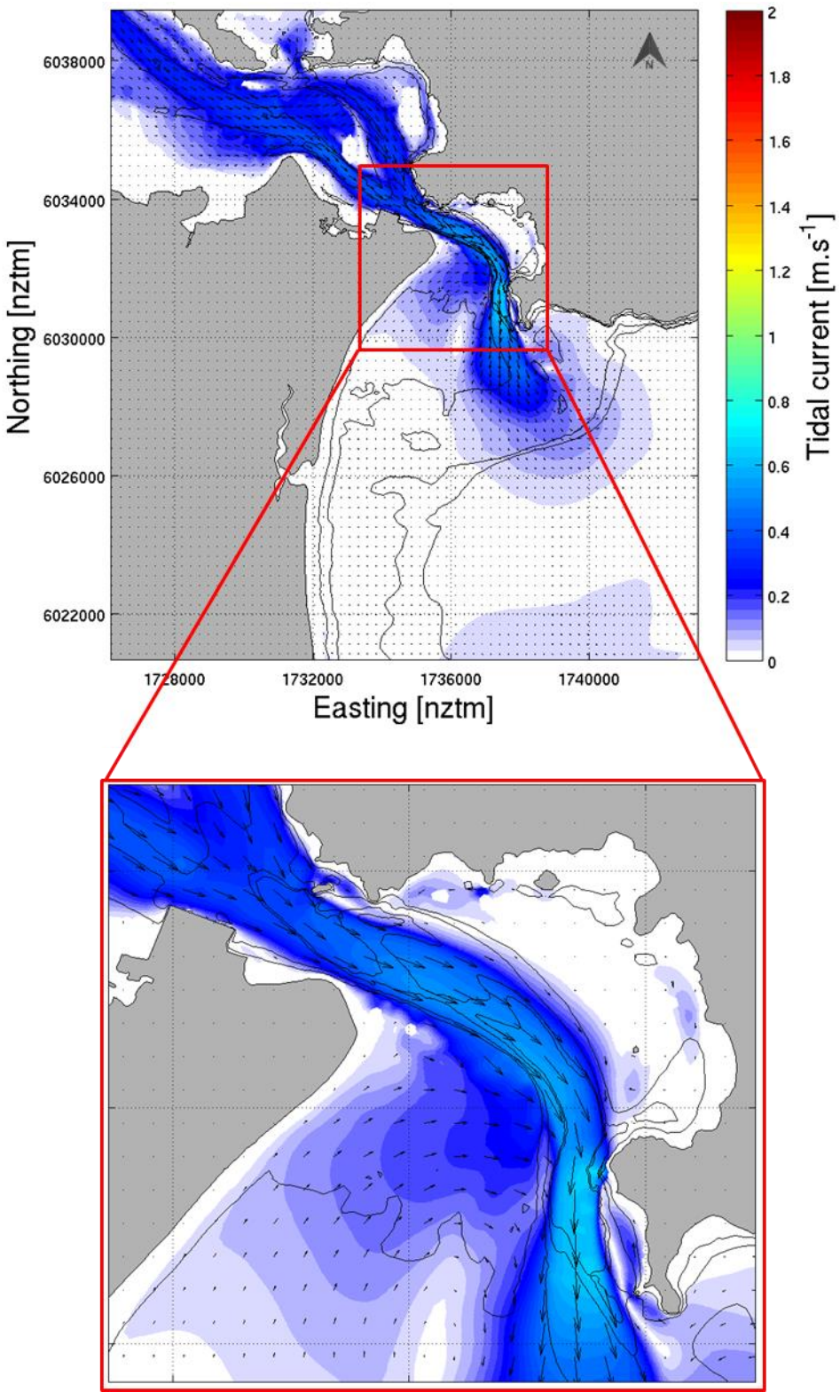

Figure 6.2 Modelled peak ebb flows during neap tide at Whangarei Harbour entrance.

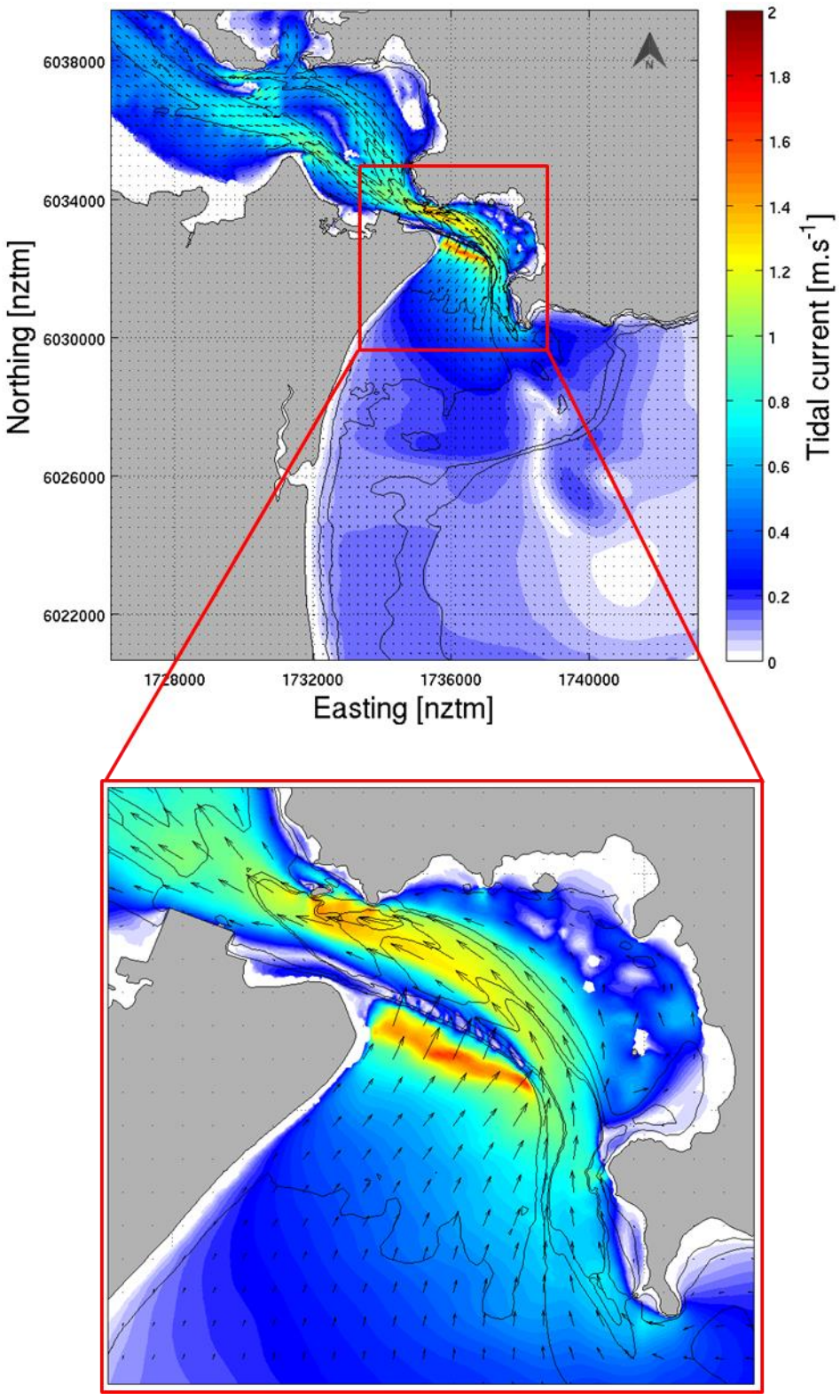

Figure 6.3 Modelled peak flood flows during spring tide at Whangarei Harbour entrance.

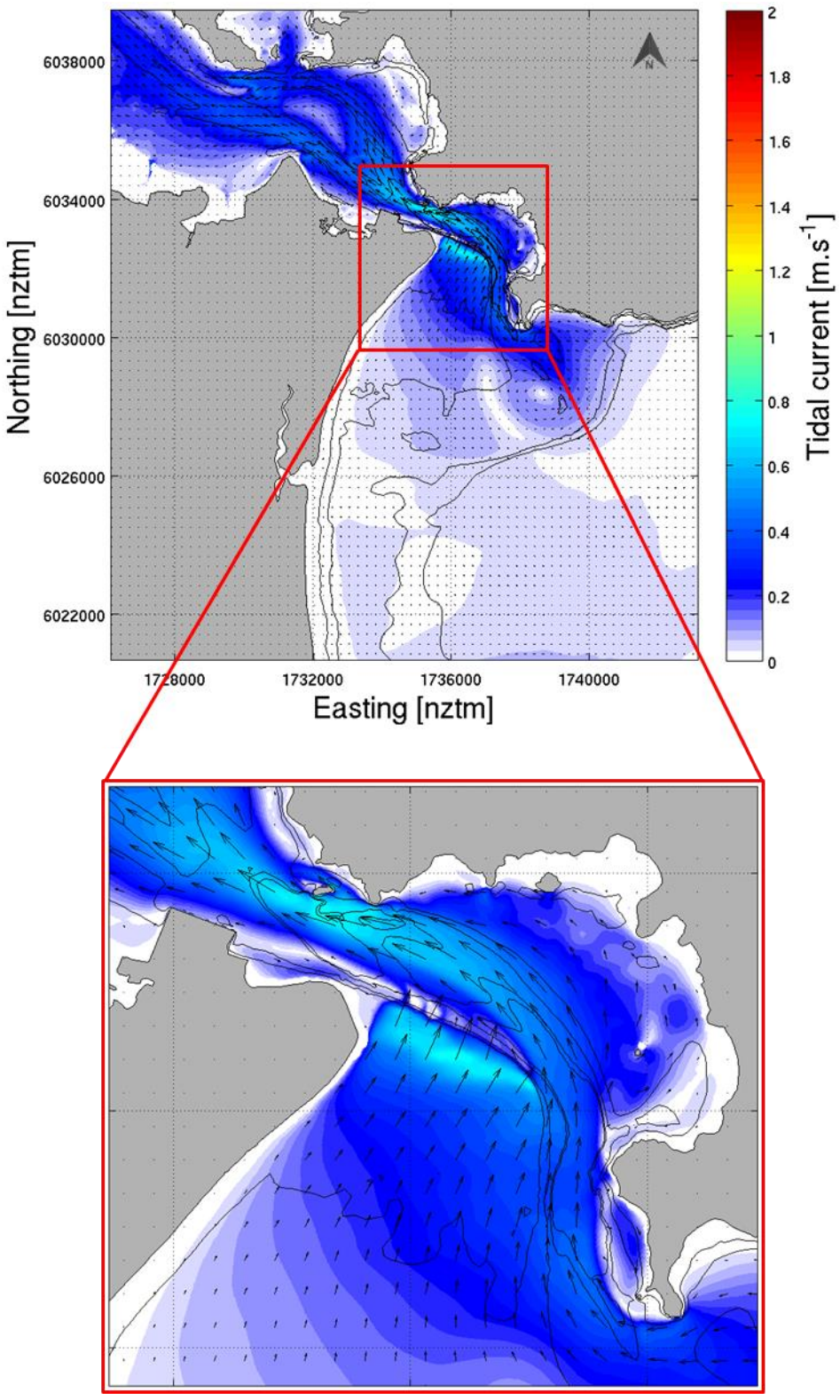

Figure 6.4 Modelled peak flood flows during neap tide at Whangarei Harbour entrance.

6.2. Effects of channel deepening on tidal hydrodynamics

The hydrodynamic model was re-run with bathymetry including the deepened channel and all other configurations remaining the same. Comparisons of depth-averaged velocities during the spring tide peak ebb flows are shown in Figure 6.5. These results indicate that the deepening causes a reduction in peak speed of up to 0.10 $m.s^{-1}$ at some locations within the main channel, and a maximum acceleration of the flows of 0.10 $m.s^{-1}$ in some areas adjacent to the channel. Note that within the areas of highest flow, this represents a very small change, but there are other areas where the localised changes are proportionally much greater, and the effect of those changes requires careful interpretation. For example, near Marsden Point the dredging of the southern flank of the channel is predicted to locally decrease the ebb current flows from 0.16 $m.s^{-1}$ to 0.06 $m.s^{-1}$. In response to this new dynamic, the current speed nearby in the marginal channel between Marsden Bank and Mair Bank is expected to increase by 0.10 $m.s^{-1}$ (i.e. some 10-15%). Removing the lobe in the central channel to the north of Mair Bank results in a decrease of the maximum ebb current speed from 0.5 to 0.35 $m.s^{-1}$ (a decrease of 0.15 $m.s^{-1}$)) along the northern flank of the inlet channel between Motukaroro Island and High Island (Figure 1.2). Conversely, there is a predicted strengthening of the ebb tidal flows from 0.05 $m.s^{-1}$ to 0.09 $m.s^{-1}$ over Little Munroe Bay and McGregor's Bay located to the west of High Island. These two areas are usually characterised by weak tidal dynamics associated with peak ebb and flood velocities ranging from 0.03 – 0.05 $m.s^{-1}$.

The changes in the flood tidal flow fields illustrated in Figure 6.6 clearly show the effect of the complex morphology on the hydrodynamics. For example, the deeper channel and subtle changes to the water level generates spatial variations in the flood tidal flows over Mair Bank. This causes a succession of flow accelerations and decelerations up to 0.20 $m.s^{-1}$ (approx. 10 - 20% change). Adjacent to the RNZ jetties, lower flows (by 0.10 $m.s^{-1}$) occur near the shore, while nearby in deeper water the flows increase by up to 0.08 $m.s^{-1}$.These changes are small compared to the strong tidal flows through the channel

The subtle realignment of the channel by removal of the 'toe' of the ebb tide shoal near Mair Bank has a localised influence on the flows for both the ebb and flood tidal stages. The maximum absolute changes along Section B (Figure 6.7, Figure 6.8 and Figure 6.9) reach 0.05 $m.s^{-1}$ on the ebb tidal stage. This is a relatively small change compared to the existing peak ebb and flood current speeds ranging between 1.2 and 1.4 $m.s^{-1}$ (less than 5%). In contrast, the deepening of the main channel body from Busby Head to the distal margin of the delta is predicted to affect a relatively large area, with some indication of a mild reorientation of the ebb tidal jet. This is predicted to lead to regions with an increase and decrease of up to 0.015 $m.s^{-1}$ of the ebb-tidal flow velocities (Figure 6.8, upper plots), which is of the order of a 20% change. The flood flows on the delta margin are slightly reoriented by the dredged channel and exhibit areas of flow acceleration and deceleration (Figure 6.9, upper plots).

Another useful comparison to make is the changes to the bed shear stress imparted by the tidal flows. Bed shear stress is a direct measure of the energy that can be transferred from the flowing water to the seabed, and is a useful analogy for potential sediment transport. Comparisons of bed shear stress at peak ebb and flood stages are presented in Figure 6.10, and these results provide an alternative examination of the potential effects, by accounting for the absolute water depth and the direct effects on the seabed. The channel deepening is not predicted to fundamentally modify the bed shear stress fields over the harbour entrance.

Nevertheless, it may induce local adjustments with a relative low degree of significance for the overall system. The deepening is predicted to reduce the peak bed shear stress in the main channel by up to 20% in the area adjacent to Marsden Point and cause localised increases and decreases up to 30% at the delta entrance during the flood tidal stage. However, these results need to be considered in the context of the absolute magnitudes and how they relate to sediment transport. Accordingly, the percentage of time the bed shear stress exceeds the critical threshold for entrainment of 200 µm sand is provided in Figure 6.11 and Figure 6.12, while the difference of these percentages of exceedance for both the ebb and the flood stages are provided in Figure 6.13.

The channel deepening is expected to decrease the ebb and flood tide values by up to 10% within the channel near Busby Head. Conversely, the percentage of time the bed shear stress exceeds the critical threshold for entrainment of 200 µm sand is predicted to increase by approximately 10% over the eastern margin of the channel close to Busby Head at flood tides (Figure 6.13). This area currently features a slight bathymetric indentation, and it may be an area of active (and asymmetric) sediment transport. Conversely, the percentage of time the bed shear stress exceeds the critical threshold for entrainment of 200 µm sand is predicted to decrease by 5 – 10% over the western margin of the channel. This typically means that the sand drift potential induced by tidal currents over the western margin is expected to be lower than over the eastern margin.

However, this is also a function of the actual sediment properties of the seabed in this area which will be evaluated in the following section.

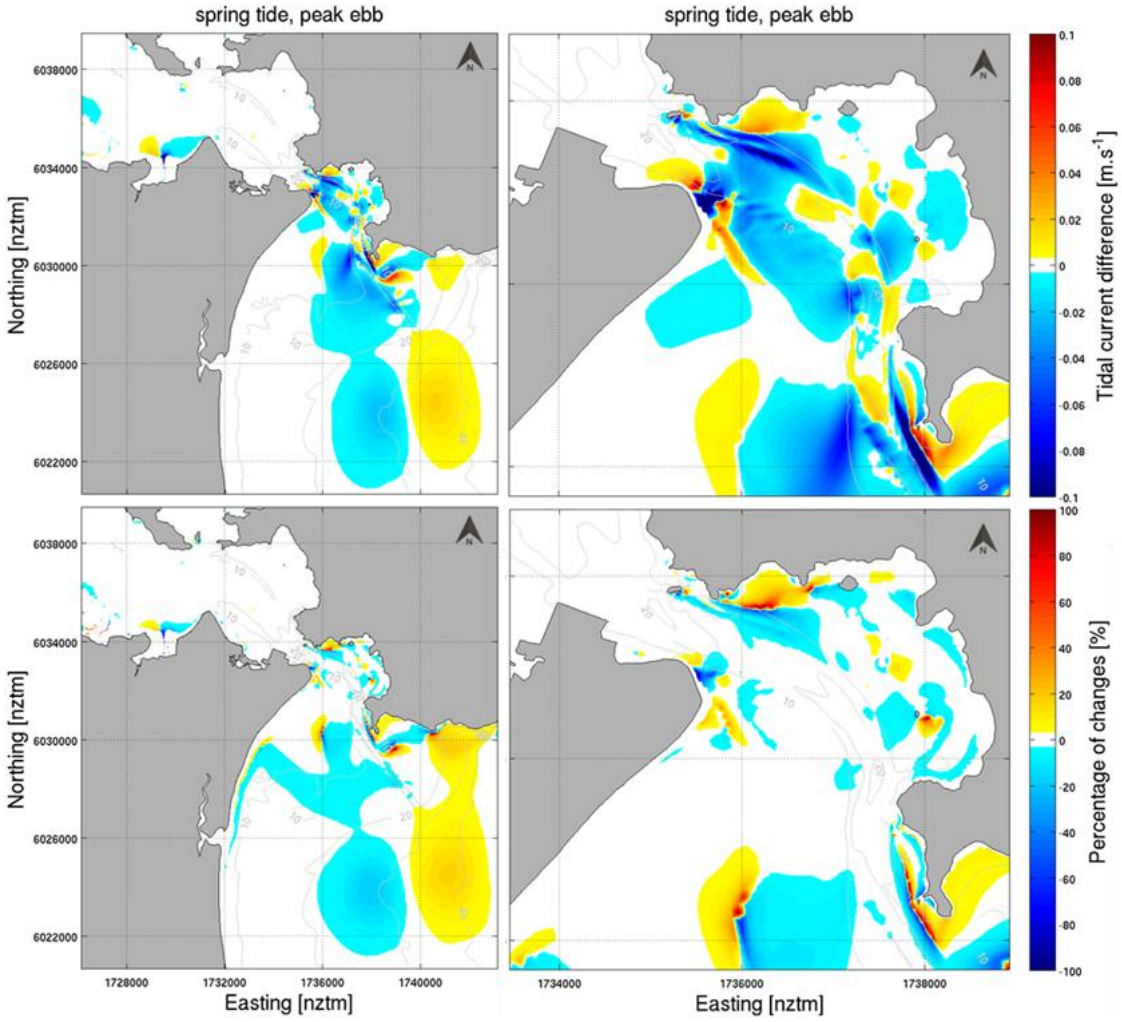

Figure 6.5 Absolute (top) and relative (bottom) difference in tidal flows post-deepening during the peak spring ebb flows. Plots on the right show a zoomed in view of the entrance region. Positive values indicate a predicted increase in flow (red scale), while the negative values indicate a decrease (blue scale).

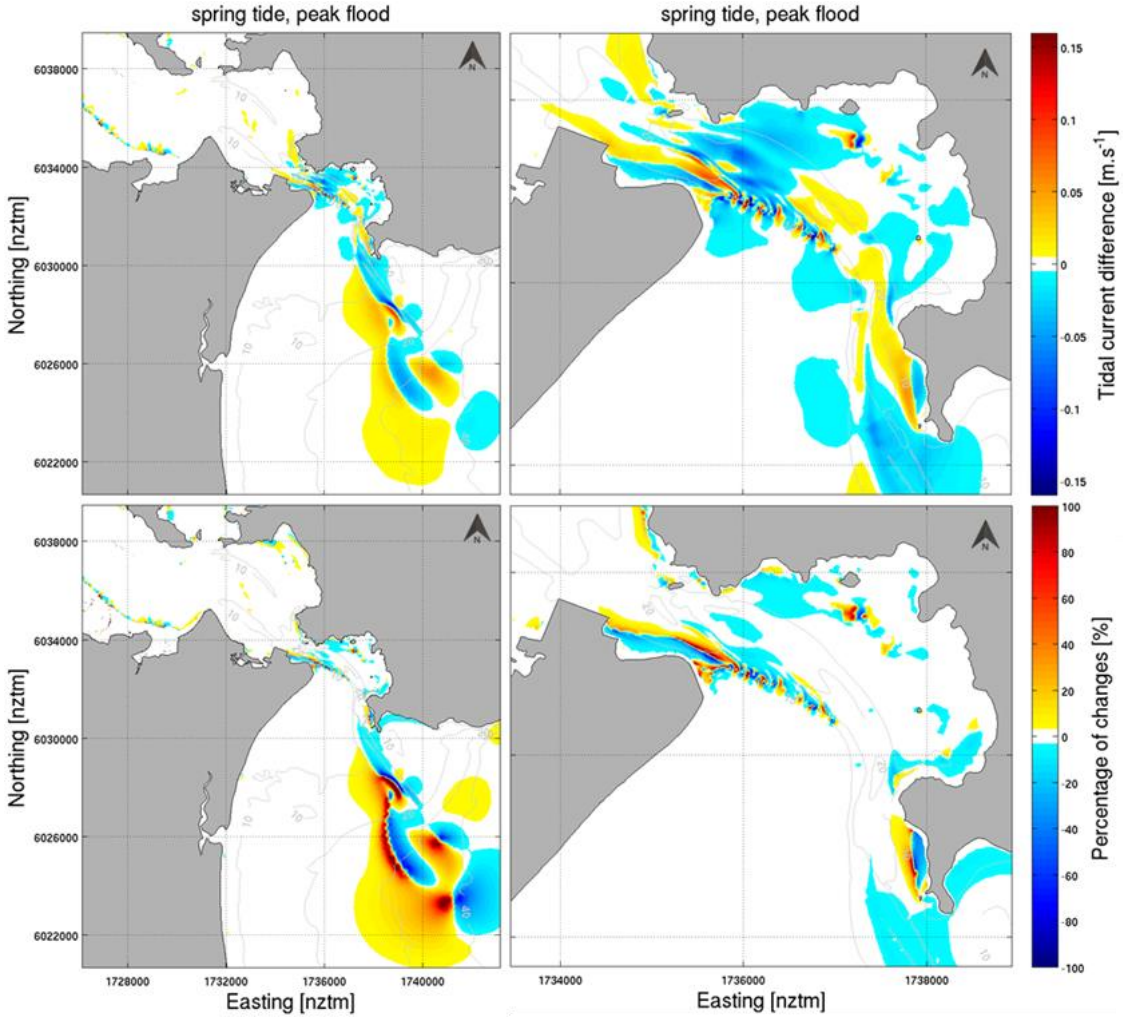

Figure 6.6 Absolute (top) and relative (bottom) difference in tidal flows post-deepening during the peak spring flood flows. Plots on the right show a zoomed in view of the entrance region. Positive values indicate a predicted increase in flow (red scale), while the negative values indicate a decrease (blue scale).

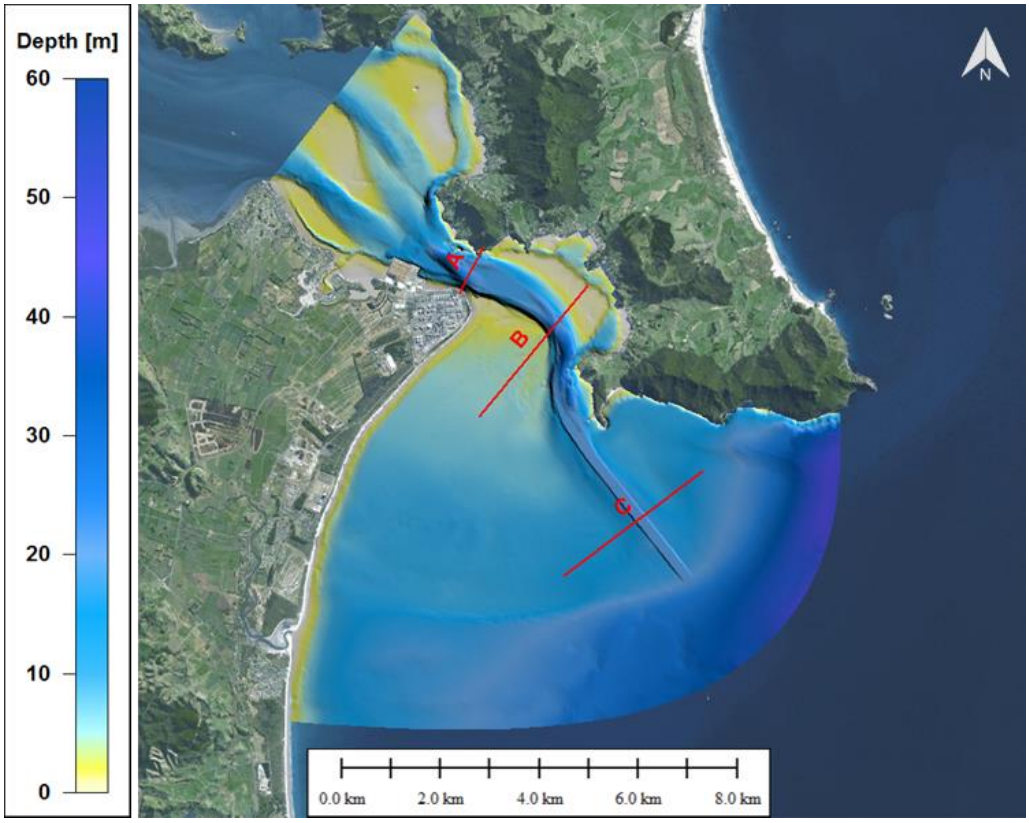

Figure 6.7 Location of the cross-sections used to evaluate the tidal flow differences following channel deepening.

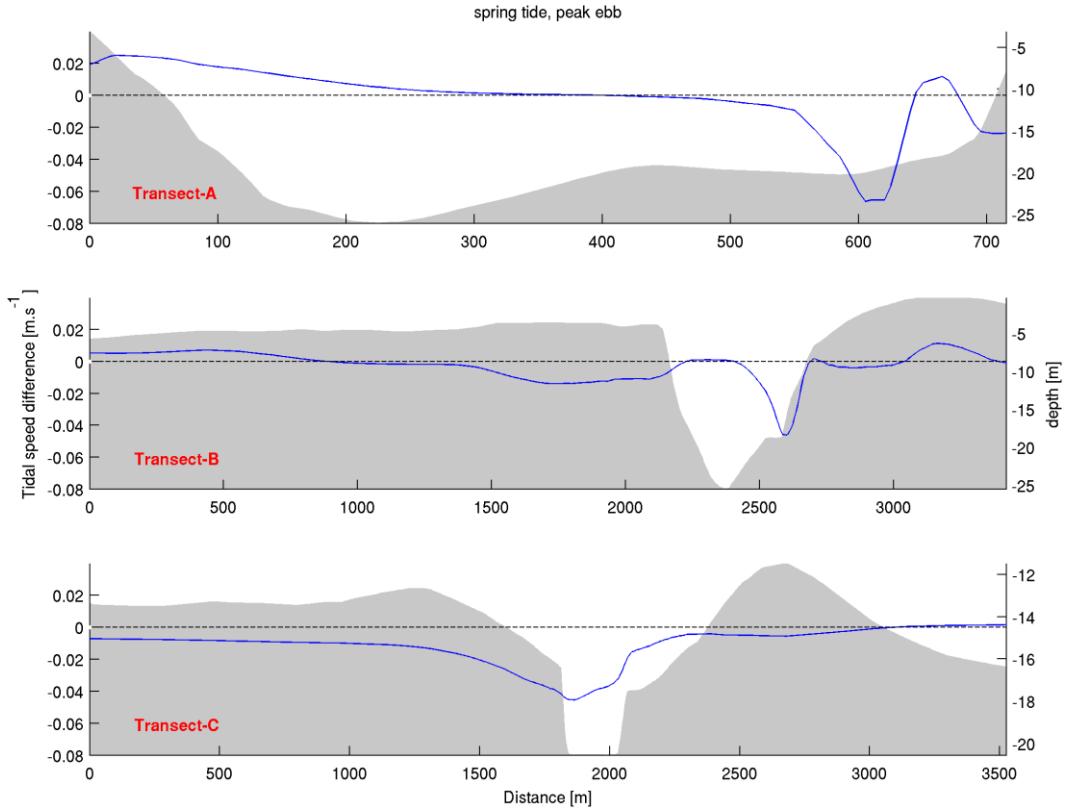

Figure 6.8 Ebb tidal flow differences during spring tide along sections A, B and C shown in Figure 6.7. The dotted line indicates the 0-m.s^{-1} velocity threshold.

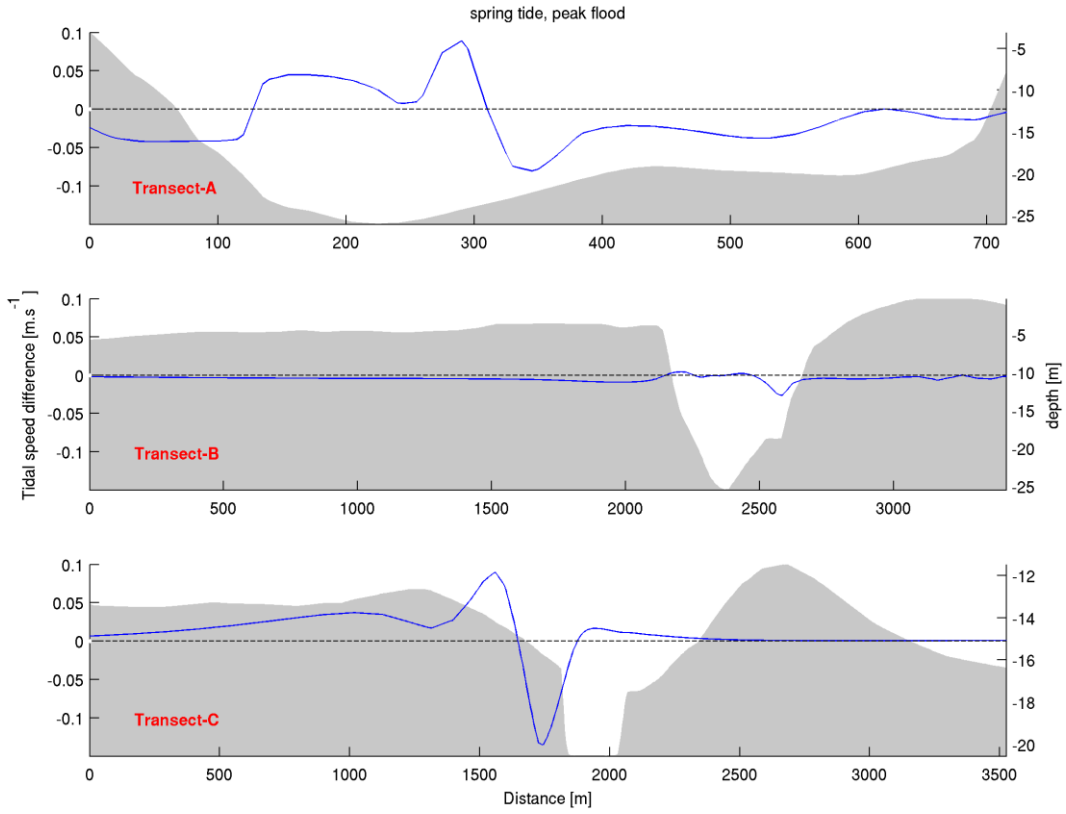

Figure 6.9 Flood tidal flow differences during spring tide along transects A, B and C shown in Figure 6.7. The dotted line indicates the 0-m.s^{-1} velocity threshold.

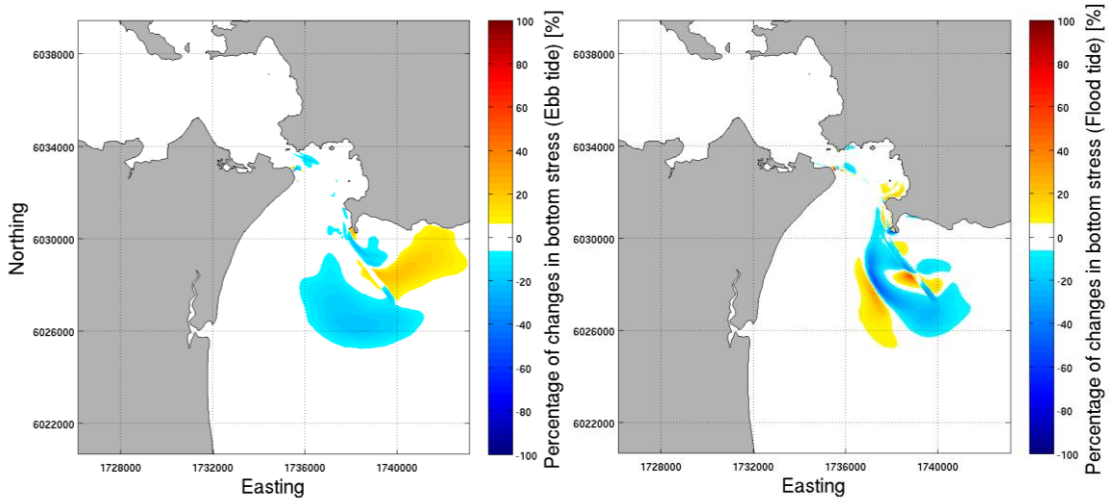

Figure 6.10 Percentage of change in the bed shear stress fields during peak spring ebb (left) and flood stages (right) between the existing and the deepened channel bathymetry.

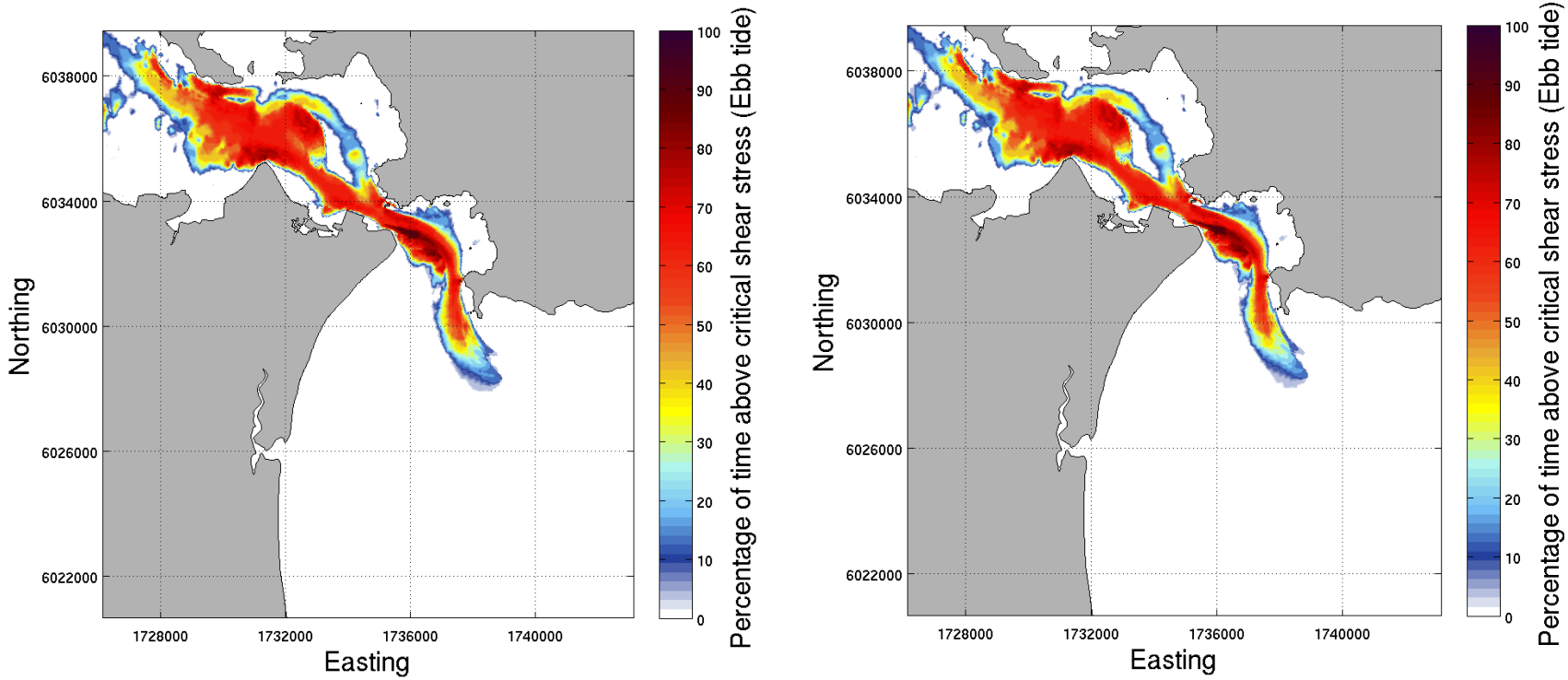

Figure 6.11 Percentage of time the bed shear stress exceeds the critical shear stress threshold for 200 µm sand at ebb tide. Calculated from a 28-day simulation of the existing harbour (left) and the deepened channel (right).

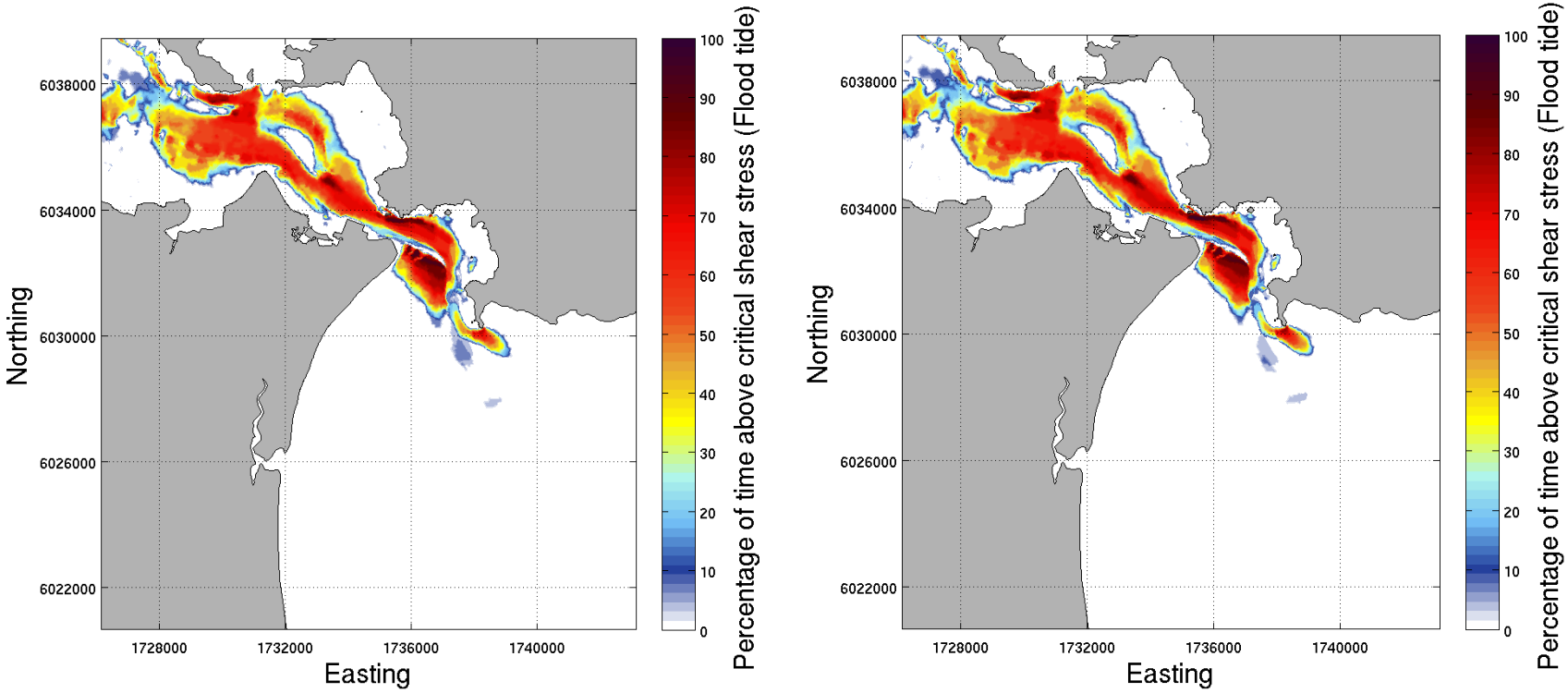

Figure 6.12 Percentage of time the bed shear stress exceeds the critical shear stress threshold for 200 µm sand at flood tide. Calculated from a 28-day simulation of the existing harbour (left) and the deepened channel (right).

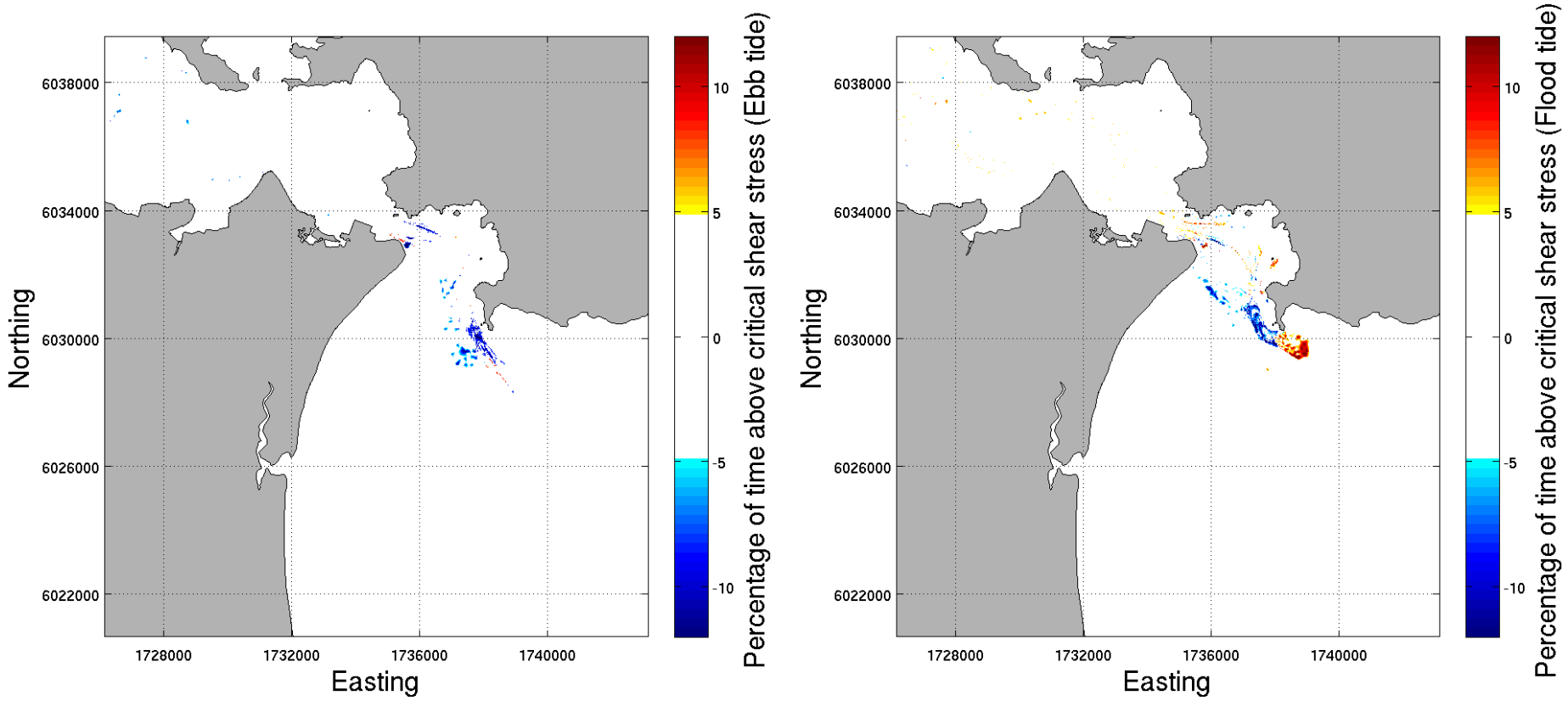

Figure 6.13 Difference of percentage of time the bed shear stress exceeds the critical shear stress threshold for 200 µm sand at ebb (left) and flood (right) tidal stages, calculated from a 28-day simulation of the existing harbour and the deepened channel. Noise in the difference fields was cleaned using an arbitrary minimum threshold of 5% to highlight the areas of significant changes.

6.3. Summary of effects on the nearshore tidal hydrodynamics

The predicted effects of the channel deepening on the hydrodynamics are:

- Reduction of the peak tidal speed by up to 0.10 $m.s^{-1}$ in the dredged channel, and acceleration up to 0.10 $m.s^{-1}$ in some adjacent areas.

- Increase of the tidal current speed by 0.10 $m.s^{-1}$ (i.e. about 10-15%) inside the marginal channel between Marsden Bank and Mair Bank.

- Removal of the lobe in the central channel between Marsden Bank and Mair Bank results in a localised decrease of tidal flow velocities of up to 0.15 $m.s^{-1}$ (from 0.5 to 0.35 $m.s^{-1}$), while the current speed is expected to increase from 0.05 to 0.09 $m.s^{-1}$ (maximum increase of 0.04 $m.s^{-1}$) along the northern flank of the inlet channel between Motukaroro Island and High Island, an area characterised by a very low hydrodynamic regime.

- The subtle realignment of the channel by removal of the 'toe' on some of the bends induce a slight acceleration of the tidal flows over the dredged areas and a deceleration over the adjacent areas for both the ebb and the flood tidal stages. These changes do not exceed 5% of the existing tidal regime.

- The deepening of the channel from Busby Head to the distal margin of the delta is predicted to lead to regions with increases and decreases of the mean ebb-tidal flow velocities of up to 0.02 $m.s^{-1}$. Both ebb and flood flows on the delta margin are slightly reoriented by the dredged channel and exhibit areas of flow acceleration and deceleration.

- Deepening the channel is not expected to fundamentally modify the bed shear stress fields over the harbour entrance but may locally induce some adjustments. A reduction of the peak bed shear stress of up to 20% at ebb and flood stages in the area adjacent to Marsden Point is expected. The dredging may also cause localised peak bed shear increases and decreases up to 30% at the delta entrance during the flood tidal stage. Such changes in the bed shear stress fields are susceptible to generate some subtle adjustments of the local morphodynamics without causing an overall transformation of the sediment transport dynamics between the harbour and the open-ocean region.

- The percentage of time the bed shear stress exceeds the critical level for entrainment of 200 µm sand is expected to decrease up to 10% in the channel due to increasing water. Conversely, this time is predicted to increase by approximately 12% along the eastern margin of the channel to the southeast of Busby Head. Along the western margin of the channel, this time is susceptible to decrease by 5 – 10%. More broadly, changes in the tidal dynamics due to the channel deepening may modify locally the potential of sand mobility inside and on either side of the channel. However, these anticipated adjustments should remain of relative low importance compared to the effect of the waves on the morphodynamics outside the harbour entrance.

- Based on the assumption of a uniform seabed composition of 200 micron sand, the asymmetry for entrainment between ebb and flood tide just east

of Busby Head may change, with the flood stage showing a 10% increase in time above the critical shear stress for 200 µm sand. Such changes may slightly increase the sand mobility induced by tidal currents near Busby Head. However, these adjustments in the sediment transport are predicted to be of relative low importance compared to the effect of waves.

- While the hydrodynamics of the internal harbour are not expected to be affected by the deepening, a very slight adjustment of the timing of the tidal phase may occur. This will likely require a period of measurement at the defined tidal stations to derive the new tidal constituents for Northport and Whangarei Port.

7. SEDIMENT TRANSPORT

A process-based numerical model was implemented to simulate the morphodynamics that are driven by the main hydrodynamic tidal and wave forces at the harbour entrance. The key processes controlling the morphodynamics of the coastal region are identified and effects of the channel deepening on sediment dynamics examined in this section. This involved different approaches to determine changes in the potential sediment fluxes, sedimentology and governing morphology of the system.

7.1. Conceptual modelling – tide only transport scenarios

Model results related to the peak flood and ebb flows for the existing environment are provided in Figure 7.1, and corresponding bed shear stress and net transport flux fields are presented in Figure 7.2 to Figure 7.6. The harbour entrance is characterised by strong tidal flows that regularly mobilise the fine and medium sands. The eastern edge and the southern areas of Mair Bank are particularly exposed to strong tidal flows during flood tide, with cross-bank velocities of up to 1.3 $m.s^{-1}$ over the shallows. Within the channel, tidal flows reach 1.4 $m.s^{-1}$ in the deeper areas. During ebb tides, the flows on the eastern edge of Mair Bank are also high, albeit to a lesser extent. Notably, the medium to high current velocities (up to 0.8 $m.s^{-1}$) over the northern area of Mair Bank results in heterogeneous bed shear stress fields that may favour local erosion and accretion. Diagrams showing the range of average current speeds at which sediment particles of different sizes are eroded and transported are shown in Figure 7.3 and Figure 7.4.

The resulting mean net transport fluxes (up to 2.10^{-4} $m^3.s^{-1}.m^{-1}$) over one tidal cycle highlight the high potential for the tidal component to mobilise sediments around Mair Bank and within the main channel. Note, however, that these potential sediment transport results consider a grain size of 200 µm (fine to medium sand) and do not take the biological component (biomass of pipi, shell hash, etc.) into account.

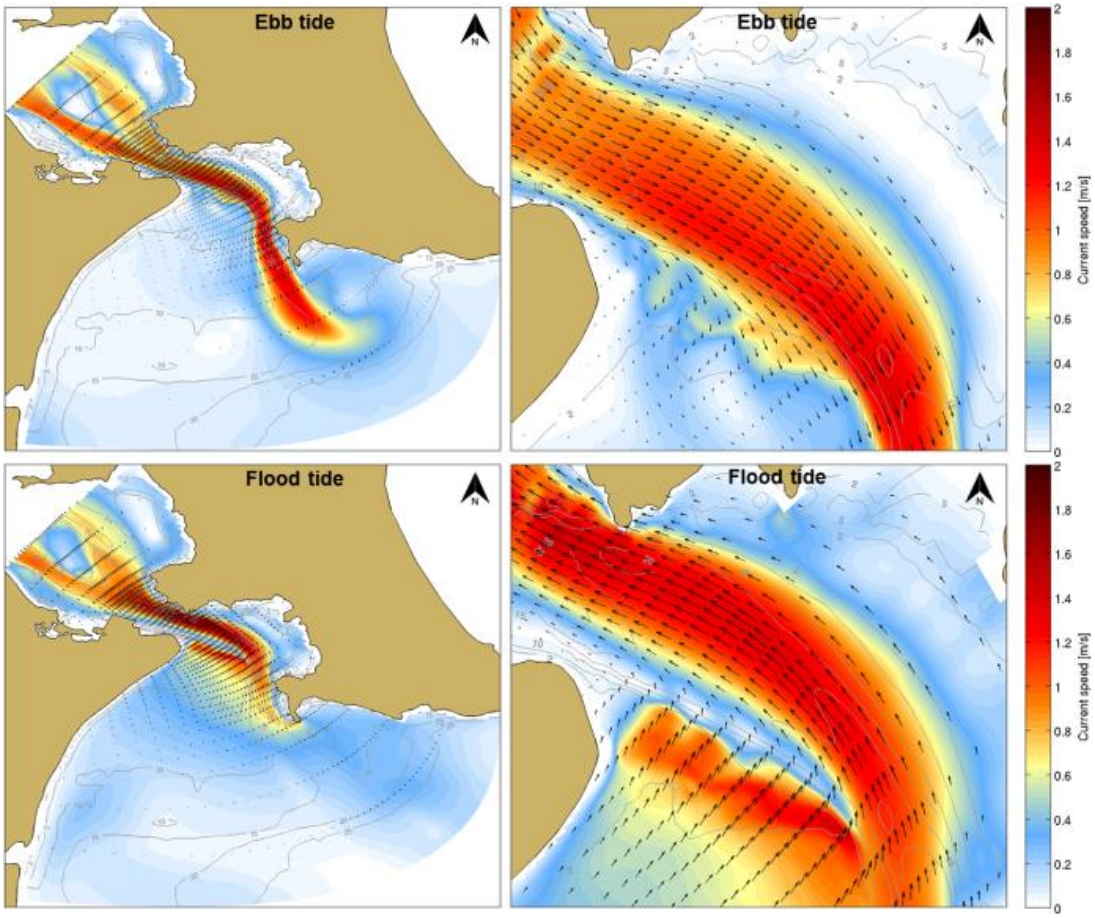

Figure 7.1 Modelled current speed fields over the whole domain (left) and over Mair Bank (right) for the tide-only scenario during spring ebb (top) and flood (bottom) tides.

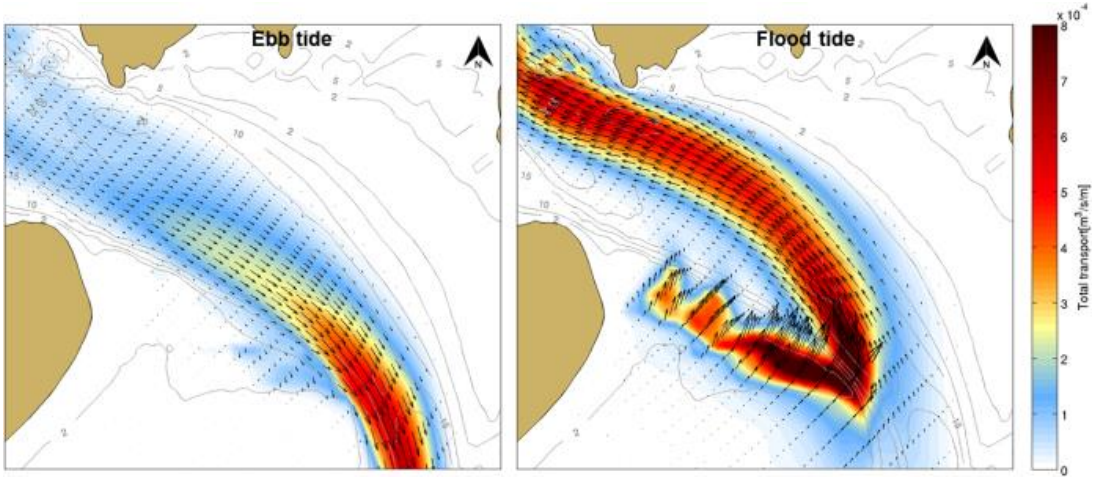

Figure 7.2 Modelled net transport fluxes over Mair Bank for the tide-only scenario during ebb (left) and flood (right) tides.

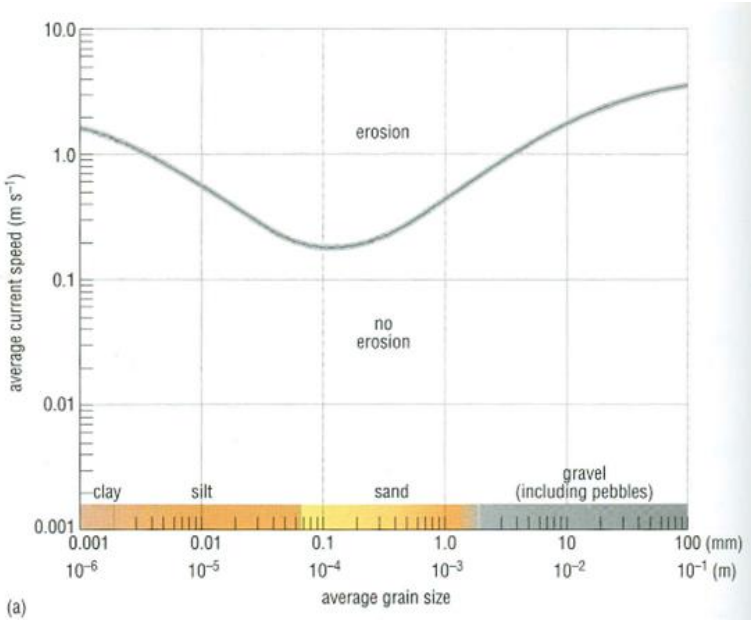

Figure 7.3 Diagram showing the range of average current speeds at which sediment particles of different sizes are eroded, i.e. set in motion. The curve for sediments finer than about 0.1 mm is for relatively uncompact silts and muds (from Wright et al. (1999)).

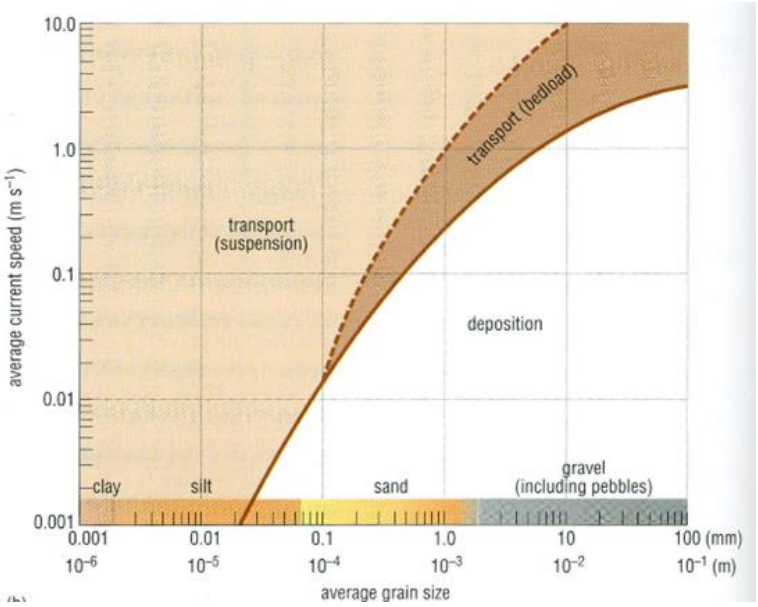

Figure 7.4 Diagram showing the range of average current speeds at which sediment particles of different sizes are transported, in suspension or as bedload, and below which they are deposited. The broken line indicates the transition between bedload and suspension transport (from Wright et al. (1999)).

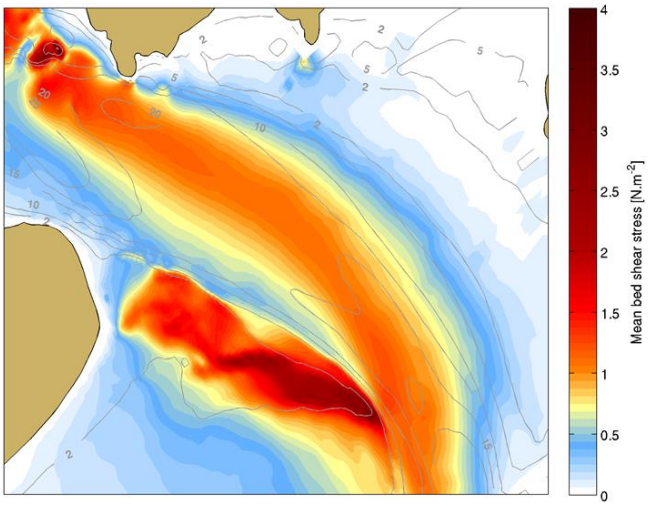

Figure 7.5 Modelled mean bed shear stress calculated over one tidal cycle for the tide-only scenario.

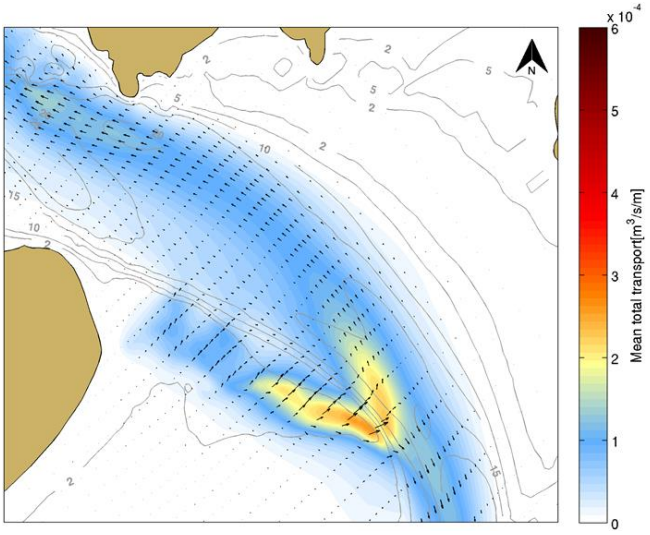

Figure 7.6 Modelled net transport fluxes calculated over one tidal cycle for the tide-only scenario.

7.2. Conceptual modelling – wave and tide scenarios

7.2.1. Existing environment

A set of 16 representative wave and tidal scenarios detailed in MSL Report 0297-01 (MSL, 2016) were run to assess the net transport fluxes through the Whangarei Harbour entrance under a range of sea conditions. The significant wave height fields corresponding to the different scenarios for the existing environment at Whangarei Harbour and the surroundings are illustrated in Figure 7.7 and Figure 7.8 while the resultant mean net transport fluxes are shown in Figure 7.9 and Figure 7.10. Using the mean net transport fluxes to investigate the existing coastal environment brings particular advantages to the study as it quantifies the potential response of the seabed to the wave and tidal forcing excluding the effect of the morphological changes during the simulation.

Whangarei Harbour entrance exhibits strong gradients in wave energy due to the coastal shape and the relative complex bathymetry. Busby Head reduces the exposure of the channel entrance and Mair Bank to the incident waves from the

dominant easterly octant (Figure 7.7) and the shoreline orientation shelters the entrance from northerly storm wave events to a large extent (Figure 7.8). In spite of the degree of shelter afforded by the topography, adding wave forcing to the sediment modelling process increases the net transport fluxes over Mair Bank and along the edge of the channel (see Figure 7.9 and Figure 7.10). Strong northward residual net transport fluxes are observed over the southern margin of Mair Bank and along Ruakaka Beach. The south-western flank of Mair Bank displayed the strongest and most localised net transport fluxes due to wave refraction. High energy wave events show a high erosive potential for sandy material over these areas with mean net transport fluxes of up to 1.10^{-3} $m^3.s^{-1}.m^{-1}$.

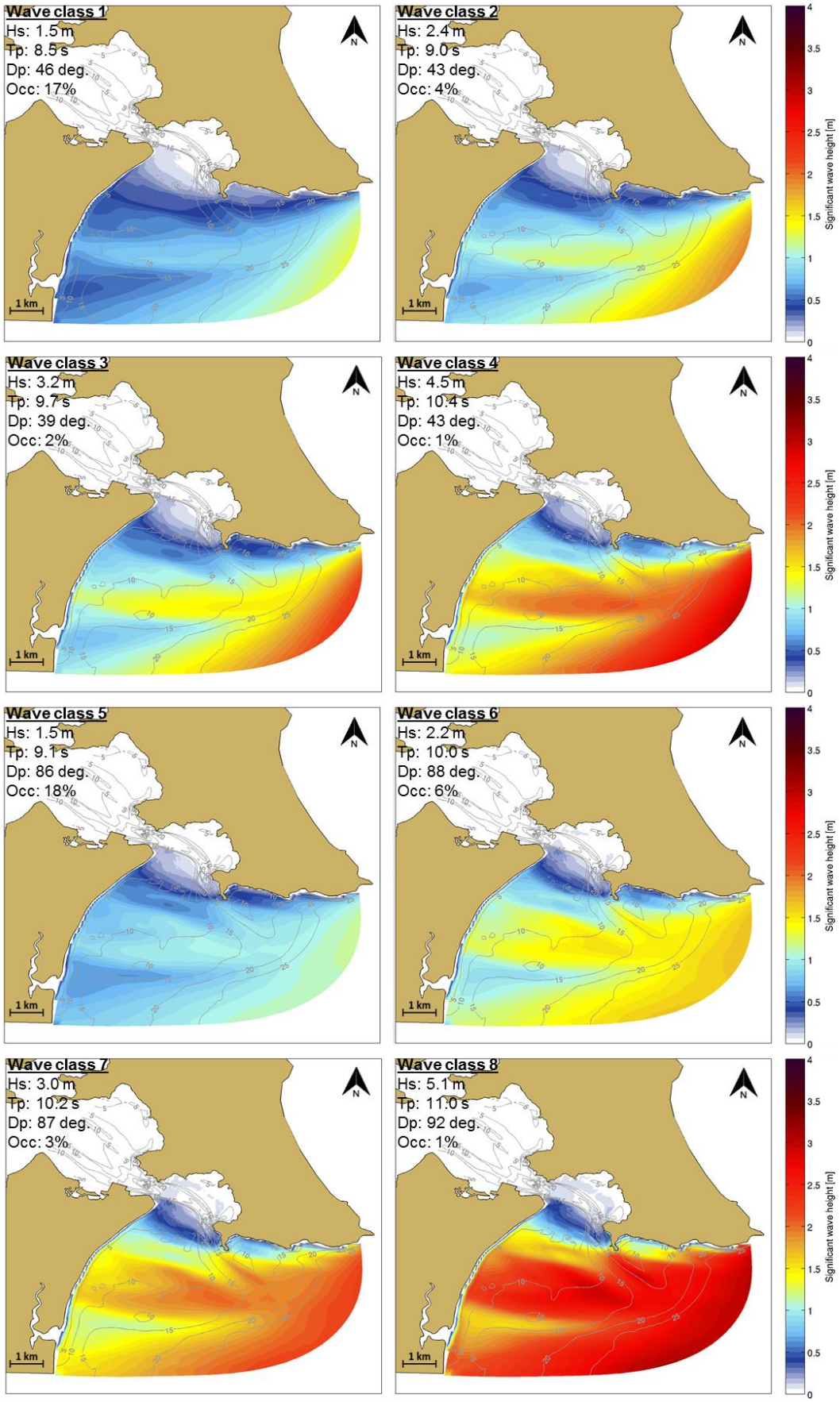

Figure 7.7 Wave height fields for Classes 1 to 8. Black arrows indicate the peak direction.

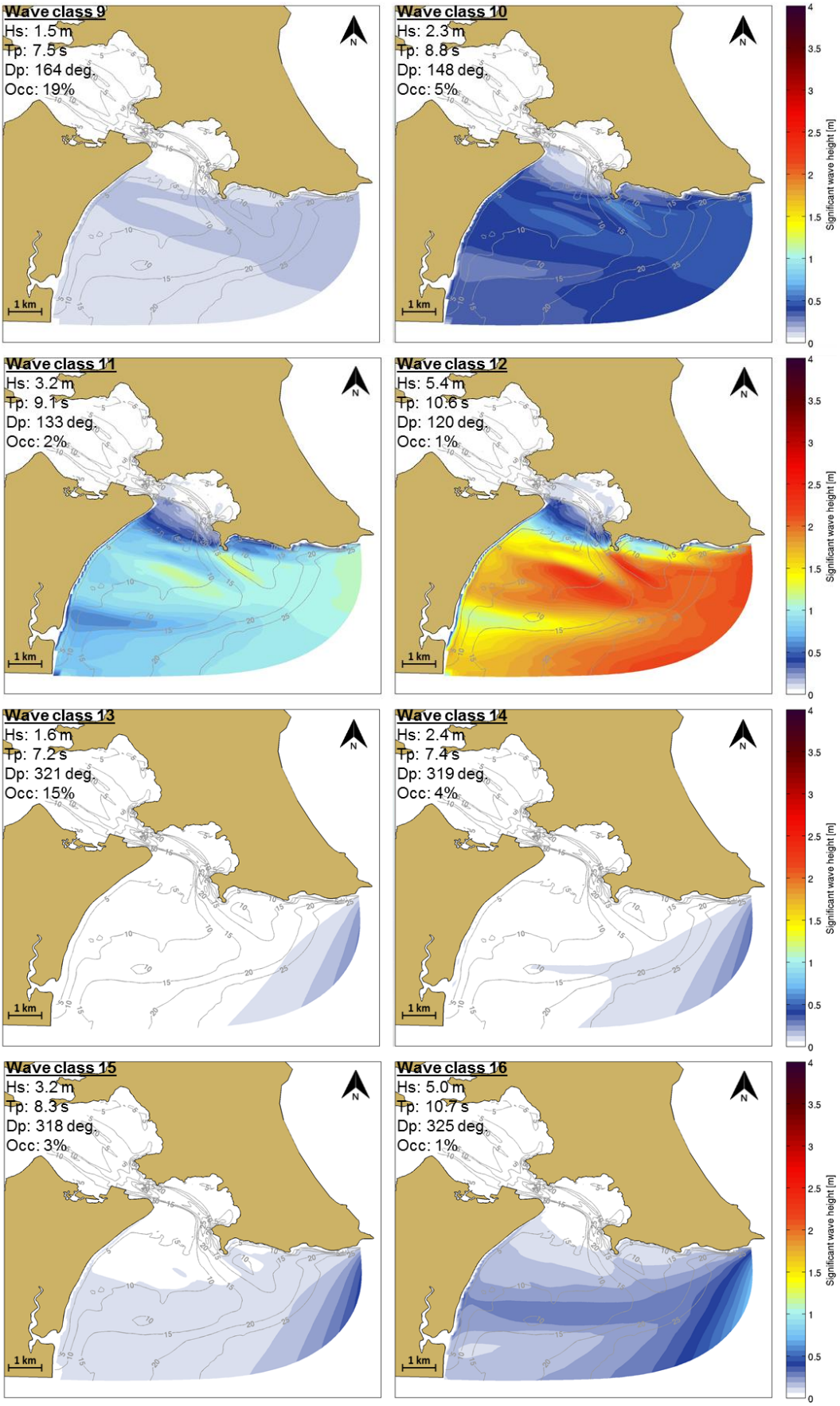

Figure 7.8 Wave height fields for Classes 9 to 16. Black arrows indicate the peak direction.

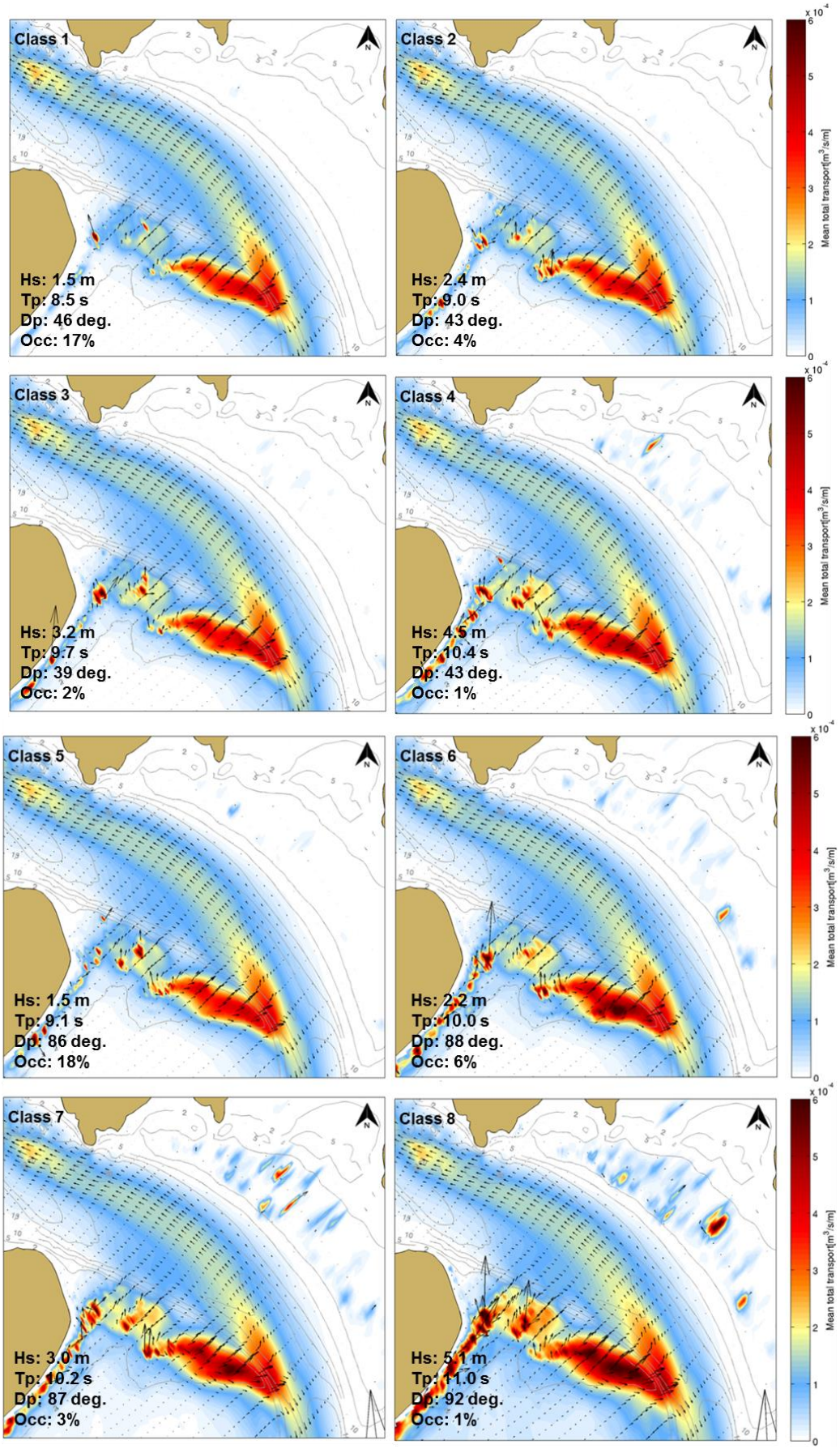

Figure 7.9 Mean net transport fluxes calculated over one tidal cycle for Classes 1 to 8.

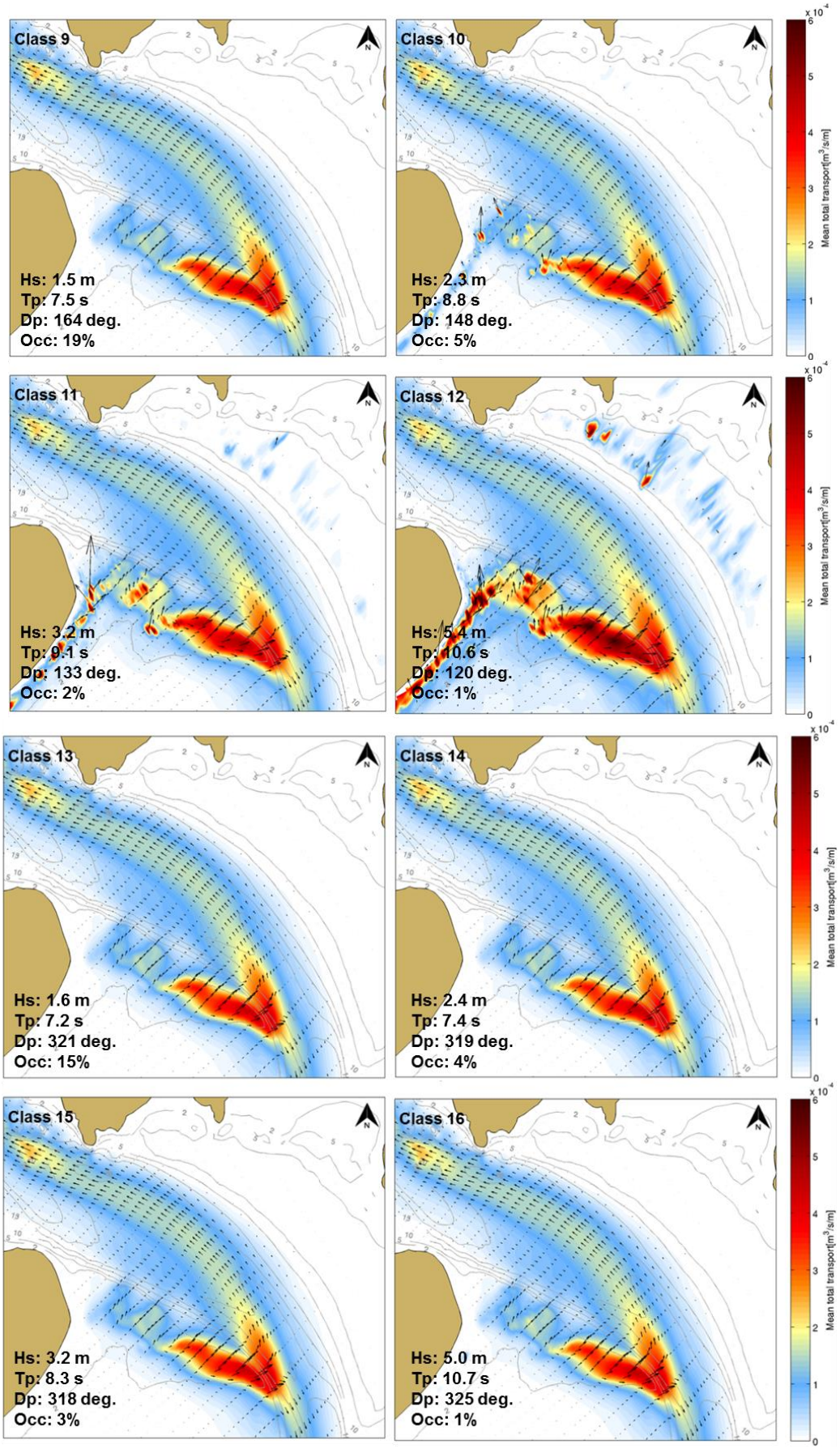

Figure 7.10 Mean net transport fluxes calculated over one tidal cycle for Classes 9 to 16.

7.2.2. Predicted changes to the sediment flux due to channel deepening

The simulations presented in Section 7.2.1 were undertaken again with the deepened channel and the two outputs were compared (Figure 7.11 to Figure 7.14). Mean net transport fluxes induced by a range of wave and tide conditions were investigated and compared to those obtained for the existing environment.

For wave classes 1, 5, 9 and 13, which represent a total of 70% of occurrence, a notable increase of up to 20% of the potential sediment flux is predicted locally along the inner flank of the channel east of Mair Bank. Over Mair Bank changes in the potential net transport fields are predicted to occur along the eastern edge of the sand bank. The increased transport pattern for wave classes 13 to 15 (i.e. low energy conditions) suggests that the effect is dominated by the tidal flows. Note, however, that changes in the wave forcing may occasionally modify somewhat the sediment transport over this particular area during extreme wave events, as illustrated for wave classes 3, 4 and 12.

All other patterns over Mair Bank, Calliope Bank and along Ruakaka Beach can be explained by the effects of the changes to the wave climate resulting from the deepened channel. The residual sediment transport is predicted to strongly increase or decrease over very shallow areas due to high-frequency wave-current interactions, represented by dark red colour and long arrows in Figure 7.11 to Figure 7.14. The high-amplitude changes highlighted in the present section are predicted to be constricted to discrete zones, without causing any overall pronounced effect of the channel deepening on the medium-term or long-term coastal morphodynamics.

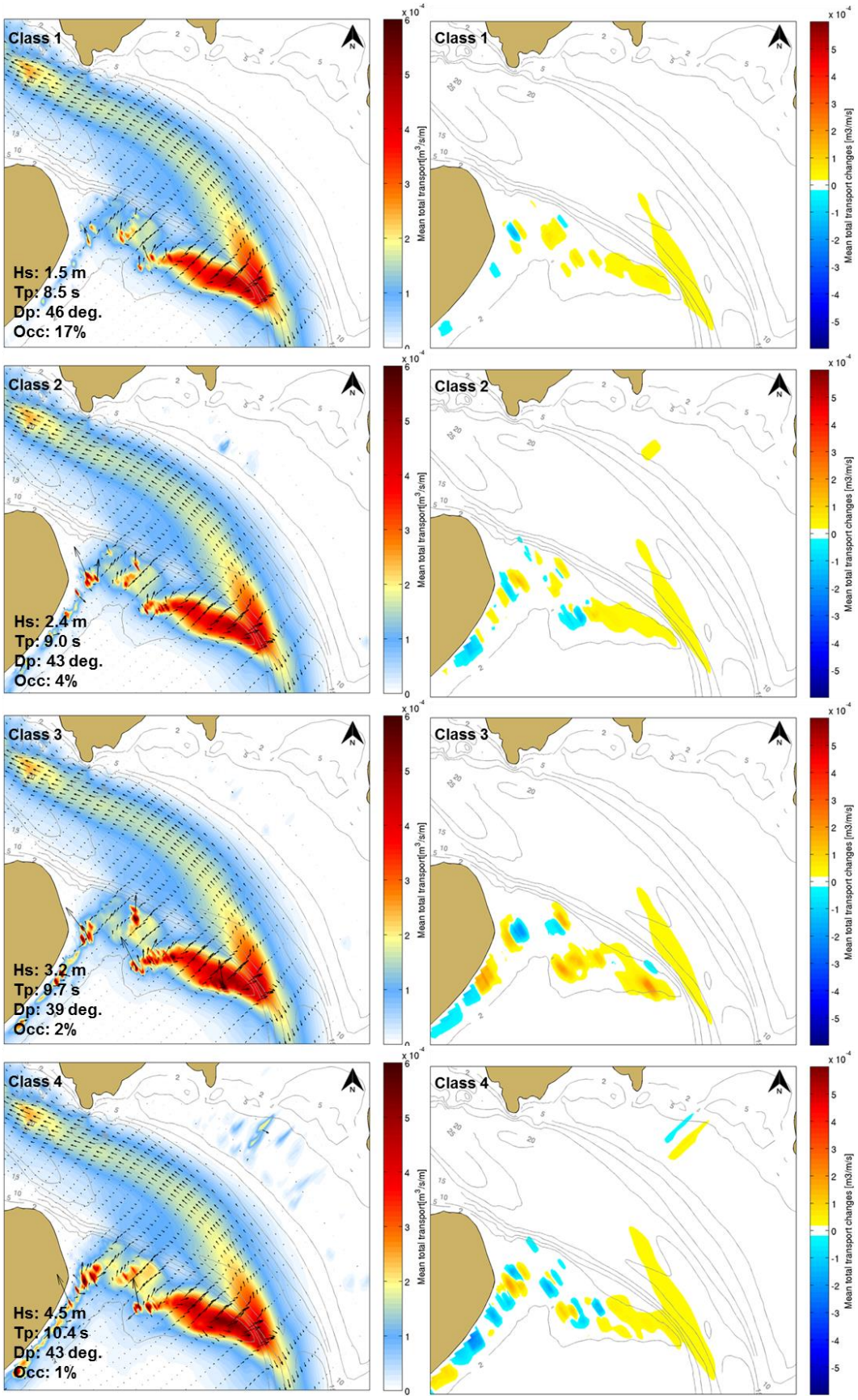

Figure 7.11 Mean net transport fluxes (left) and mean net transport differences (right) between pre- and post-dredge scenarios over one tidal cycle for Classes 1 to 4. A positive magnitude represents an increase.

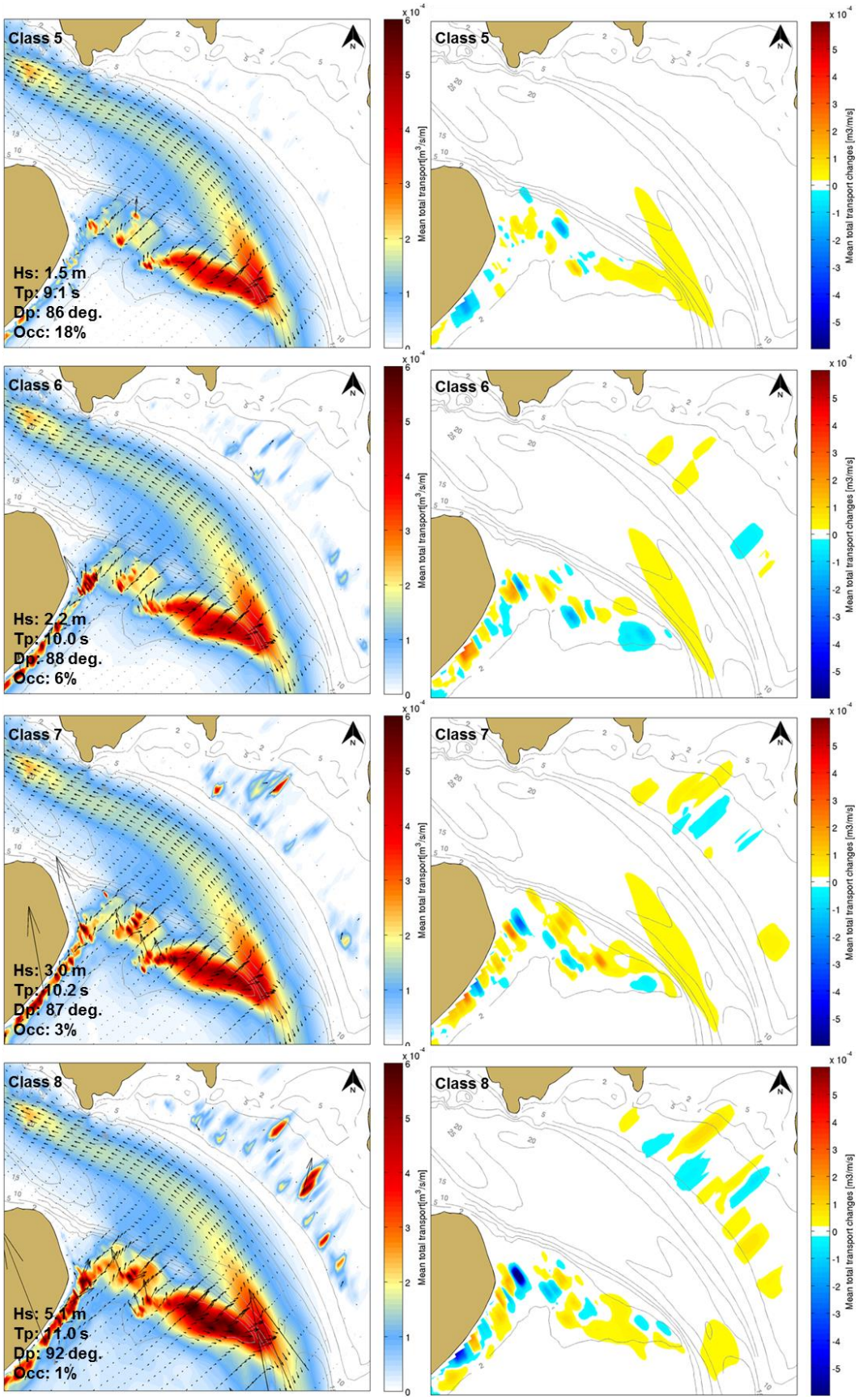

Figure 7.12 Mean net transport fluxes (left) and mean net transport differences (right) between pre- and post-dredge scenarios over one tidal cycle for Classes 5 to 8. A positive magnitude represents an increase.

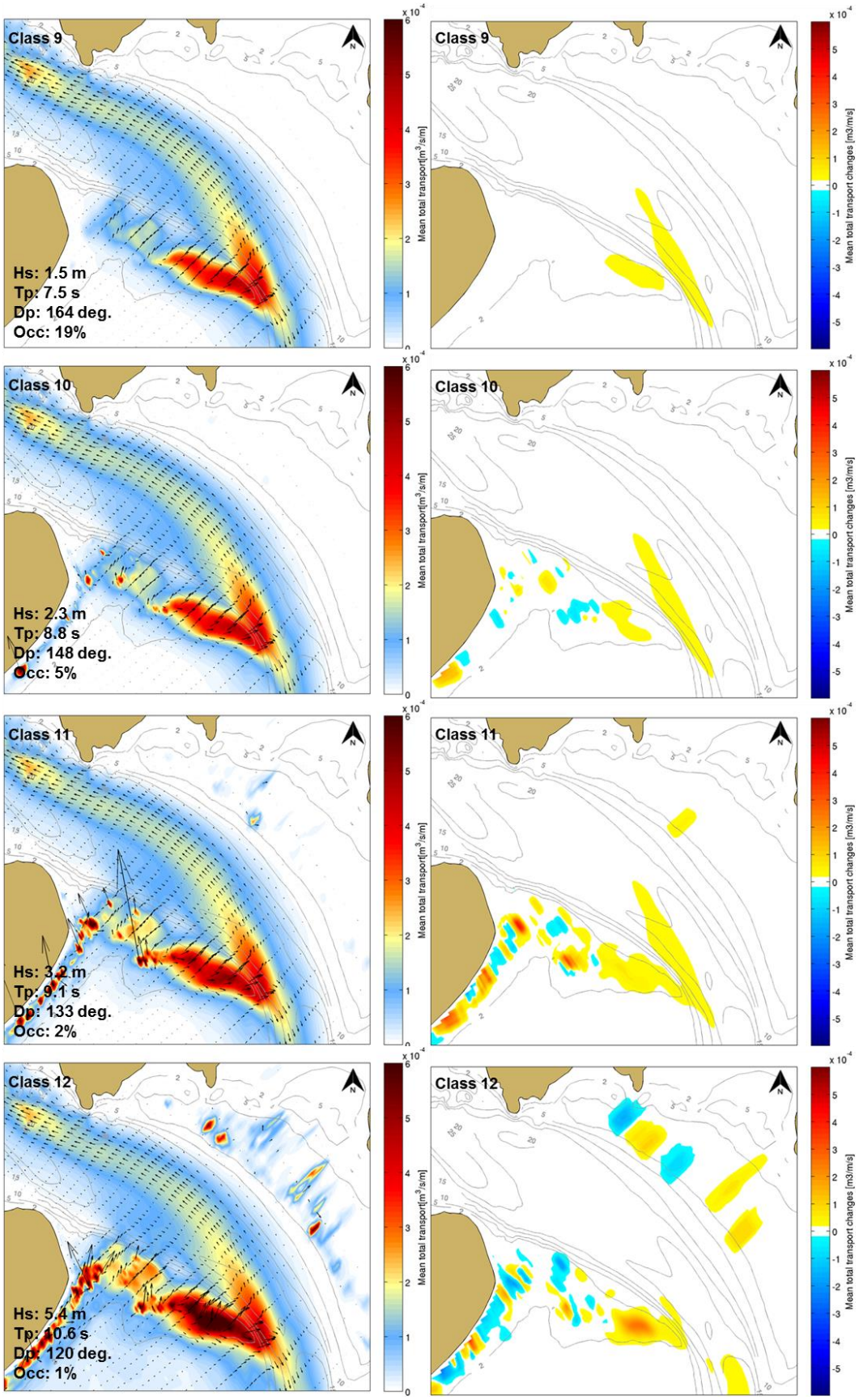

Figure 7.13 Mean net transport fluxes (left) and mean net transport differences (right) between pre- and post-dredge scenarios over one tidal cycle for Classes 9 to 12. A positive magnitude represents an increase.

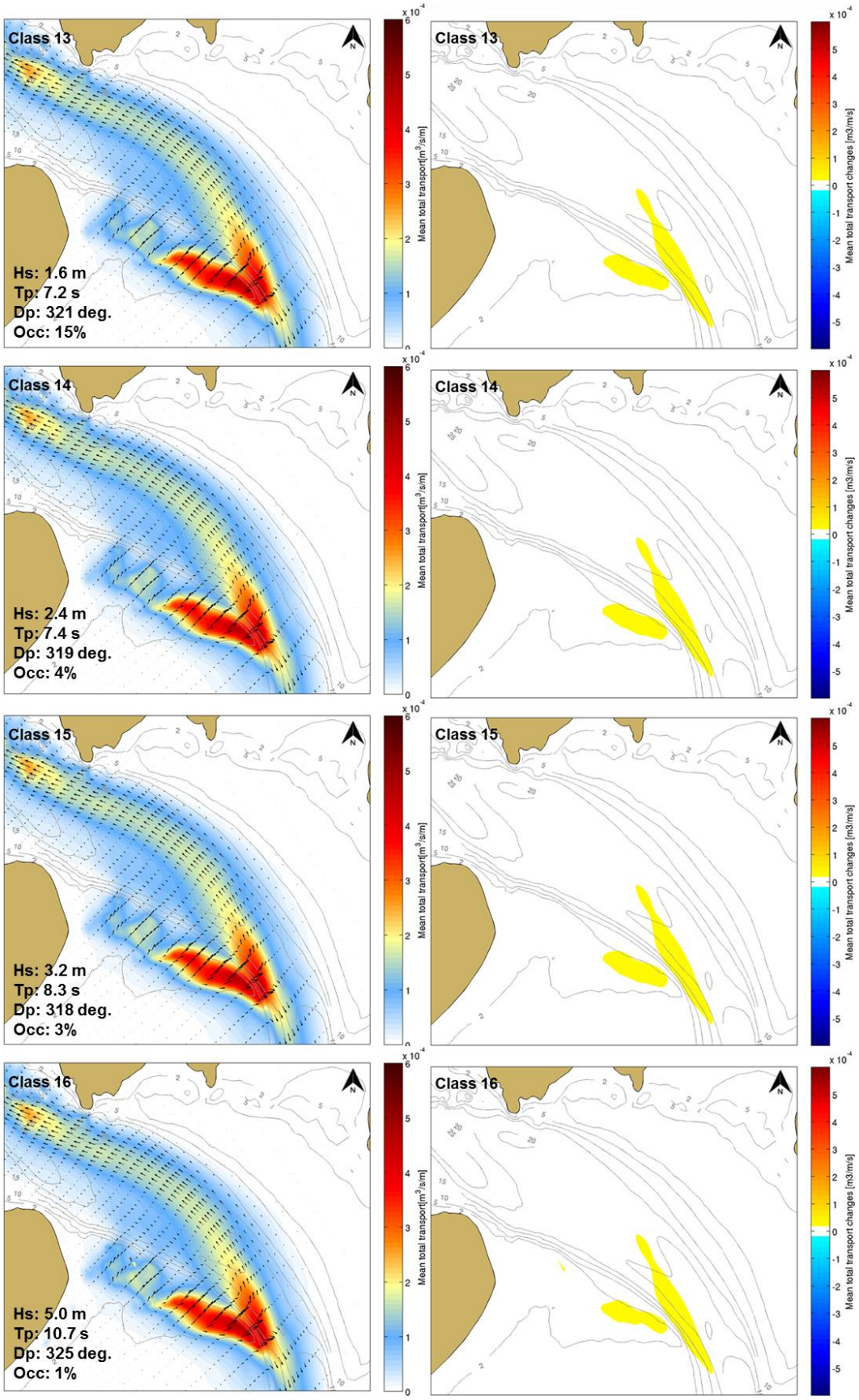

Figure 7.14 Mean net transport fluxes (left) and mean net transport differences (right) between pre- and post-dredge scenarios over one tidal cycle for Classes 13 to 16. A positive magnitude represents an increase.

7.3. Sediment dynamics

The adequate initialisation of spatially varying grain size distribution of bottom sediment in a process-based model is often constrained by a lack of appropriate field data for the entire model domain. In the present study, a synthetic simulation was initiated with a uniform sediment type distribution over two bed layers using 6 sediment fractions to replicate a realistic bed composition over the entire domain and thus avoid the problem of data constriction. This "sedimentological spin-up" was performed over a 6-month fair-weather period to promote the vertical and horizontal redistribution of sediment grain size fractions in response to the combination of tide-induced currents and low energy wave conditions, and thus recreate a realistic bed composition. The purpose of this technique was to provide the realistic bed composition required to initialise both the pre- and post-dredging simulations. The same bed composition was used for both configurations to allow comparison of model results. Note, however, that the "sedimentological spin-up" was also performed using the post-dredging bathymetry to investigate the resultant changes in the sedimentology due to potential changes in the tide-induced currents and wave conditions.

This section details firstly the final sediment grain-size distributions obtained for the existing configuration and some qualitative comparisons with the sediment sampling results over the navigation channel. Secondly, the pre- and post-dredging bed compositions were compared to assess the potential changes caused by the channel deepening on the sedimentology at the entrance to Whangarei Harbour.

7.3.1. Bed composition generation (BCG) simulation

Sediment distributions for each fraction generated by the BCG run (i.e. 100, 150, 200µm…) are presented in Figure 7.15 to Figure 7.21. Note that this BCG run corresponds to the existing bathymetry. The BCG technique is fully described in MSL Report P0297-01.

The surficial sediment grain size distribution shown in Figures 7.15-7.21 illustrate a significant coarsening within the main channel. Most of the sandy material (between 100 and 500 µm) is actively washed away from the channel. Fine sand is deposited at the outermost ebb-tidal delta lobe where ebb-directed current velocities decrease due to increasing water depths. This is supported by the sediment sampling results, where the fine sand fraction increases to 17% in the furthest offshore section of the channel.

The modelled channel bed was initially composed of medium and coarse sand particles. Field data showed the medium sandy sediment fraction to dominate the channel bed composition (~60%; Tonkin and Taylor, 2016) while modelled sediment distribution suggested a higher fraction of coarse sediments. This is probably related to the low frequency of sediment grain sizes between 500 and 1000 µm in the bed composition initialisation. The presence of 500 µm grain size material in the channel indicates that the overall bed shear stress exerted by tidal flows in the inlet throat is not much higher than the critical bed shear stress corresponding to medium to coarse sediment grain size. Adding fractions of grain size in the range of 500 – 800 µm may limit the overestimation of the coarse sediment fraction within the bed composition of the channel. However, the BCG run was limited to seven sediment fractions because of the computational expenses related to the implementation of the bed stratigraphy module and the 3D mode in the model. Note that the shell fragment layers found in the sediment samples (Tonkin and Taylor, 2016b) were not considered in these simulations. Shell

fragments may shelter the underlying grains from the flow and thus reduce the erosion of medium grained sediments. The interactions between the biological, morphological and hydrodynamic components in the model do not allow a full reproduction of the frictional forces acting on the surface transport layer. This bias is nevertheless compensated to some degree by the morphological spin-up process which modifies the bed composition based on the modelled friction fields. However, the model reproduces the relative stability of the fine sediment layer observed over the southern bottom edge of the channel section located north of Mair Bank well. Measured data indicated the presence of 16% fine sand in the bed composition, which agrees qualitatively with the modelled top layer composition shown in Figure 7.15.

The dredged area adjacent to NorthPort berths was shown by the model to be particularly favourable for the deposition of medium grain size sediments. In the vicinity of the berth, medium and coarse sediment fractions dominated the bed composition in the channels while fine sediments were largely present over the different shoals. The overall modelled sediment pattern was consistent with the configuration described in Longdill and Healy (2007).

The high bed shear stress fields over the intertidal area of Mair Bank lead to rapid redistribution of sediments in this type of simulation. Over subtidal areas of the shoal, fine sediments entrained by tidal flows are transported offshore through the harbour. Medium grain size sediments are washed away from Mair Bank and deposited offshore. These results are not consistent with the sediment sampling reported in Williams and Hume (2014) which indicated a predominance of fine sand (~50%). Such discrepancies can be expected as the reduction of the bed shear stress provided by the shell hash layer and the biomass of pipi on the seabed cannot be reproduced in the model. The discrepancies clearly illustrate the morphological stability provided by the biological component on Mair Bank. The model showed a substantial amount of fine and medium sand sediments located along the harbour flank of the bank controlled by the flood-tidal flows. The southern margin of Mair Bank was predicted to show the largest range of sediment grain sizes from 100 to 1000 µm, with a predominance of coarse sand.

The overall qualitative validation of the bed composition over the particular areas of the domain where sediment samples were available highlighted that it was difficult for the model to recreate the existing bed composition. Most of the results obtained with this technique were nevertheless coherent with the observations, although some differences were identified over specific sections of the channel or over Mair Bank. The armouring of both the channel and Mair Bank provided by the shell layer and the biomass of pipi is not fully resolved by the morphological model. However, the implementation of the “morphodynamic spin-up” technique introduces balancing mechanisms through the adaptation of the bed composition to the model bed shear stress, thus avoiding the occurrence of very large erosion processes in further simulations initiated with this synthetic bed composition. The main purpose of the BCG run is not to replicate the real sea bed composition but rather a sea bed composition that will allow realistic replication of sediment fluxes and depth changes over the domain, including the effect of the processes not implicitly resolved by the model.

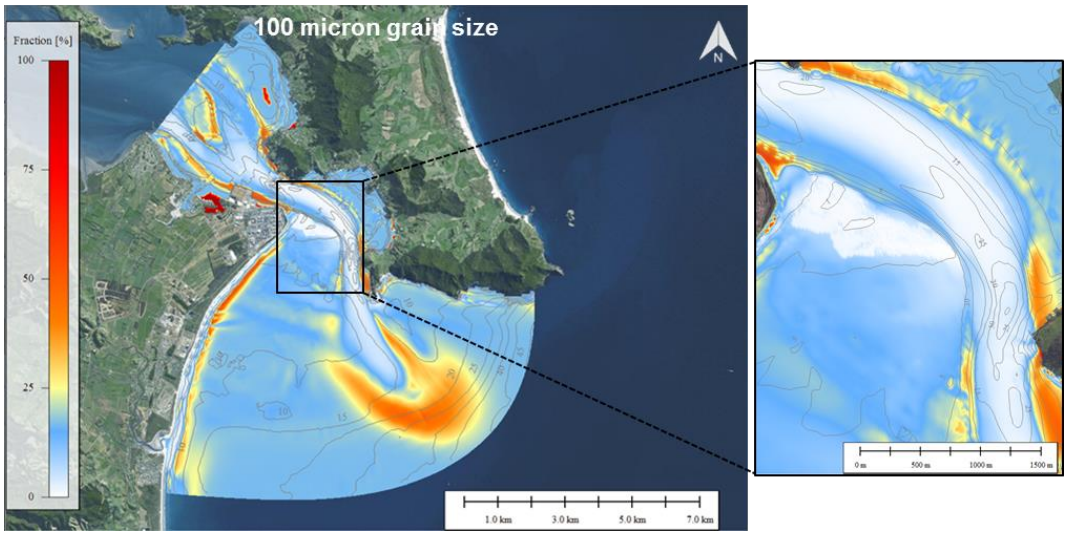

Figure 7.15 Distribution of 100 µm grain size sediments in the active layer generated by the BCG run for a 6-month fair-weather period.

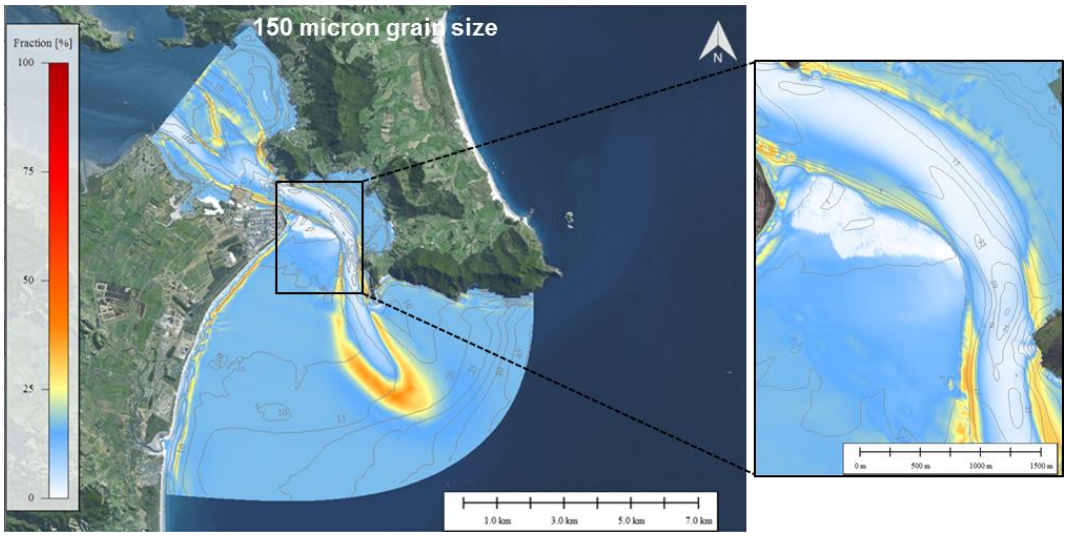

Figure 7.16 Distribution of 150 µm grain size sediments in the active layer generated by the BCG run for a 6-month fair-weather period.

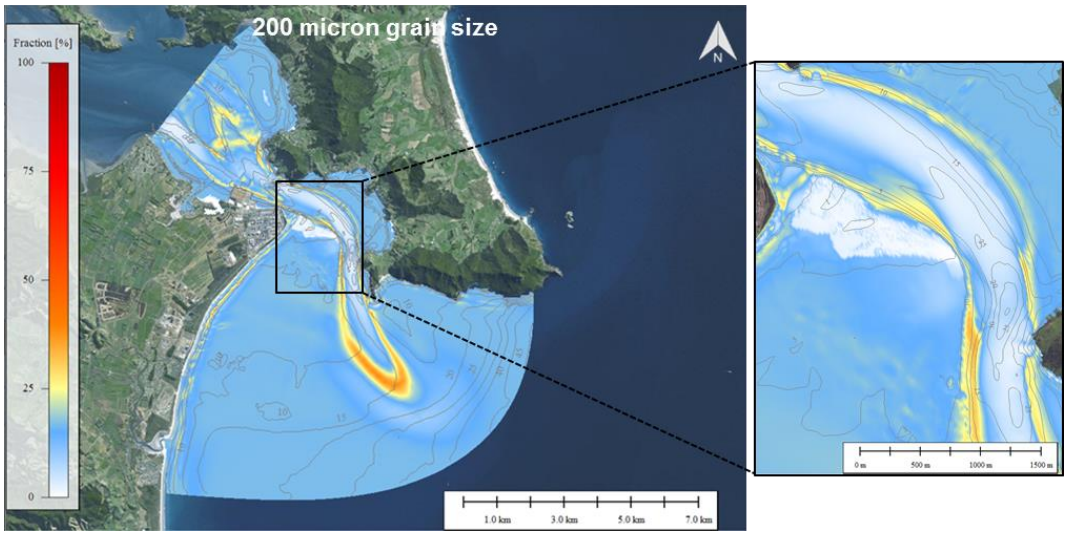

Figure 7.17 Distribution of 200 µm grain size sediments in the active layer generated by the BCG run for a 6-month fair-weather period.

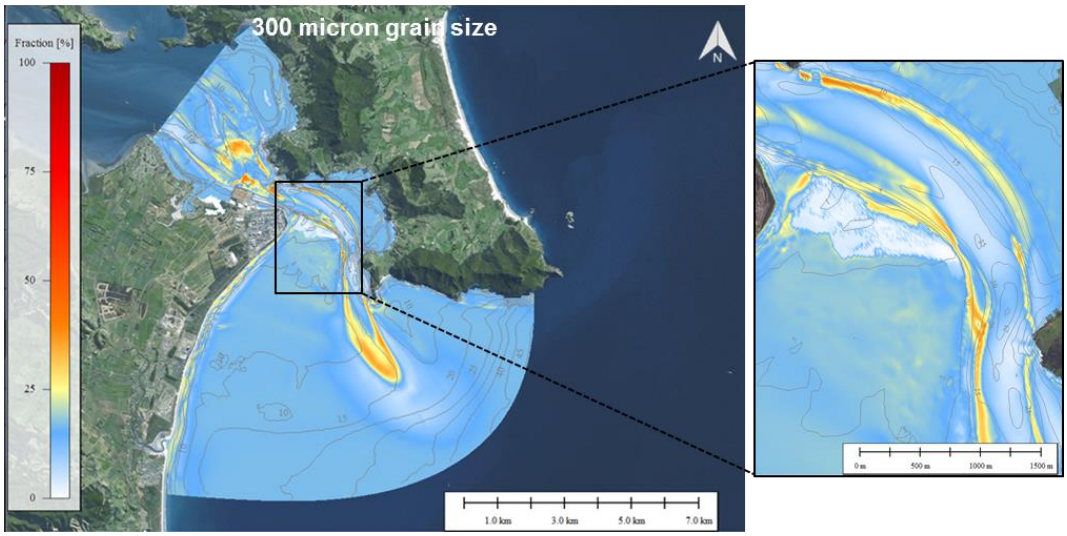

Figure 7.18 Distribution of 300 µm grain size sediments in the active layer generated by the BCG run for a 6-month fair-weather period.

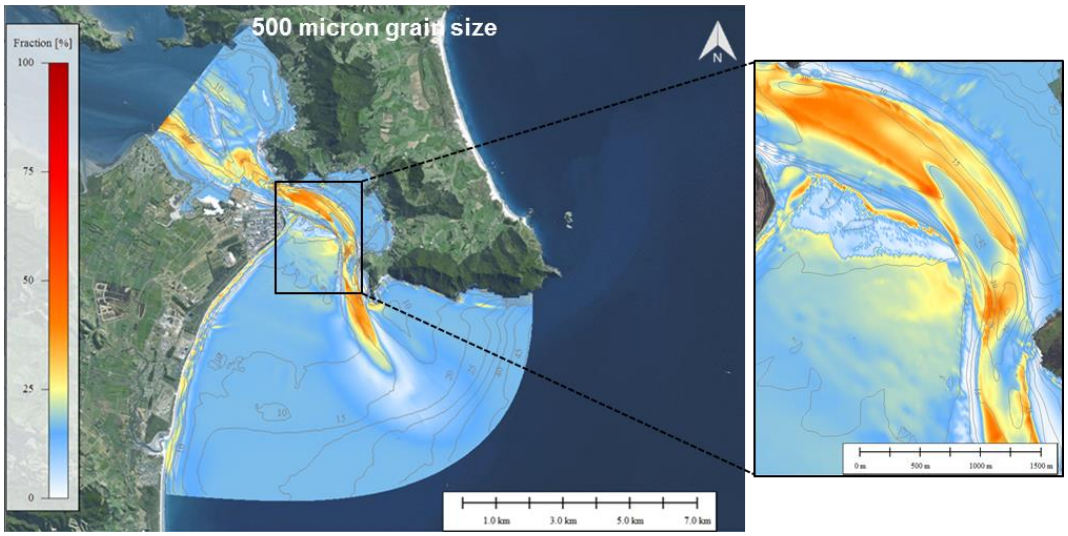

Figure 7.19 Distribution of 500 µm grain size sediments in the active layer generated by the BCG run for a 6-month fair-weather period.

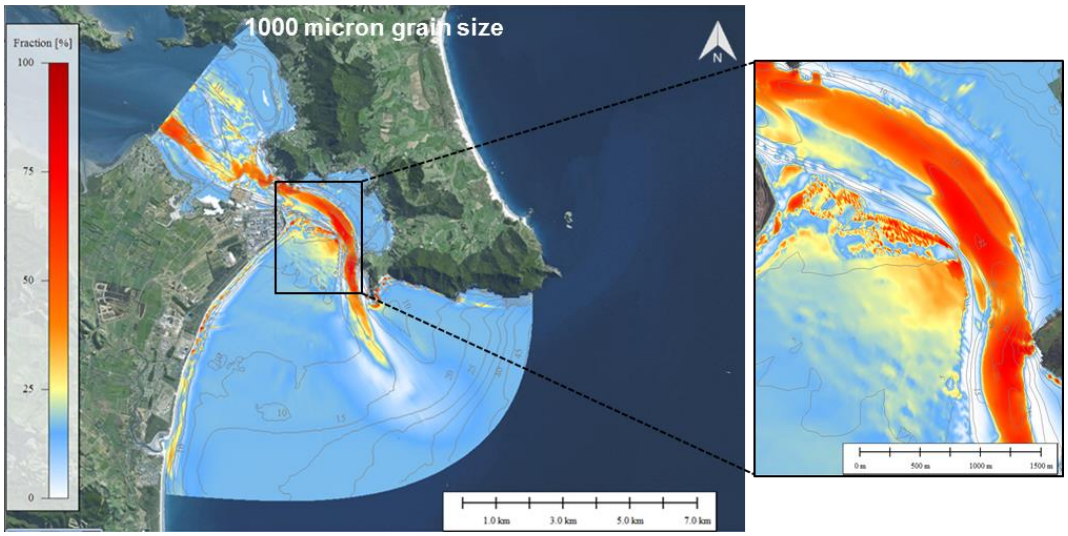

Figure 7.20 Distribution of 1 mm grain size sediments in the active layer generated by the BCG run for a 6-month fair-weather period.

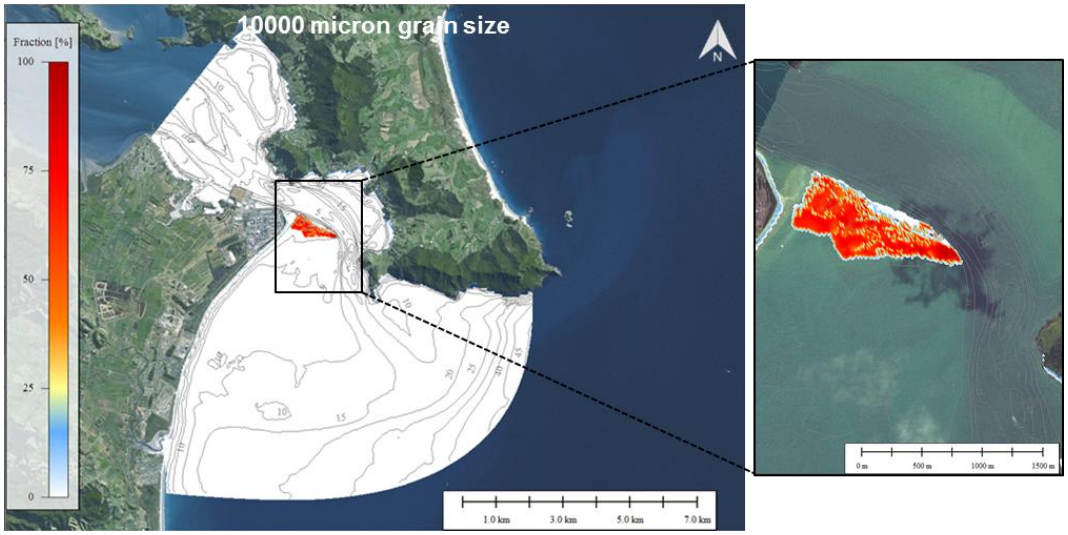

Figure 7.21 Distribution of 10 mm grain size sediments in the active layer generated by the BCG run for a 6-month fair-weather period.

7.3.1. Predicted changes in the spatial distribution of sediment fractions

The complex interplay of tidal and wave driven forces in the entrance region leads to characteristic spatial changes in the sediment grain-size distributions. Some of this has been described in the field report on the seabed survey (Tonkin and Taylor, 2016b). In this section the numerical model was used to examine the underlying processes that lead to grain-size sorting, applying the same technique to the existing state and the deepened channel scenario. A comparison of the results of those simulations is provided in Figure 7.22 for the various sediment grain size fractions. The results indicate that the overall changes in grain size sorting are very subtle and less than about 5%. Isolated areas with larger changes in grain sorting correlate directly with the magnitude of the deepening. For example, within the outer part of the channel the increased depth is predicted to increase the finer (100 µm) grain size fraction due to the reduced tidal flows. The realignment and deepening near Busby Head has a similar effect on the 200 µm fraction. Conversely, the slight changes to the wave climate due to refraction on the channel margins reduce the fine fractions in some areas and increase them in other. These subtle changes in the sedimentology described in this section are predicted to be constricted to discrete zones within the entrance system and are not expected to be discernible in the context of long-term morphological changes.

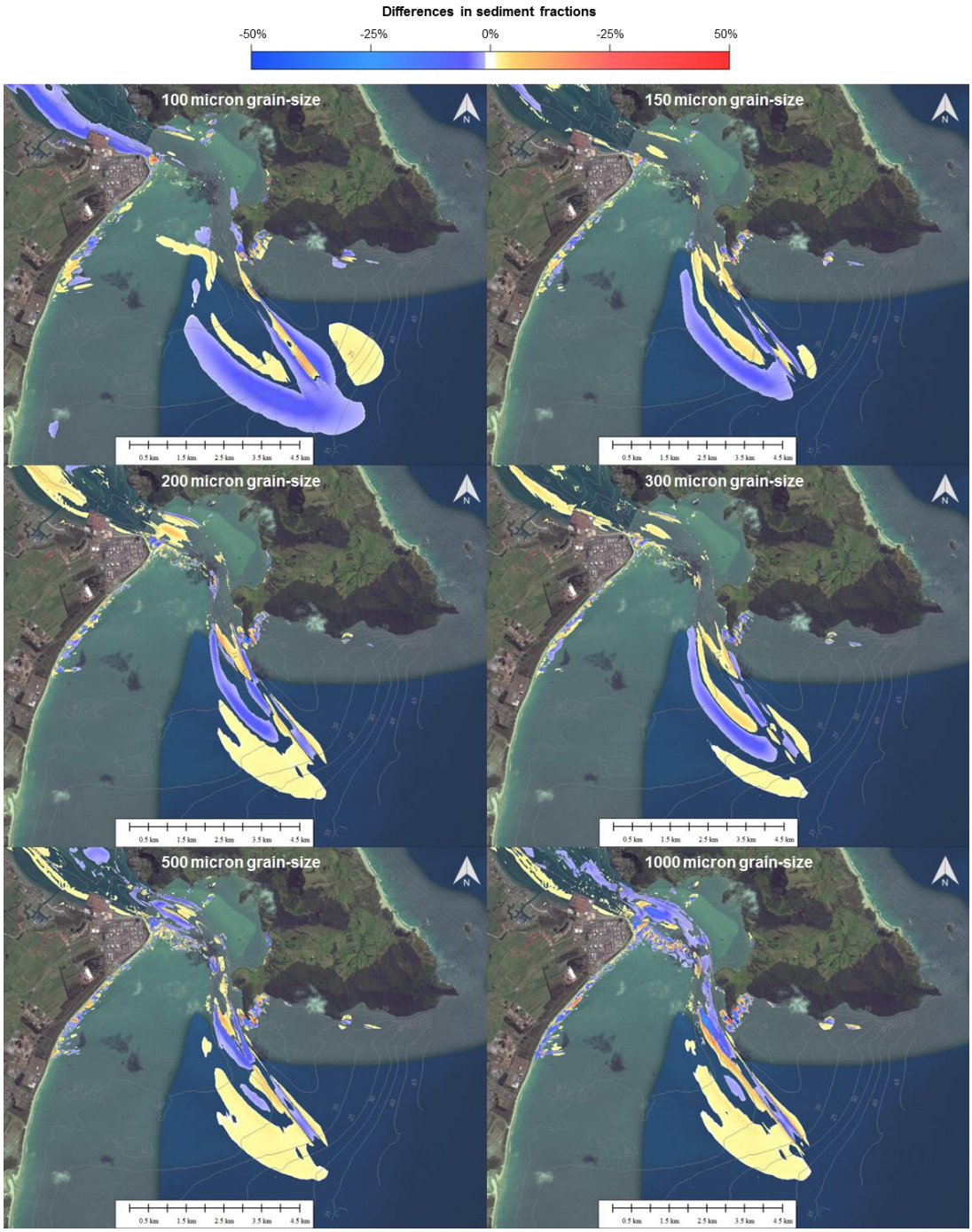

Figure 7.22 Differences in spatial sediment fraction distributions. Positive amplitude indicates an increase of the given sediment fraction in the post-deepening configuration.

7.4. Predicted morphological changes

A sequence of storm and fair-weather conditions was used to examine the evolution of the sea bed at the harbour entrance. An historical 21-day period was used for this purpose.

During storm wave conditions (i.e. peak conditions for the existing environment shown in Figure 7.23), significant morphological and sedimentological adjustments occur along Ruakaka Beach and east of Busby Head due to increased sediment transport fluxes (Figure 7.24) generated by refracted waves. This is clearly highlighted by the patterns of accretion (red colour) and erosion (blue colour) along Ruakaka Beach and at Busby Head in Figure 7.25. The residual bed load transport is predominantly directed southward. The erosion of the northern section of Ruakaka Beach during episodic storm events is counteracted by the replenishment of the nearshore regions during the fair-weather conditions (Figure 7.26). Within the channel itself, however, the model predicts more influence from the tidal flows under the fair weather condition than under stormy conditions. This indicates the dominance of the tidal regime on the sediment dynamics. Modelled morphodynamic results exhibit subtle change (in the order of cm) in the channel. Lag deposits of shell effectively armour the seabed and change the hydraulic roughness and the model can only mimic that with an increased grain size in defined areas. Nonetheless, the model remains a useful tool for the integration of the highly non-linear aspects of the sediment transport dynamics, and the direct comparison of the deepened channel with the existing environment is a valid technique to identify potential effects.

Comparison of the predicted morphological changes from the storm and fair weather simulations are presented in Figure 7.27 to Figure 7.32. The results show:

- The outermost section of the channel to the southeast of Busby Head is predicted to infill in the order of few cm over the 21-day period under the sequence of stormy and fair-weather conditions.

- Adjacent to Busby Head, the morphological changes suggest increased critical bed shear stress due to an increase in wave energy directed at this area in a storm caused by enhanced refraction along the eastern margin of the dredged channel. This environment is occasionally subjected to 4-m wave heights during storms. However, photos of the sea bed presented in the Kerr & Associates Report - Ecology Stage One Pilot Study (2016) indicate the seabed comprises coarser sediment than modelled, with a sandy / shelly / gravel sediment top layer near Busby Head. Considering such bed composition, changes in wave height due to the channel deepening are not expected to have a significant influence on the morphodynamics near Busby Head.

- Morphological changes along the northern section of Ruakaka Beach suggest that the migration patterns of shore-oblique sand bars during storm events will be modified, but this is a minor spatial adjustment and not a fundamental change to the overall sediment budget.

- Increased tidal flows between Marsden Bank and Mair Bank are predicted to limit the accretion of sand in this area. This phenomenon may be of importance given the historical observations have highlighted the formation of a marginal channel in this area.

- Subtle changes in the tidal and wave-driven currents over the eastern part of Mair Bank may result in zones of deposition and erosion on the toe of the Bank. Note that the historical survey data have shown that this area is dynamic and that natural bed variability of the order of 0.5 m already occurs.

Overall the conclusion drawn from the sediment transport simulations is that the channel deepening produces a minor redistribution of the sediments, but does not create a change to the governing dynamics. While storm events produce localised changes, it is the tidal regime that dominates over time, acting to smooth out the storm changes as well as mobilise large areas of the delta. The deepening slightly reduces the peak velocities within the channel and slightly increases the velocities on the areas adjacent to the channel. However, large areas of the channel are presently armoured with shall lag and in these areas the sediment transport flux potential is very high and the mobile sediments are entrained for a high percentage every day (see Figure 7.11 and Figure 7.12).

The short-term erosion/accretion patterns modelled over Mair Bank during storm and fair-weather conditions reflect the general consistency between the model and the observations presented in Section 2. The wave action over the southern margin of Mair Bank appears to lead to a slow landward net transport as described in Morgan et al. (2011). The extended accretion pattern for wave conditions over the intertidal area of Mair Bank is difficult to interpret as the morphodynamics in this region are highly related to the biological component. Indeed, the elevation of the ridges observed in Morgan et al. (2011) were interpreted as the migration of the shell swash bar. The gravel layer defined on the top of Mair Bank in the model to mimic the biological component seems to reproduce this behaviour leading to steeper lee slopes on the northern margin of the bank. The bathymetry changes observed between 2011 and 2015 suggest a strong inter-annual variability of this accretion pattern. This may be due to the impact of cyclones on the wave climate which generate wave heights of up to 1.5 m adjacent to Mair Bank leading to a strong erosion of the sand bank over a very short period of time.

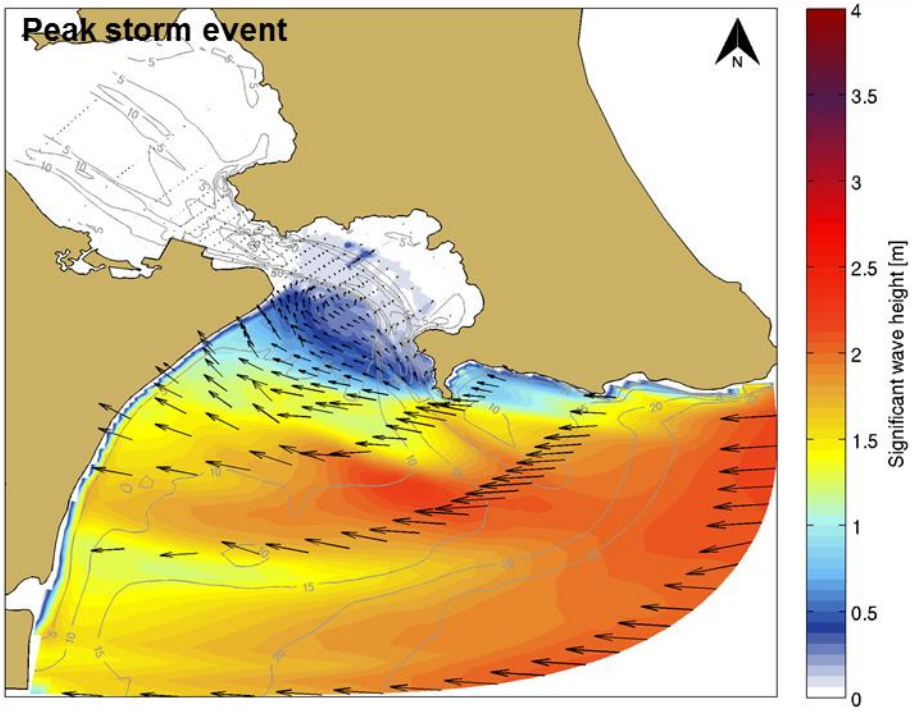

Figure 7.23 Wave height fields during storm event. Black arrows indicate the peak direction.

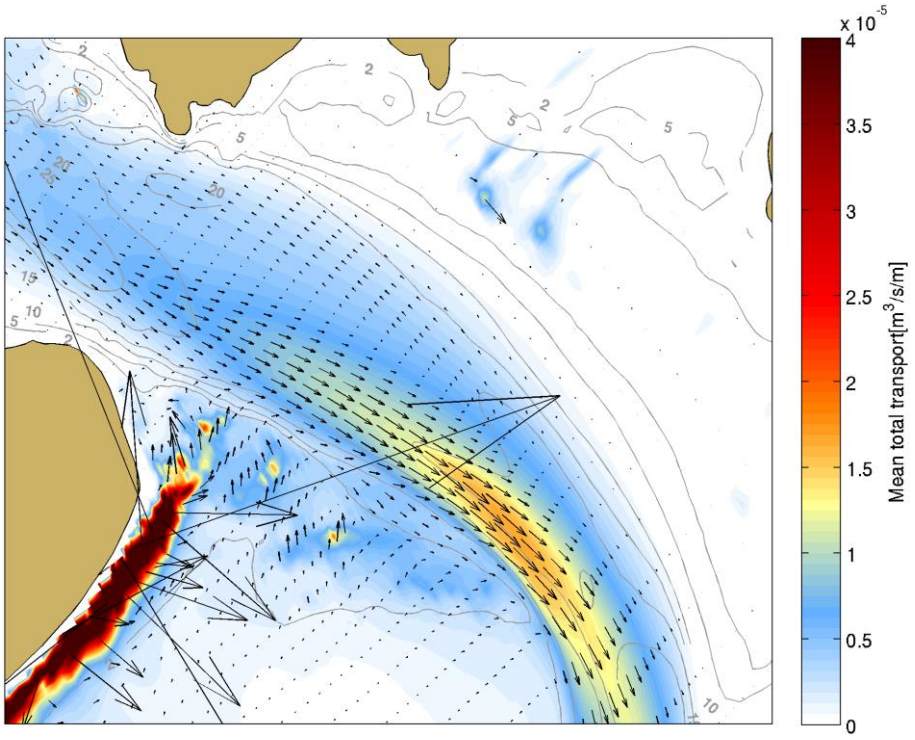

Figure 7.24 Mean total transport calculated during the 5-day storm period. Note that sediment transport was calculated over a complete number of tidal cycles (peak to peak).

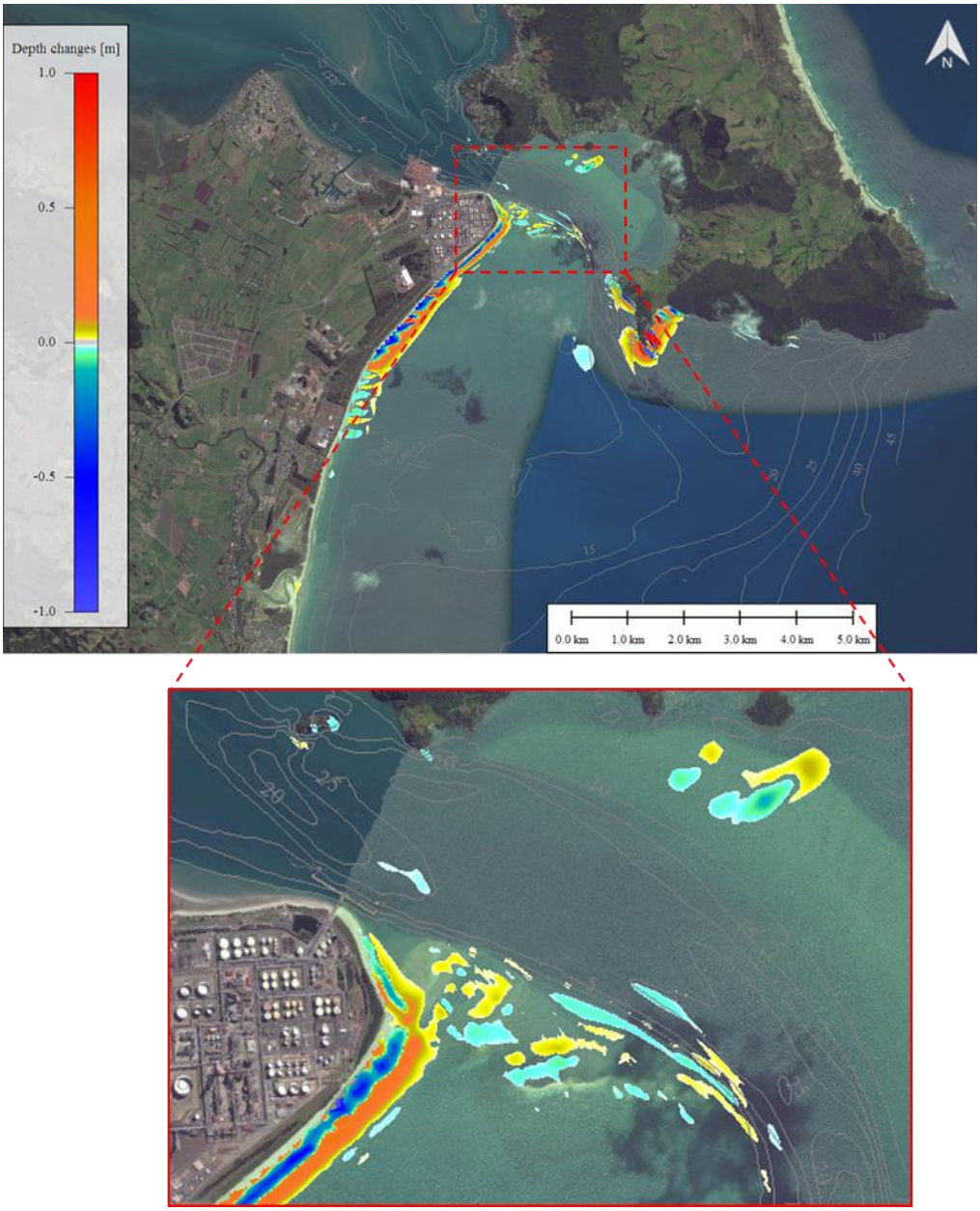

Figure 7.25 Simulated depth changes after 5 days of storm conditions. Positive and negative magnitudes indicate sedimentation and erosion patterns, respectively.

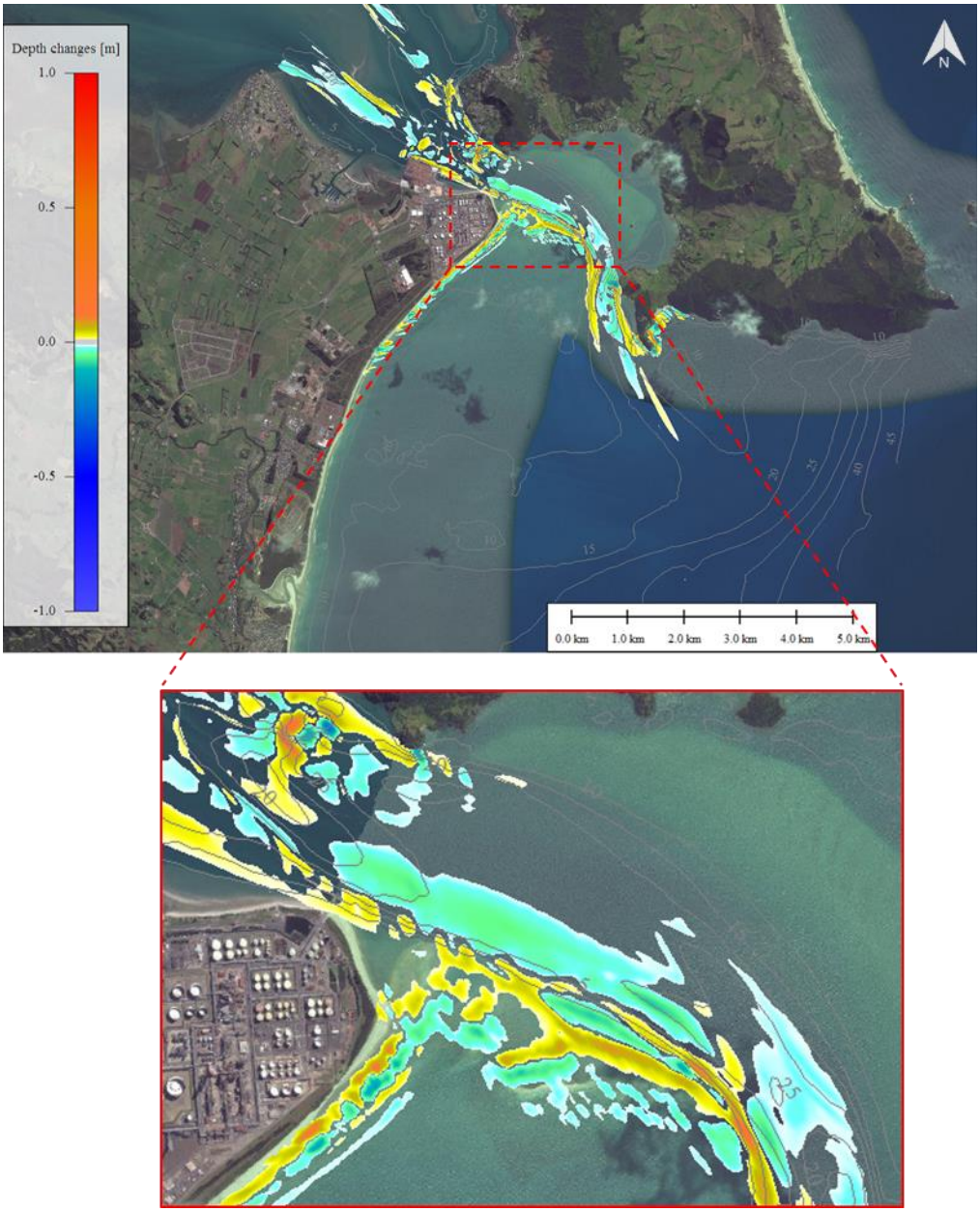

Figure 7.26 Simulated depth changes after 16-day simulation of low energy waves. Positive and negative magnitudes indicate sedimentation and erosion patterns, respectively.

Figure 7.27 Changes in sedimentation and erosion patterns over the study area between the existing and post-deepening configurations over a 5-day storm event.

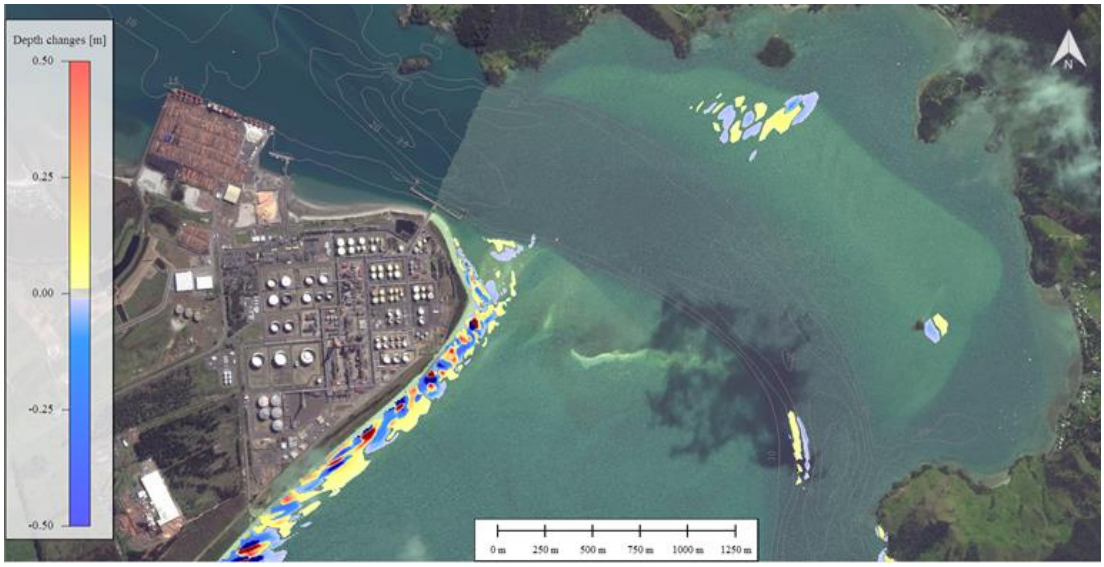

Figure 7.28 Changes in sedimentation and erosion patterns over the entrance to Whangarei Harbour between the existing and post-deepening configurations over a 5-day storm event. Zoom.

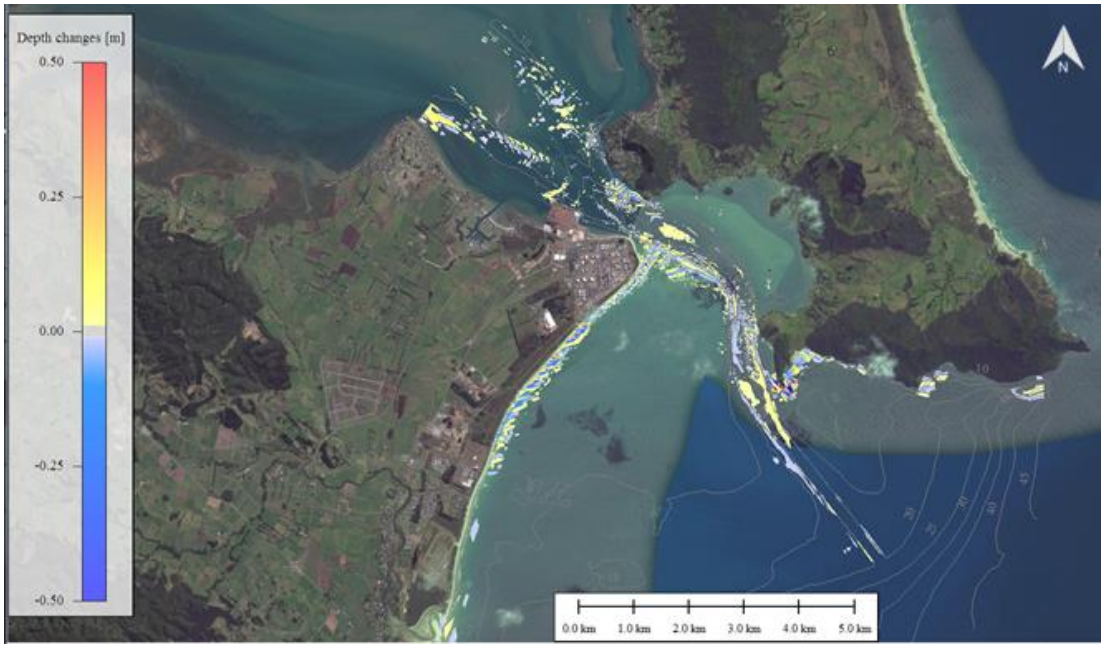

Figure 7.29 Changes in sedimentation and erosion patterns over the study area between the existing and post-deepening configurations over a 16-day fair weather event.

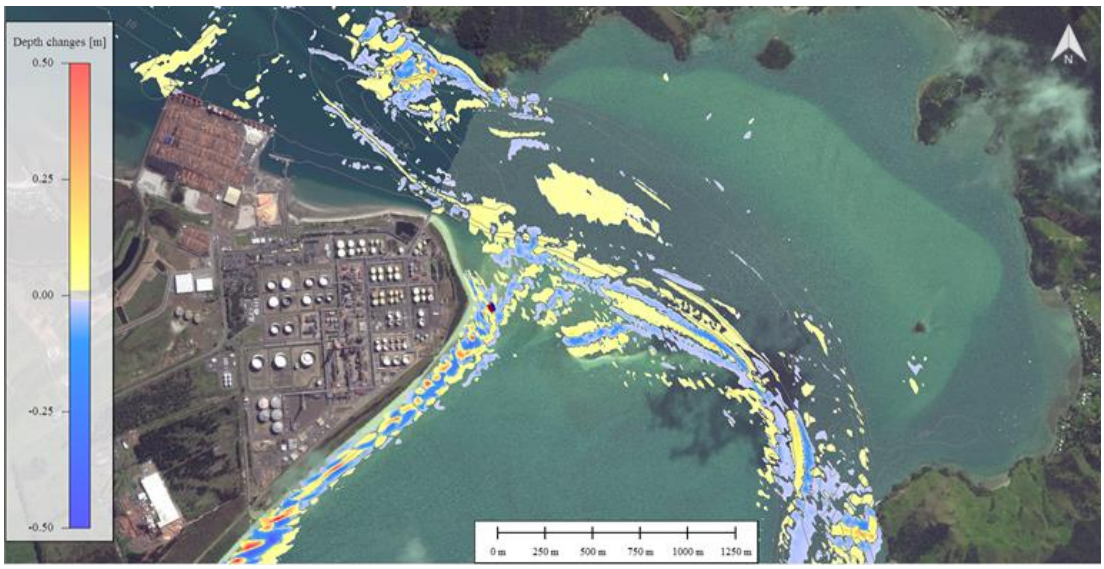

Figure 7.30 Changes in sedimentation and erosion patterns over the entrance to Whangarei Harbour between the existing and post-deepening configurations over a 16-day fair weather event.

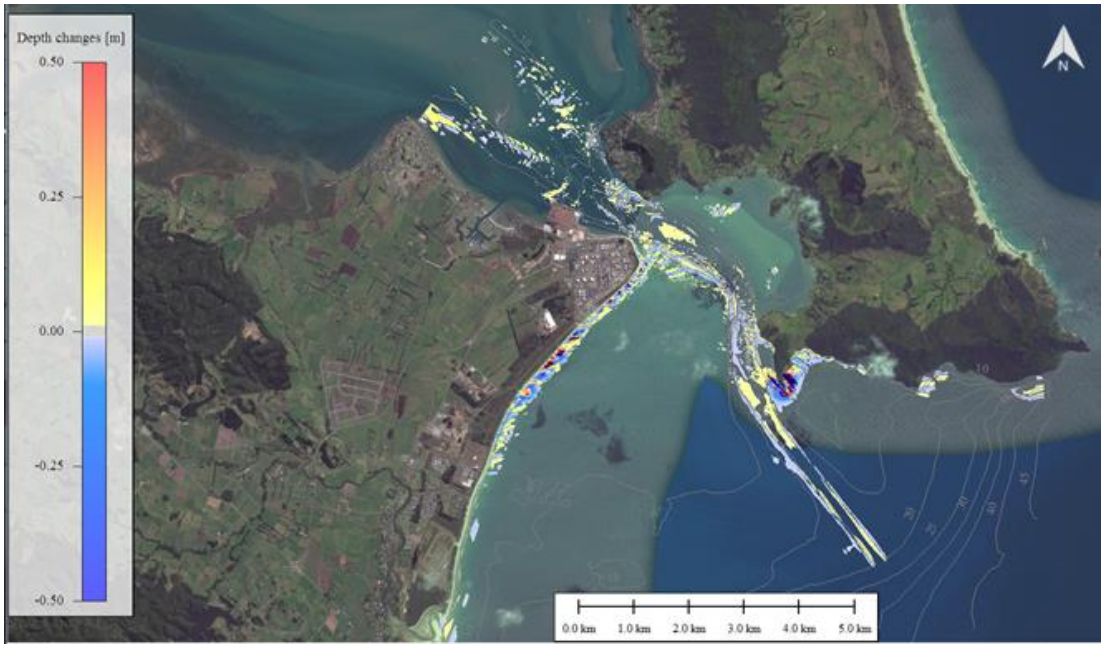

Figure 7.31 Changes in sedimentation and erosion patterns over the study area between the existing and post-deepening configurations over a 21-day sequence of storm and fair weather conditions.

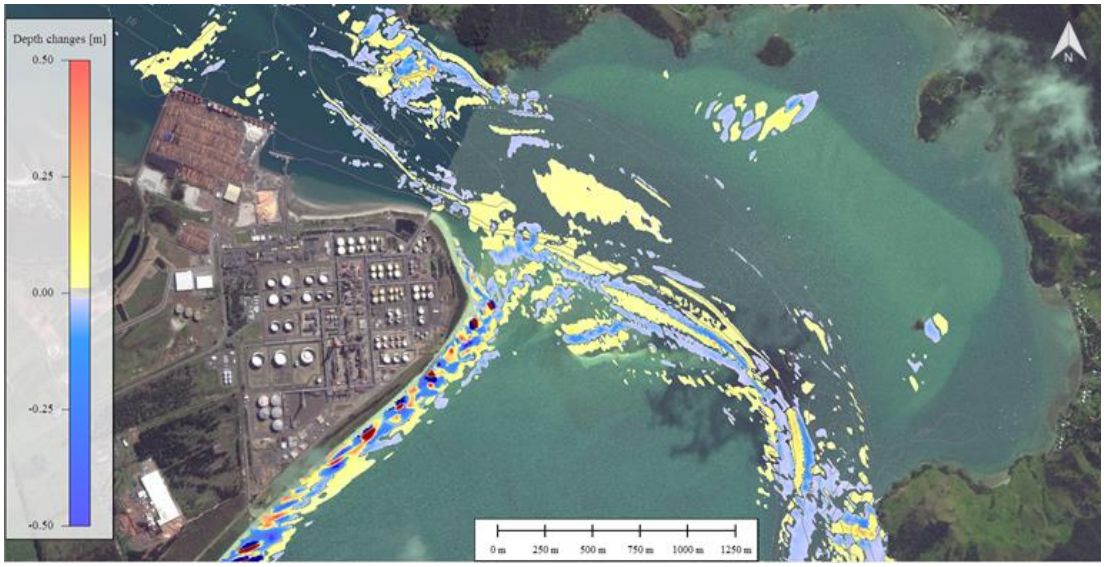

Figure 7.32 Changes in sedimentation and erosion patterns over the entrance to Whangarei Harbour between the existing and post-deepening configurations over a 21-day sequence of storm and fair weather conditions.

7.5. Estimates of channel infilling

Infilling of the deepened channel is expected to occur in some areas, and this will likely require a maintenance dredging programme to maintain the navigable design depth over time. While the historical 21-day simulation, which included both stormy and calm weather periods, indicates accretion of the order of a few centimetres in discrete parts of the channel, these results cannot simply be multiplied out to infer the annual accretion rate. First, there will be a period of adjustment as the margins of the new channel adjust to the new hydrodynamics. Then, the sequence of storms and daily tidal entrainment will actively redistribute a fraction of the mobile sediments. Finally, the source of sediment for infilling is primarily the adjacent ebb tidal delta. Interpretation of the model simulations and analysis of the historical observations suggest there will be two areas of channel accretion:

The first is the deepened area immediately adjacent to the Marsden Point jetty. Here the tidal flows are predicted to reduce by around 0.10 $m.s^{-1}$ and survey data shows over-wash of sediment from the ebb tide shoal. The sedimentation process at this location will be tidally dominated and relatively constant. The likely evolution pattern will be accretion from the southern shore of the ebb tidal delta outward into the main channel. This is different to the ebb tide migration of sand waves within the central channel, which is a phenomenon reported in the contemporary survey data. Based on the results provided by the short- and medium-term simulations, such accretion within the central channel is not expected to exceed 10 - 15 cm per year.

The second is the area within the offshore extent of the channel, south of Busby Head toward the distal margin. Here, the deepened channel is exposed to diffusive infilling from wave action but notably there are no strong cross-channel fluxes to drive rapid asymmetric infilling, as observed at other ports such as the Otago Harbour entrance (Weppe et al., 2015) and Port Taranaki (McComb et al., 1999). However, a change in the location and focussing of the ebb tide jet is predicted, and also in the magnitude of wave-driven currents near Busby Head. The source of infilling material to the channel is the immediate channel margins and the adjacent delta, and the rate of accretion is expected to decrease over time until equilibrium is reached.

A simulation of the annual infilling for the outermost section of the channel (i.e. from Busby Head to the distal margin) was made for the existing and the deepened channel. The difference in infilling is presented in Figure 8.33, and it highlights the two infilling processes in operation. Over this region, the interactions between biology and physics are not as critical as observed for other parts of the harbour entrance, thus allowing a more accurate medium-term prediction of the infilling processes. For the southern half of this section of channel, the accretion pattern is symmetrical and caused by diffusive sedimentation under wave action, with material being sourced from the adjacent areas of the delta. For the section immediately south of Busby Head, the accretion pattern is highly asymmetrical, with infilling occurring on the eastern side in response to the increased wave driven flows in storm conditions, as described in Section 4.2.

The anticipated post-dredging infilling rate over the section of the channel between Busby Head and the distal margin is 86,000 m^3 per year (based on a 0.4 - 0.8 m infilling along the flank of the channel and 0.1 m at the centre), with a margin of error of ± 36,000 m^3 per year. This margin was derived from the infilling predicted by the model for the existing channel, which in fact is stable and has not shown historical accretion. A practical volumetric estimate following establishment of an

equilibrium after several years would be 50,000- 100,000 m^3 per year, which corresponds approximately to 1 – 3 % of the total capital dredging volume.

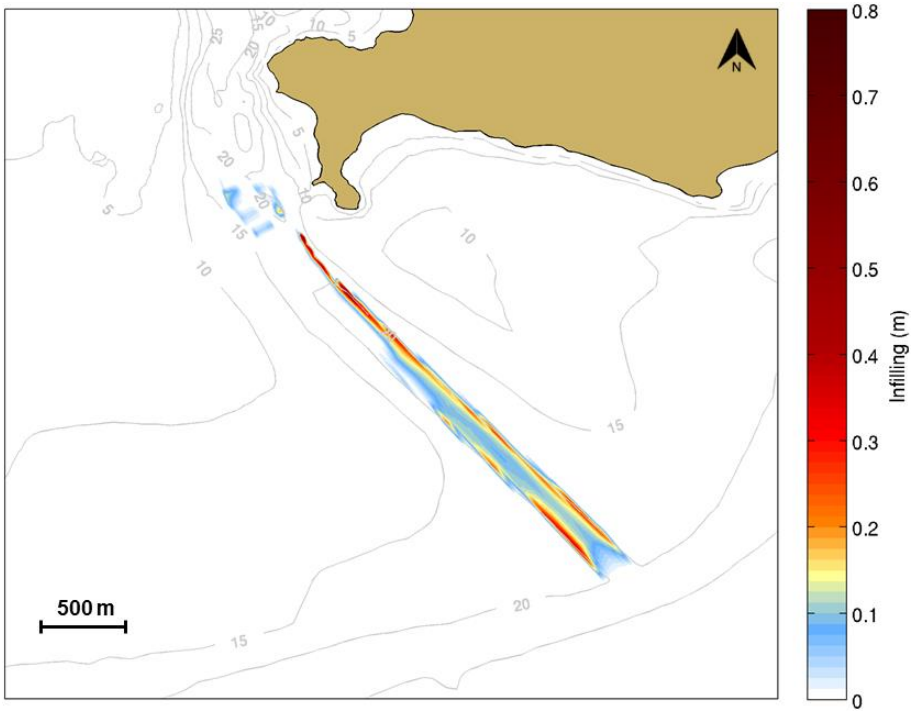

Figure 7.33 Predicted infilling in the outermost section of the channel between Busby Head and the distal margin to the delta estimated from a 1-year simulation including the post-dredging bathymetry.

7.6. Summary of effects on sediment transport

Several techniques were used to investigate the potential changes to the harbour entrance as a result of deepening. The first technique was to use a sediment transport pathway approach in which the spatial distribution of the important sediment fractions was simulated over a 6-month period. The second technique was to estimate the effect of a deeper channel on the potential sediment fluxes for a single representative sediment grain size. The third technique consisted of running a sequence of storm and fair-weather conditions over a 21-day historical period to simulate the cumulative morphological changes with a realistic seabed composition. Using these numerical techniques, changes in the erosion and accretion patterns were examined to allow a qualitative estimate of the effects of channel deepening. The findings are as follows:

- The sediment dynamics of the harbour entrance, controlled by the tide-induced currents and waves, are not expected to be fundamentally modified by the channel deepening project. The anticipated changes in the sediment transport fluxes are predicted to occur in spatially discrete zones and are expected to appear negligible compared to the total net sediment transport fluxes occurring through the main channel between the harbour and the open-ocean region.

- The morphodynamics of Mair Bank are largely influenced by the bio-stabilisation provided by live shellfish and their residual shell fragments. This bio-stabilisation is expected to have a more significant effect on future evolution of the Bank than the effect predicted by the proposed channel

deepening. The numerical model results infer that the shell armouring allowed Mair Bank to prevail in the presence of an energetic tidal regime and large temporal and spatial gradients in wave energy, consistent with historical observations and the wealth of previous investigations of this area. While the complexity of the interactions between the biological, morphological and hydrodynamic components do not allow quantitative predictions to be made with confidence, the model studies have confirmed the significance of the biomass of shellfish on the enduring stability of Mair Bank. Inside the high flow areas of the main channel the coarsening of the seabed by shell lagged sediments provides significant armouring and resistance to erosion. Within this context, and constrained by the model limitations, the simulations have reproduced the overall stability of the channel and the ebb tide delta. The stability of Mair Bank is largely controlled by the bio-stabilisation provided by the inhabiting populations of shellfish. The studies undertaken do not indicate that deepening within the channel will significantly change the sedimentary outcomes on Mair Bank.

- The sedimentary stability of Ruakaka Beach is not expected to be influenced by the slight variation in the wave conditions caused by channel deepening.

- Enhanced wave refraction along the eastern ridge of the channel may increase the potential "erodibility" of the seabed around Busby Head. However, this effect is likely to be mitigated by the sandy shelly-gravel top layer of the seabed, rendering it relatively high resistance to suspension and bedload transport processes. This assertion is further supported by the fact that Busby Head is currently occasionally subjected to 4-m wave height suggesting a relative high degree of stability of the sea bed.

- Sedimentation is expected to occur immediately adjacent to the Marsden Point jetty. Here, the tidal flows are predicted to reduce and the tidal asymmetry is expected to promote infilling of the deepened areas over time at a relatively constant rate. While a reliable volumetric estimate is difficult to provide, the likely evolution pattern will be accretion outward from the southern shore.

- A degree of infilling at the toe of Mair Bank may occur where the channel has been realigned.

- A 1–year simulation of the infilling of the channel south of Busby Head toward the distal margin was made. The results confirm a programme of maintenance dredging will likely be required for ongoing navigability. At this location, the deepened channel is exposed to diffusive infilling from wave action and there is a predicted change to the location and width of the ebb tide jet along with an increase in the sediment flux from the adjacent channel margins. The source of infilling material to the channel is the adjacent delta, and the rate of accretion is expected to decrease over time until equilibrium is reached. The infilling of this area is predicted by the model to be 86,000 m^3 per year with a margin of error of ±36,000 m^3/year. A practical estimate of infilling rates after several years is 50,000-122,000. m^3/year.

8. DREDGING PLUMES

The dispersion of a plume caused by dredging activities was simulated at several sites along the dredged channel design using the ERCore lagrangian particle modelling technique developed by MSL, forced by tidal currents provided by the SELFE tidal nearshore model. A detailed description of the processes that give rise to a plume for each dredger is provided in MSL Report P0297-01. The model settings considered include the typical type and size range of dredging vessels that might be used on the Crude Shipping Project. The plume dispersion associated with two different (large and small) trailing suction hopper dredgers (TSHD), one cutter suction dredger (CSD) and one Backhoe Dredger (BHD) was simulated in the present study. Different production and discharge rates were used for each dredger, leading to differences in the predicted plume dispersion. In this section, probabilistic assessments of the dispersion dynamics are provided for the dredging and overflow scenarios during the channel deepening operations.

As discussed in MSL Report P0297-01, the TSHD is the preferred option for the dredging operations. The use of a CSD at the jetty pocket and within the inner section of the channel was included in the present study for completeness in case it is required as an option. BHD operations will be restricted to the jetty pocket. Consequently, from the nine sites tested for the TSHD dredge plume modelling, only one site located in the proposed jetty pocket was set up, examining the potential effects of using a CSD and a BHD. The sediment release associated with the CSD was predicted to be confined to the near bottom layer due to the effect of the rotating cutter head. No overflow or propeller source terms were considered for this dredger (see methodology in MSL Report P0297-01). The large TSHD configuration was considered a worst case scenario, which is why only one site was tested for the CSD as the CSD generated plumes were proven to fall within the small and large TSHD plume effect ranges.

8.1. Dredging plume modelling results

A large number of scenarios were simulated representing typical conditions. A selection is provided here, while all the results are included in Appendix D. Specific areas including Marine Management Areas (as identified within the Operative Regional Coastal Plan), Marine Reserves and sensitive areas have been considered (see Figure 8.1) to show the limited impact of the dredging on the environment.

The results for the TSHD dredging and overflow stages in the present section are based on a 3% production rate for the drag head source and the maximum period of overflow (79 or 95 minutes depending of the size of the dredge). This is a conservative approach which aims to provide results for the "worst case" outcome. The modelled plume dispersions considering a 1.5% of production rate for the drag head source are provided in Appendix D.

The discharge rate associated with the rotating cutter head (CSD) was set up based on a 5% production rate near the bottom. This corresponds to the upper value of the range proposed in the literature. The bucket source term associated with the BHD was defined using a 4% discharge rate over the entire water column due to the excavation, hoisting and slewing phases during the dredging operations.

The exact timing of the dredging operations is unknown and will depend on a range of factors such as weather conditions, tides, or other time-dependent factors (e.g.

travel to and from disposal site, maintenance etc.). In that sense it is not meaningful to predict a suspended sediment concentration (SSC) time history over a defined period. Instead, a more informative way is to employ a probabilistic approach whereby the entire range of hydrodynamic forcing conditions are considered and from this produce a robust description of the range of SSC plumes that could be expected at a given site, for a given aspect of the operation.

Sediment releases associated with dredging and disposal operations may cause a significant increase of the turbidity over the adjacent areas affecting the light penetration, and consequently the adjacent ecological communities. In this context, a complementary literature review of the existing ecological systems and water quality was undertaken in Brian T. Coffey and Associates Limited (2016a) to provide a solid background for the environmental impact assessment of the Crude Shipping Project. Different levels of disturbance associated with the proposed dredging and spoil disposal activities were provided in Brian T. Coffey and Associates Limited (2016b) to support the interpretation of the dredge and disposal plume modelling results. On this basis, a minimum 12 mg/L SSC threshold was applied to delimit the plume dispersion. Such threshold corresponds to the difference between the 15 NTU level 2 Response Limit (based on one-hour average) indicated in Brian T. Coffey and Associates Limited (2016b) and the 3 NTU existing background level considering a 1:1 relationship between SSC and Turbidity. This linear relationship was established by Stewart (2017) analysing vibrocore samples from the dredging footprint. This methodology aims to assess the predicted SSC levels based on the level of tolerance for the adjacent communities, and thus to status on the degree of disturbance for the existing ecology. Details about the levels and the methodology applied to determine these thresholds are provided in Brian T. Coffey and Associates Limited (2016b).

In Whangarei Harbour entrance, where tidal forcing dominates, two complete spring-neap tidal cycles were used as a reference period to produce the probabilistic SSC plumes associated with the dredging and overflow phases. The SSC plumes were obtained by overlaying the successive particle clouds throughout the 28-day period and computing the SSC fields based on the combined particle clouds. These were computed for the dredging-only phase (i.e. no overflow) and also the four overflow durations, i.e. 10, 20, 50 and 79 minutes for the large TSHD. For the small TSHD, the overflow durations were 10, 20, 50 and 95 minutes. Probabilistic SSC plumes associated with the TSHD for both the dredging and the overflow phases at sites R0, R1, R5 and R6, for the existing hydrodynamics, are given in Figure 8.2 to Figure 8.5. The locations of the sites are shown in MSL Report P0297-01. Comparison between tidal and residual current velocities at the outermost sites R4 and R5 are provided in Appendix C. Although the non-tidal component is somewhat more significant at the seaward entrance of the delta than inside the channel, the tidal component remains dominant, which justifies the use of the *tide-only* nearshore model to force the particle tracking model. Moreover, the occasional high wind-driven flow acceleration highlighted by the non-tidal time series corresponds to storm events. Periods such as these are typical of storm events associated with high waves and strong winds and would not permit any dredging operations.

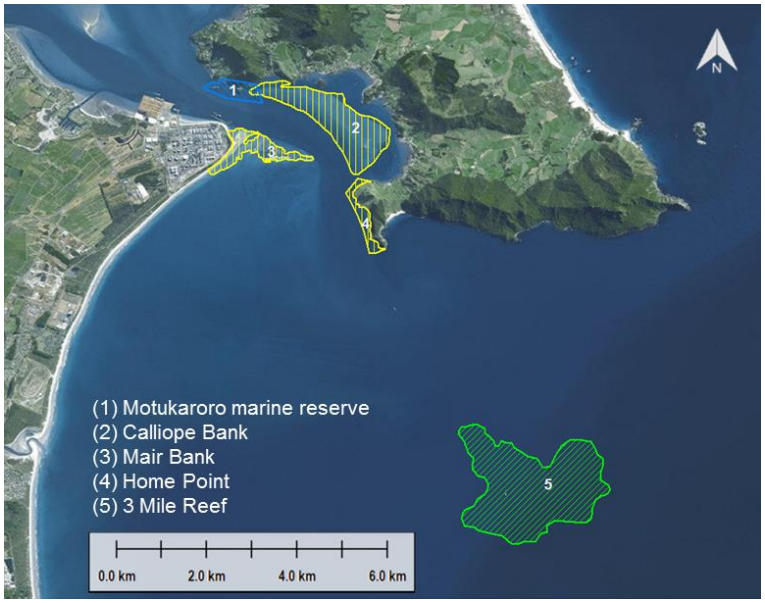

Figure 8.1 Location of the sensitive areas considered for the investigation of the dredging plume dispersion. The blue, yellow and green polygons depict Marine Reserves, Marine 1 (Protection) Management Areas and sensitive areas, respectively, used for the mapping of the dredging plume modelling results.

- Plumes associated with the use of large TSHD

The results show that SSC plumes produced by the drag head are constrained within the lower water column (bottom layer on plots), with negligible SSC levels predicted at mid-water and surface levels. In contrast, the overflow SSC plumes were widely spread across the entire water column, primarily due to the shallower release point and larger quantity of sediment involved.

The plume predictions exhibit considerable variation along the channel; consistent with the tidal flow regime. The plumes follow the channel orientations at sites R0, R1, and R6 while the patterns becomes more elliptical at site R5 where the tidal currents are less bi-directional due to increasing water depth near the delta entrance. Note that the dredging and overflow activities associated with the large TSHD generate larger SSC plumes than with the small TSHD. The maximum extension of the SSC plumes over a 24 h period do not exceed 1200 m at any of the sites examined (considering a minimum threshold of 12 mg/L), and are all constrained within the navigation channel. There is no dispersion of the plume over the adjacent beaches, sand banks, Marine Management Areas and Marine Reserves.

The overflow phase consists in releasing a highly concentrated mixture of water-sediment to maximise the amount of sediment stored in the hopper. The process is generally highly turbulent and will result in suspended sediment within the entire water column. The predicted SSC plumes associated with different overflow periods at sites R0 and R1 are illustrated in Figure 8.6 to Figure 8.9; the overflow duration has a significant effect on the magnitude and extent of the SSC plume.

The difference in the predicted SSC plumes between the existing channel and the post-dredging channel at sites R2 and R3 are illustrated in Figure 8.10 to Figure 8.13. A deeper channel results in a reduced excursion of the plume, as the tidal velocities are slightly decreased. This is particularly evident at site R3 where the

SSC plume dispersion due to the ebb-tidal flows is much more constrained in the post-dredging scenario than in the existing channel one.

The sensitivity analysis undertaken to examine the effect on the predicted plume dispersion of higher silt fraction (10%), lower settling velocity (0.4 mm/s) associated with silt particles and different release extensions (cylinders of 20 m x 100 m and 40 m x 60 m) during overflow did not reveal any fundamental changes in the plume dispersion as shown in Appendix H. The low fraction of silt particles within the tested release (from 5 to 10%) explains largely the relative low impact of these conservative parameters on the plume delimited by the 12 mg/L threshold.

- Plumes associated with the use of CSD

The results show that SSC plumes produced by the rotating cutter head are constrained to the bottom layer of the water column (Figure 8.14), with a relative small horizontal extension (< 200m) due to low current velocities near the seabed. The use of floating pipelines to discharge the sediment sucked up by dredge pumps avoid any sediment losses associated with overflow which tend to considerably limit the plume dispersion within the water column compared to the TSHD. The plume modelling of the CSD was limited to Site R0. The TSHD configuration was considered a worst-case option, and this plume modelling option was used for the other sites in the inner section of the channel, considering that the plume dispersion for the CSD would be always lower in SSC. The use of a CSD is not expected to produce any significant plume extension over Marine Management Areas, Marine Reserve, sand banks or adjacent beaches. The sediment settling is expected to be quick, particularly for the sandy particles.

- Plumes associated with the use of BHD

The use of a BHD is predicted to cause sediment losses over the entire water column at the RNZ Jetty pocket (Site R0). Although the discharge rate is relatively high (up to 4% over the entire water column), the absolute sediment releases dependent on the hourly production rate estimated for the operations using the BHD (source: RHDHV) remains relative low compared to the TSHD configuration. The results show that SSC plumes produced by the excavation, hoisting and slewing phases are expected to create a maximum horizontally extended plume of 210 m after 24 h. The BHD plume dispersion is thus less than that modelled for the TSHD which was considered the worst case scenario in the present study. No sediment depositions over Marine Management Areas, Marine Reserve, sand banks or adjacent beaches were predicted.

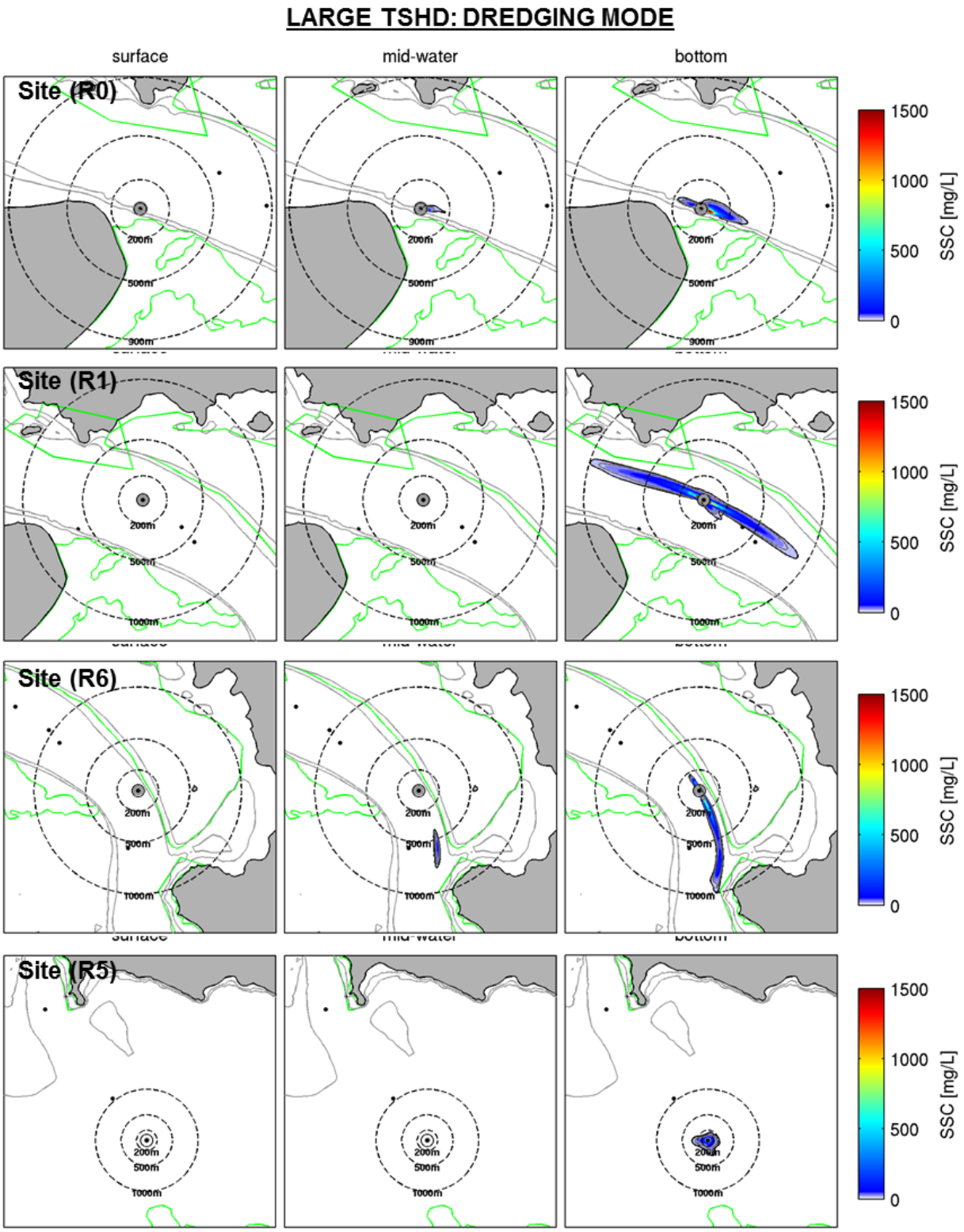

Figure 8.2 Probabilistic *SSC* plumes during dredging phase (large trailing suction hopper dredger, TSHD) at sites R0, R1, R6 and R5 at three levels of the water column presented in MSL Report P0297-01. The drag head source rate used is 3% and the minimum threshold of SSC is 12 mg/L (black line). The grey contours indicate the 10 and 20 m isobaths delimiting the channel. The green polygons show the area of interest in terms of environment impact.

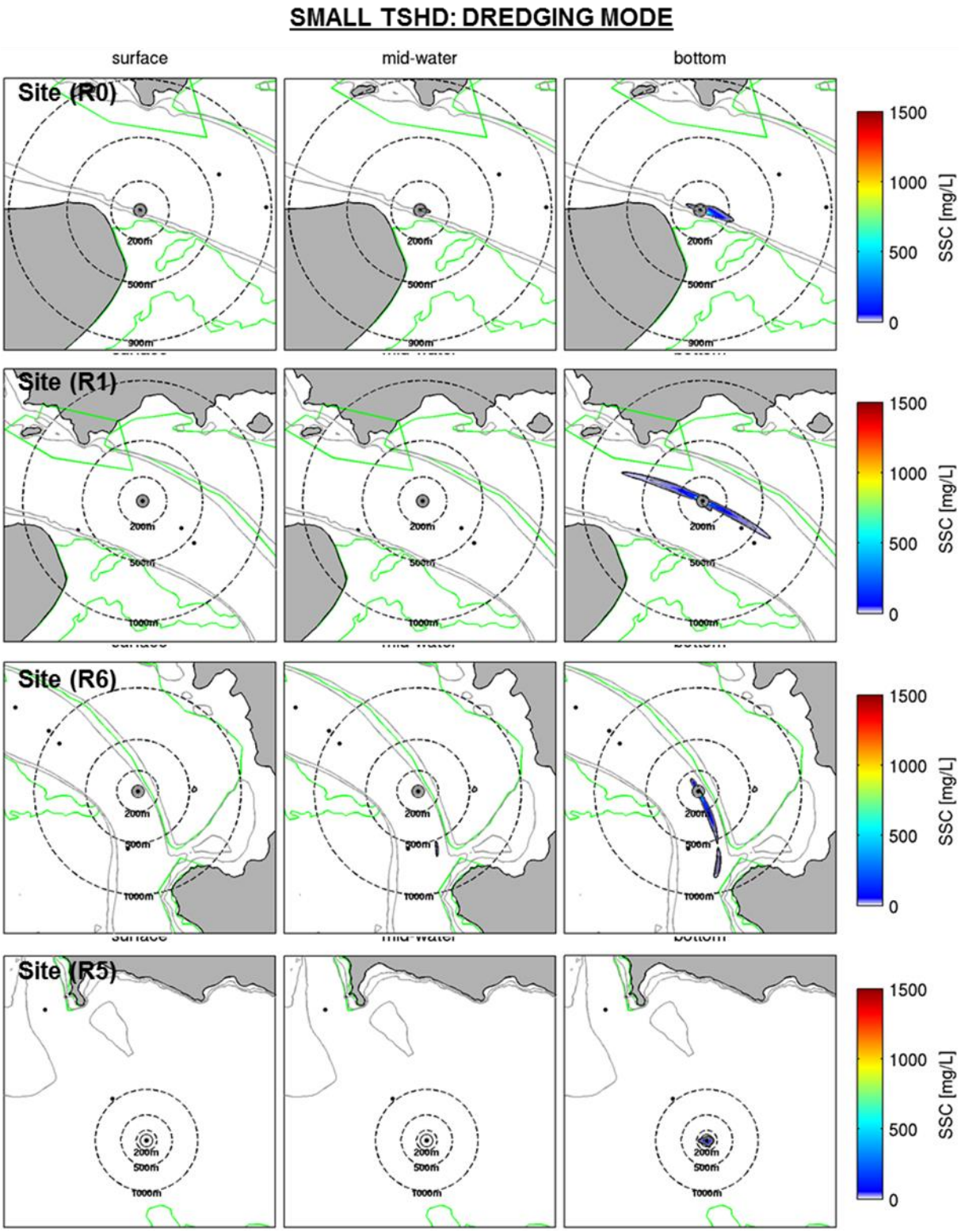

Figure 8.3 Probabilistic *SSC* plumes during dredging phase (small trailing suction hopper dredger, TSHD) at sites R0, R1, R6 and R5 at three levels of the water column presented in MSL Report P0297-01. The drag head source rate used is 3% and the minimum threshold of SSC is 12 mg/L (black line). The grey contours indicate the 10 and 20 m isobaths delimiting the channel. The green polygons show the areas of interest in terms of environment impact.

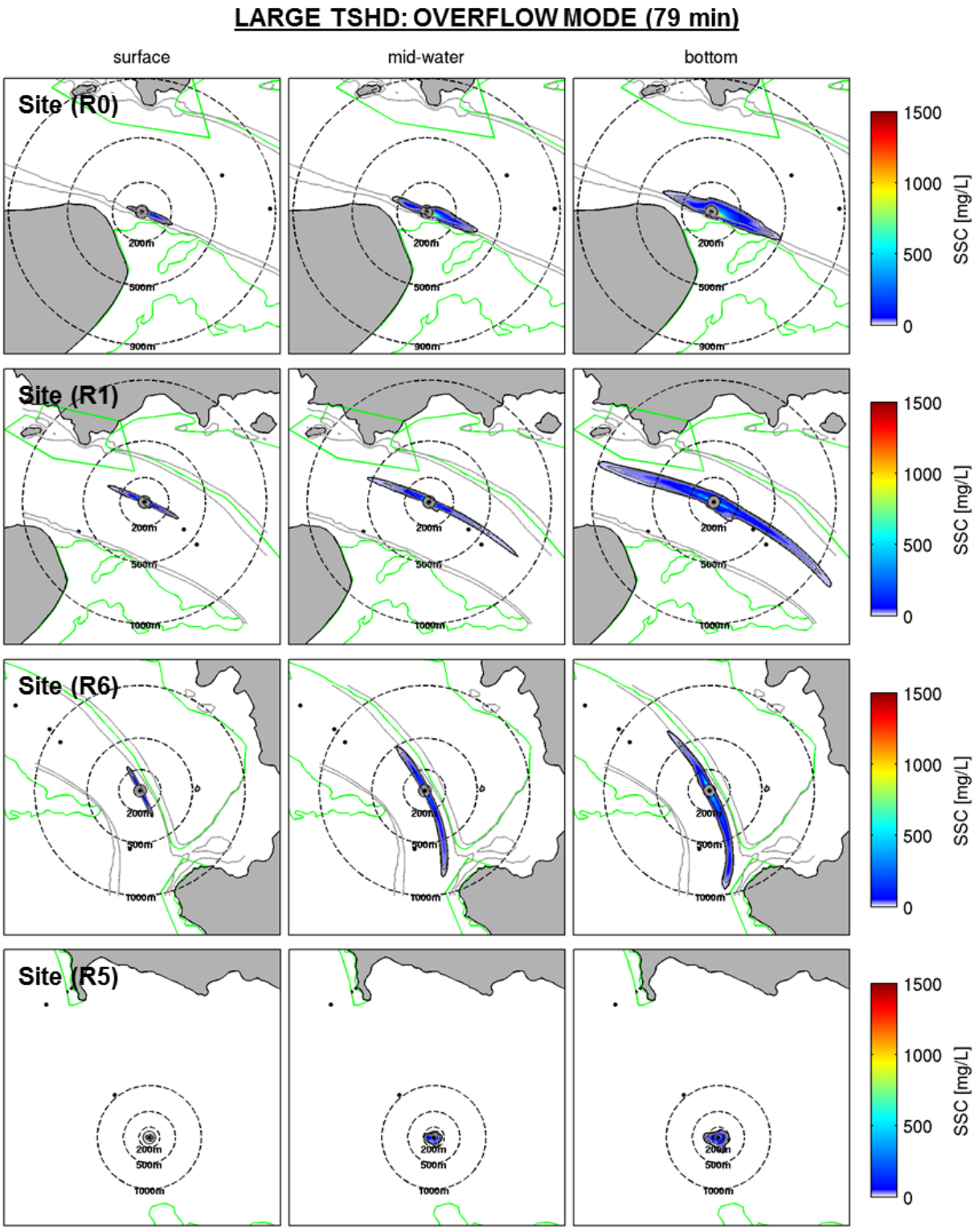

Figure 8.4 Probabilistic *SSC* plumes during overflow phase (large trailing suction hopper dredger, TSHD) at sites R0, R1, R6 and R5 at three levels of the water column presented in MSL Report P0297-01. SSC plumes are illustrated for a 79 min period. The minimum threshold of SSC is 12 mg/L (black line). The grey contours indicate the 10 and 20 m isobaths delimiting the channel. The green polygons show the areas of interest in terms of environment impact.

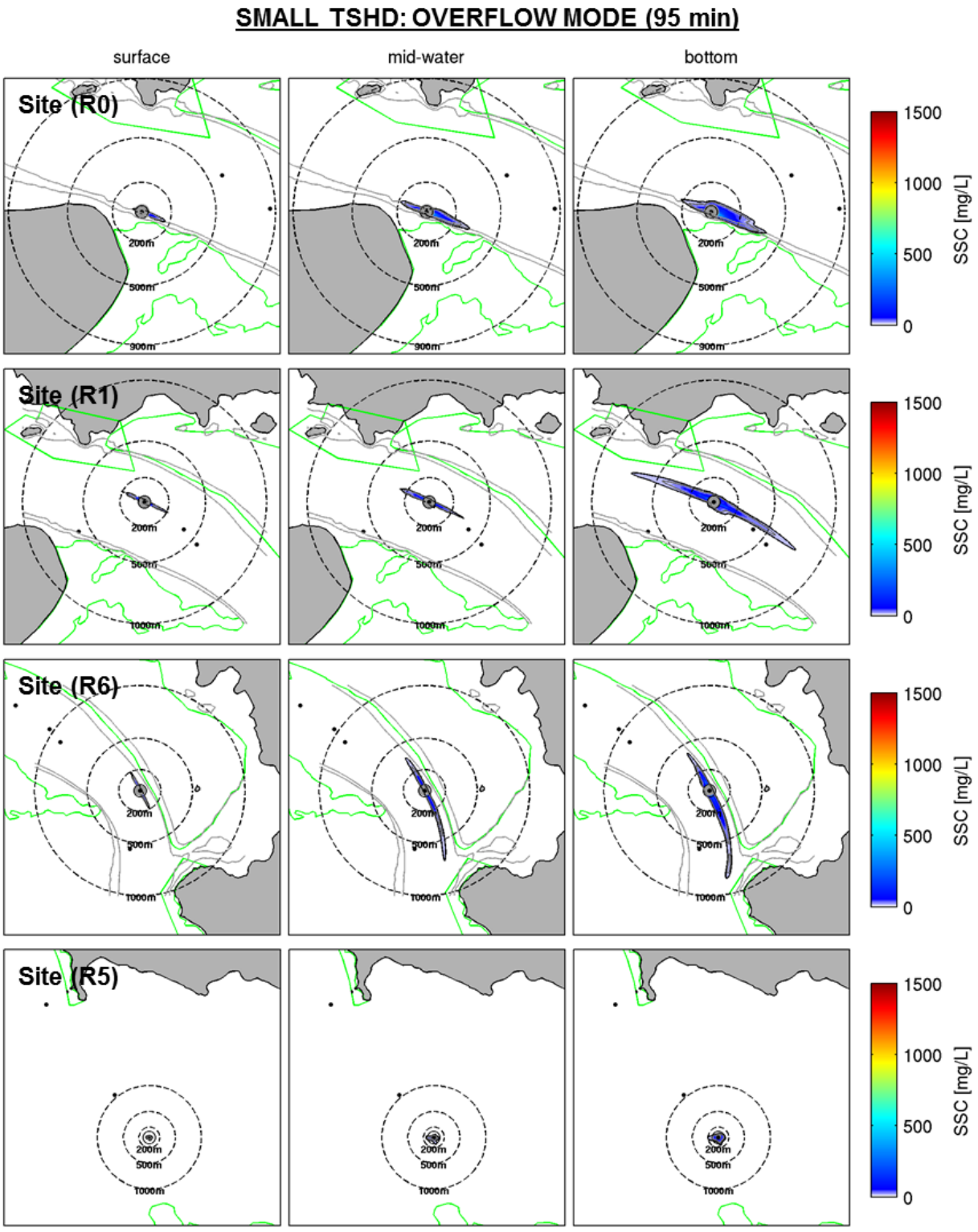

Figure 8.5 Probabilistic *SSC* plumes during overflow phase (small trailing suction hopper dredger, TSHD) at sites R0, R1, R6 and R5 at three levels of the water column presented in MSL Report P0297-01. SSC plumes are illustrated for a 95 min period. The minimum threshold of SSC is 12 mg/L (black line). The grey contours indicate the 10 and 20 m isobaths delimiting the channel. The green polygons show the areas of interest in terms of environment impact.

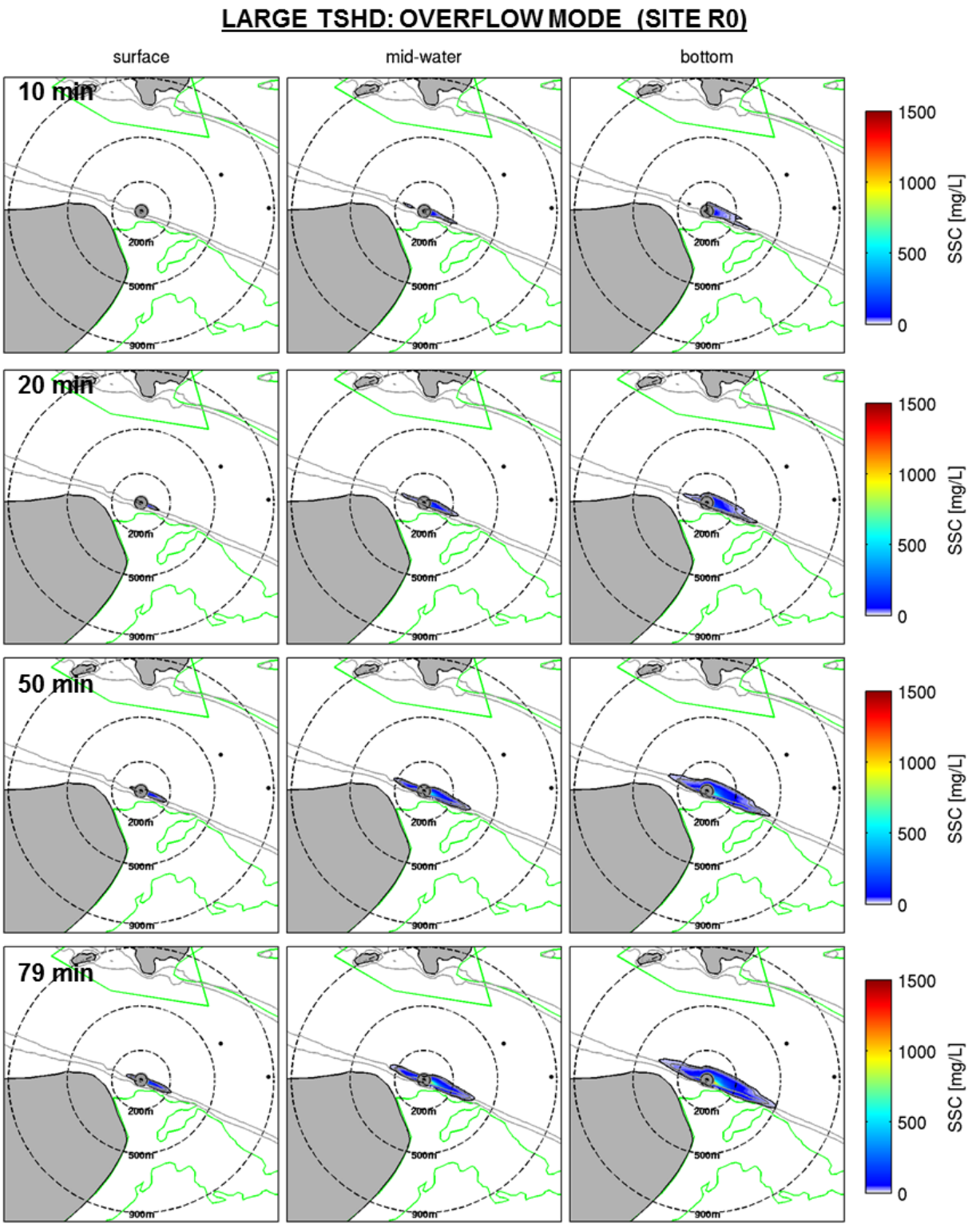

Figure 8.6 Probabilistic *SSC* plumes during overflow phase (large trailing suction hopper dredger, TSHD) at site R0 at three levels of the water column presented in MSL Report P0297-01. SSC plumes are illustrated for a 10, 30, 50 and 79 min period of overflow. The minimum threshold of SSC is 12 mg/L (black line). The grey contours indicate the 10 and 20 m isobaths delimiting the channel. The green polygons show the areas of interest in terms of environment impact.

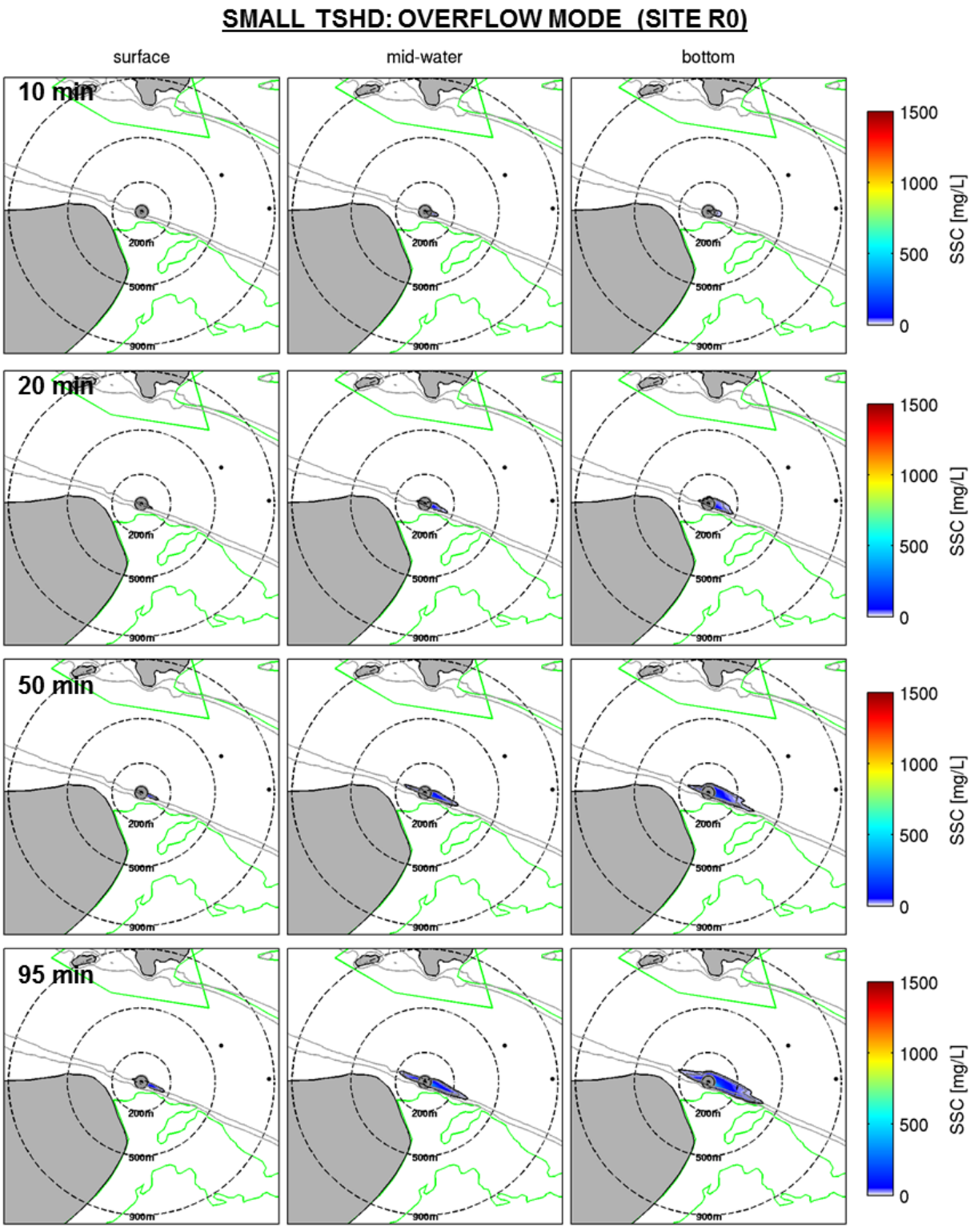

Figure 8.7 Probabilistic *SSC* plumes during overflow phase (small trailing suction hopper dredger, TSHD) at site R0 at three levels of the water column presented in MSL Report P0297-01. SSC plumes are illustrated for a 10, 30, 50 and 95 min period of overflow. The minimum threshold of SSC is 12 mg/L (black line). The grey contours indicate the 10 and 20 m isobaths delimiting the channel. The green polygons show the areas of interest in terms of environment impact.

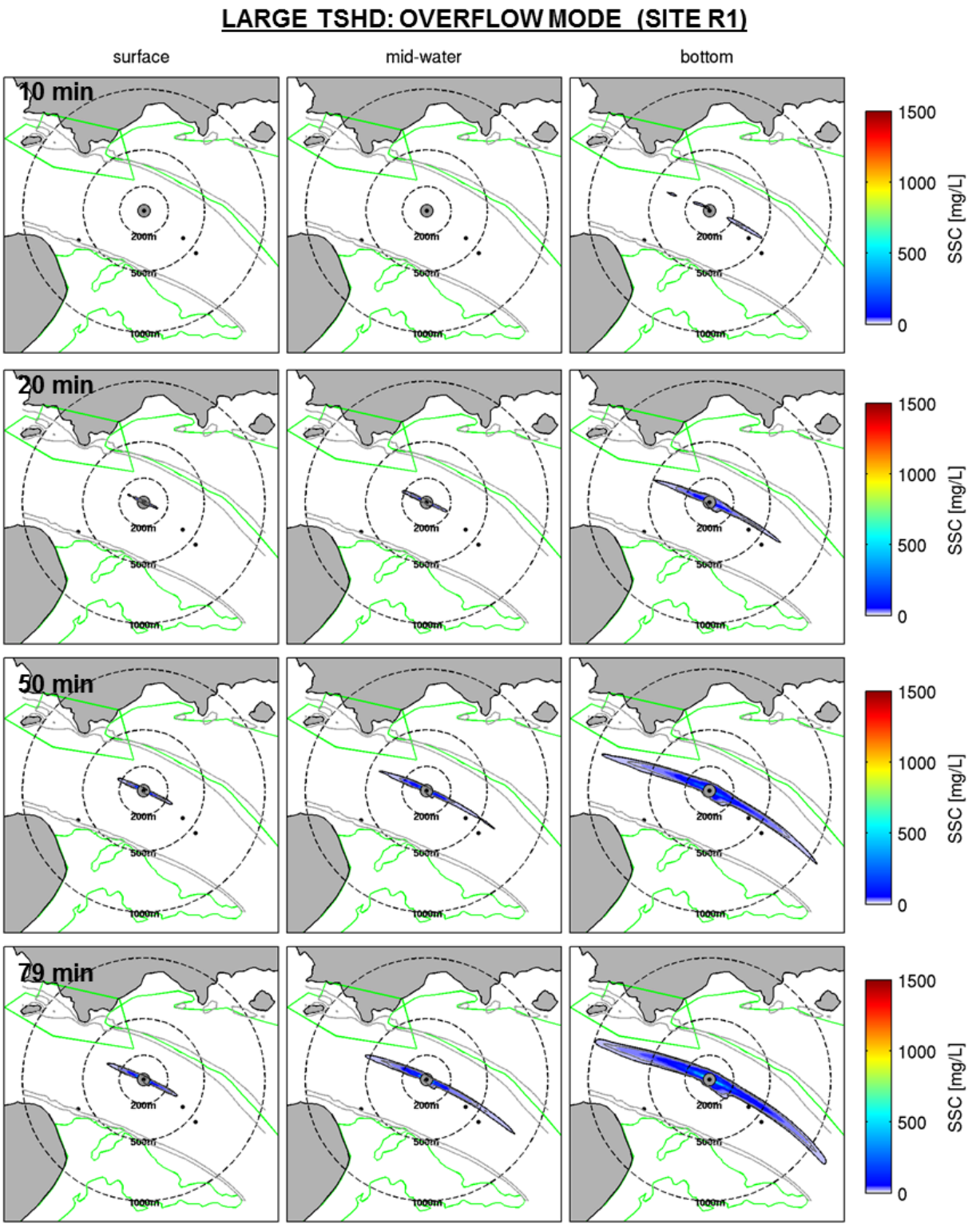

Figure 8.8 Probabilistic *SSC* plumes during overflow phase (large trailing suction hopper dredger, TSHD) at site R1 at three levels of the water column presented in MSL Report P0297-01. SSC plumes are illustrated for a 10, 30, 50 and 79 min period of overflow. The minimum threshold of SSC is 12 mg/L (black line). The grey contours indicate the 10 and 20 m isobaths delimiting the channel. The green polygons show the areas of interest in terms of environment impact.

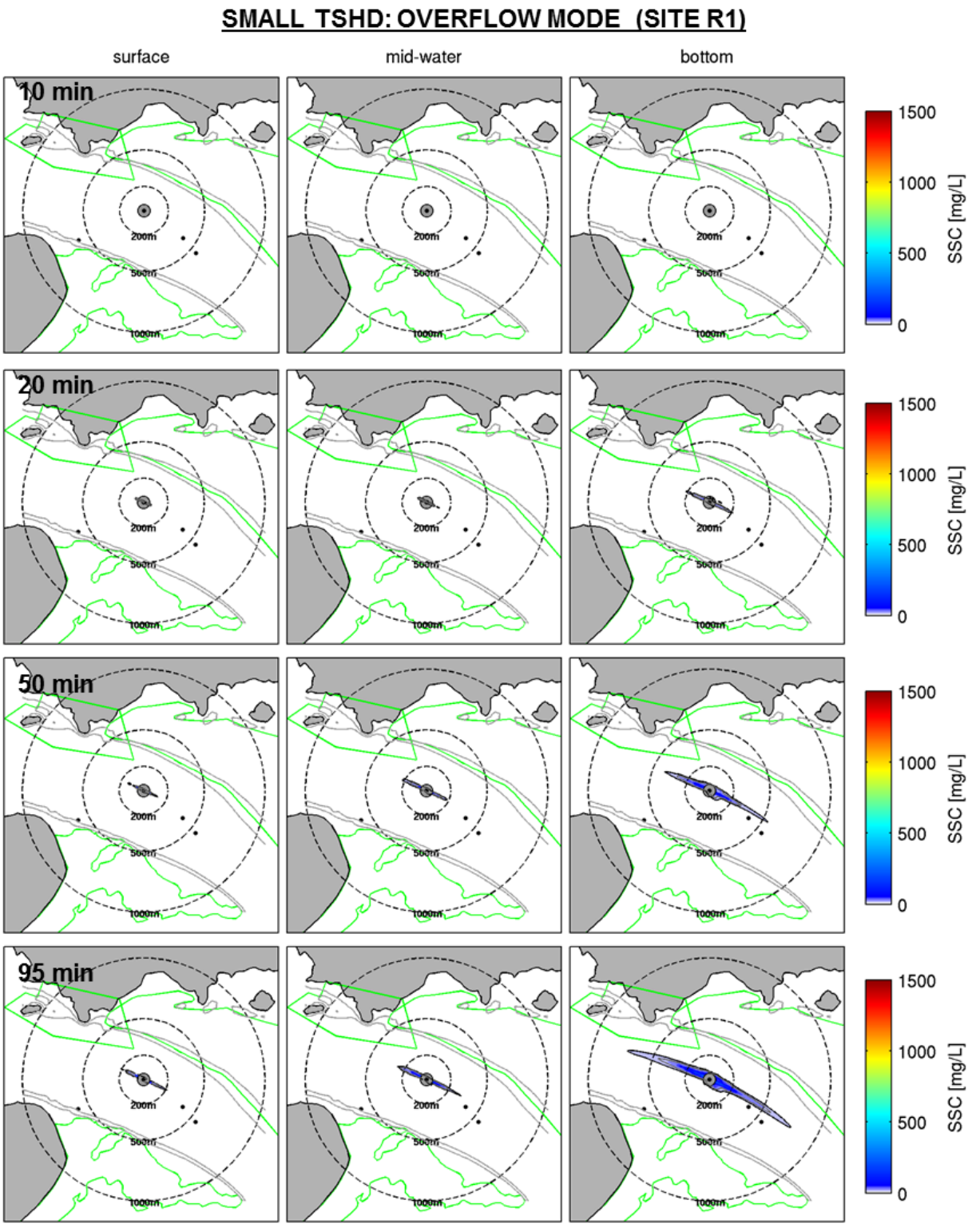

Figure 8.9 Probabilistic *SSC* plumes during overflow phase (small trailing suction hopper dredger, TSHD) at site R1 at three levels of the water column. SSC plumes are illustrated for a 10, 30, 50 and 95 min period of overflow. The minimum threshold of SSC is 12 mg/L (black line). The grey contours indicate the 10 and 20 m isobaths delimiting the channel. The green polygons show the areas of interest in terms of environment impact.

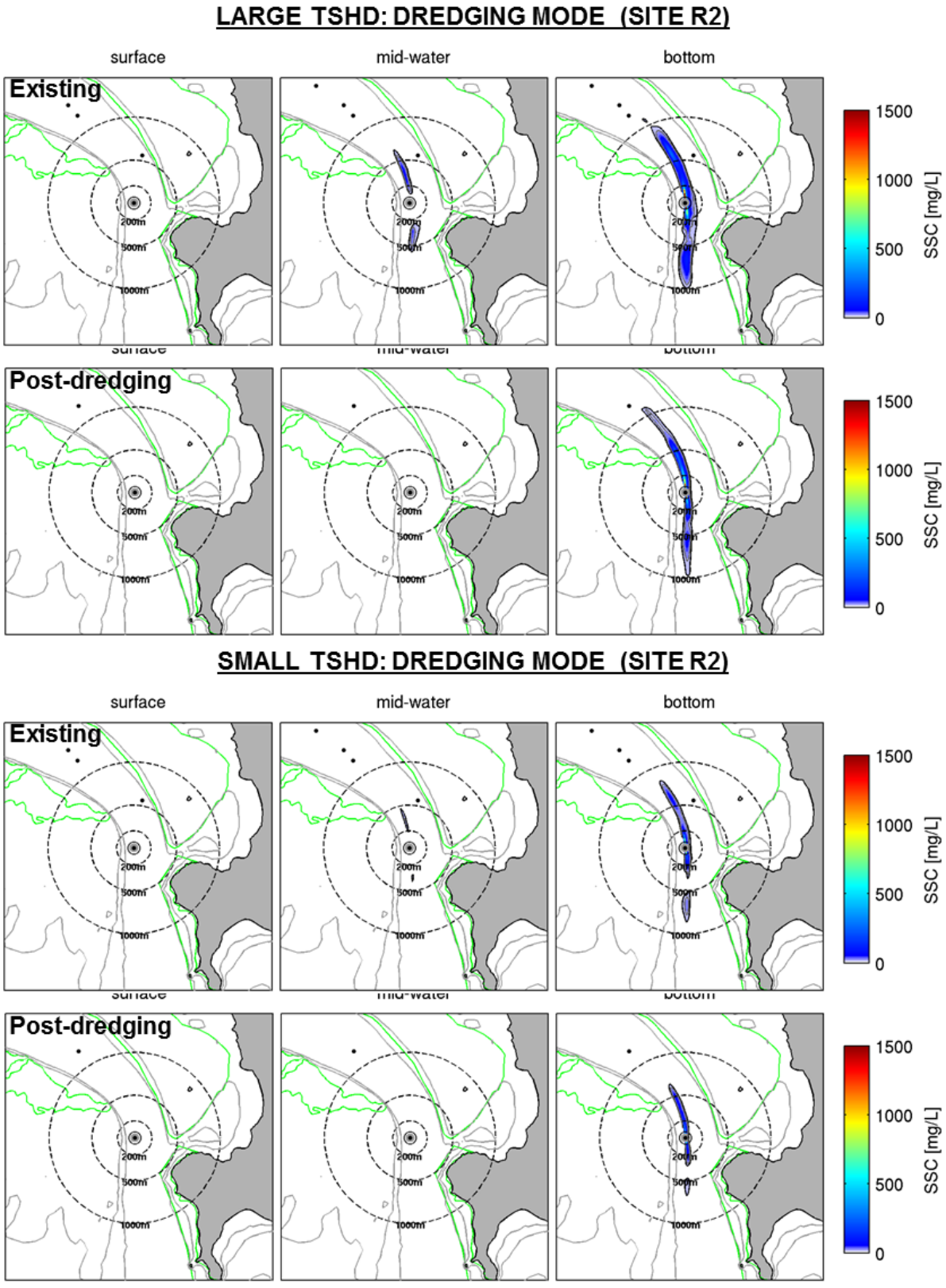

Figure 8.10 Probabilistic *SSC* plumes during dredging phase at site R2 for both the large (top) and the small (bottom) trailing suction hopper dredger (TSHD) considering the existing and the post-dredging configurations. The minimum threshold of SSC is 12 mg/L (black line). The grey contours indicate the 10 and 20 m isobaths delimiting the channel. The green polygons show the areas of interest in terms of environment impact.

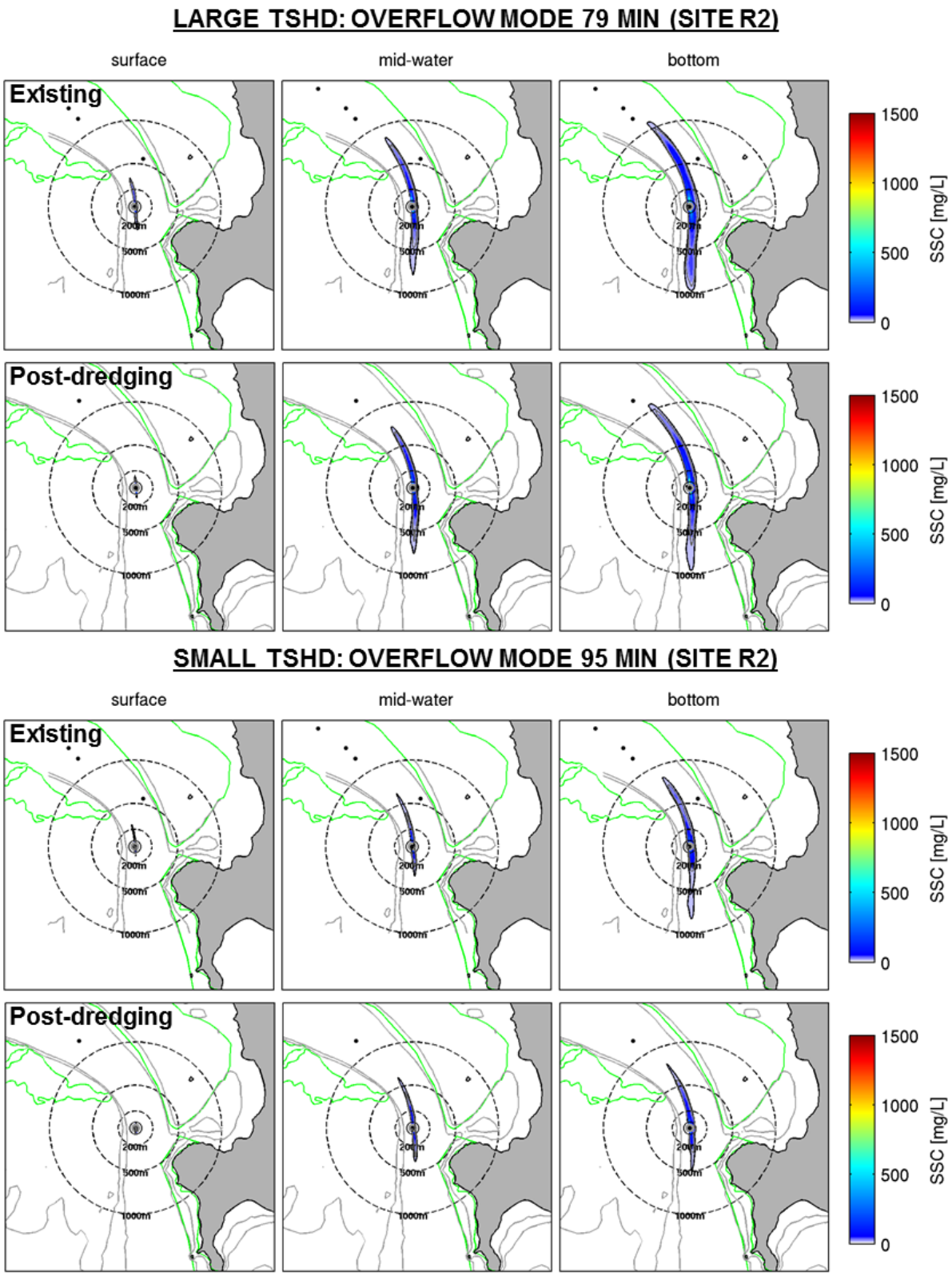

Figure 8.11 Probabilistic *SSC* plumes during overflow phase at site R2 for both large (top) and small (bottom) trailing suction hopper dredger (TSHD) considering the existing and the post-dredging configurations. SSC plumes are illustrated for a 79 min and 95 min period of overflow depending on the barge. The minimum threshold of SSC is 12 mg/L (black line). The grey contours indicate the 10 and 20 m isobaths delimiting the channel. The green polygons show the areas of interest in terms of environment impact.

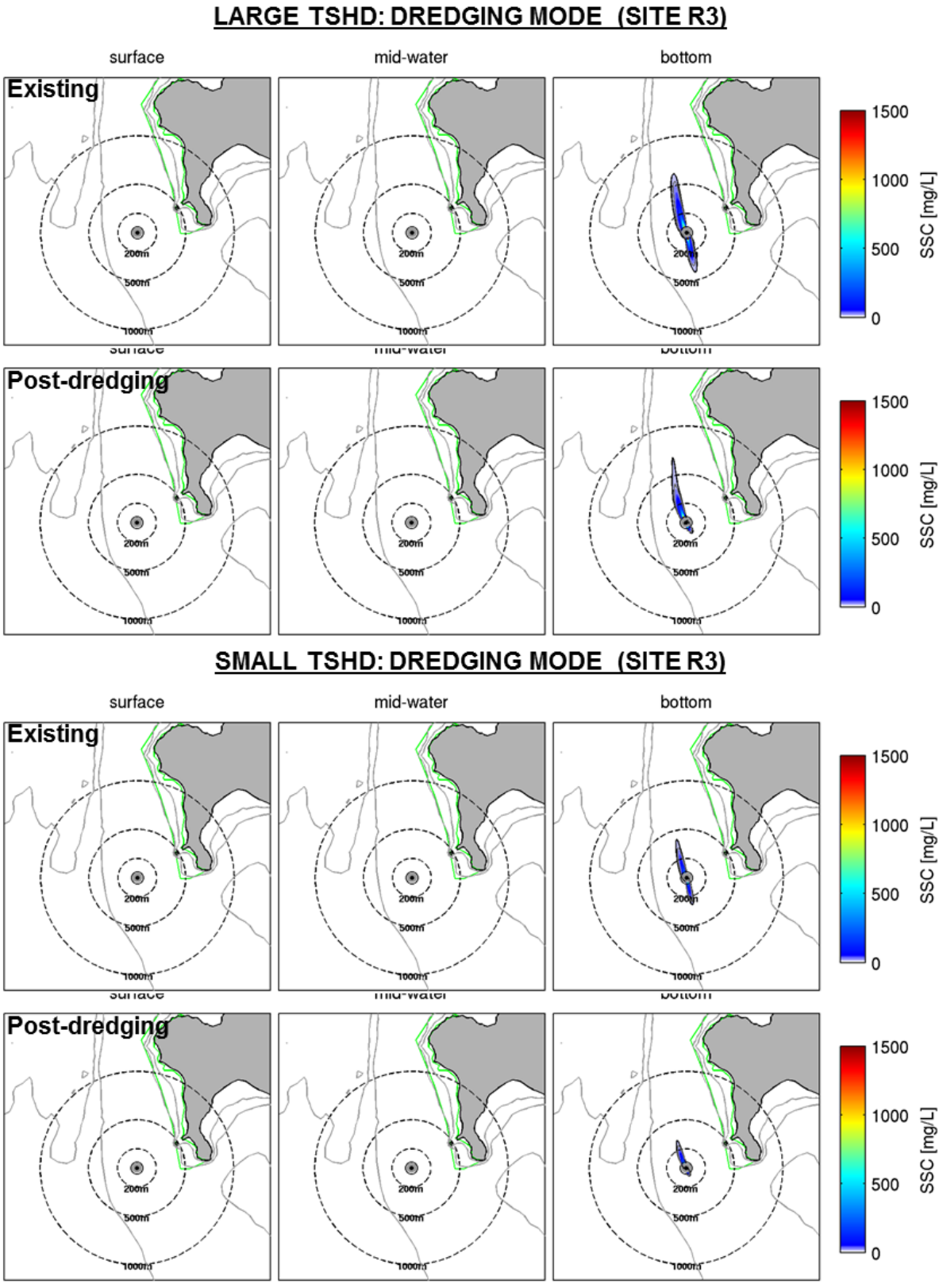

Figure 8.12 Probabilistic *SSC* plumes during dredging phase at site R3 for both the large (top) and the small (bottom) trailing suction hopper dredger (TSHD) considering the existing and the post-dredging configurations. The minimum threshold of SSC is 12 mg/L (black line). The grey contours indicate the 10 and 20 m isobaths delimiting the channel. The green polygons show the areas of interest in terms of environment impact.

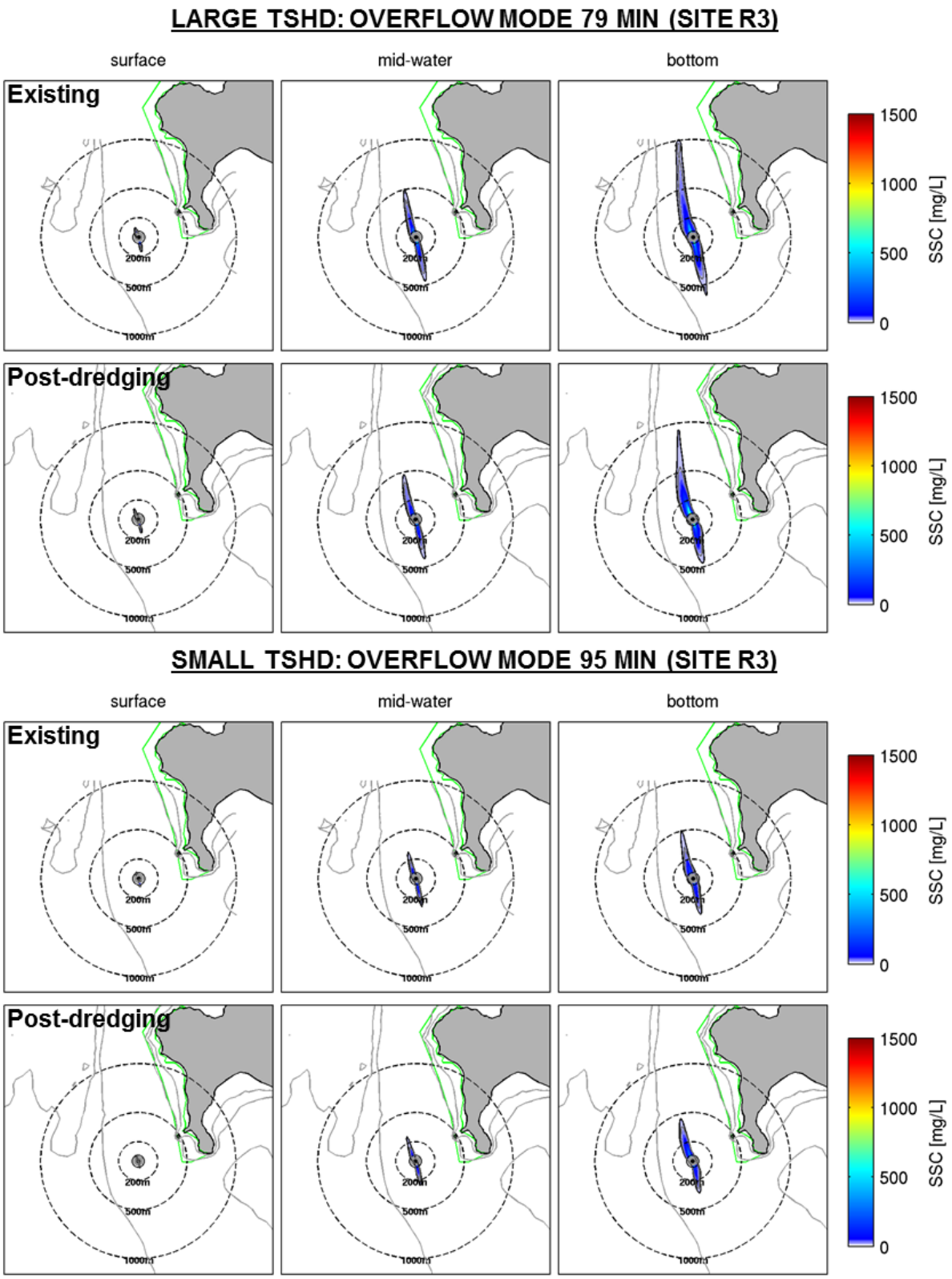

Figure 8.13 Probabilistic *SSC* plumes during overflow phase at site R3 for both large (top) and small (bottom) trailing suction hopper dredger (TSHD) considering the existing and the post-dredging configurations. SSC plumes are illustrated for a 79 min and 95 min period of overflow depending on the barge.

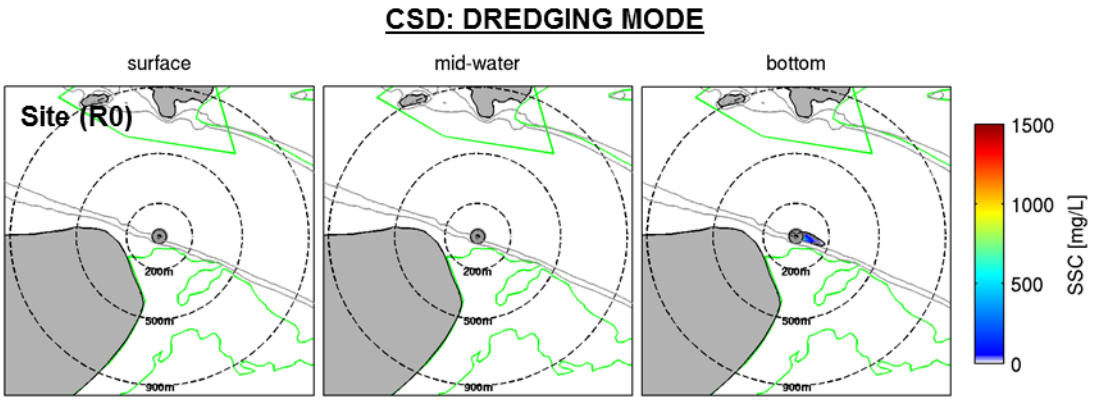

Figure 8.14 Probabilistic *SSC* plumes during dredging at site R0 for cutter suction dredger (CSD) considering the existing configuration.

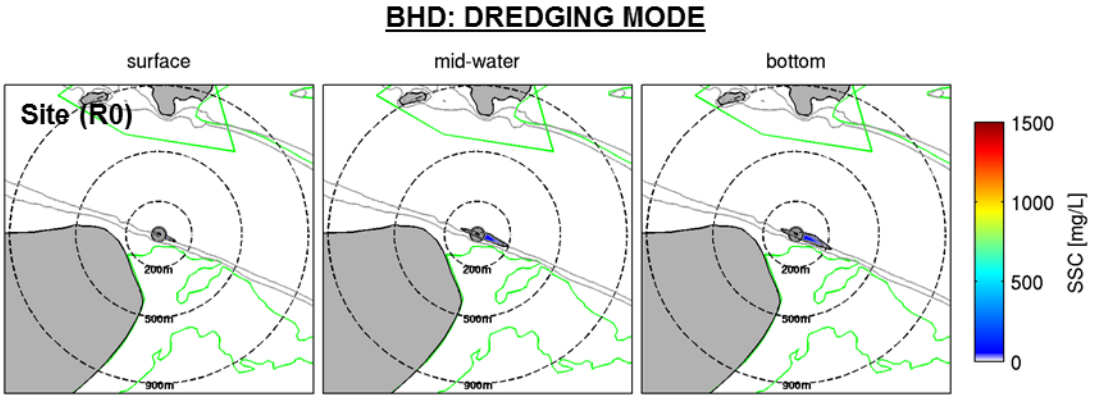

Figure 8.15 Probabilistic *SSC* plumes during dredging at site R0 for backhoe dredger (BHD) considering the existing configuration.

8.2. Summary of dredging plumes

The modelling of the dredging plumes has showed that:

- The sediment plumes associated with dredging and caused by the action of the drag head (TSHD) are predicted to remain constrained within the lower water column, with negligible expression at mid-water and surface levels. In contrast, the sediment plumes associated with the overflow phase are predicted to be spread across the entire water column.

- The resultant plumes from either source are predicted to follow the general channel alignment, consistent with the tidal currents. The maximum modelled excursion of any plume did not exceed 1200 m, with the plume constrained to the channel. The modelling shows no evidence of plume dispersion to the adjacent beaches, sand banks, Marine 1 (Protection) Management Areas or Marine Reserves. The sensitivity analysis carried out using conservative configurations of the sediment release during dredging did not show any fundamental changes in the plume dispersion.

- The modelling shows that the large TSHD generates more extended and concentrated plumes than the smaller vessel. The overflow duration has a significant effect on the magnitude and extent of the plumes.

- The sediment plumes associated with dredging and caused by the action of the rotating cutter head (CSD case) are predicted to remain constrained within the lower water column, with no expression at mid-water and surface levels.

- The sediment plumes associated with dredging and caused by the excavation, hoisting and slewing phases (BHD case) are expected to generate sediment losses over the entire water column. The low production rate associated with the BHD lead, however, to a low discharge rate compared to the TSHD case.

- Comparisons between plumes generated for the existing channel and the post-dredging scenario indicates that the plume excursions will decrease slightly as the channel becomes deeper due to the slightly reduced tidal velocities.

- No plume dispersion extending to the adjacent beaches, sand banks, Marine 1 Management Areas and Marine Reserves were generated by the dredging plume modelling for any of the dredge scenarios.

9. DISPOSAL GROUND DYNAMICS

9.1. Wave climate

The region of Bream Bay where the proposed offshore disposal Area 3.2 is located (Figure 1.4) is characterised by a relatively low energy wave climate, occasionally affected by short-duration storms and cyclonic events. The wave rose, calculated at the centre of the ground from 10-year hindcast data and illustrated in Figure 9.1, indicates that the wave propagation over the disposal ground is largely dominated by the north-eastern direction. The site is partially sheltered by Bream Head and the offshore islands from northerly and easterly swells, respectively. The modelled wave height fields shown in Figure 9.3 and Figure 9.4 for different wave scenarios exhibit these features explicitly.

At the disposal ground the water depth exceeds 40 m and therefore the wave orbital velocities near the seabed are generally below the threshold required to initiate sediment transport (i.e. less than 0.2 m/s). During storm events involving wave heights between 4 – 6 m (see Figure 9.2) and peak wave periods higher than 10 – 12 s, the near bed wave orbital velocities exceed 0.4 $m.s^{-1}$ (Figure 9.5 and Figure 9.6) which is strong enough to initiate entrainment and transport of sand particles (in suspension or by bedload), depending on the grain size (see diagrams in Figure 7.3 and Figure 7.4).

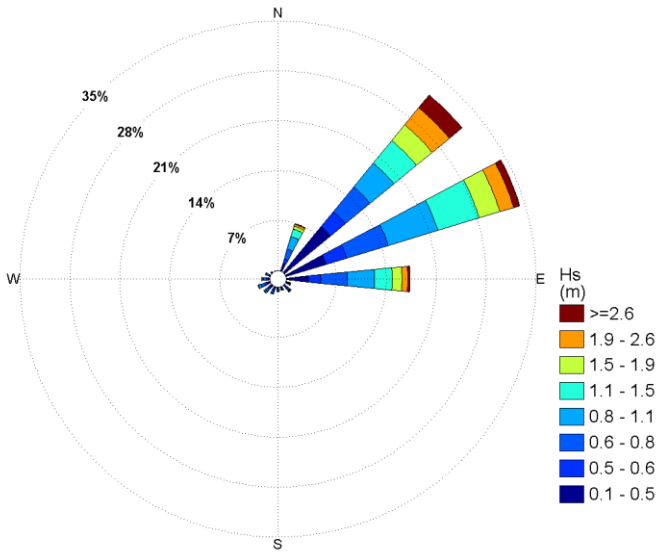

Figure 9.1 Wave rose for the proposed disposal ground from 10-year wave hindcast (2005 – 2014). Wave directions are in the ‘‘coming from’’ convention.

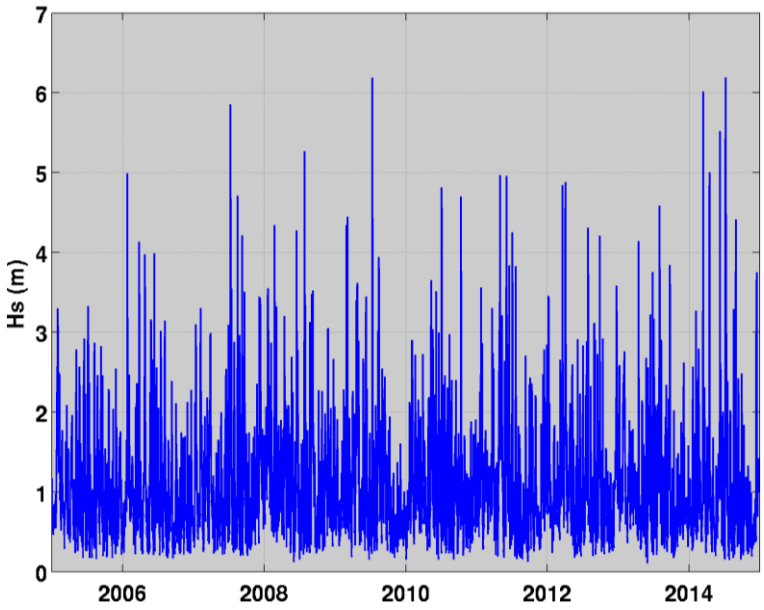

Figure 9.2 Time series (2005 – 2014) of modelled significant wave height (Hs) within the proposed disposal ground.

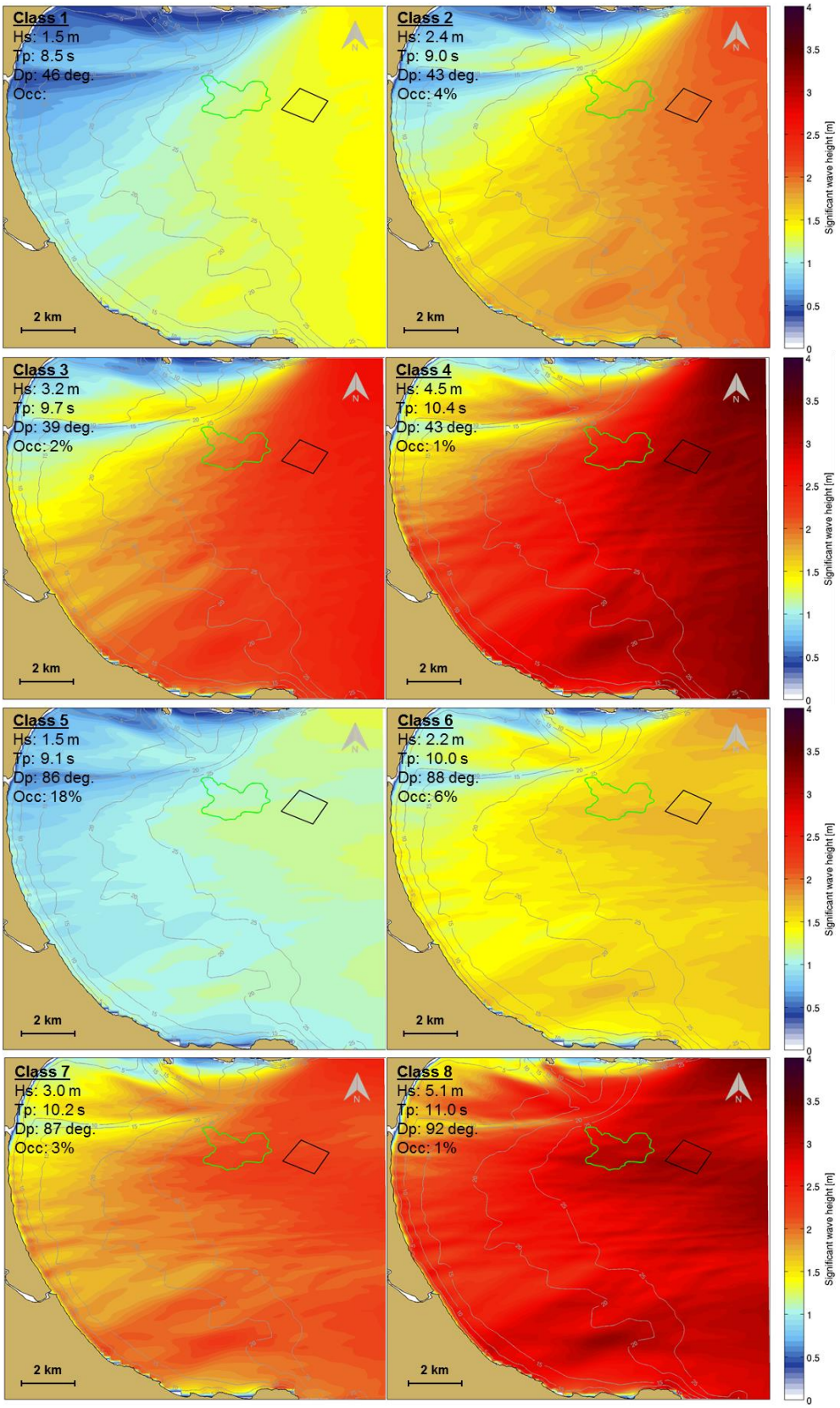

Figure 9.3 Wave height fields over Bream Bay for wave classes 1 to 8. Hs, Tp, Dp and Occ (% Occurrence) presented in the upper left corner indicate the wave conditions at the offshore position BND (see MSL Report P0297-01).

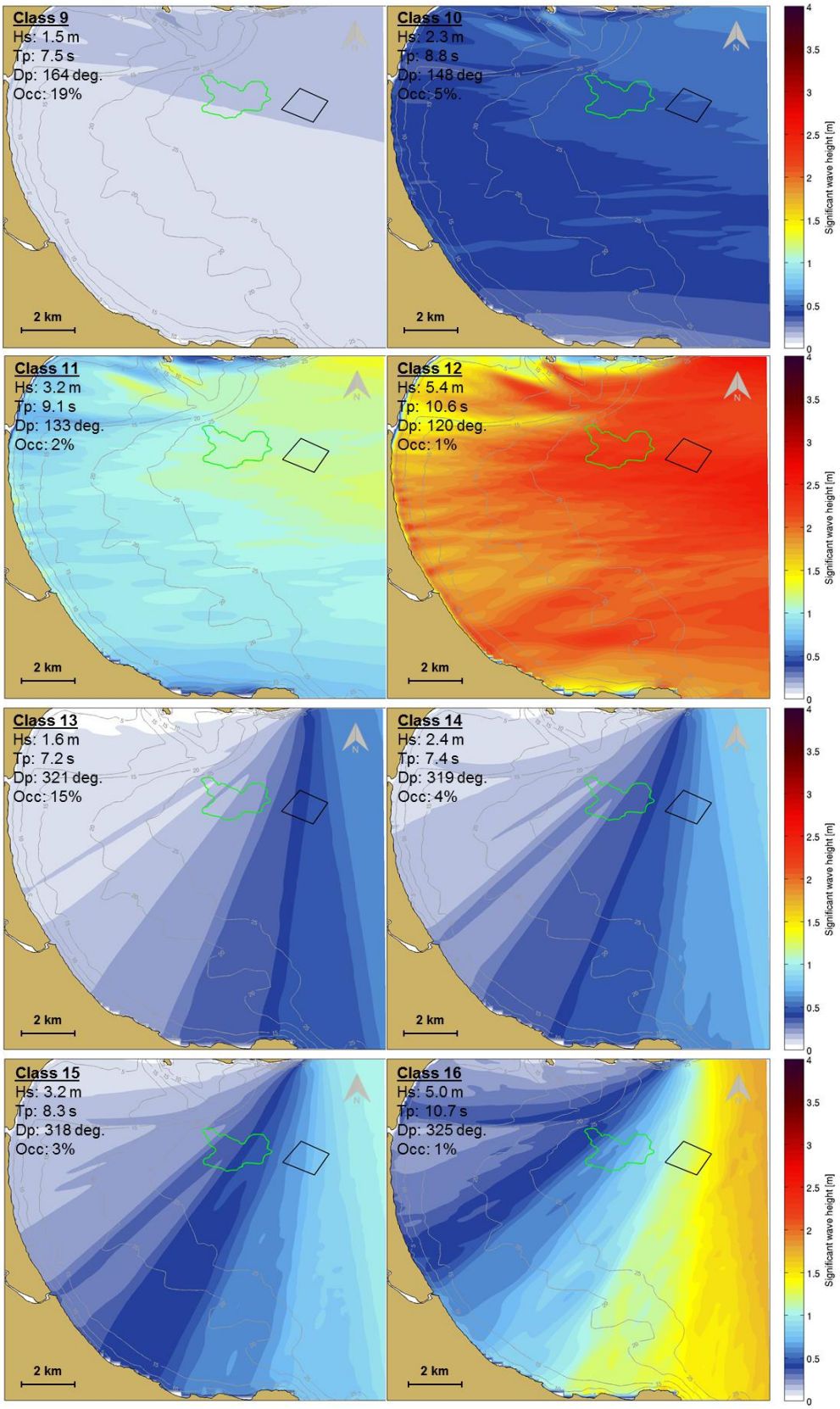

Figure 9.4 Wave height fields over Bream Bay for wave classes 9 to 16. Hs, Tp, Dp and Occ (% Occurrence) presented in the upper left corner indicate the wave conditions at the offshore position BND (see MSL Report P0297-01).

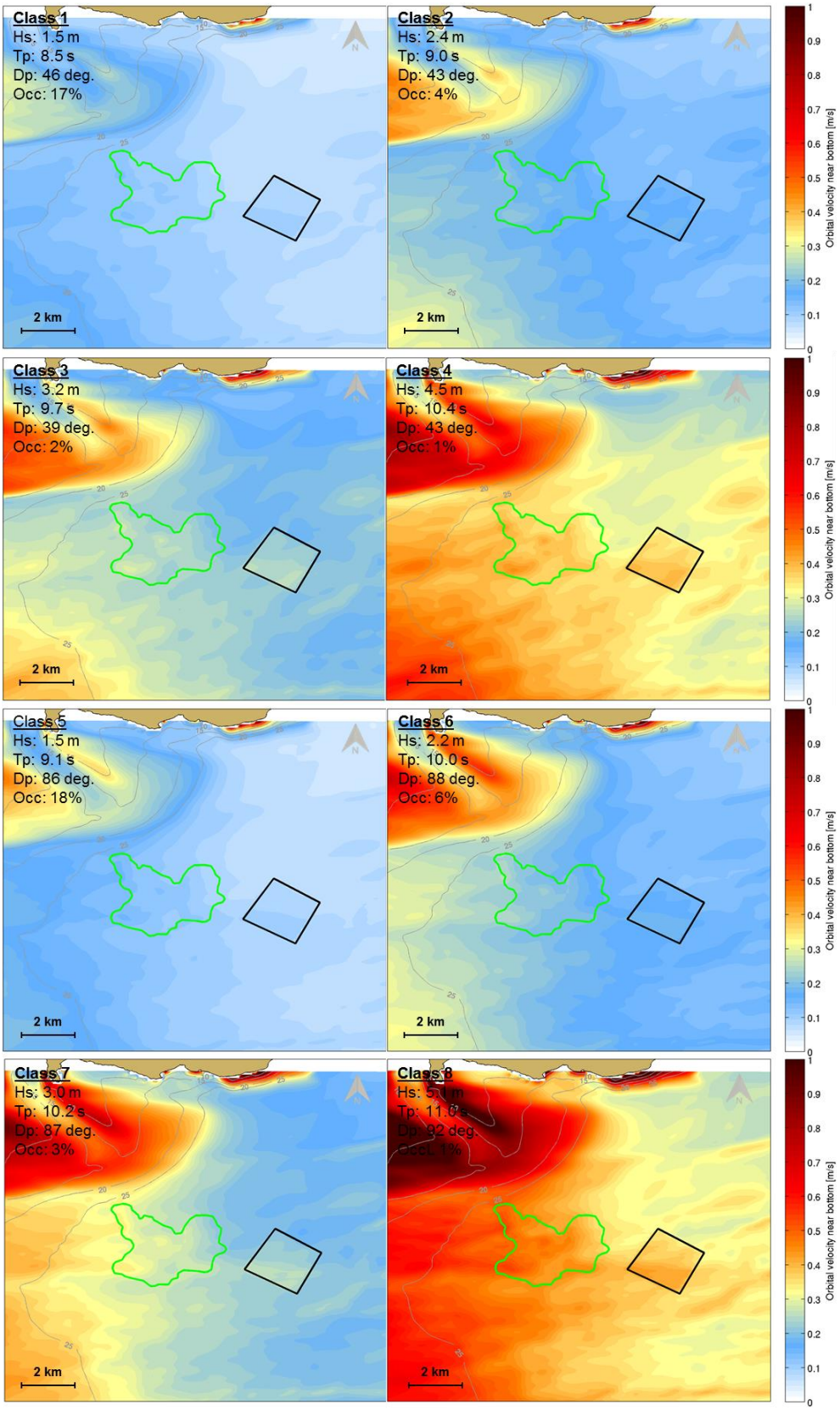

Figure 9.5 Near bottom orbital velocity fields over the disposal ground for wave scenarios 1 to 9. Hs, Tp, Dp and Occ (% Occurrence) presented in the upper left corner indicate the wave conditions at the offshore position BND (see MSL Report P0297-01).

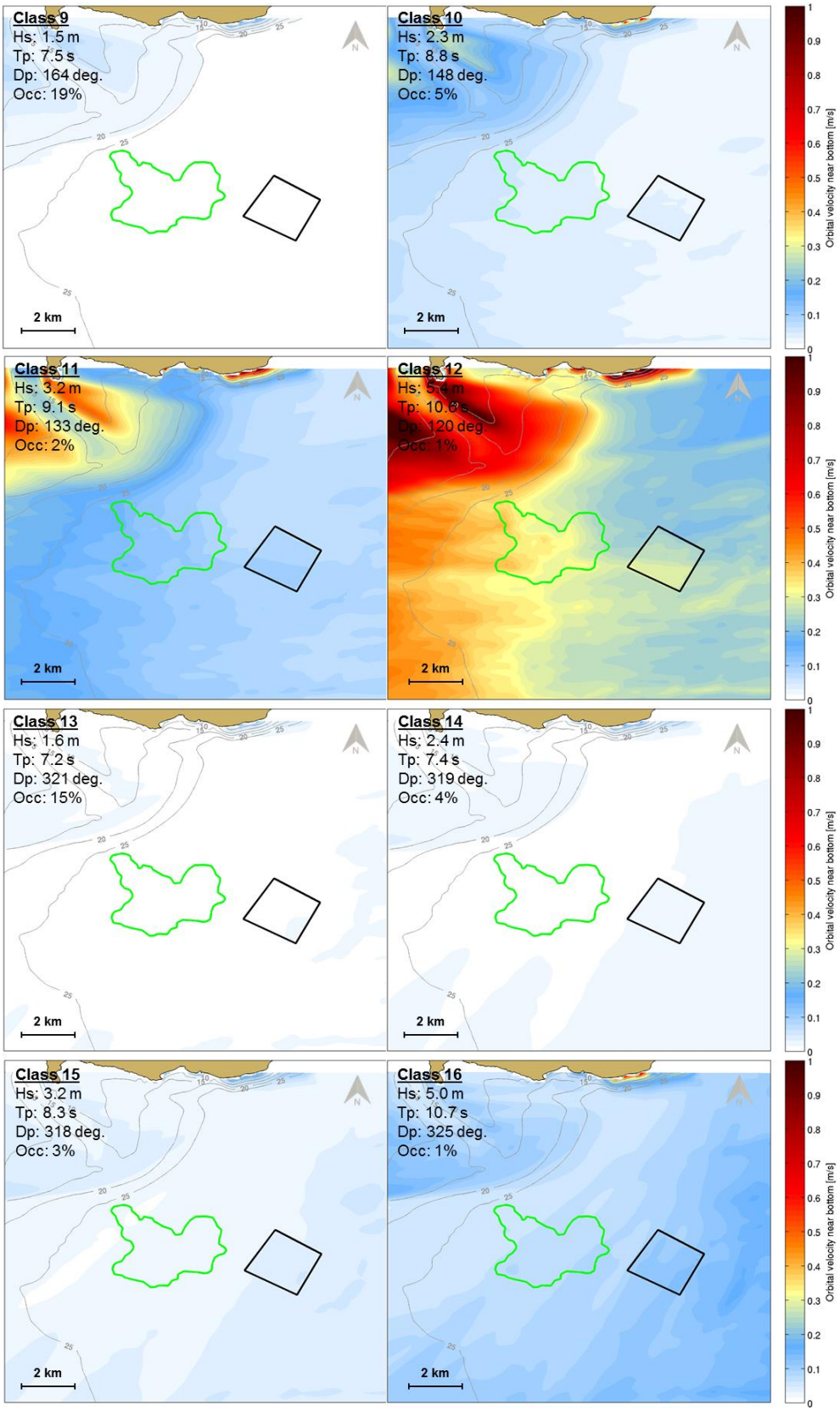

Figure 9.6 Near bottom orbital velocity fields over the disposal ground for wave scenarios 9 to 16. Hs, Tp, Dp and Occ (% Occurrence) presented in the upper left corner indicate the wave conditions at the offshore position BND (see MSL Report P0297-01).

9.2. Hydrodynamics

Current roses extracted from a 10-year ROMS hindcast at the centre of the disposal ground and for three different levels (5, 15 and 30 m below sea surface) are presented in Figure 9.7. These data show that the flows (including the tidal and the residual components) are mainly directed toward the south-west, with velocities lower than 0.3 $m.s^{-1}$. During storm events, these velocities may exceed 0.4 $m.s^{-1}$ when increased by an intense wind-driven circulation. Note that the current rose near bottom also exhibits a secondary mode in the north-eastern direction with a 10 – 20% of occurrence due to the tidal asymmetry and the westerly wind episodes.

As described in the previous section, current velocities of such magnitudes have the ability to directly initiate the transport of fine grained non-cohesive particles from the disposal ground. Moreover, the validation of the ROMS hindcast at the centre of Disposal Site 3.2 (MSL Report P0297-01) showed that the model was under-predicting the current speed by up to 20%. The consequences of such bias on the model outcomes regarding the predicted disposal ground dynamics are discussed in Sections 9.3 and 9.4.

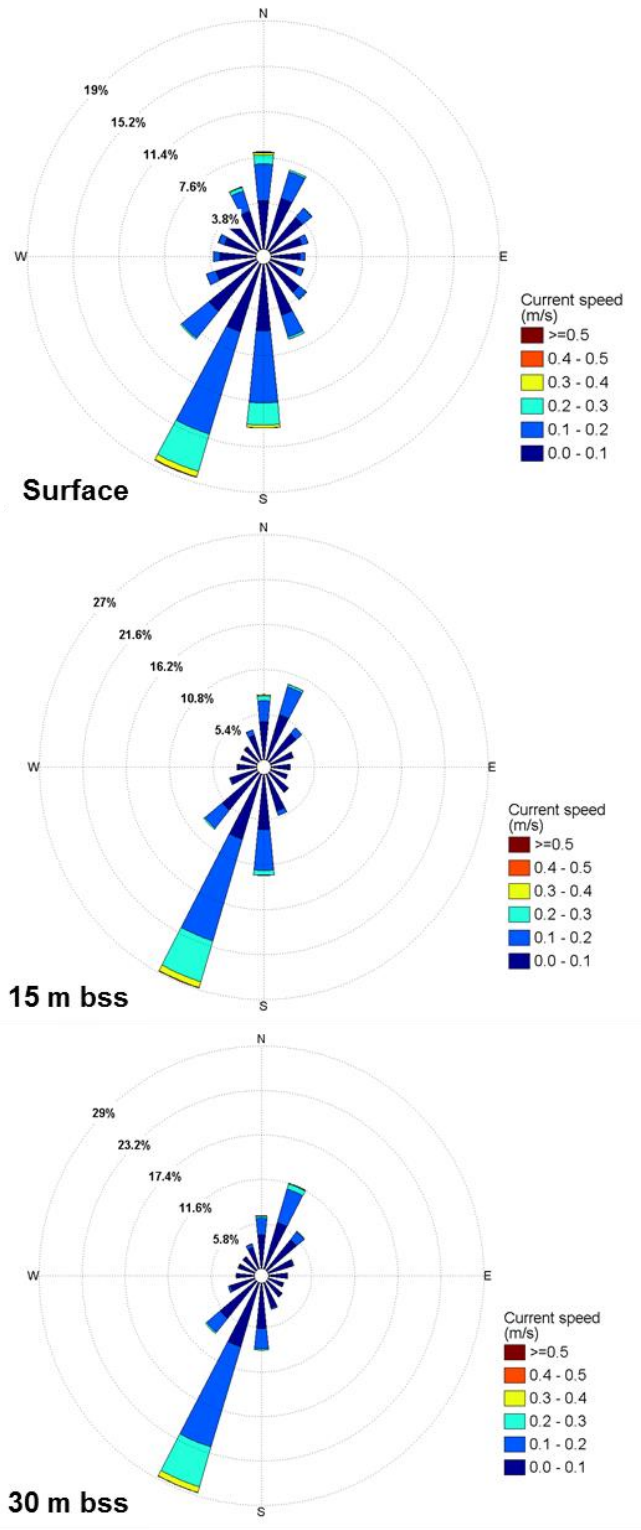

Figure 9.7 Current roses showing total current speed at 0, 15 and 30 m below sea surface (bss) from ROMS hindcast data for the period 2000 – 2010 in the proposed disposal ground. Current directions are in the "going to" convention.

9.3. Sediment dynamics for disposal ground 3.2

The characterisation of the wave climate and the near bed hydrodynamic regime at the proposed disposal ground shows that both components were occasionally of sufficient magnitude to initiate sediment transport of the finer fractions in the disposed sediments. A more integrated assessment of the dynamics of the ground was made with the Delft3D model. This model was used to predict the disposal ground 3.2 morphodynamics using an input reduction approach, which is fully described in Section 9 of MSL Report 0297-01. In this technique, a limited number of representative forcing conditions (including tides, waves, residual currents and residual water elevations) are used to reproduce the medium-term residual sediment transport patterns and associated morphological evolutions. The methodology was combined with a morphological acceleration factor based on the occurrence of each scenario to improve computational efficiency by acceleration computed morphological evolution. Using this technique, the disposal ground dynamics were simulated over a 1-year period.

A highly conservative approach was also adopted for the height of the mound in these simulations. A maximum height of 4 m (corresponding to a total volume of 8 million m^3) was adopted, in order to replicate a scenario in which the disposal operation is constrained to limited areas in order to minimise the footprint of deposition, and being a reasonable upper value to represent some overlapping deposition of the dredged hopper loads. This maximum height of 4 m is less than 10% of water depth at Area 3.2.

The annual morphological changes presented in Figure 9.8 (based on a conservative configuration of the model) show a very slight west-southwest migration of the sediments by bedload transport due to wave effects. The erosion of the disposal mound after 1 year reveals a marked gradient in the transport based on water depth. This suggests that both high energy wave and current conditions are necessary to initiate the entrainment of the disposed sediments. Less than 5% of the disposed material (based on an 8 million m^3 volume) is expected to be eroded and transported over a 1-year period. In this context, under-predicting the current velocity by 5 – 20% at the offshore disposal ground location is not expected to fundamentally change the numerical modelling outcomes. Indeed, the near-bottom current velocities over areas characterised by water depths ranging between 40 – 45 m are relatively low. The high degree of stability highlighted by the 1-year morphodynamic numerical modelling is not expected to be compromised by a ~0.05 $m.s^{-1}$ absolute error in the model velocities.

The extent of movement of sediment is very limited and does not reach any sensitive area such as beaches, Marine Reserves, Marine 1 Management Areas or sensitive areas. The adjacent 3 Mile Reef is not expected to receive a detectable amount of sediments from disposal ground 3.2. Given the receiving environment already has a similar grain size composition to the dredged sediments, there will be no material change to the sedimentary character of 3 Mile Reef. Disposal ground 3.2 is expected to be stable over a long-term period given the very low amplitude of transport shown by the model. The ratio of deposited to eroded material indicates that small amounts of fine sediments are transported during storms and spread in undetectable quantities over the adjacent areas.

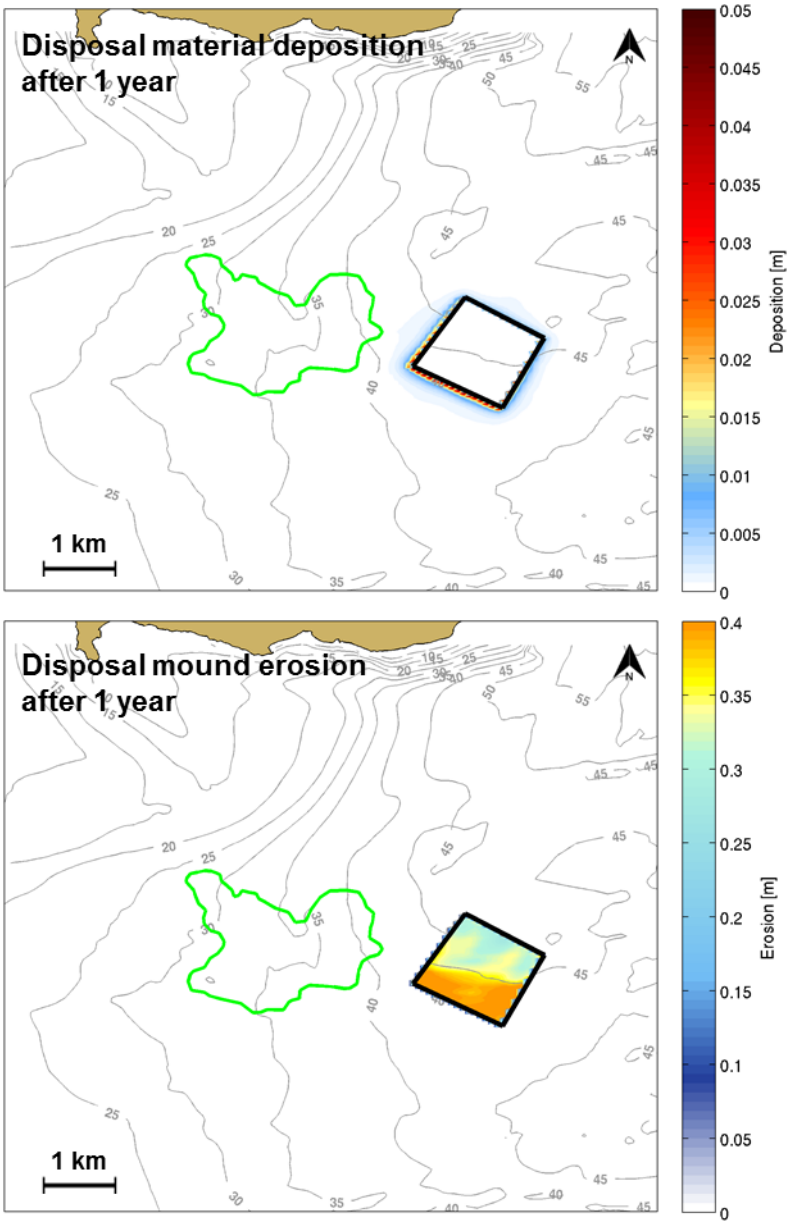

Figure 9.8 Disposal ground 3.2 dynamics simulated for a 1 year period.

9.4. Sediment dynamics for Disposal ground 1.2

For disposal site 1.2, a 0.6-m mound (1.5 million m^3) was considered for the maintenance dredging volume and up to 5% of the capital dredging volume based on the consultation between RNZ and the relevant experts. The site is located over the southern extension of the ebb-tidal delta where depths range from 7 – 15 m. The hydrodynamic study showed that the tidal currents over this region of Bream Bay are not particularly strong, with peak ebb and flood velocities lower than 0.2 $m.s^{-1}$ and oriented northeast. Conversely, the maximum orbital velocities due to the effect of waves over shallow areas are predicted by the model to reach 0.4 – 0.5 m/s during storms, making the disposal ground dynamics dominated by waves. This area is exposed to refracted waves propagating in the eastern direction, causing high bottom friction fields over the tidal delta. Results of the 1-year morphodynamic simulation shown in Figure 9.9 clearly confirm the wave-dominated transport of dredged material after disposal. Sediments were predicted to be dispersed in south-western to north-western directions, by waves, and tidal

currents to a lesser extent. The erosion of the disposal mound is predicted to reach approximately 8% of the total volume after 1 year. No connection between the disposed material and the channel is predicted by the model. This disposal site will likely promote the replenishment of the adjacent beach and sand bank areas over years under the effect of waves during storm conditions.

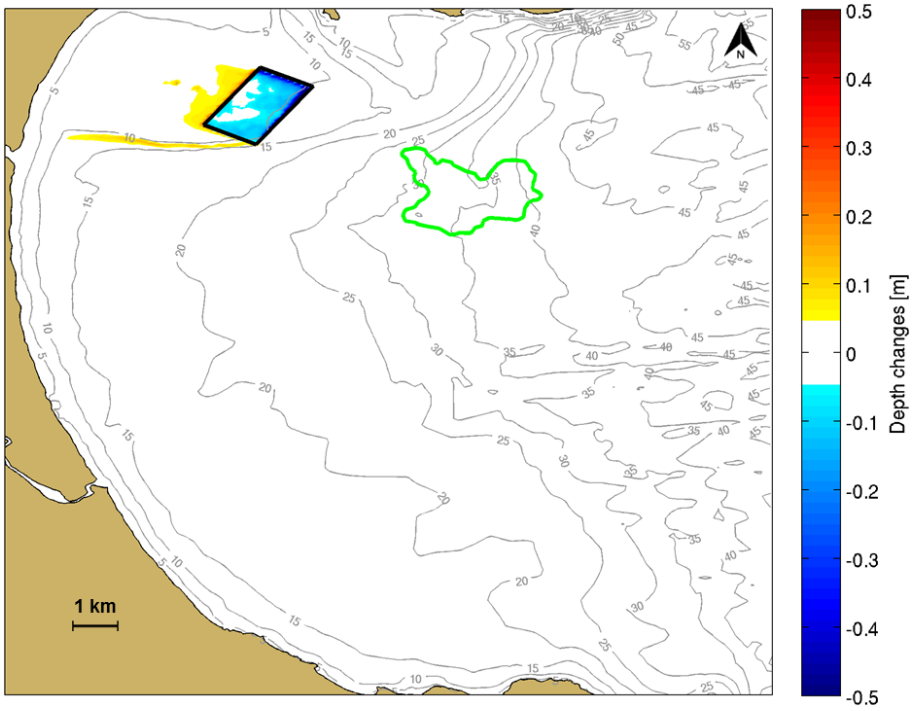

Figure 9.9 Disposal ground 1.2 dynamics simulated for a 1 year period.

9.5. Effects of disposal grounds on the wave climate

Changing the shape of the seabed potentially influences the nearshore wave climate through the process of wave refraction. Wave height and direction at the shore can be changed if a disposal mound is of sufficient size, and a local example is the modification of waves by the shape of the ebb tide delta.

To examine this potential, the 16 representative wave classes were simulated with the spectra wave model (DELFT3D – WAVE) to examine the effects of the disposal mounds 1.2 and 3.2 on the wave climate near Ruakaka Beach and over the wider Bream Bay. No hydrodynamic forcing was included. Highly conservative mound heights of 1.75 m and 4 m corresponding to the Disposal grounds 1.2 and 3.2, respectively, were used.

In the case of the Disposal Site 3.2, the results presented in Figure 9.10 and Figure 9.11 for the modelled cases (with incoming waves of 0.5 to 4.0 m in height at the disposal site 3.2) show that the difference in wave height (illustrated by yellow/orange colours for an increase and blue colours for a decrease) is very small (less than 10 cm). Maximum changes are observed near the mound itself while changes along Ruakaka Beach do not exceed 5 cm. These subtle differences in the significant wave height fields are mainly due to the relative high water depth (~40 – 45 m) at the disposal site. The effect near the shore is a slight modulation, with areas of increase and areas of decrease, dependent on the incident wave direction.

Changes in significant wave heights caused by the Disposal Site 1.2 illustrated in Figure 9.12 and Figure 9.13 are not expected to exceed 5 cm and 10 cm along the adjacent beaches and near the mound, respectively. The wave energy is susceptible to be slightly redistributed due to changes in wave refraction and wave breaking, particularly during storm events. The wave height along the adjacent beaches to the north-west of the mound is predicted to increase by less than 10 cm for moderate / high energy wave events. During extreme events characterised by offshore wave height of more than 5 m, the reduction of the water depth due to the presence of the mound may promote wave breaking processes over the disposal Site reducing the wave height along the shoreline by 5 – 10 cm (< 5%). Note that during such exceptional events, the northern area of Ruakaka Beach can be subjected to an increase of a few centimetres in wave heights. The erosion of the disposal mound over years driven by the effect of waves is expected to reduce notably the changes in significant wave heights caused by the mound. The methodology applied in the present study is thus highly conservative as it considers a non-erodible disposal mound over 10 years. The effect of the disposal mound 1.2 on the existing wave climate is largely negligible. Surfing conditions along Ruakaka Beach are therefore not expected to be affected by the disposal mounds 1.2 and 3.2.

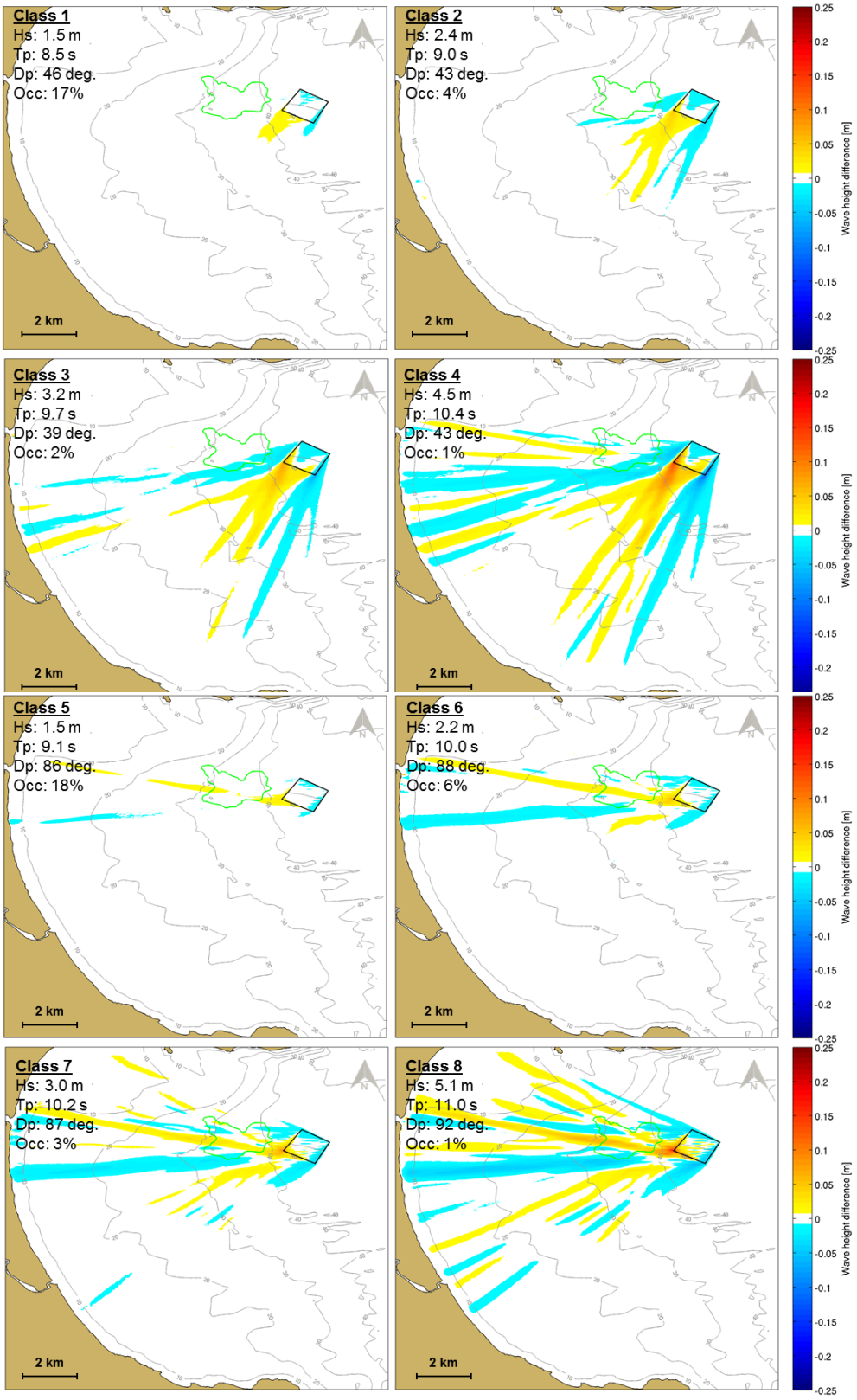

Figure 9.10 Difference in wave height fields caused by the disposal mound 3.2 over Bream Bay for wave scenarios 1 to 8. Hs, Tp, Dp and Occ (% Occurrence) presented in the upper left corner indicate the wave conditions at the offshore position BND (MSL Report P0297-01).

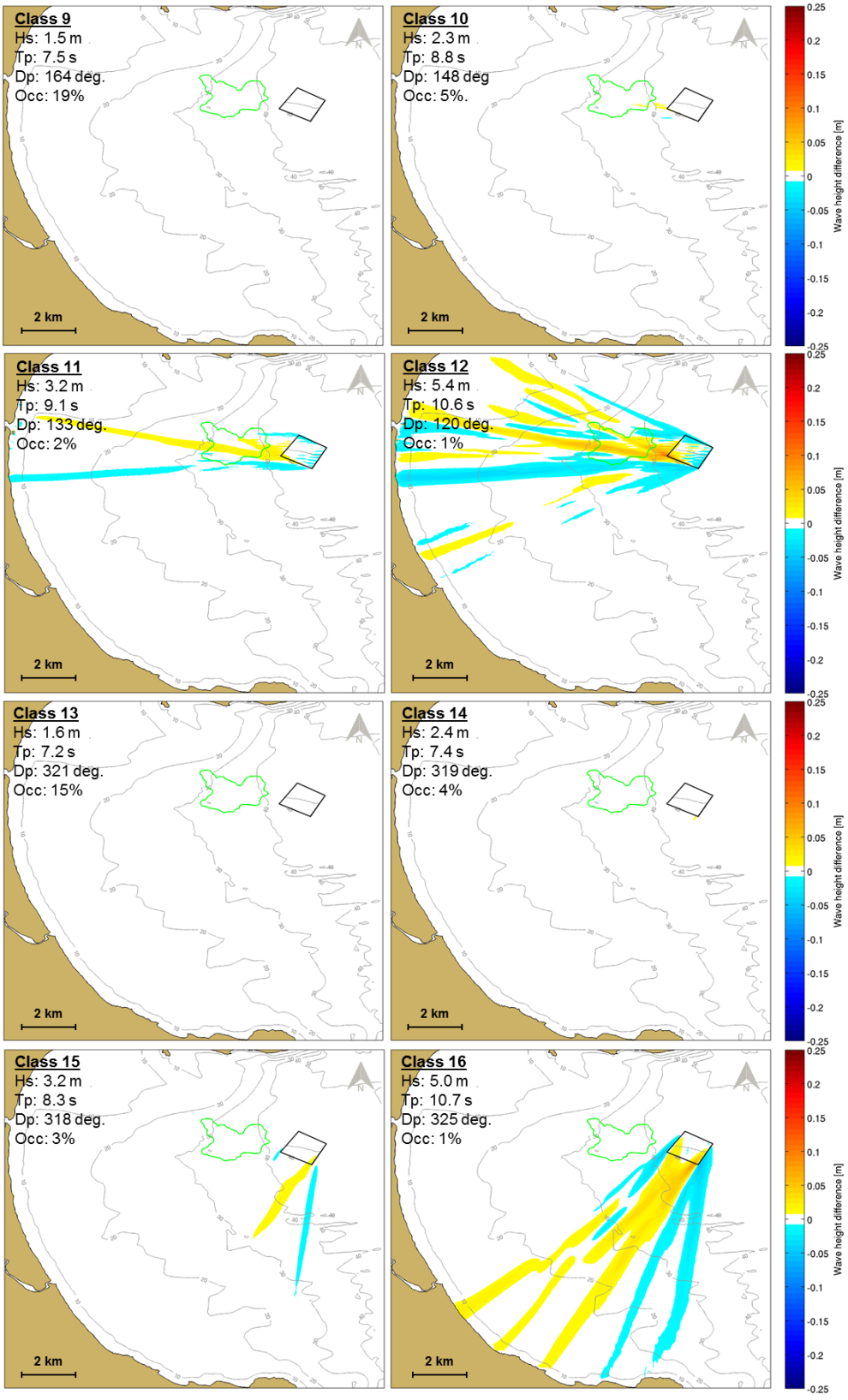

Figure 9.11 Difference in wave height fields caused by the disposal mound 3.2 over Bream Bay for wave scenarios 9 to 16. Hs, Tp, Dp and Occ (% Occurrence) presented in the upper left corner indicate the wave conditions at the offshore position BND (MSL Report P0297-01).

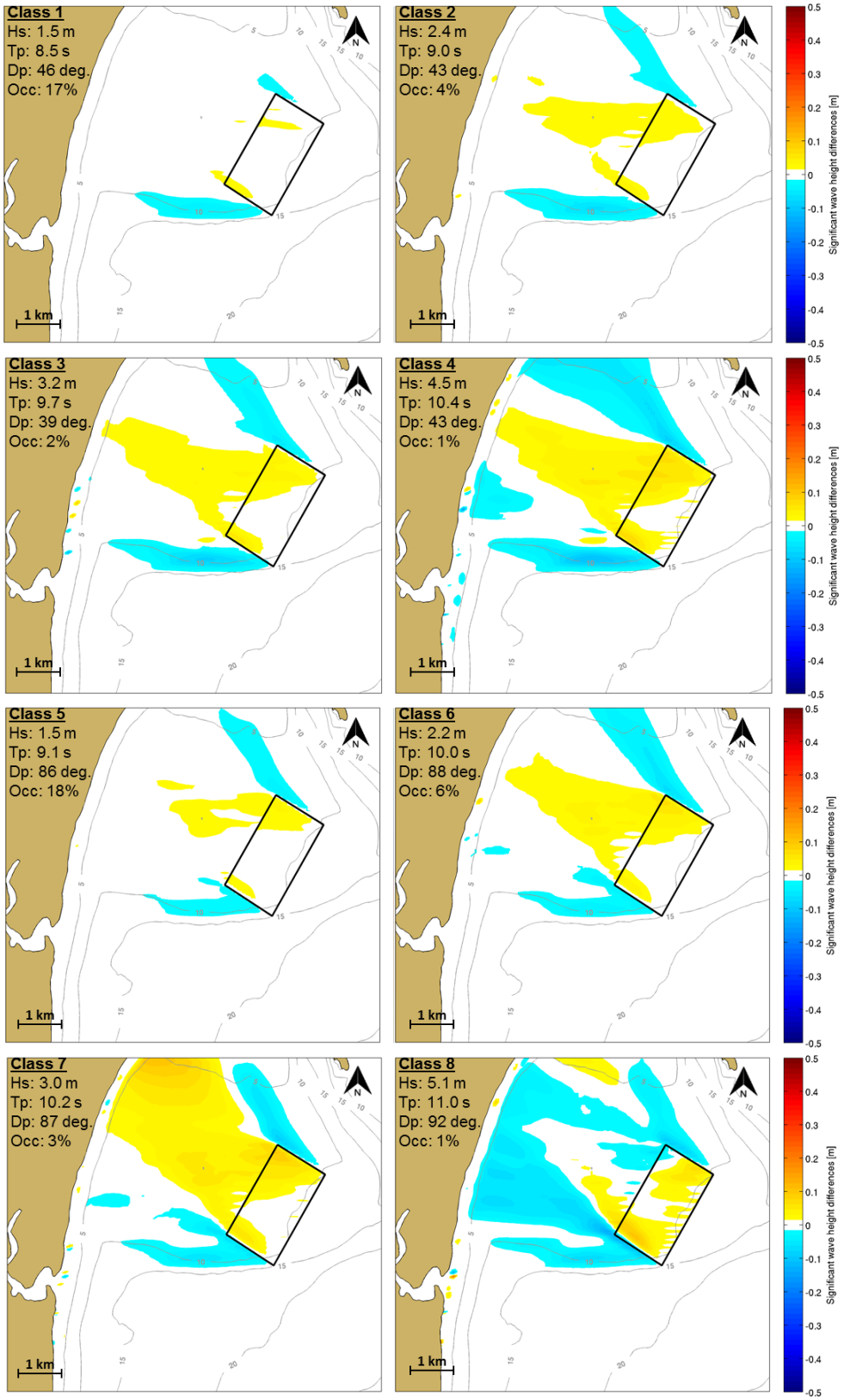

Figure 9.12 Difference in wave height fields caused by the disposal mound 1.2 near Ruakaka Beach for wave scenarios 1 to 8. Hs, Tp, Dp and Occ (% Occurrence) presented in the upper left corner indicate the wave conditions at the offshore position BND (MSL Report P0297-01).

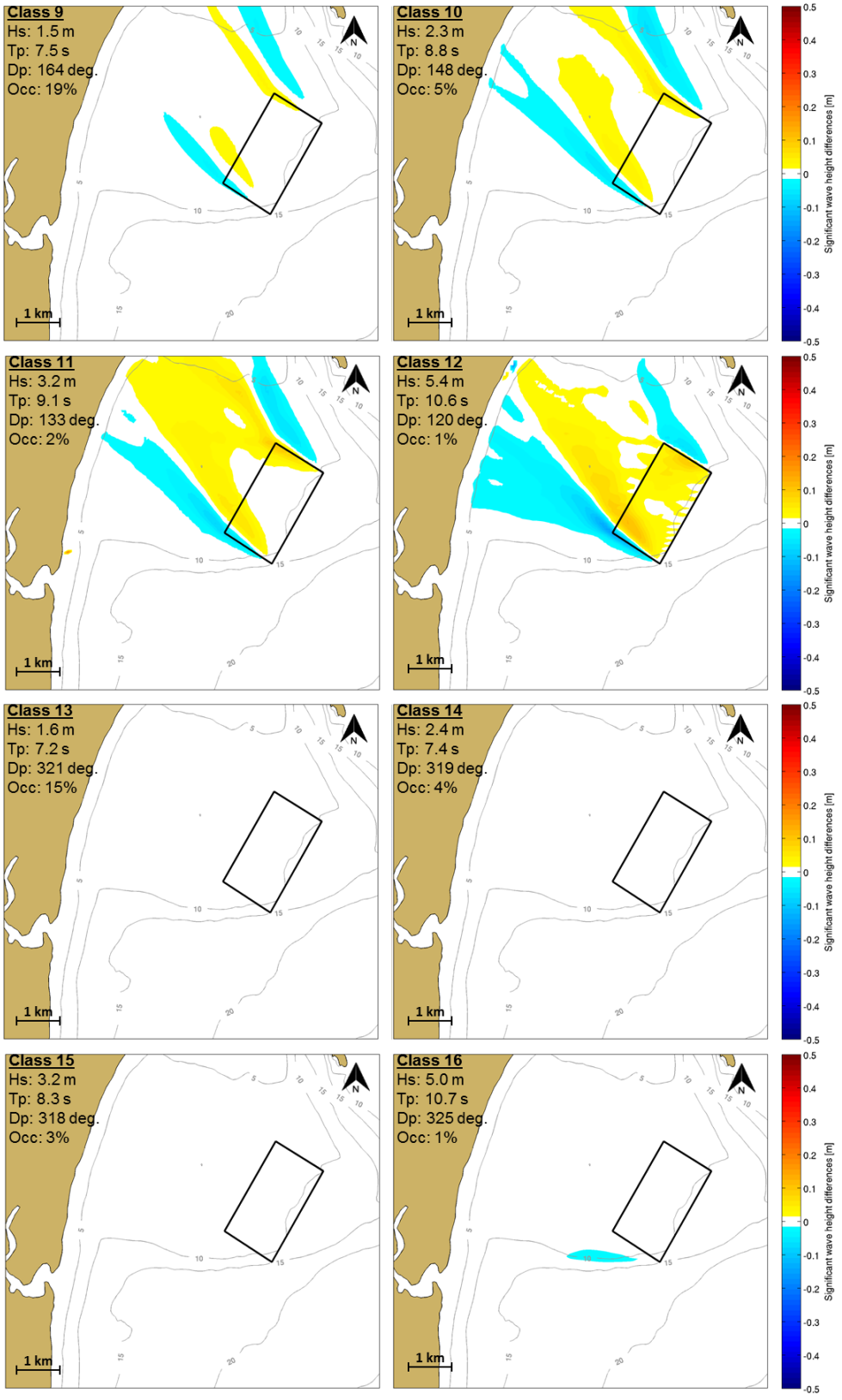

Figure 9.13 Difference in wave height fields caused by the disposal mound 1.2 near Ruakaka Beach for wave scenarios 9 to 16. Hs, Tp, Dp and Occ (% Occurrence) presented in the upper left corner indicate the wave conditions at the offshore position BND (MSL Report P0297-01).

9.6. Summary of effects of the disposal grounds

The numerical modelling of the sediment dynamics of the proposed offshore disposal ground in 40-45 m depth in Bream Bay shows that:

- The wave and current regime can occasionally mobilise sediments in this area. This will only occur during more energetic storm conditions, when sediments can be transported in suspension or by bedload processes.

- The predicted rate of movement of sediment from disposal ground 3.2 is very low and essentially omnidirectional, although results suggest a slight bias to the south.

- After one year, the extent of movement from disposal ground 3.2 will have a very limited excursion. This region of Bream Bay is characterised by 40-m water depths, and the erosion of the seabed in the area is not predicted to exceed a few centimetres by current and wave actions. The relative high depth favours a high degree of stability of the disposal mound.

- The adjacent 3 Mile Reef is not expected to receive a detectable amount of sediments coming from disposal ground 3.2. Moreover, given the receiving environment already has a similar grain size composition to the dredged sediments, there will be no material change to the sedimentary character of the 3 Mile Reef.

- The dredged material disposed at Disposal ground 1.2 is predicted to be transported in the south-western and north-western directions over the adjacent beach and sand bank areas by waves. The circulation induced by tidal and wave forcing in this region is not predicted to connect the disposal mound system with the channel system, thus the risk of channel infilling by the dredged material after disposal is limited.

- Predicted maximum changes to the nearshore wave climate by the presence of both the nearshore and the offshore mounds (disposal Site 1.2 and 3.2) are very minor and not expected to exceed +/- 0.05 m along the shoreline under energetic wave conditions. Therefore, no consequences on the beach or nearshore processes are expected. This includes no consequences to the recreational surfing activities along Ruakaka Beach.

10. DISPOSAL PLUMES

The dispersion of a plume caused by disposal operations was simulated at several sites within the proposed offshore disposal ground using a lagrangian particle modelling technique (ERcore model) nested within the hindcast regional 3D hydrodynamic flow fields. A detailed description of the methodology is provided in MSL Report P0297-01. As with the dredging plumes, a probabilistic modelling approach has been adopted to capture the range of possible plume outcomes.

10.1. Disposal plume modelling results

The mean suspended sediment concentrations (SSC) after 24h of continuous disposal for two different sizes of dredger (small and large trailing suction hopper dredger, TSHD) were determined from a 6-month simulation using the combined tidal and non-tidal currents as the environmental forcing. The results are presented in Figure 10.1 and Figure 10.2. The same conservative 12 mg/L SSC threshold used and discussed in the dredging plume section was applied in the disposal plume modelling.

The predicted SSC plumes clearly follow a northeast-southwest axis, which was expected given the current climate at the disposal ground (see Figure 9.1). Surface plumes are constrained to the mixing zone around the boat and do not extend more than 50 m from the release location. The SSC progressively increases with increasing depth due to the rapid settlement of the sediments through the water column. The simulations suggest that the mid water plume may extend about 500 m from the release location for both the small and the large dredge, to the minimum concentration threshold of 12 mg/L. However, most of the plume is constrained within a radius of 50 and 100 m for the small and the large dredge, respectively. Notably, the highest SSC levels within the lower water column are predicted to the southwest of the disposal ground; consistent with the flow regime being biased to this octant. The plumes do not show significant differences in extent or direction between sites inside the disposal ground. At site PW, the closest to the 3 Mile Reef, it is important to note that the plume does not intersect with the reef area, and the probability of a plume reaching the reef is considered very low.

As a form of corroboration, a disposal plume modelling scenario was also undertaken using the current velocity profiles recorded inside the proposed disposal ground from 15 January to 5 March, 2016. For this scenario, the plume results for both the large and the small vessels over a 24 h period exhibit a different behaviour (Figure 10.4), likely due to the shorter duration and the particular weather patterns at the time. Nonetheless, the results show less dispersion than the longer term modelling and no evidence of trajectory over the reef to the west of the disposal ground. These results confirm that the 5 – 20% bias identified in the model depth-averaged current velocities at the offshore disposal site has no significant impact on the plume dispersion. We therefore conclude that even taking into account this bias there is a very low probability of the plume reaching 3 Mile Reef.

Another useful metric for assessing the disposal plumes is the percentage of time a certain SSC level is exceeded. Exceedance time estimations were undertaken relative to reference SSC levels of 10, 50 and 100 $mg.L^{-1}$. Two specific 48 h periods involving strong west surface and bottom currents were selected and results are provided in Figure 10.5 to Figure 10.8 for the large and small dredges. Also, two month-long simulations (January and August, 1995 – selected at random

to illustrate the summer and winter conditions) were run to investigate the seasonal variability of the exceedance time estimations. The results are presented in Figure 10.9 to Figure 10.12.

The exceedance time estimates suggest that plume dispersion and elevated SSC levels are not expected over the reef. The scenario corresponding to the disposal activities with the large vessel during overall strong westerly-directed currents on surface (Figure 10.5) indicate that even during a short-term non-favourable event, no dispersion over the reef is predicted to occur. Most of the fine sand particles were transported northward (within 3000 m for >10 $mg.L^{-1}$) on the surface while the medium sands settle quickly over a limited area (of less than 50 m radius). Note that the relatively strong westerly-directed bottom current scenario exhibits very similar results. The hydrodynamic conditions in summer do not promote large scale dispersions. The northward maximum extension of the exceeding time area considering a 12 $mg.L^{-1}$ threshold is not predicted to exceed 1000 m over a 24 h period. In winter, the exceedance time patterns for thresholds of 12 and 50 $mg.L^{-1}$ suggest a southward dominated dispersion within a 1500 m maximum radius.

10.2. Disposal plume summary

The disposal plume modelling undertaken for disposal ground 3.2 indicates that:

- The plumes caused by disposal are short lived and not highly dispersive. They typically extend along a northeast – southwest axis, preserving the adjacent reef from settlement, and 99% of the plume material settles to the seabed within 14 hours.

- The disposal plumes calculated from the measured current profiles have a lesser excursion than those determined from the long term current hindcast, and does not show incursion with the adjacent 3 Mile reef to the west of the proposed disposal ground.

- The SSC plumes over the disposal area are not expected to extend more than 550 m from the release locations and should only play a moderate role.

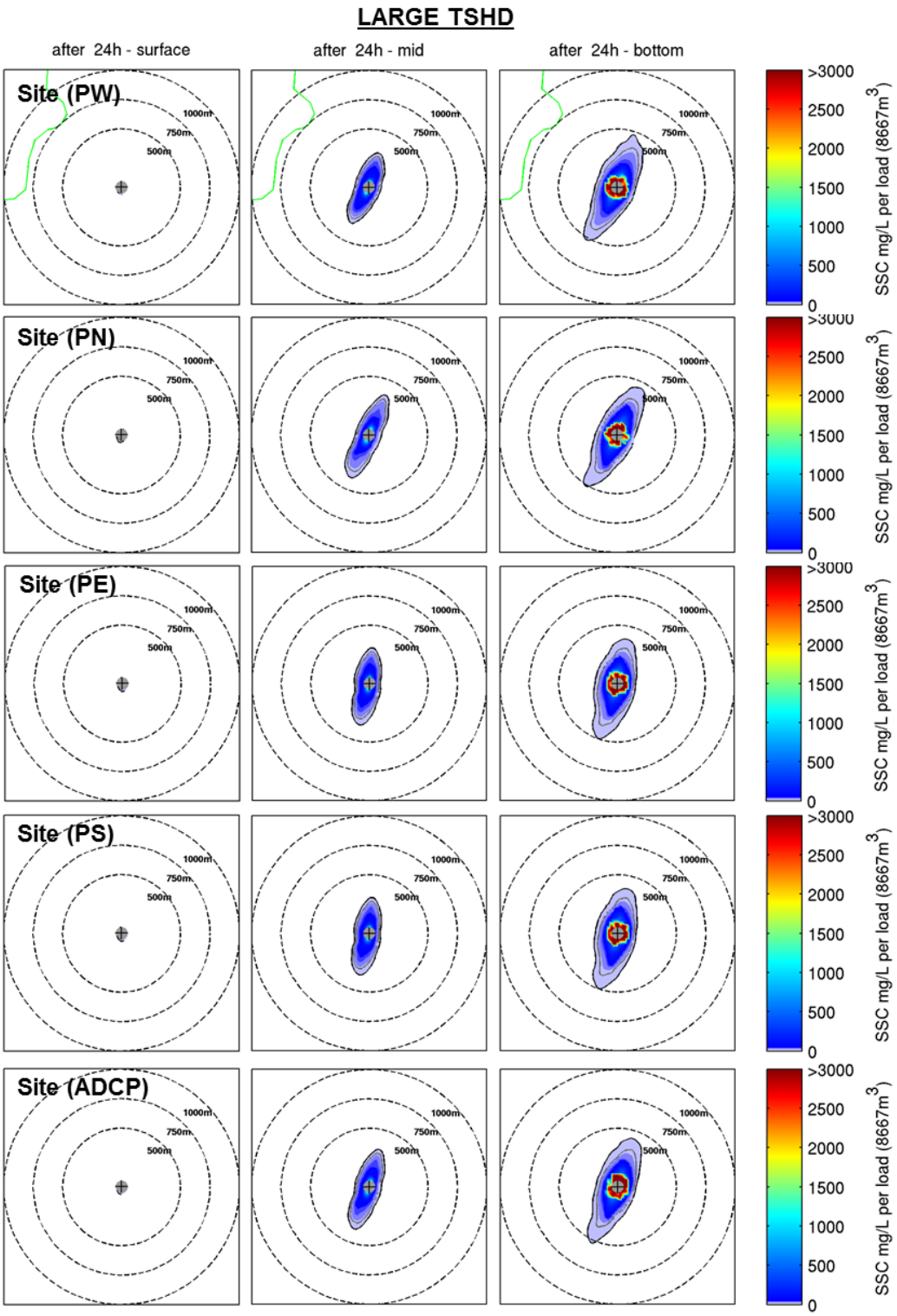

Figure 10.1 Predicted suspended sediment concentrations (SSC) after 24h at bottom, mid water and surface levels for a release at sites PW, PN, PE, PS and ADCP. Note that a large TSHD is considered here for the amount of released sediments. The green polygon indicates the contour of 3 Mile Reef. The black and grey lines indicate the 12- and 20-mg/L SSC threshold corresponding to the critical threshold for rocky reef systems and to the highest background concentration recorded near the entrance to Whangarei Harbour.

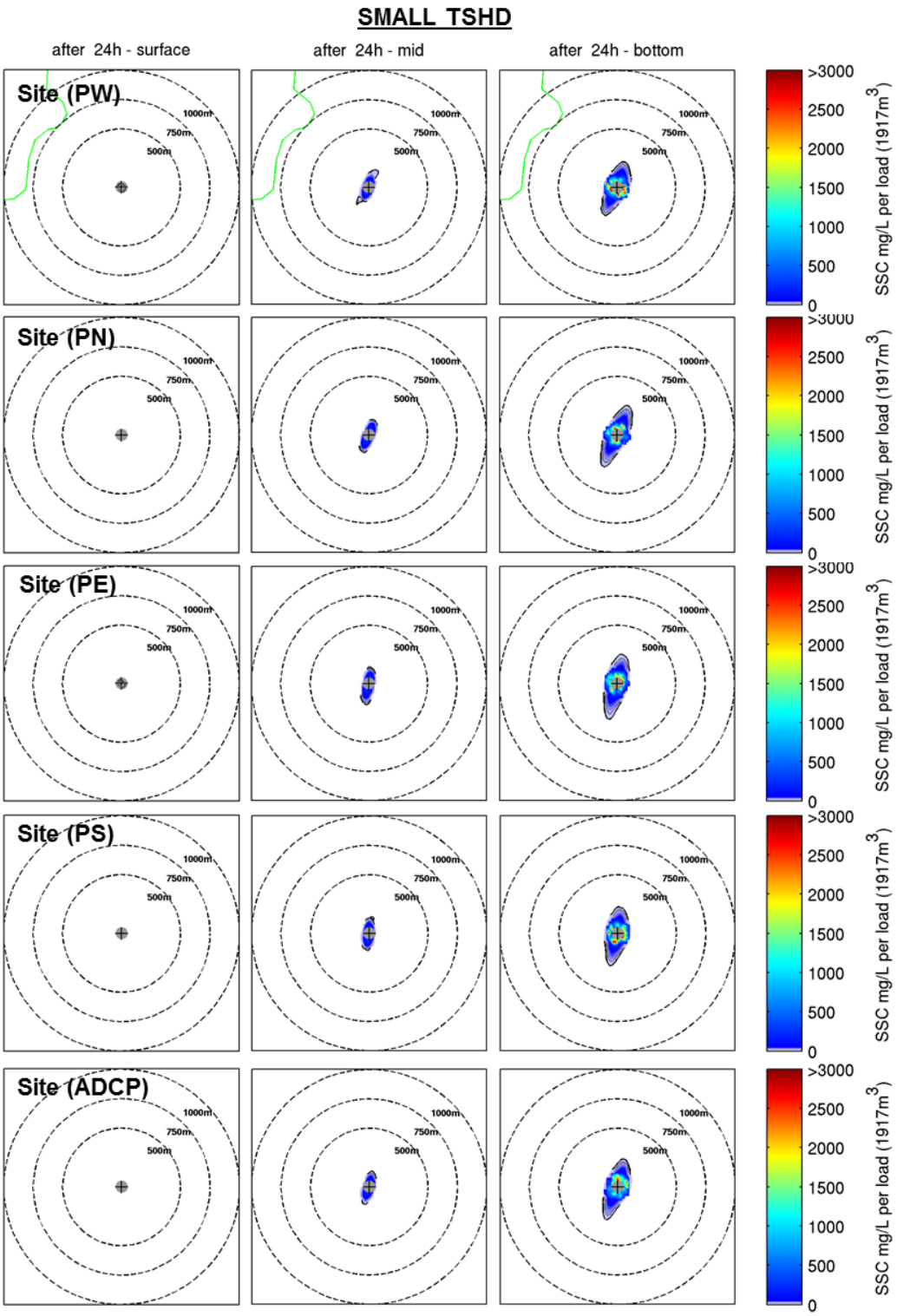

Figure 10.2 Predicted suspended sediment concentrations (SSC) after 24h at bottom, mid water and surface levels for a release at sites PW, PN, PE, PS and ADCP. Note that a small TSHD is considered here for the amount of released sediments. The green polygon indicates the contour of the adjacent reef. The black and grey lines indicate the 12- and 20- mg/L SSC threshold corresponding to the critical threshold for rocky reef systems and to the highest background concentration recorded near the entrance to Whangarei Harbour.

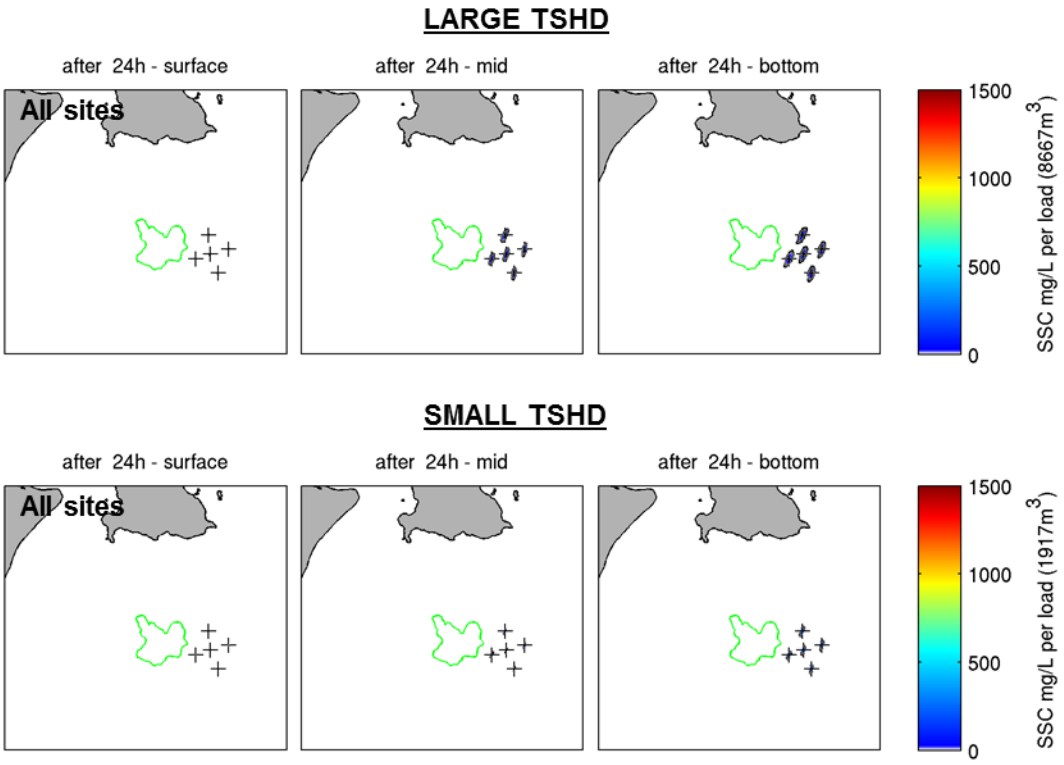

Figure 10.3 Overview of the predicted suspended sediment concentrations (SSC) after 24h at sites PW, PN, PE, PS and ADCP, for both the large and the small TSHD.

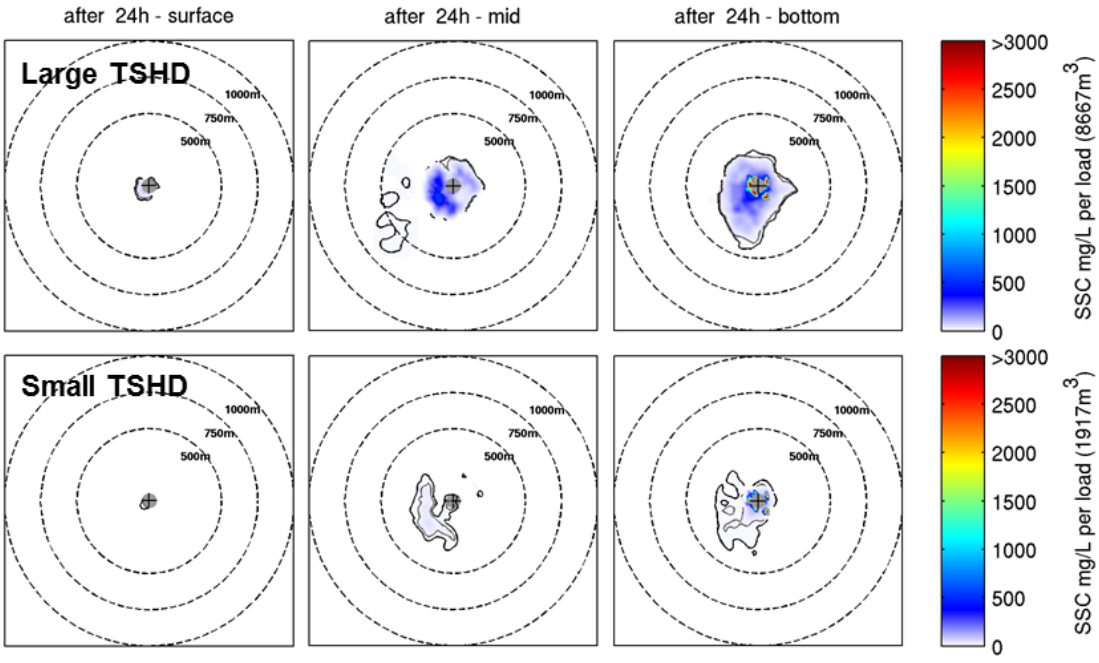

Figure 10.4 Predicted suspended sediment concentrations (SSC) after 24h at bottom, mid water and surface levels for a release at site ADCP forced by measured current data.

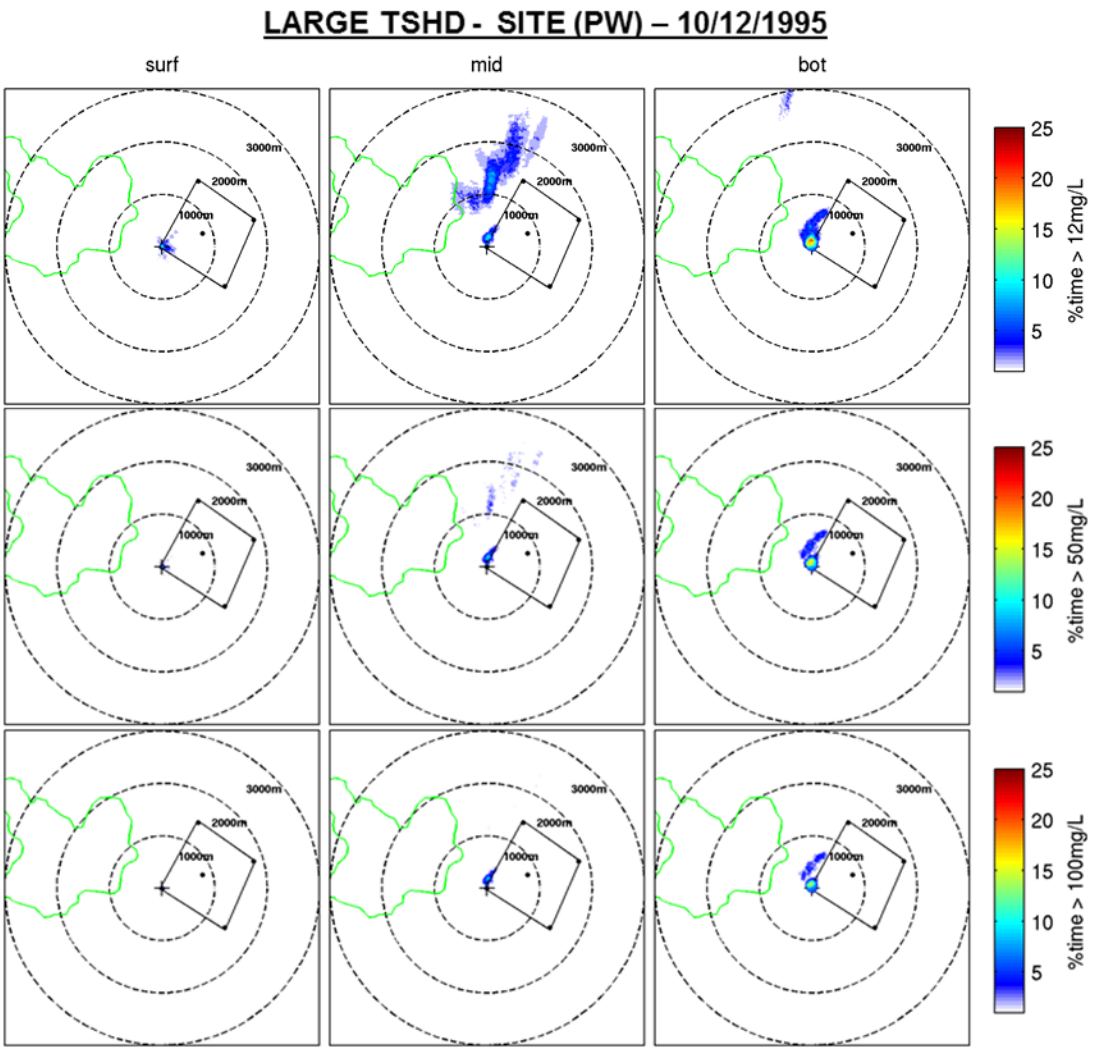

Figure 10.5 Percentage of time *SSC* thresholds of 12, 50, 100 mg.L^{-1} are exceeded between 10/12/1995 12:00 and 12/12/1995 12:00, assuming disposal at site PW with the large TSHD. The green polygon indicates an adjacent reef classified as sensitive.

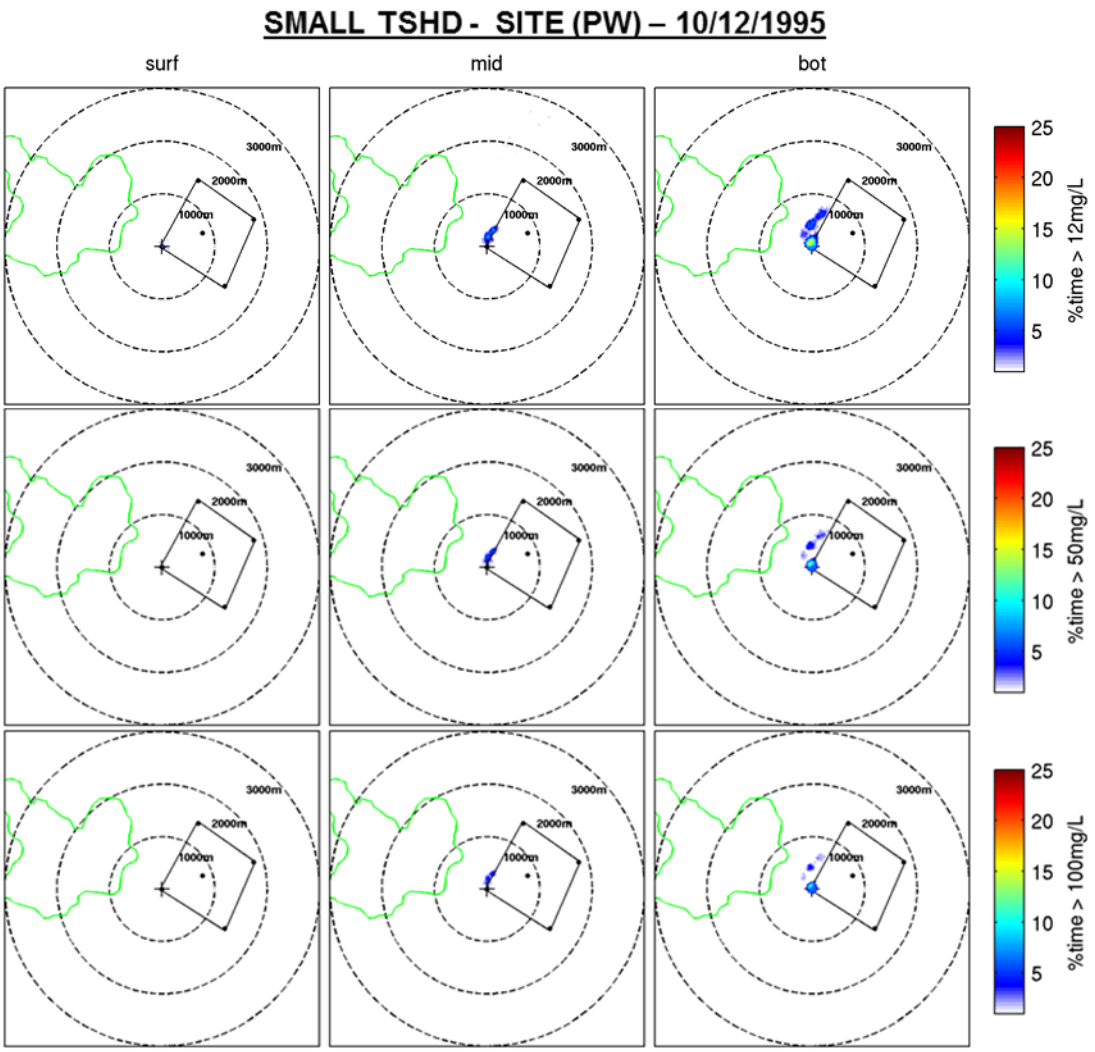

Figure 10.6 Percentage of time *SSC* thresholds of 12, 50, 100 mg.L^{-1} are exceeded between 10/12/1995 12:00 and 12/12/1995 12:00, assuming disposal at site PW with the small TSHD. The green polygon indicates an adjacent reef classified as sensitive.

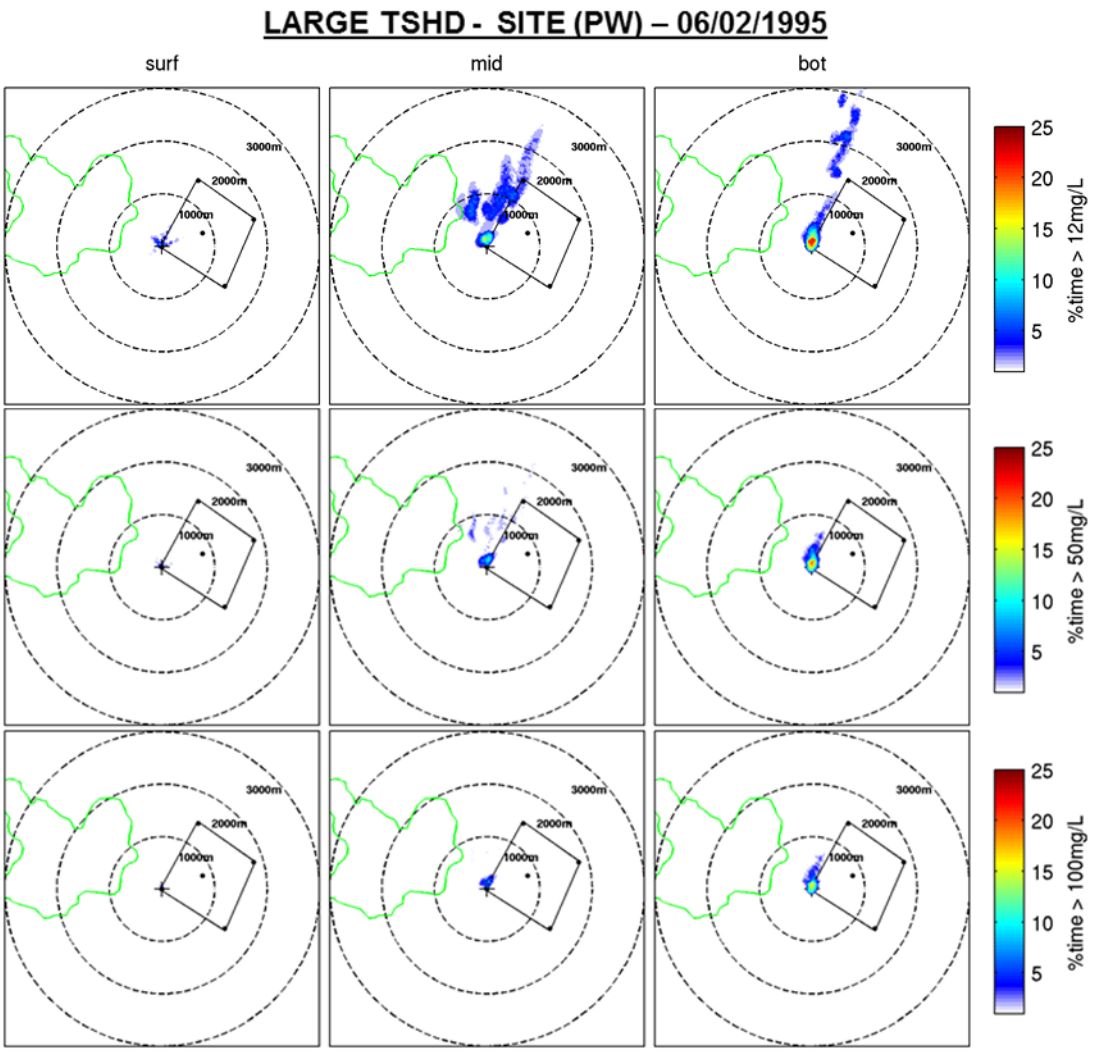

Figure 10.7 Percentage of time *SSC* thresholds of 12, 50, 100 mg.L^{-1} are exceeded between 06/02/1995 12:00 and 08/02/1995 12:00, assuming disposal at site PW with the large TSHD. The green polygon indicates an adjacent reef classified as sensitive.

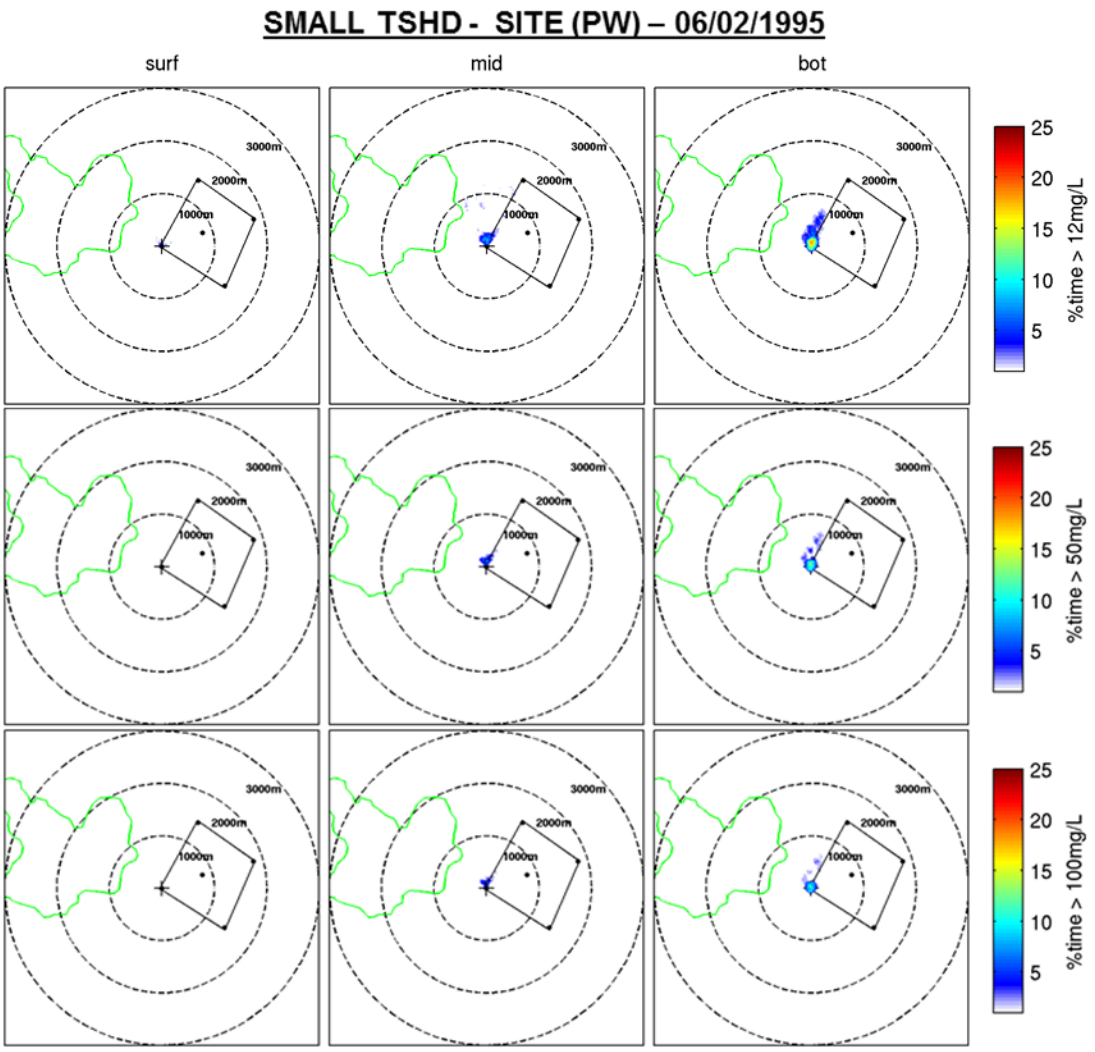

Figure 10.8 Percentage of time *SSC* thresholds of 12, 50, 100 mg.L^{-1} are exceeded between 06/02/1995 12:00 and 08/02/1995 12:00, assuming disposal at site PW with the small TSHD. The green polygon indicates an adjacent reef classified as sensitive.

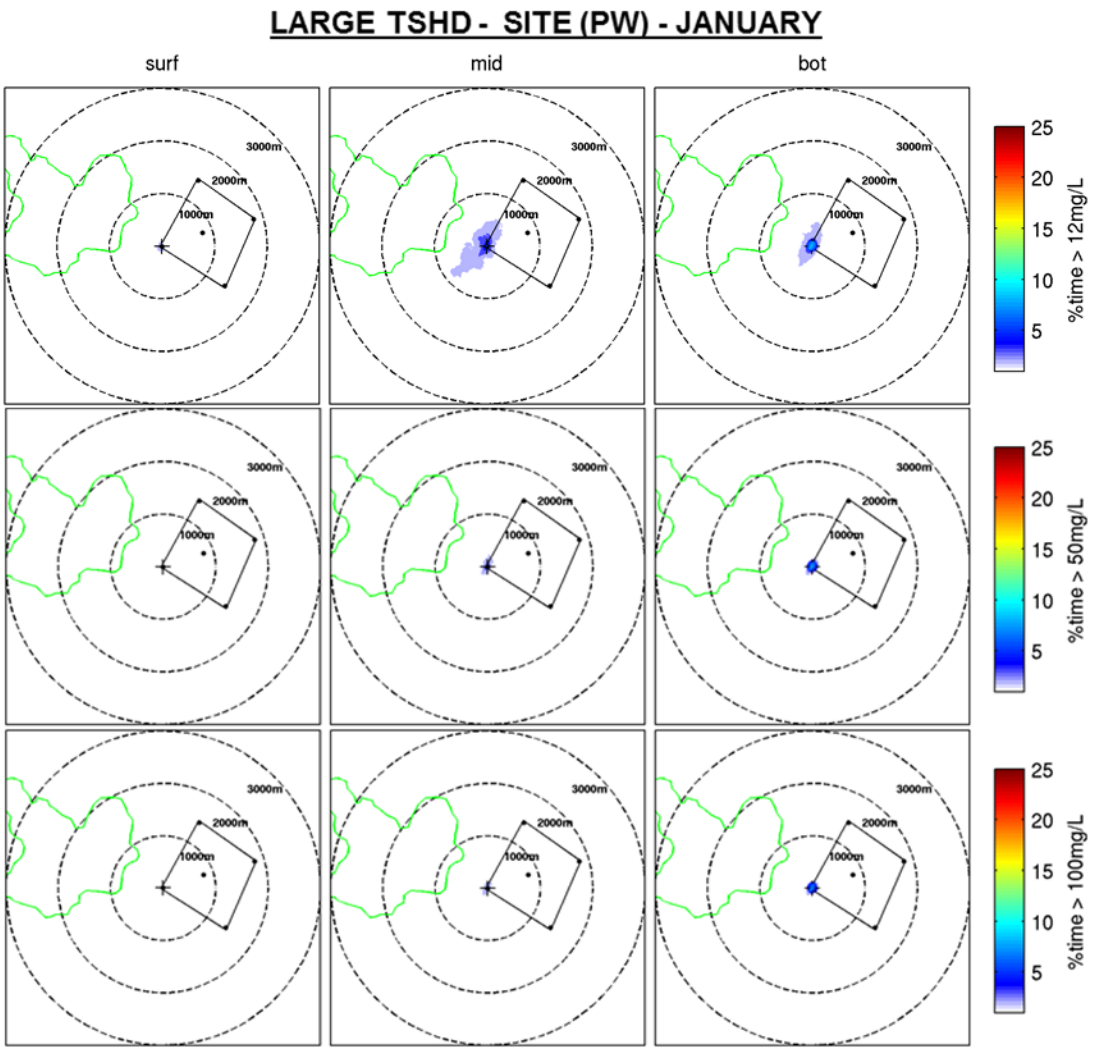

Figure 10.9 Percentage of time *SSC* thresholds of 12, 50, 100 mg.L^{-1} are exceeded during the summer month of January, assuming disposal at site PW with the large TSHD. The green polygon indicates an adjacent reef classified as sensitive.

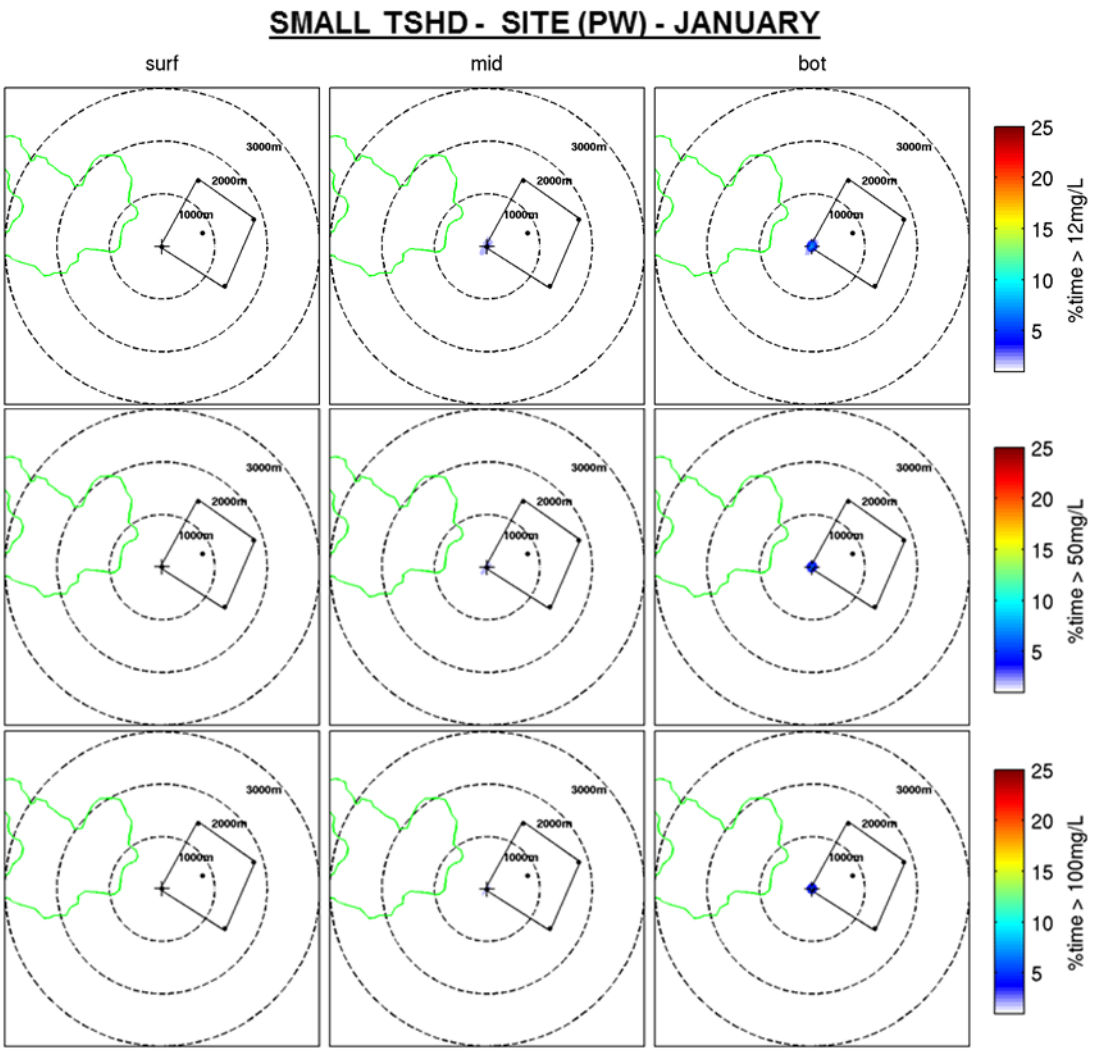

Figure 10.10 Percentage of time *SSC* thresholds of 12, 50, 100 mg.L^{-1} are exceeded during the summer month of January, assuming disposal at site PW with the small TSHD. The green polygon indicates an adjacent reef classified as sensitive.

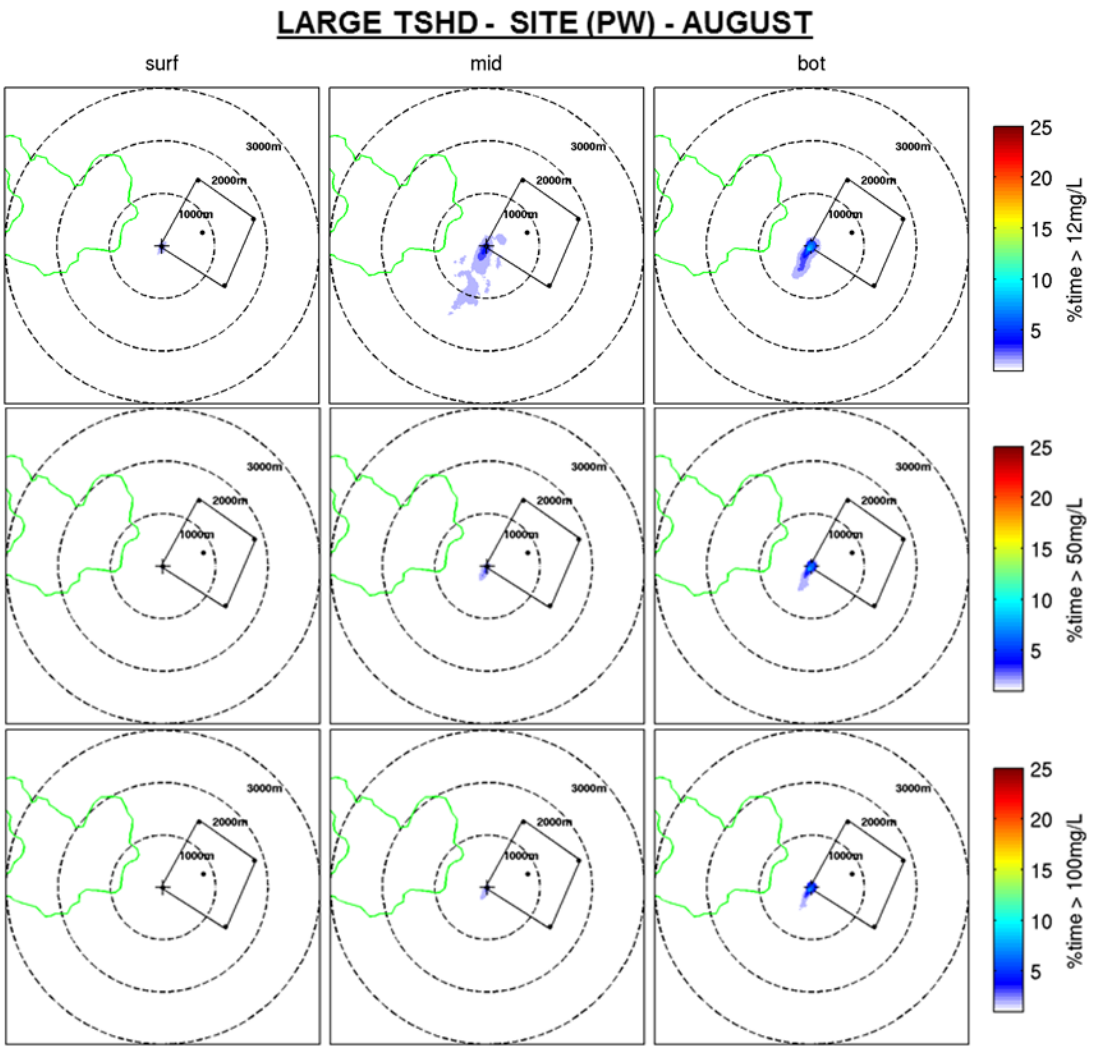

Figure 10.11 Percentage of time *SSC* thresholds of 12, 50, 100 $mg.L^{-1}$ are exceeded during the winter month of August, assuming disposal at site PW with the large TSHD. The green polygon indicates an adjacent reef classified as sensitive.

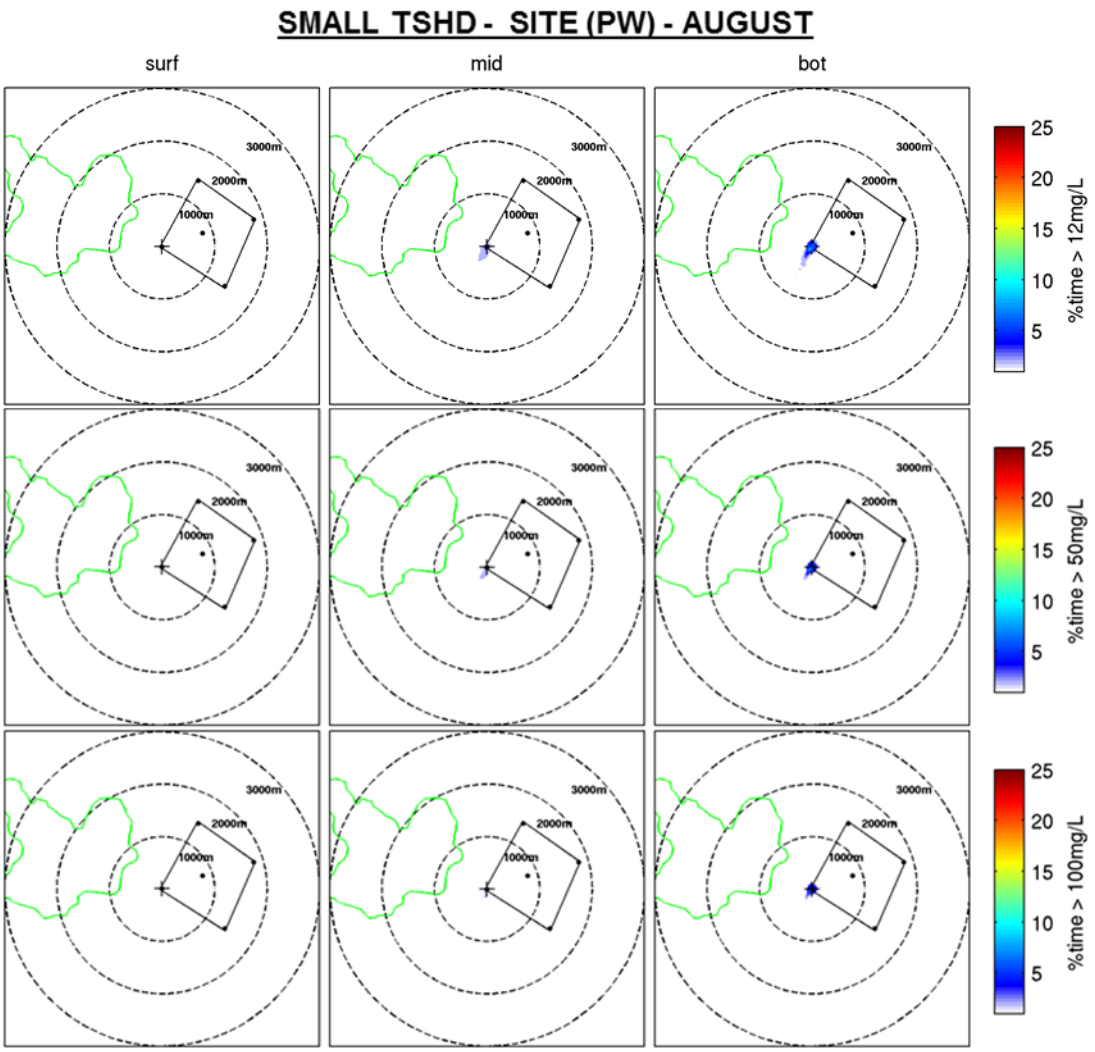

Figure 10.12 Percentage of time *SSC* thresholds of 102, 50, 100 mg.L^{-1} are exceeded during the winter month of August, assuming disposal at site PW with the small TSHD. The green polygon indicates an adjacent reef classified as sensitive.

REFERENCES

Brian T. Coffey and Associates Limited, 2016a. Refining New Zealand Crude Shipping Project - Complementary literature review to inform survey work and report requirements to assess the environmental effects of proposed dredging and spoil disposal activites in the approaches to Mardsen Point.

Brian T. Coffey and Associates Limited, 2016b. Refining New Zealand Crude Shipping Project, Modelling sedimentation effects associated with proposed dredging / Spoil disposal activities - Provisional turbidity / Suspended solids thresholds nominated for the protection of adjacent communities. Prepared for Chancery Green for Refining NZ.

Folk, R.., 1954. The distinction between grain size and mineral composition in sedimentary rock nomenclature. J. Geol. 62, 344–359.

Kerr & Associates Report - Ecology Stage One Pilot Study, 2016.

Kerr, V.C., 2016. Mair Bank channel edge additional characterisation: Crude Freight shipping project, Bream Bay, Whangarei. For Chancery Green on behalf of Refining NZ by Kerr and Associates.

Longdill, P.C., Healy, T.R., 2007. Sediment dynamics surrounding a flood tidal delta adjacent to reclamation and a dredged turning basin. J. Coast. Res. 1097–1105.

McComb, P., Black, K., Atkinson, P., Lim, Y.T., Heafy, T., 1999. The accretion of a breakwater-tip shoal following dredging, in: Proceedings of the 14th Australasian Coastal and Ocean Engineering Conference and the 7th Australasian Port and Harbour Conference. Australia, pp. 394–399.

Morgan, K.M., Kench, P.S., Ford, R.B., 2011. Geomorphic change of an ebb-tidal delta: Mair Bank, Whangarei Harbour, New Zealand. N. Z. J. Mar. Freshw. Res. 45, 15–28.

MSL, 2016. Crude Shipping Project, Whangarei Harbour - Establishment of numerical models of wind, wave, current and sediment dynamics.

OMC International, 2016. Mardsen Point Channel Optimisation.

Royal HaskoningDHV, 2016a. Shipping Channel - Concept Design Report, prepared for Refining NZ., Refining NZ Crude Freight Project.

Royal HaskoningDHV, 2016b. Dredging Methodology Assessment.Technical Memo, prepared for Refining NZ., Refining NZ Crude Freight Project.

Royal HaskoningDHV, 2015. Desktop Simulation Study, prepared for Refining NZ., Refining NZ Crude Freight Project.

Stewart, 2017. Evaluating TSS/NTU Relationship for CSP, Refining NZ. Ryder Consulting January 2017.

Tonkin and Taylor, 2016a. Crude Shipping project, Mid-point multi-criteria alternatives assessment. Prepared for ChanceryGreen for Refining NZ.

Tonkin and Taylor, 2016b. Marsden point Refinery - Crude Freight Project, Vibrocore report (No. 30488.1000). Prepared for Chancery Green on behalf of Refining NZ.

Tonkin and Taylor, 2010. Coastal Erosion Hazard Zone Review. Prepared for Whangarei District Council.

Weppe, S., McComb, P., Coe, L., 2015. Numerical Model Studies to Support the Sustainable Management of Dredge Spoil Deposition in a Complex Nearshore Environment, in: The Proceedings of the Coastal Sediments 2015. World Scientific.

Williams, J.R., Hume, T.M., 2014. Investigation into the decline of pipi at Mair Bank, Whangarei Harbour. Prepared for Northland Regional Council (No. AKL2014-022). NIWA.

Wright, J., Colling, A., Park, D., 1999. Waves, Tides, and Shallow-water Processes, 2nd ed. Butterworth-Heinemann and Open University.

APPENDIX A – WIND STATISTICS

Annual and monthly wind speed statistics at WRB.

Wind speed (m/s))	Parameter					
	Mean ($m\ s^{-1}$)	Median ($m\ s^{-1}$)	P90 ($m\ s^{-1}$)	P95 ($m\ s^{-1}$)	P99 ($m\ s^{-1}$)	Max ($m\ s^{-1}$)
Jan	5.71	5.45	9.28	10.52	13.22	19.24
Feb	5.58	5.35	9.09	10.33	13.33	17.32
Mar	5.75	5.54	9.34	10.71	13.61	23.74
Apr	5.64	5.36	9.25	10.61	13.14	20.01
May	6.10	5.84	10.04	11.21	13.59	19.54
Jun	6.50	6.23	10.60	12.18	14.99	20.09
Jul	6.69	6.26	11.22	13.02	16.14	22.76
Aug	6.46	6.14	10.75	12.09	14.79	20.02
Sep	6.48	6.25	10.44	11.92	14.87	19.88
Oct	6.43	6.24	10.32	11.52	13.65	18.91
Nov	6.17	5.99	9.82	10.95	13.77	20.05
Dec	5.70	5.47	9.31	10.46	13.06	18.56
1979	5.82	5.46	9.60	10.96	13.72	18.91
1980	6.25	6.06	10.26	11.61	14.62	20.08
1981	6.19	5.81	10.37	11.60	13.78	18.11
1982	5.87	5.57	9.62	11.14	13.51	20.39
1983	6.16	5.89	9.76	11.21	14.15	21.08
1984	5.83	5.53	10.03	11.39	14.06	18.49
1985	6.23	6.01	10.35	11.46	14.41	19.63
1986	5.64	5.35	9.39	10.84	13.91	19.24
1987	5.95	5.69	9.86	11.09	13.41	17.13
1988	6.35	6.09	10.34	11.86	15.01	23.74
1989	6.34	5.92	10.59	12.36	15.30	20.02
1990	5.71	5.45	9.34	10.55	13.27	18.49
1991	6.13	6.00	9.65	10.71	12.82	16.61
1992	6.35	6.20	10.10	11.22	14.15	19.20
1993	5.89	5.66	9.71	10.89	13.91	20.07
1994	6.42	6.25	10.20	11.37	13.81	18.30
1995	6.09	5.94	9.64	10.87	13.20	19.88
1996	6.52	6.31	10.33	11.82	14.35	20.09
1997	6.11	5.74	10.05	11.66	14.74	19.21
1998	6.34	5.90	10.70	12.36	15.67	20.05
1999	6.02	5.79	9.87	11.00	13.61	16.56
2000	6.14	5.74	10.09	12.20	14.95	18.20
2001	6.27	6.10	9.92	11.22	14.34	18.08
2002	6.45	6.29	10.16	11.22	13.70	19.58
2003	6.14	5.77	10.03	11.55	14.09	18.51
2004	6.21	6.01	10.07	11.51	13.81	17.13
2005	5.78	5.48	9.65	10.82	14.21	17.98
2006	5.93	5.68	9.66	10.81	14.09	19.58
2007	6.07	5.78	10.12	11.69	14.74	21.62
2008	6.36	6.10	10.19	11.90	14.65	20.83
2009	6.08	5.84	9.87	11.22	14.51	22.76
2010	6.00	5.63	9.94	11.70	14.08	18.89
2011	6.05	5.61	10.27	11.79	14.20	17.27
2012	6.25	6.06	9.99	11.34	13.75	17.29
2013	5.72	5.38	9.63	11.08	13.83	17.39
2014	6.09	5.68	10.15	11.97	15.53	20.85
Annual	6.10	5.83	9.99	11.36	14.27	23.74

Monthly and annual wind speed exceedance probabilities at WRB.

Wind speed (m/s)	Exceedance (%)												
	January	**February**	**March**	**April**	**May**	**June**	**July**	**August**	**September**	**October**	**November**	**December**	**Year**
>2	92.95	92.33	92.53	92.19	93.22	94.07	94.37	94.33	94.21	94.69	94.46	93.18	93.55
>4	70.93	69.37	71.42	70.12	74.10	77.45	78.45	77.18	78.00	78.02	76.81	71.38	74.46
>6	42.44	40.78	43.49	41.48	48.07	52.86	53.24	51.59	53.15	53.42	49.92	42.11	47.75
>8	19.37	17.88	19.44	18.92	24.94	29.84	30.19	29.00	28.91	28.67	24.29	19.05	24.24
>10	6.72	5.94	7.34	6.76	10.22	13.11	15.47	13.65	12.33	12.12	8.85	6.65	9.96
>12	2.51	2.09	2.58	2.23	2.99	5.38	7.43	5.34	4.77	3.77	2.60	2.03	3.65
>14	0.59	0.66	0.72	0.54	0.80	1.86	3.24	1.76	1.66	0.74	0.88	0.50	1.17
>16	0.16	0.14	0.24	0.15	0.15	0.58	1.10	0.43	0.42	0.16	0.24	0.11	0.32
>18	0.04	0.00	0.11	0.03	0.03	0.17	0.38	0.10	0.08	0.04	0.06	0.03	0.09
>20	0.00	0.00	0.07	0.01	0.00	0.02	0.13	0.01	0.00	0.00	0.01	0.00	0.02
>22	0.00	0.00	0.03	0.00	0.00	0.00	0.01	0.00	0.00	0.00	0.00	0.00	0.00

Annual joint probability distribution (parts per thousand) of the wind speed and wind direction at WRB.

Wind speed (m/s)	Wind direction (degT, from)								
	337.5-22.5	**22.5-67.5**	**67.5-112.5**	**112.5-157.5**	**157.5-202.5**	**202.5-247.5**	**247.5-292.5**	**292.5-337.5**	**Total**
0 - 2	6.3	6.2	7.0	7.0	8.1	10.5	11.0	8.3	64.4
2 - 4	17.0	19.3	21.9	18.6	22.5	33.0	35.2	23.4	190.9
4 - 6	25.5	26.1	26.3	20.1	26.1	56.1	49.9	37.1	267.2
6 - 8	25.9	20.2	25.8	14.3	16.2	59.9	43.9	28.9	235.1
8 - 10	19.9	12.4	17.3	9.6	7.8	31.1	29.6	15.2	142.9
10 - 12	10.3	8.0	9.6	5.6	2.8	9.8	11.5	5.5	63.1
12 - 14	4.2	4.6	4.7	3.3	1.0	2.5	3.0	1.6	24.9
14 - 16	1.3	1.9	2.4	1.0	0.4	0.5	0.6	0.3	8.4
16 - 18	0.3	0.5	0.7	0.4	0.1	0.1	0.1	0.0	2.2
18 - 20	0.1	0.2	0.3	0.1	0.0	0.0	0.0	0.0	0.7
20 - 22	0.0	0.0	0.1	0.0	0.0	0.0	0.0	0.0	0.1
Total	110.8	99.4	116.1	80.0	85.0	203.5	184.8	120.3	1000.0

APPENDIX B – WAVE STATISTICS

Annual and monthly total significant wave height statistics at WRB.

H_s (m)	Parameter					
	Mean (m)	**Median (m)**	**P90 (m)**	**P95 (m)**	**P99 (m)**	**Max (m)**
Jan	0.82	0.68	1.48	1.89	2.82	3.85
Feb	0.92	0.79	1.63	1.98	2.85	4.51
Mar	0.90	0.75	1.62	1.94	2.74	5.86
Apr	0.86	0.73	1.59	1.93	2.68	4.63
May	0.80	0.67	1.46	1.82	2.64	5.09
Jun	0.81	0.64	1.59	1.98	2.87	4.89
Jul	0.90	0.66	1.88	2.45	3.68	5.35
Aug	0.78	0.61	1.51	2.01	3.08	4.97
Sep	0.74	0.58	1.41	1.80	2.80	4.51
Oct	0.66	0.55	1.22	1.52	2.16	4.29
Nov	0.69	0.54	1.30	1.62	2.56	5.00
Dec	0.75	0.63	1.33	1.62	2.35	3.59
1979	0.81	0.67	1.44	1.84	2.69	3.69
1980	0.73	0.58	1.31	1.72	3.01	4.15
1981	0.88	0.73	1.63	1.97	2.73	4.16
1982	0.75	0.58	1.39	1.91	3.01	4.33
1983	0.76	0.61	1.43	1.83	2.91	4.54
1984	0.88	0.70	1.71	2.00	3.06	5.09
1985	0.94	0.75	1.75	2.09	3.01	3.88
1986	0.71	0.59	1.33	1.62	2.35	3.37
1987	0.73	0.61	1.24	1.66	2.92	3.50
1988	0.84	0.65	1.59	2.05	3.52	5.86
1989	0.99	0.82	1.89	2.28	3.44	4.97
1990	0.68	0.59	1.23	1.46	1.88	2.34
1991	0.70	0.60	1.26	1.56	2.16	2.89
1992	0.70	0.56	1.26	1.65	2.73	4.63
1993	0.71	0.54	1.42	1.81	2.48	4.22
1994	0.75	0.60	1.39	1.79	2.30	3.31
1995	0.78	0.65	1.38	1.64	2.36	3.15
1996	0.78	0.62	1.48	1.93	2.89	4.89
1997	0.77	0.62	1.37	1.85	2.96	4.51
1998	0.95	0.81	1.64	2.10	2.92	5.00
1999	0.88	0.76	1.53	1.87	2.51	2.91
2000	0.85	0.62	1.71	2.14	3.58	4.40
2001	0.90	0.75	1.67	1.97	3.13	4.05
2002	0.73	0.61	1.33	1.71	2.73	4.21
2003	0.86	0.72	1.58	2.09	2.99	4.51
2004	0.72	0.62	1.26	1.51	2.25	2.92
2005	0.79	0.63	1.58	1.91	2.57	3.14
2006	0.71	0.58	1.31	1.82	2.72	3.38
2007	0.83	0.65	1.59	1.93	3.04	5.02
2008	0.87	0.71	1.57	1.98	2.85	4.12
2009	0.79	0.59	1.54	1.91	2.63	5.35
2010	0.80	0.68	1.47	1.77	2.49	4.29
2011	0.87	0.73	1.62	2.07	2.77	3.88
2012	0.85	0.68	1.61	1.91	2.80	4.63
2013	0.83	0.70	1.59	1.92	2.64	3.41
2014	0.80	0.62	1.51	2.08	3.50	4.84
Annual	0.80	0.65	1.50	1.89	2.85	5.86

Annual and monthly significant swell wave statistics at WRB.

H_s (m)	Parameter					
	Mean (m)	**Median (m)**	**P90 (m)**	**P95 (m)**	**P99 (m)**	**Max (m)**
Jan	0.50	0.39	1.00	1.39	2.09	3.22
Feb	0.57	0.45	1.17	1.42	2.04	3.24
Mar	0.55	0.41	1.13	1.39	2.00	4.85
Apr	0.53	0.40	1.15	1.44	2.03	3.83
May	0.45	0.31	1.00	1.32	2.10	4.03
Jun	0.43	0.26	1.04	1.40	2.13	4.08
Jul	0.52	0.28	1.36	1.85	2.78	4.28
Aug	0.44	0.28	0.98	1.42	2.39	3.99
Sep	0.40	0.25	0.91	1.25	2.01	3.33
Oct	0.33	0.21	0.77	1.06	1.70	2.96
Nov	0.38	0.25	0.84	1.13	1.95	4.05
Dec	0.46	0.35	0.91	1.14	1.76	3.16
1979	0.46	0.35	0.96	1.23	1.91	2.73
1980	0.37	0.23	0.83	1.15	1.96	3.11
1981	0.51	0.40	1.12	1.41	1.80	3.01
1982	0.42	0.28	0.85	1.35	2.31	3.34
1983	0.44	0.31	0.97	1.28	2.12	3.55
1984	0.55	0.38	1.24	1.50	2.55	4.03
1985	0.55	0.39	1.21	1.50	2.26	3.07
1986	0.40	0.29	0.86	1.13	1.72	2.30
1987	0.40	0.29	0.88	1.21	2.12	2.71
1988	0.50	0.31	1.11	1.43	2.88	4.85
1989	0.60	0.43	1.39	1.76	2.63	3.99
1990	0.36	0.28	0.76	0.97	1.33	1.67
1991	0.37	0.25	0.85	1.08	1.54	2.00
1992	0.34	0.22	0.66	1.02	1.96	3.50
1993	0.39	0.23	0.92	1.19	1.78	2.92
1994	0.40	0.25	0.99	1.29	1.94	2.43
1995	0.43	0.30	0.95	1.19	1.94	2.69
1996	0.43	0.29	0.91	1.27	2.38	4.08
1997	0.43	0.30	0.88	1.24	2.32	3.63
1998	0.60	0.47	1.10	1.47	2.21	4.05
1999	0.53	0.40	1.13	1.31	1.73	2.12
2000	0.52	0.30	1.27	1.69	2.74	3.49
2001	0.54	0.40	1.16	1.49	2.34	3.11
2002	0.36	0.20	0.86	1.17	2.20	3.23
2003	0.52	0.36	1.16	1.55	2.32	3.55
2004	0.39	0.27	0.82	1.14	1.80	2.37
2005	0.47	0.31	1.17	1.43	2.04	2.89
2006	0.40	0.27	0.86	1.24	2.23	2.95
2007	0.48	0.34	1.04	1.34	2.08	4.12
2008	0.48	0.34	1.09	1.39	1.98	2.92
2009	0.47	0.32	1.05	1.33	1.88	4.28
2010	0.47	0.33	1.03	1.27	1.65	2.96
2011	0.54	0.40	1.16	1.45	2.18	2.92
2012	0.52	0.39	1.19	1.46	2.11	3.83
2013	0.55	0.41	1.21	1.55	2.00	2.58
2014	0.49	0.35	1.05	1.56	2.59	3.85
Annual	0.46	0.32	1.03	1.36	2.13	4.85

Annual and monthly significant windsea wave statistics at WRB.

H_s (m)	Parameter					
	Mean (m)	**Median (m)**	**P90 (m)**	**P95 (m)**	**P99 (m)**	**Max (m)**
Jan	0.62	0.52	1.13	1.39	2.03	2.76
Feb	0.69	0.60	1.21	1.46	2.10	3.17
Mar	0.68	0.59	1.19	1.45	2.06	3.37
Apr	0.64	0.55	1.14	1.38	1.97	2.68
May	0.62	0.53	1.10	1.35	1.97	3.11
Jun	0.64	0.53	1.19	1.49	2.17	3.03
Jul	0.68	0.53	1.35	1.78	2.54	3.31
Aug	0.60	0.48	1.15	1.51	2.12	3.11
Sep	0.58	0.48	1.06	1.31	2.09	3.05
Oct	0.53	0.46	0.96	1.15	1.65	3.11
Nov	0.55	0.45	1.00	1.21	1.87	2.99
Dec	0.57	0.48	1.03	1.23	1.76	2.73
1979	0.63	0.52	1.12	1.40	2.07	2.74
1980	0.59	0.49	1.09	1.37	2.31	2.88
1981	0.68	0.58	1.19	1.50	2.12	2.97
1982	0.58	0.46	1.07	1.35	2.22	2.88
1983	0.59	0.49	1.08	1.31	2.15	2.85
1984	0.64	0.53	1.17	1.48	2.00	3.11
1985	0.72	0.61	1.34	1.59	2.12	2.61
1986	0.55	0.47	0.97	1.20	1.87	2.76
1987	0.57	0.49	1.00	1.25	2.02	2.53
1988	0.64	0.52	1.23	1.53	2.26	3.37
1989	0.74	0.63	1.28	1.68	2.32	3.11
1990	0.54	0.48	0.96	1.20	1.62	1.85
1991	0.55	0.46	0.99	1.17	1.77	2.51
1992	0.58	0.48	1.05	1.26	2.10	3.31
1993	0.55	0.43	1.11	1.33	2.13	3.05
1994	0.59	0.52	1.03	1.27	1.61	2.45
1995	0.61	0.52	1.05	1.23	1.60	2.38
1996	0.62	0.51	1.17	1.45	2.09	2.84
1997	0.60	0.49	1.09	1.43	2.14	3.04
1998	0.70	0.59	1.26	1.55	2.29	3.04
1999	0.67	0.59	1.18	1.44	1.93	2.55
2000	0.64	0.50	1.18	1.59	2.29	3.07
2001	0.68	0.59	1.18	1.46	2.27	2.65
2002	0.59	0.50	1.04	1.27	1.77	2.94
2003	0.64	0.55	1.12	1.43	2.06	3.17
2004	0.56	0.49	0.96	1.15	1.61	2.32
2005	0.60	0.51	1.10	1.31	1.77	2.17
2006	0.54	0.46	0.96	1.21	1.83	2.62
2007	0.64	0.51	1.21	1.52	2.36	3.05
2008	0.68	0.58	1.23	1.47	2.18	2.94
2009	0.60	0.47	1.10	1.48	2.08	3.21
2010	0.62	0.53	1.09	1.38	2.09	3.12
2011	0.64	0.54	1.23	1.50	2.09	2.65
2012	0.63	0.53	1.21	1.43	2.04	2.77
2013	0.58	0.50	1.04	1.26	1.86	2.65
2014	0.59	0.45	1.11	1.56	2.39	3.06
Annual	0.62	0.51	1.12	1.39	2.09	3.37

Monthly and annual total significant wave height exceedance probabilities at WRB.

H_s (m)	Exceedence (%)												
	January	**February**	**March**	**April**	**May**	**June**	**July**	**August**	**September**	**October**	**November**	**December**	**Year**
>0.5	71.68	79.24	76.61	72.69	69.06	63.54	66.11	62.24	60.01	56.10	55.23	65.57	66.45
>1	24.35	33.68	31.82	30.45	25.18	26.96	29.41	22.61	20.66	16.32	18.52	22.66	25.17
>1.5	9.72	13.21	13.03	11.54	9.33	11.54	15.99	10.09	8.52	5.14	6.27	6.68	10.07
>2	4.22	4.84	4.41	4.24	3.72	4.80	8.40	5.05	3.13	1.69	2.48	2.13	4.09
>2.5	1.95	1.68	1.46	1.56	1.38	1.92	4.82	2.45	1.40	0.35	1.16	0.80	1.75
>3	0.53	0.71	0.73	0.51	0.48	0.83	2.64	1.24	0.72	0.11	0.30	0.36	0.77
>3.5	0.08	0.20	0.40	0.16	0.20	0.42	1.38	0.34	0.31	0.03	0.20	0.02	0.31
>4	0.00	0.02	0.21	0.07	0.08	0.20	0.57	0.13	0.05	0.01	0.14	0.00	0.12
>4.5	0.00	0.01	0.10	0.02	0.03	0.05	0.19	0.02	0.01	0.00	0.08	0.00	0.04
>5	0.00	0.00	0.08	0.00	0.01	0.00	0.03	0.00	0.00	0.00	0.00	0.00	0.01
>5.5	0.00	0.00	0.02	0.00	0.00	0.00	0.00	0.00	0.00	0.00	0.00	0.00	0.00

Annual joint probability distribution (parts per thousand) of the total significant wave height and mean wave direction at peak energy at WRB.

H_s (m)	Wave direction (degT)								
	337.5 -22.5	**22.5 -67.5**	**67.5 -112.5**	**112.5 -157.5**	**157.5 -202.5**	**202.5 -247.5**	**247.5 -292.5**	**292.5 -337.5**	**Total**
0 - 0.5	0.2	6.5	269.3	11.9	10.8	17.2	12.5	8.4	336.8
0.5 - 1	0.1	6.8	337.8	15.6	17.0	23.9	6.8	4.0	412.0
1 - 1.5	0.0	0.3	143.6	3.8	1.5	1.4	0.1	0.0	150.7
1.5 - 2	0.0	0.0	58.5	1.1	0.0	0.0	0.0	0.0	59.6
2 - 2.5	0.0	0.0	22.9	0.5	0.0	0.0	0.0	0.0	23.4
2.5 - 3	0.0	0.0	9.8	0.0	0.0	0.0	0.0	0.0	9.8
3 - 3.5	0.0	0.0	4.5	0.0	0.0	0.0	0.0	0.0	4.5
3.5 - 4	0.0	0.0	1.8	0.0	0.0	0.0	0.0	0.0	1.8
4 - 4.5	0.0	0.0	0.8	0.0	0.0	0.0	0.0	0.0	0.8
4.5 - 5	0.0	0.0	0.3	0.0	0.0	0.0	0.0	0.0	0.3
5 - 5.5	0.0	0.0	0.1	0.0	0.0	0.0	0.0	0.0	0.1
Total	0.3	13.6	849.4	32.9	29.3	42.5	19.4	12.4	1000.0

Annual joint probability distribution (parts per thousand) of the total significant wave height and peak wave period at WRB.

H_s (m)	Peak wave period T_p (s)									
	2-4	**4-6**	**6-8**	**8-10**	**10-12**	**12-14**	**14-16**	**16-18**	**18-20**	**Total**
0 - 0.5	60.0	13.5	27.9	138.2	63.9	19.6	5.7	1.5	0.1	330.4
0.5 - 1	62.8	42.8	61.1	159.2	62.4	19.7	3.5	0.5	0.1	412.1
1 - 1.5	2.1	11.3	37.2	62.7	29.1	7.4	0.7	0.1	0.0	150.6
1.5 - 2	0.0	1.1	11.0	27.6	16.2	3.7	0.2	0.0	0.0	59.8
2 - 2.5	0.0	0.1	4.2	9.9	7.1	2.1	0.0	0.0	0.0	23.4
2.5 - 3	0.0	0.0	0.9	4.7	3.2	0.9	0.0	0.0	0.0	9.7
3 - 3.5	0.0	0.0	0.2	1.8	2.0	0.4	0.1	0.0	0.0	4.5
3.5 - 4	0.0	0.0	0.0	0.7	0.9	0.3	0.0	0.0	0.0	1.9
4 - 4.5	0.0	0.0	0.0	0.3	0.4	0.1	0.0	0.0	0.0	0.8
4.5 - 5	0.0	0.0	0.0	0.1	0.2	0.0	0.0	0.0	0.0	0.3
5 - 5.5	0.0	0.0	0.0	0.0	0.1	0.0	0.0	0.0	0.0	0.1
Total	124.9	68.8	142.5	405.2	185.5	54.2	10.2	2.1	0.2	1000.0

Annual persistence non-exceedance (%) for total significant wave height at WRB.

Hs (m)	Duration (hours)											
	> 6	**> 12**	**> 18**	**> 24**	**> 30**	**> 36**	**> 42**	**> 48**	**> 54**	**> 60**	**> 66**	**> 72**
<= 0.5	33.06	32.11	31	29.63	28.29	26.66	25.27	23.51	21.73	20.21	18.71	17.16
<= 1	74.75	74.54	74.2	73.87	73.42	72.93	72.4	71.73	71.18	70.59	69.99	69.37
<= 1.5	89.89	89.83	89.71	89.56	89.32	89.13	88.99	88.86	88.71	88.53	88.33	88.17
<= 2	95.88	95.83	95.8	95.77	95.75	95.69	95.63	95.55	95.5	95.41	95.33	95.28
<= 2.5	98.24	98.22	98.21	98.19	98.19	98.18	98.17	98.12	98.11	98.11	98.11	98.06
<= 3	99.23	99.22	99.21	99.19	99.19	99.18	99.18	99.18	99.18	99.18	99.18	99.18
<= 3.5	99.68	99.68	99.68	99.68	99.67	99.67	99.67	99.67	99.67	99.67	99.67	99.67
<= 4	99.87	99.87	99.87	99.87	99.87	99.87	99.87	99.87	99.87	99.87	99.85	99.85

APPENDIX C – TIDAL AND NON-TIDAL TIME SERIES

Tidal (blue) and non-tidal (red) time series of the current velocities extracted from SELFE and ROMS, respectively, at the positions R4 and R5 at the seaward entrance of the delta.

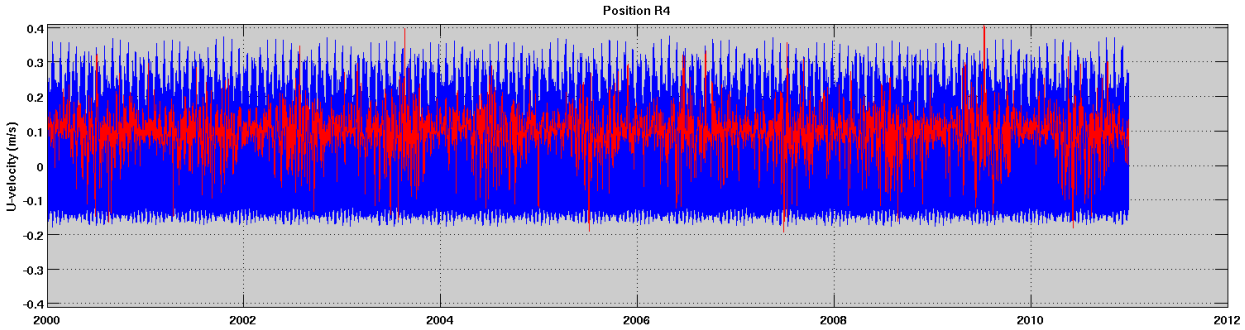

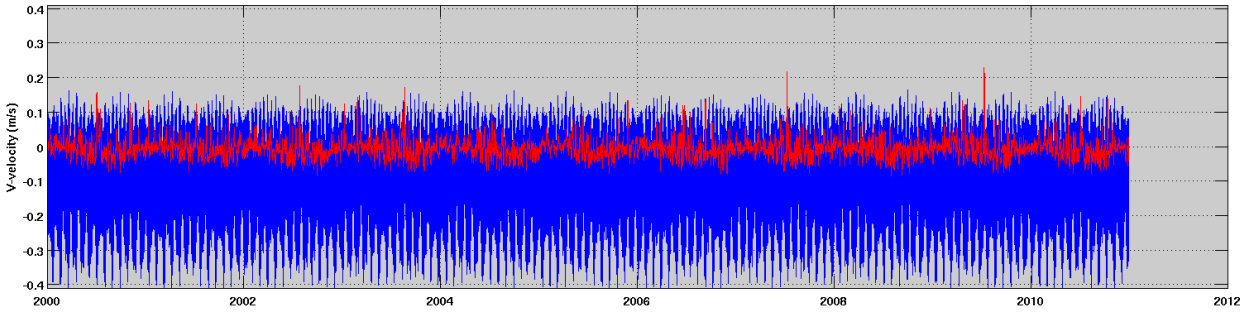

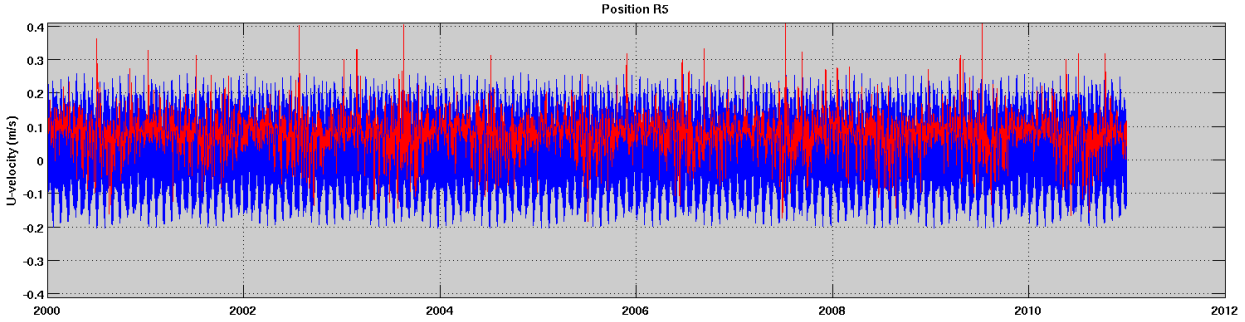

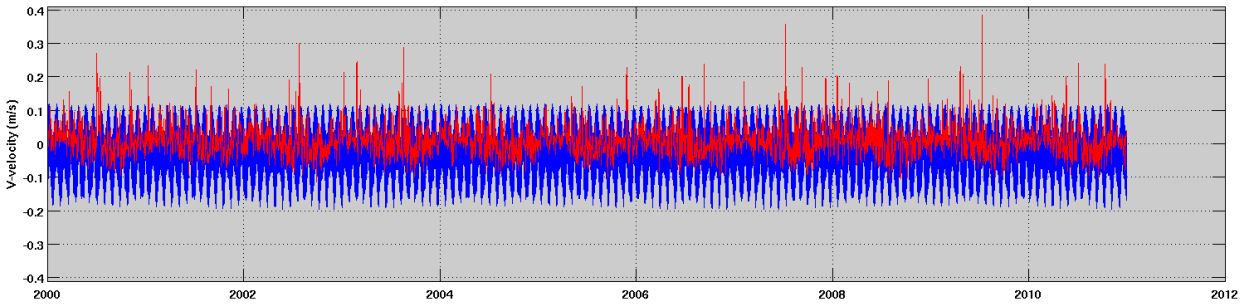

APPENDIX D – ADDITIONAL DREDGING PLUME RESULTS

Probabilistic *SSC* plumes during overflow phase (large TSHD) at site R2 at three levels of the water column. SSC plumes are illustrated for a 10, 30, 50 and 79 min period of overflow.

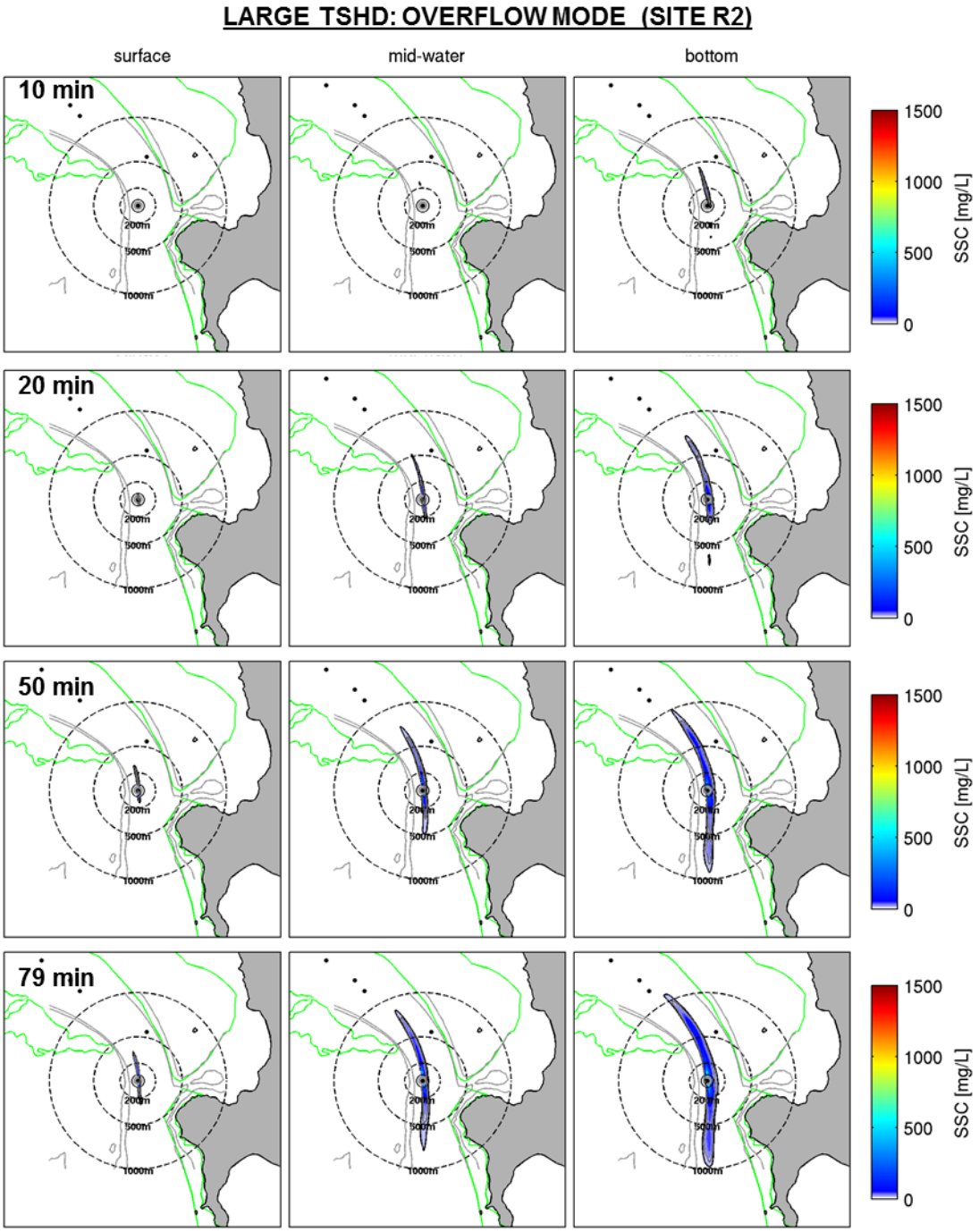

Probabilistic *SSC* plumes during overflow phase (large TSHD) at site R3 at three levels of the water column. SSC plumes are illustrated for a 10, 30, 50 and 79 min period of overflow.

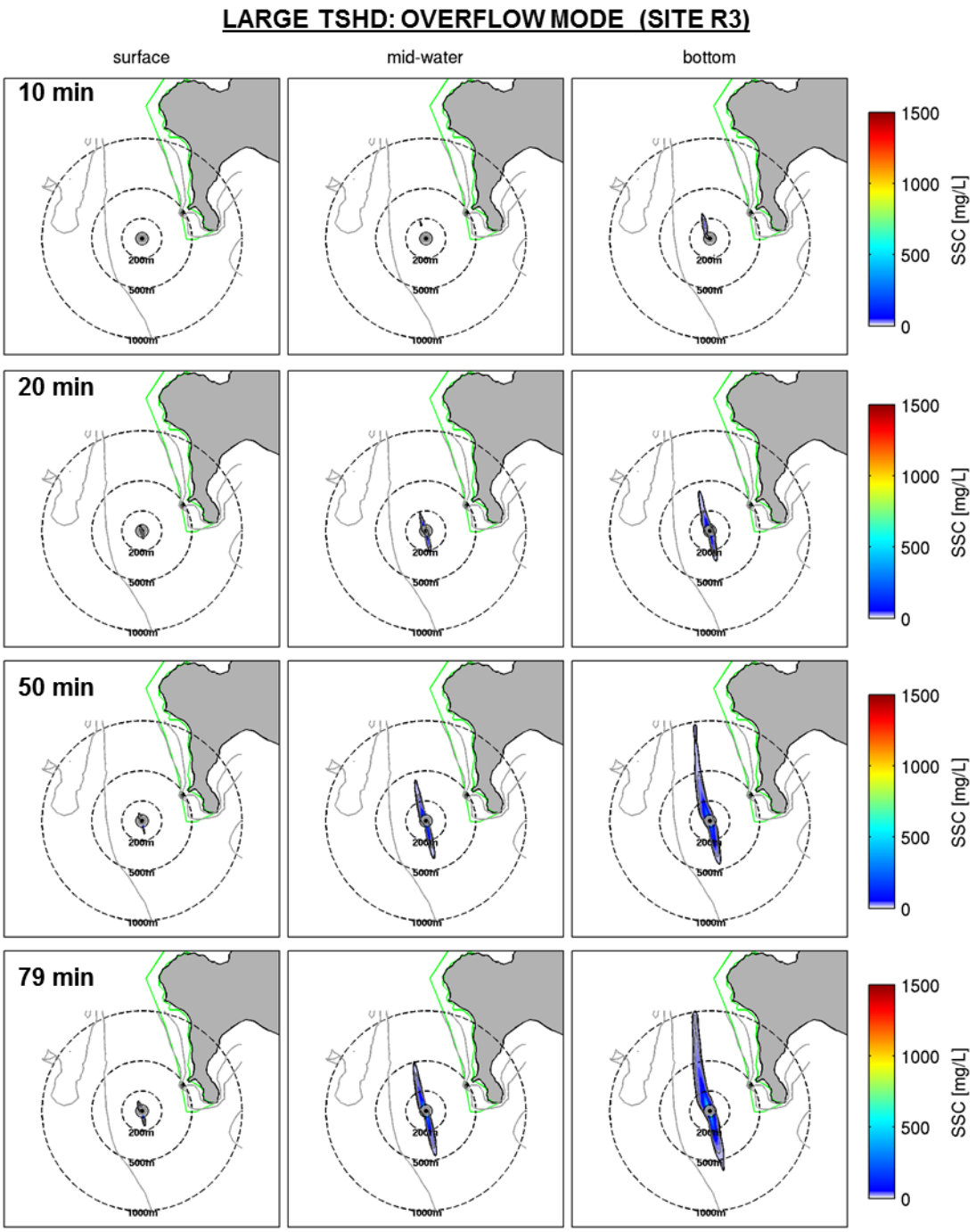

Probabilistic *SSC* plumes during overflow phase (large TSHD) at site R4 at three levels of the water column. SSC plumes are illustrated for a 10, 30, 50 and 79 min period of overflow.

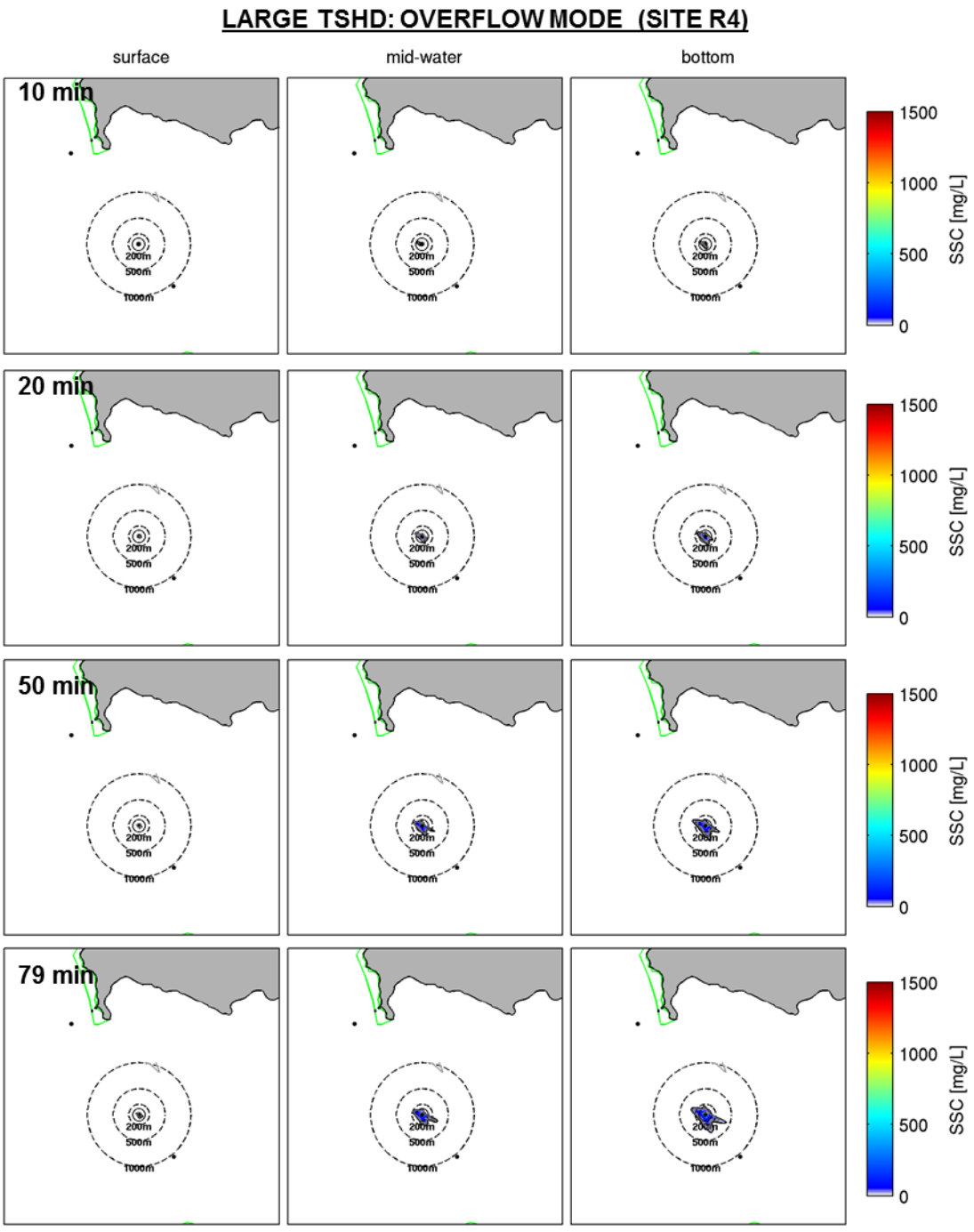

Probabilistic *SSC* plumes during overflow phase (large TSHD) at site R7 at three levels of the water column. SSC plumes are illustrated for a 10, 30, 50 and 79 min period of overflow.

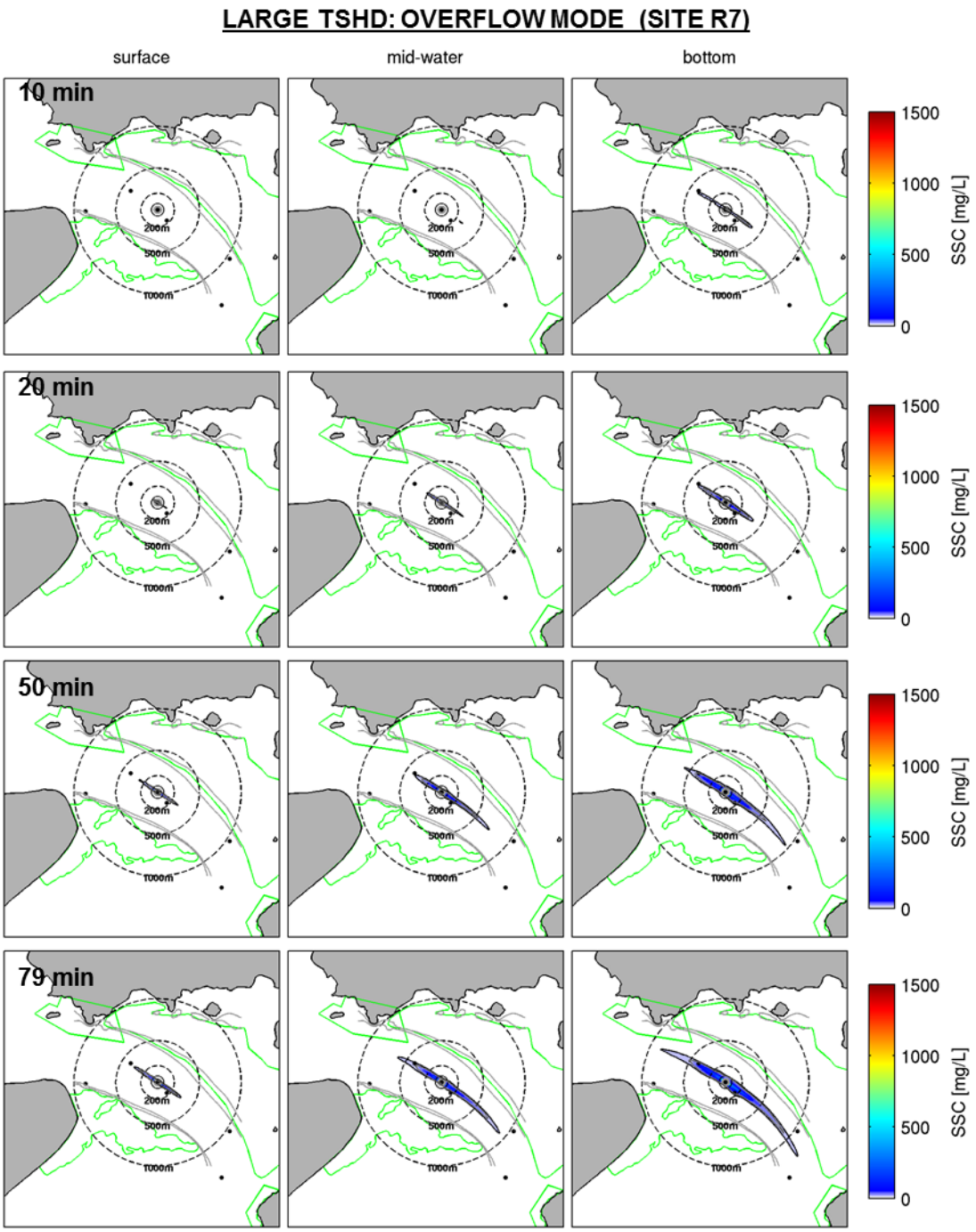

Probabilistic *SSC* plumes during overflow phase (large TSHD) at site R8 at three levels of the water column. SSC plumes are illustrated for a 10, 30, 50 and 79 min period of overflow.

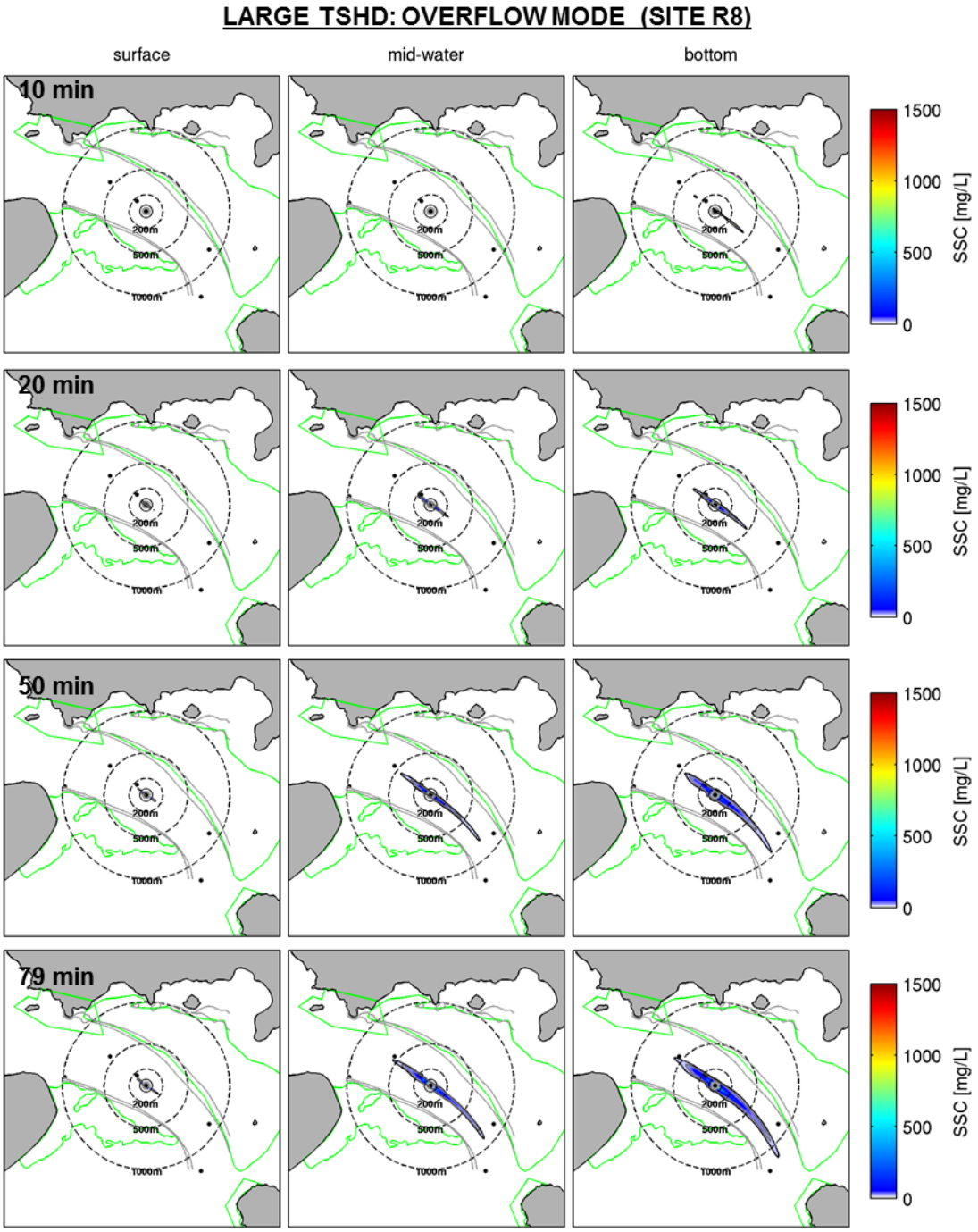

Probabilistic *SSC* plumes during overflow phase (small TSHD) at site R2 at three levels of the water column. SSC plumes are illustrated for a 10, 30, 50 and 95 min period of overflow.

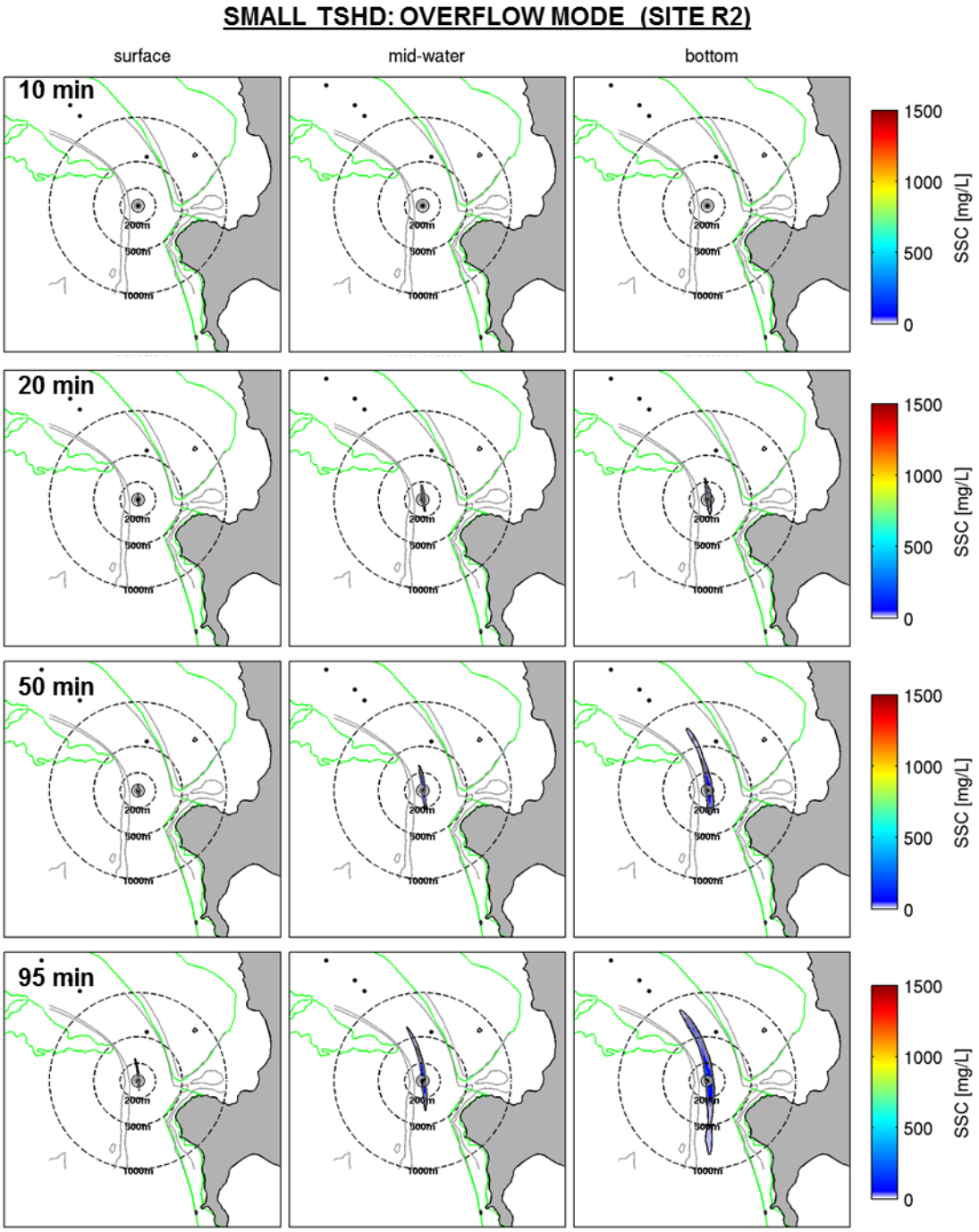

Probabilistic *SSC* plumes during overflow phase (small TSHD) at site R3 at three levels of the water column. SSC plumes are illustrated for a 10, 30, 50 and 95 min period of overflow.

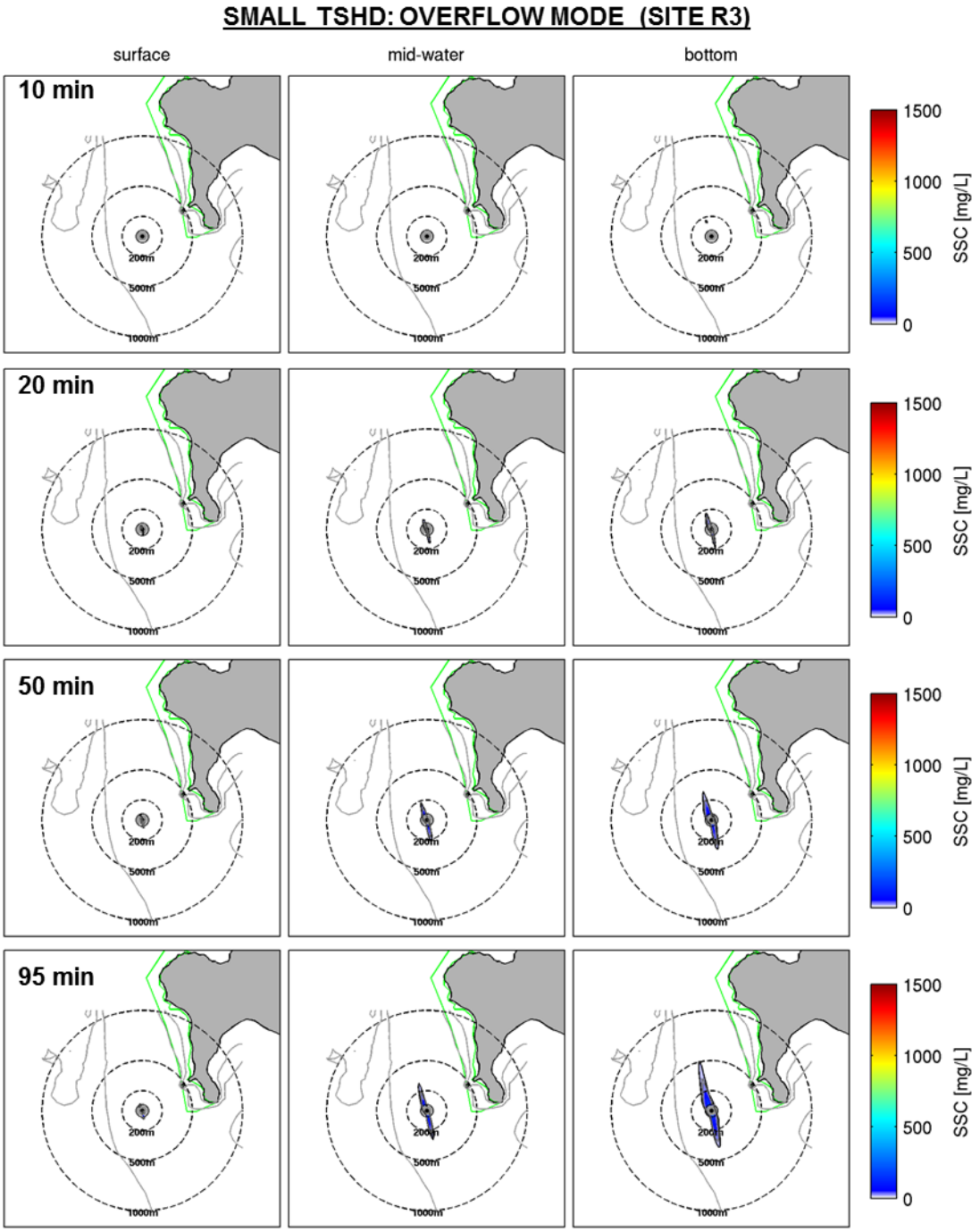

Probabilistic *SSC* plumes during overflow phase (small TSHD) at site R4 at three levels of the water column. SSC plumes are illustrated for a 10, 30, 50 and 95 min period of overflow.

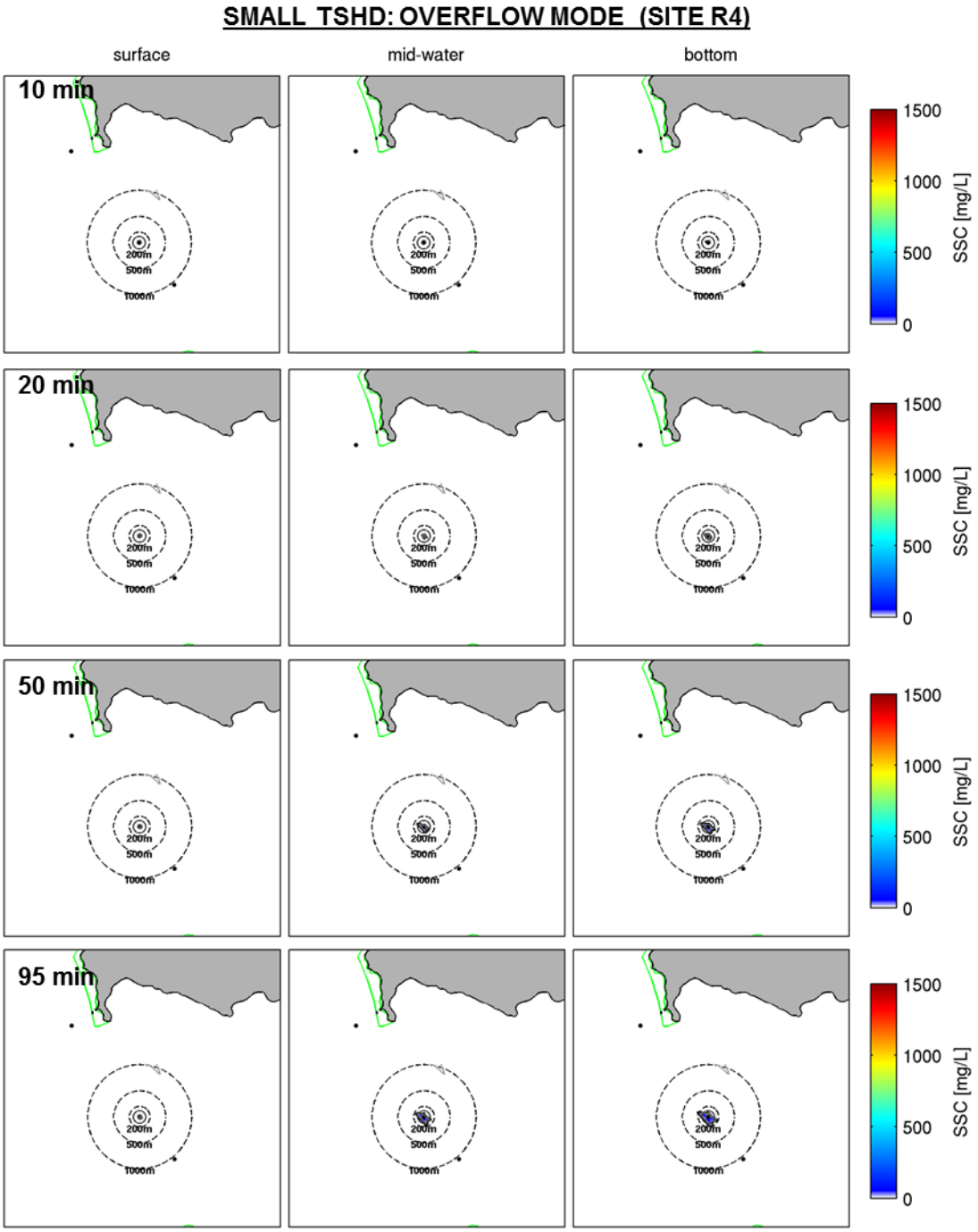

Probabilistic *SSC* plumes during overflow phase (small TSHD) at site R7 at three levels of the water column. SSC plumes are illustrated for a 10, 30, 50 and 95 min period of overflow.

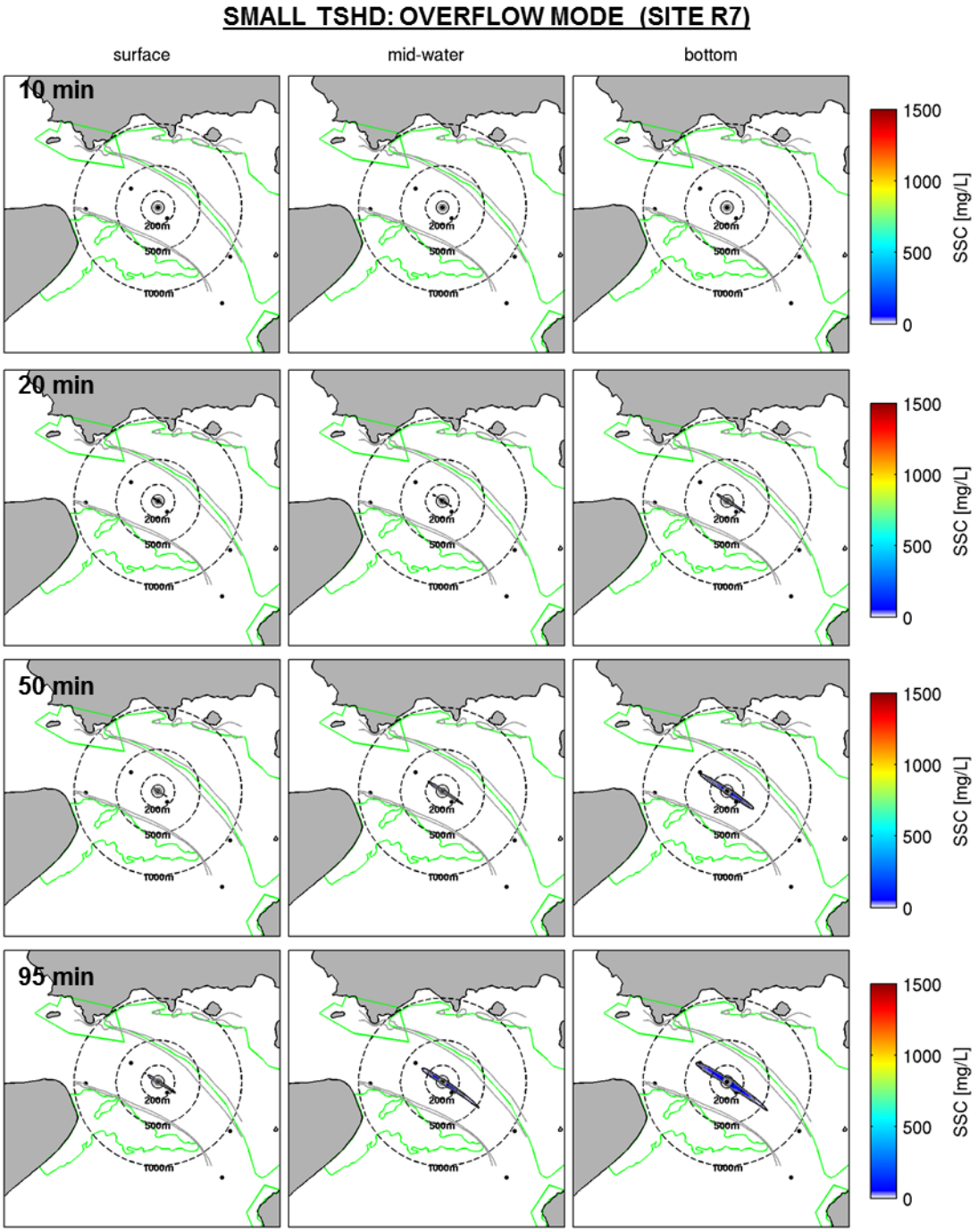

Probabilistic *SSC* plumes during overflow phase (small TSHD) at site R8 at three levels of the water column. SSC plumes are illustrated for a 10, 30, 50 and 95 min period of overflow.

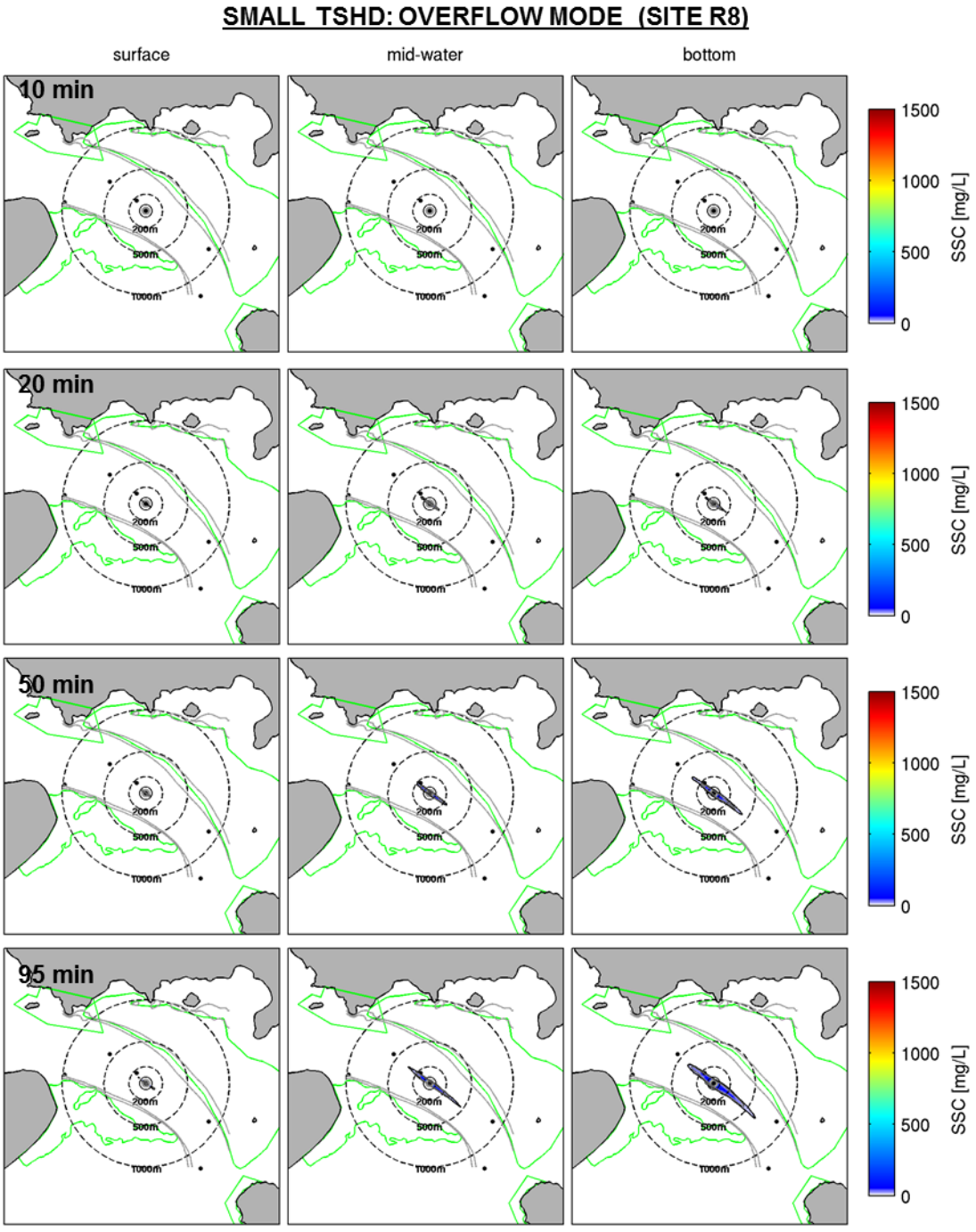

APPENDIX E – ADDITIONAL DREDGING PLUME RESULTS

Probabilistic *SSC* plumes during dredging phase (large TSHD) at sites R0 to R4 at three levels of the water column considering a 1.5 % production rate for the drag head source.

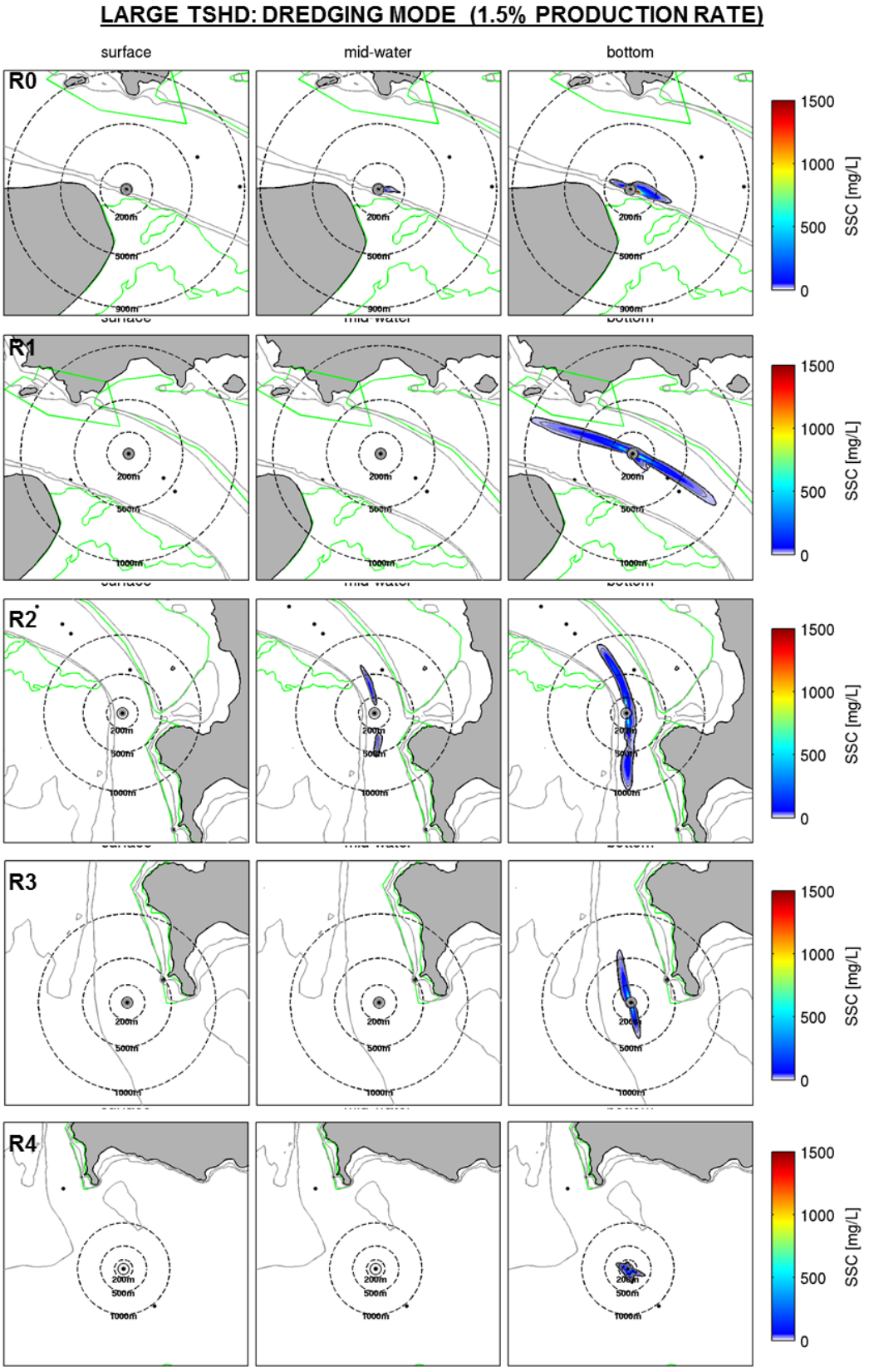

Probabilistic *SSC* plumes during dredging phase (large TSHD) at sites R0 to R4 at three levels of the water column considering a 3.0 % production rate for the drag head source.

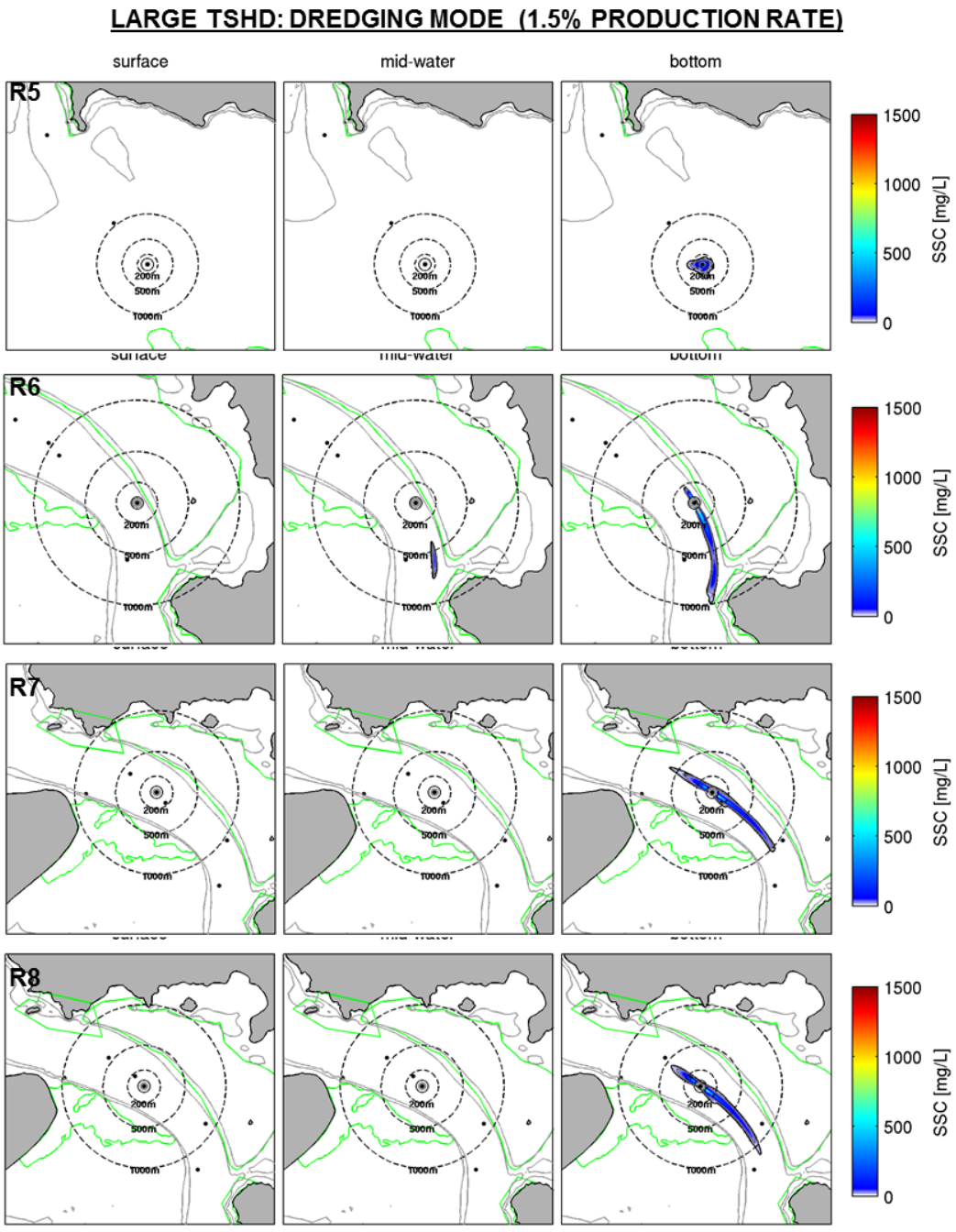

Probabilistic *SSC* plumes during dredging phase (large TSHD) at sites R5 to R8 at three levels of the water column considering a 1.5 % production rate for the drag head source.

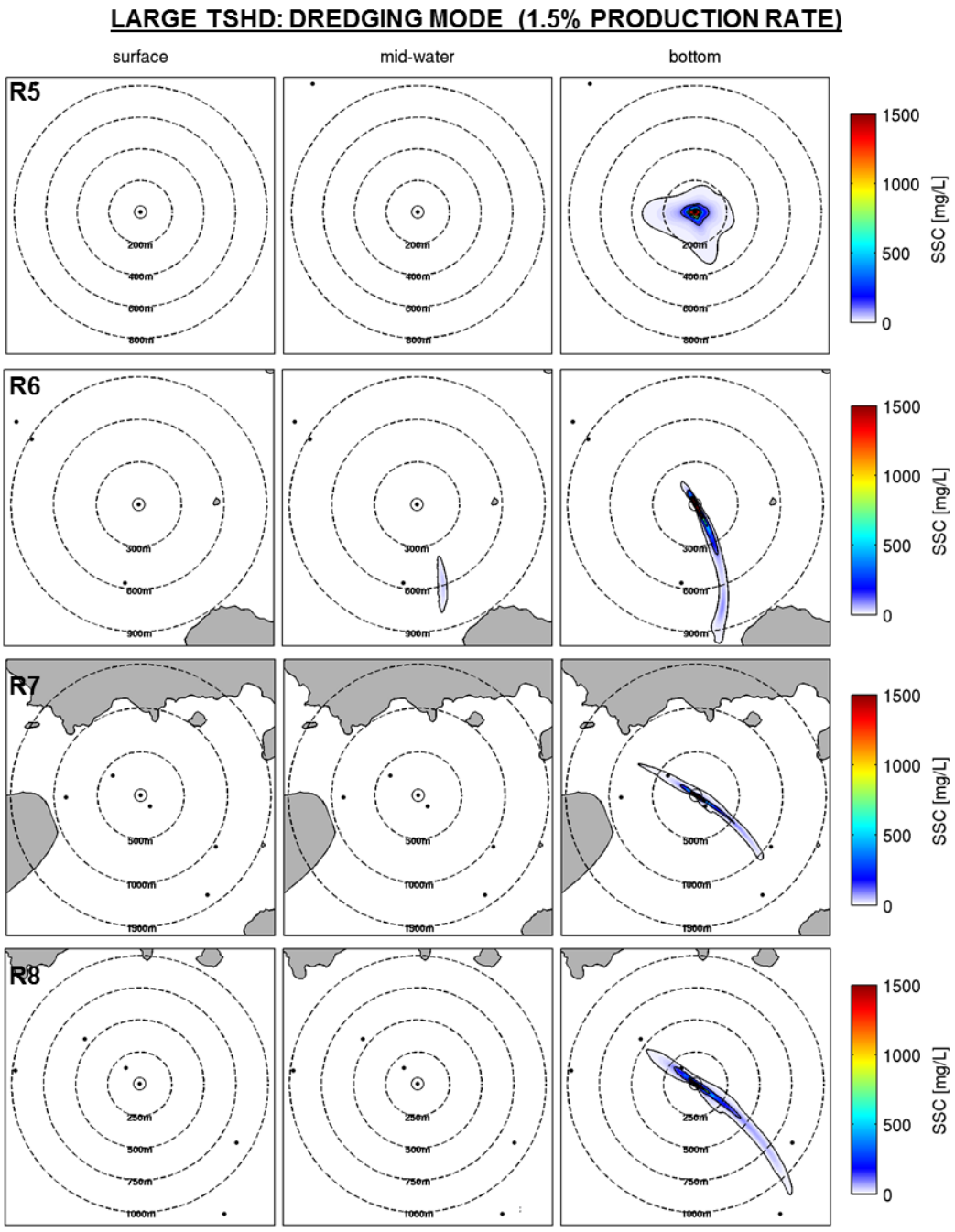

Probabilistic *SSC* plumes during dredging phase (small TSHD) at sites R0 to R4 at three levels of the water column considering a 1.5 % production rate for the drag head source.

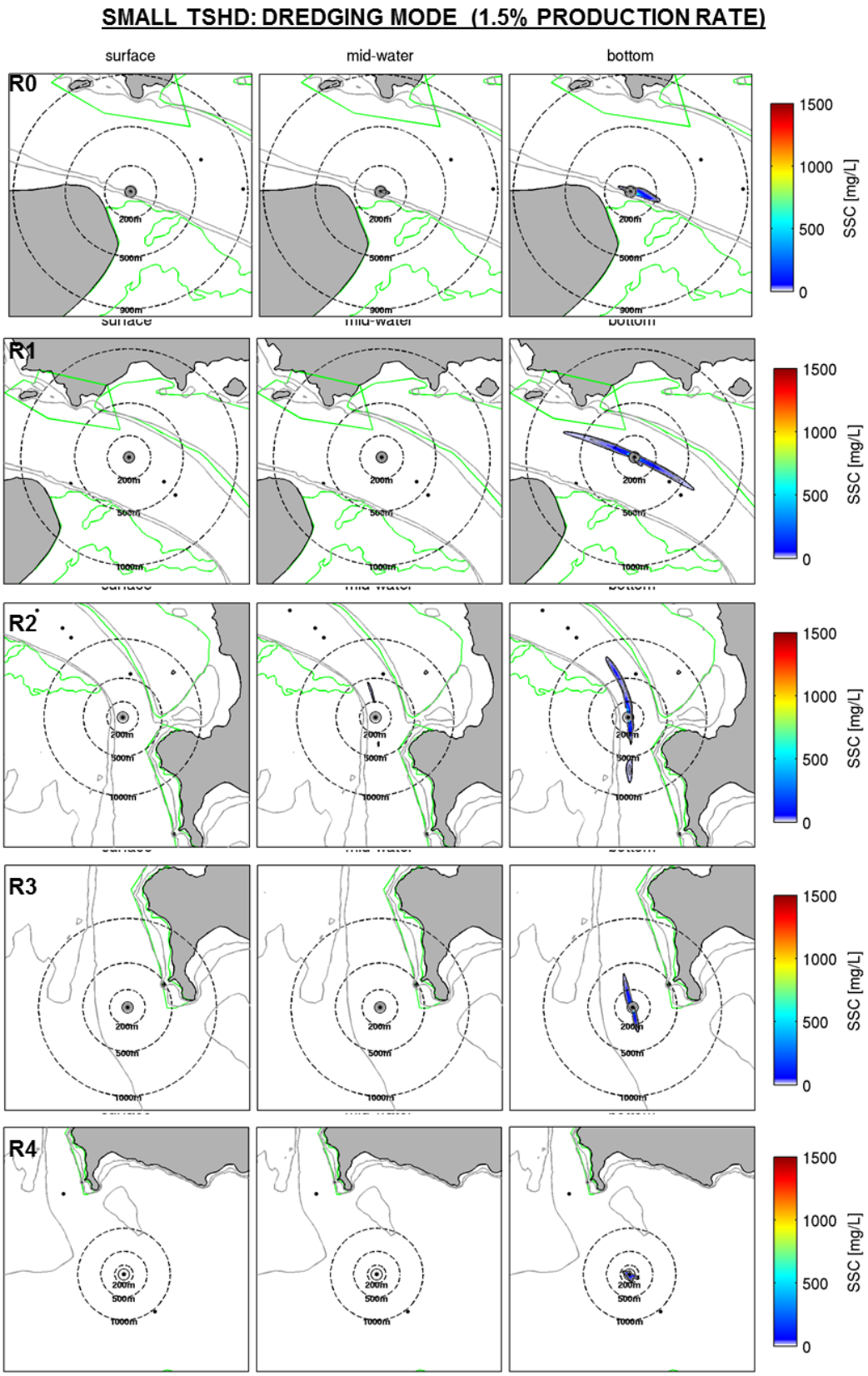

Probabilistic *SSC* plumes during dredging phase (small TSHD) at sites R5 to R8 at three levels of the water column considering a 1.5 % production rate for the drag head source.

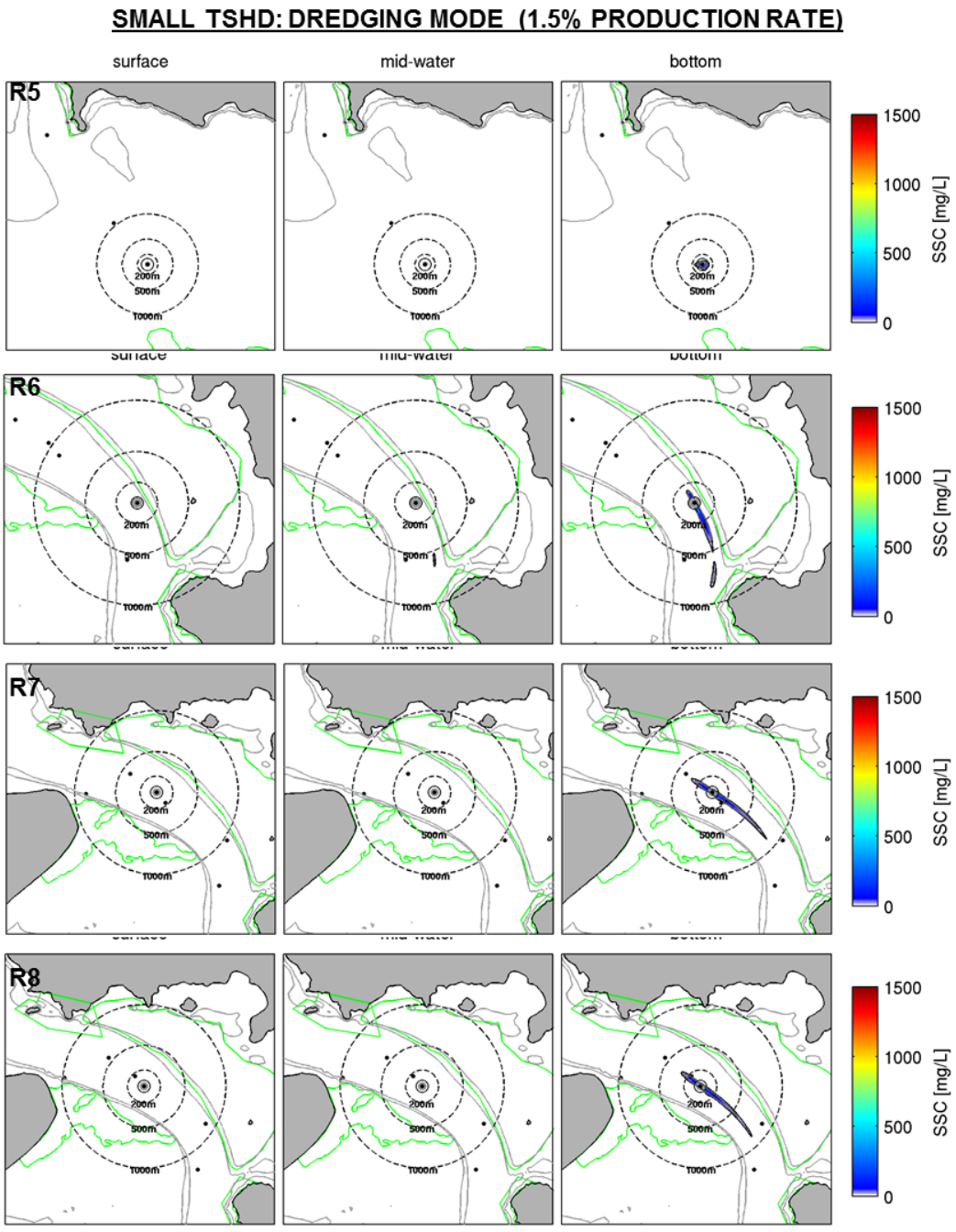

APPENDIX F – PLUME MODELLING AT DIFFERENT TIDE STAGES

Probabilistic *SSC* plumes at Neap ebb tide during dredging phase (large TSHD) at sites R0 to R4 at three levels of the water column considering a 3.0 % production rate for the drag head source.

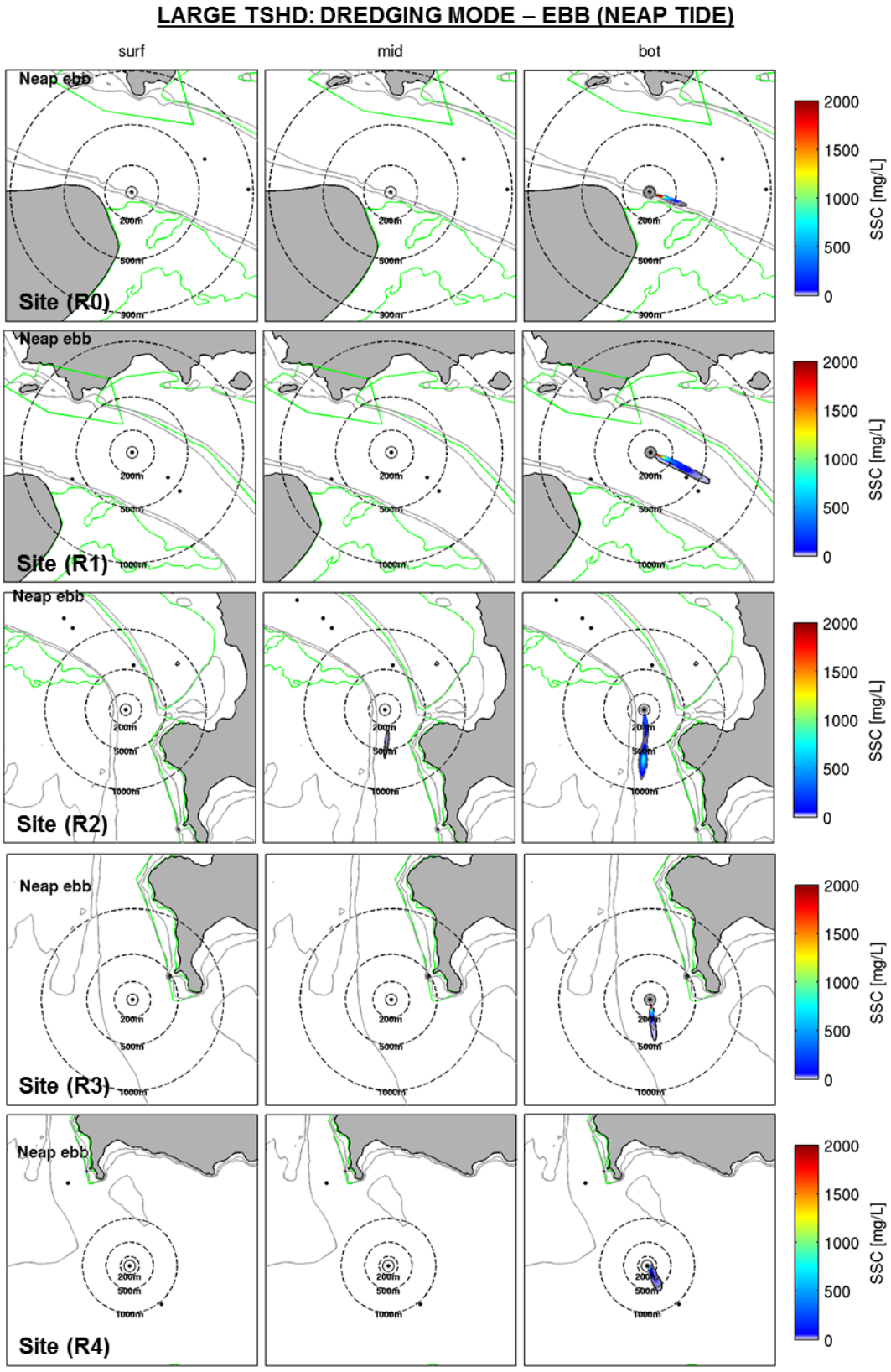

Probabilistic *SSC* plumes at Neap ebb tide during dredging phase (large TSHD) at sites R5 to R8 at three levels of the water column considering a 3.0 % production rate for the drag head source.

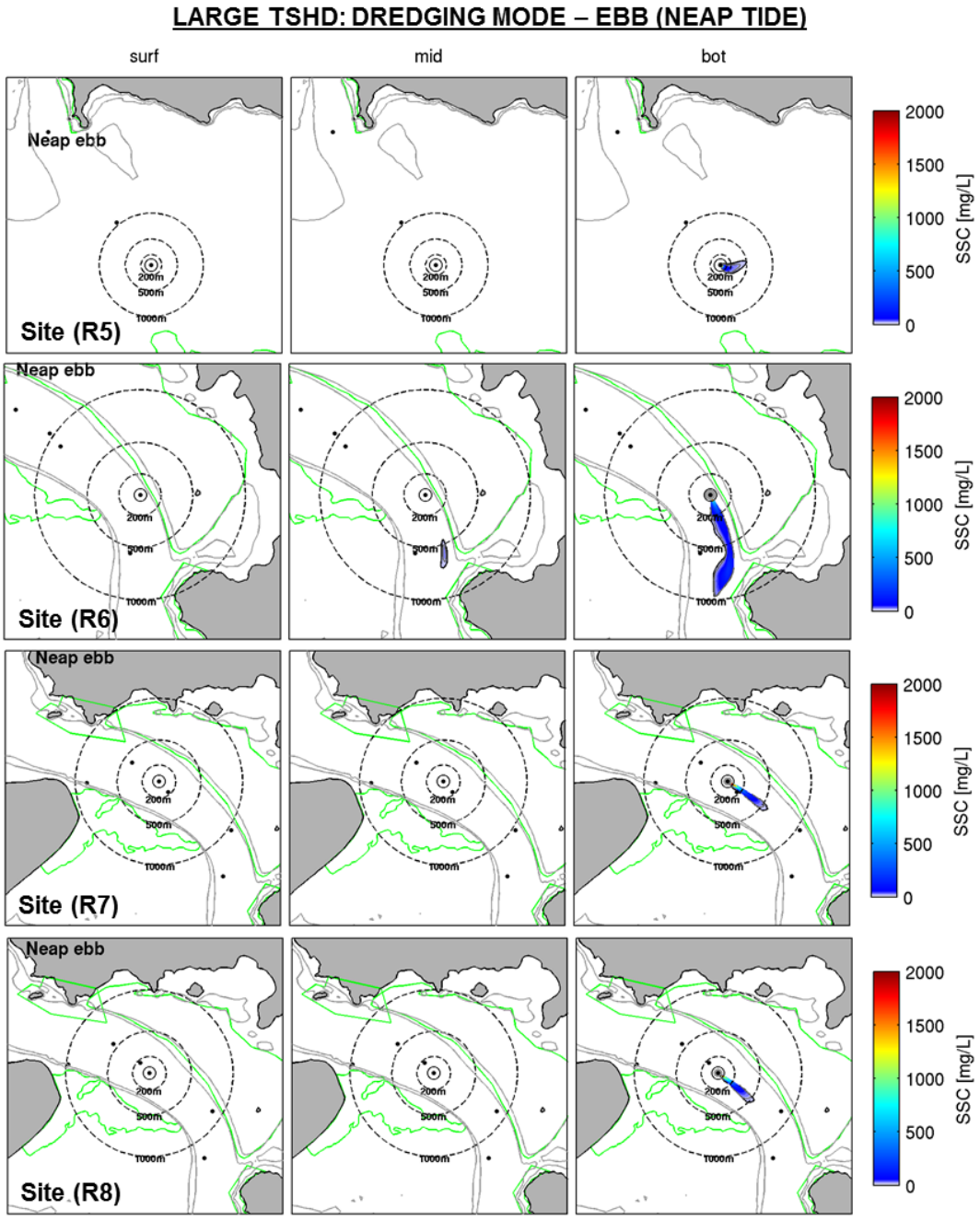

Probabilistic *SSC* plumes at Neap ebb tide during dredging phase (small TSHD) at sites R0 to R4 at three levels of the water column considering a 3.0 % production rate for the drag head source.

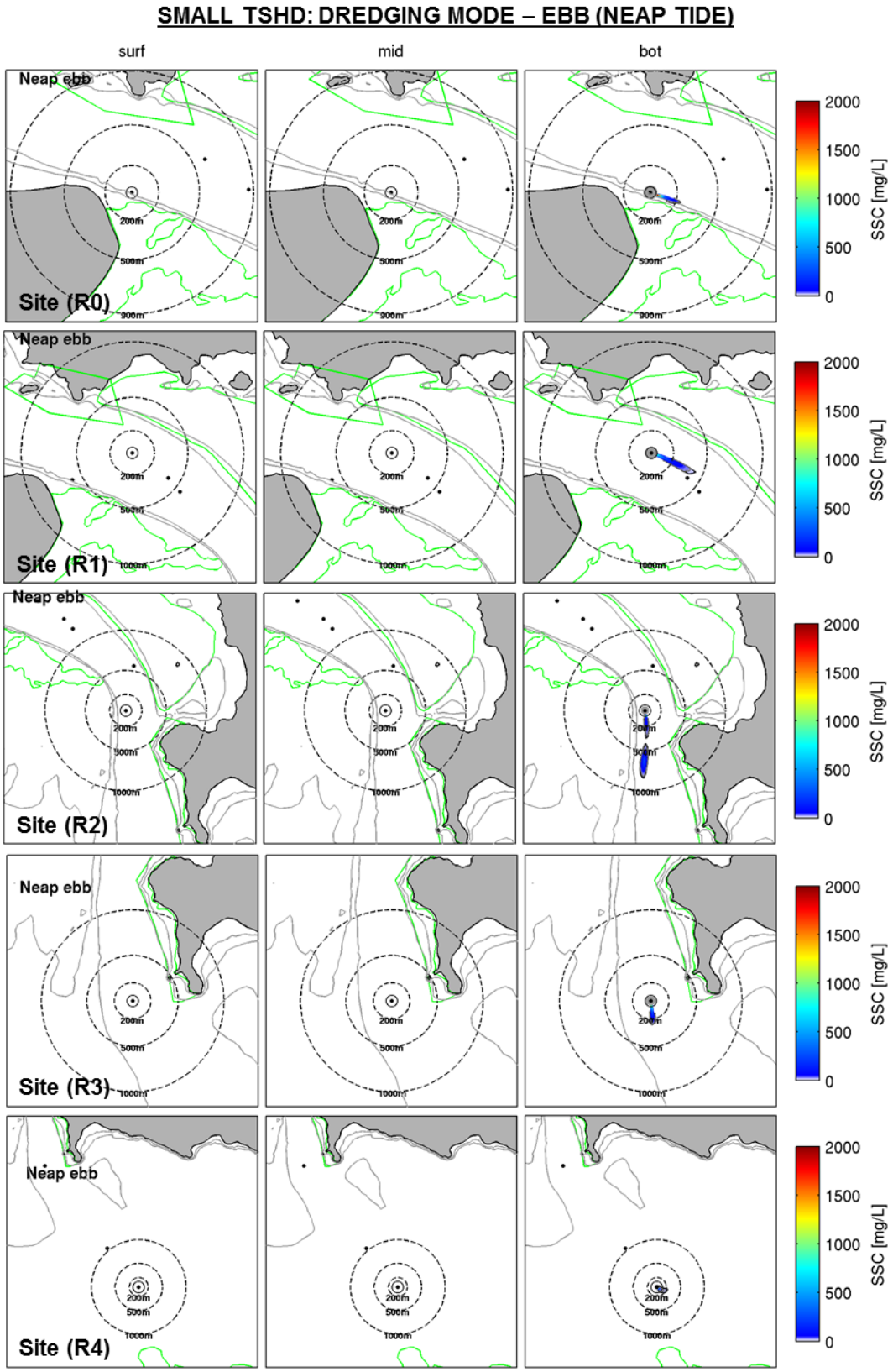

Probabilistic *SSC* plumes at Neap ebb tide during dredging phase (small TSHD) at sites R5 to R8 at three levels of the water column considering a 3.0 % production rate for the drag head source.

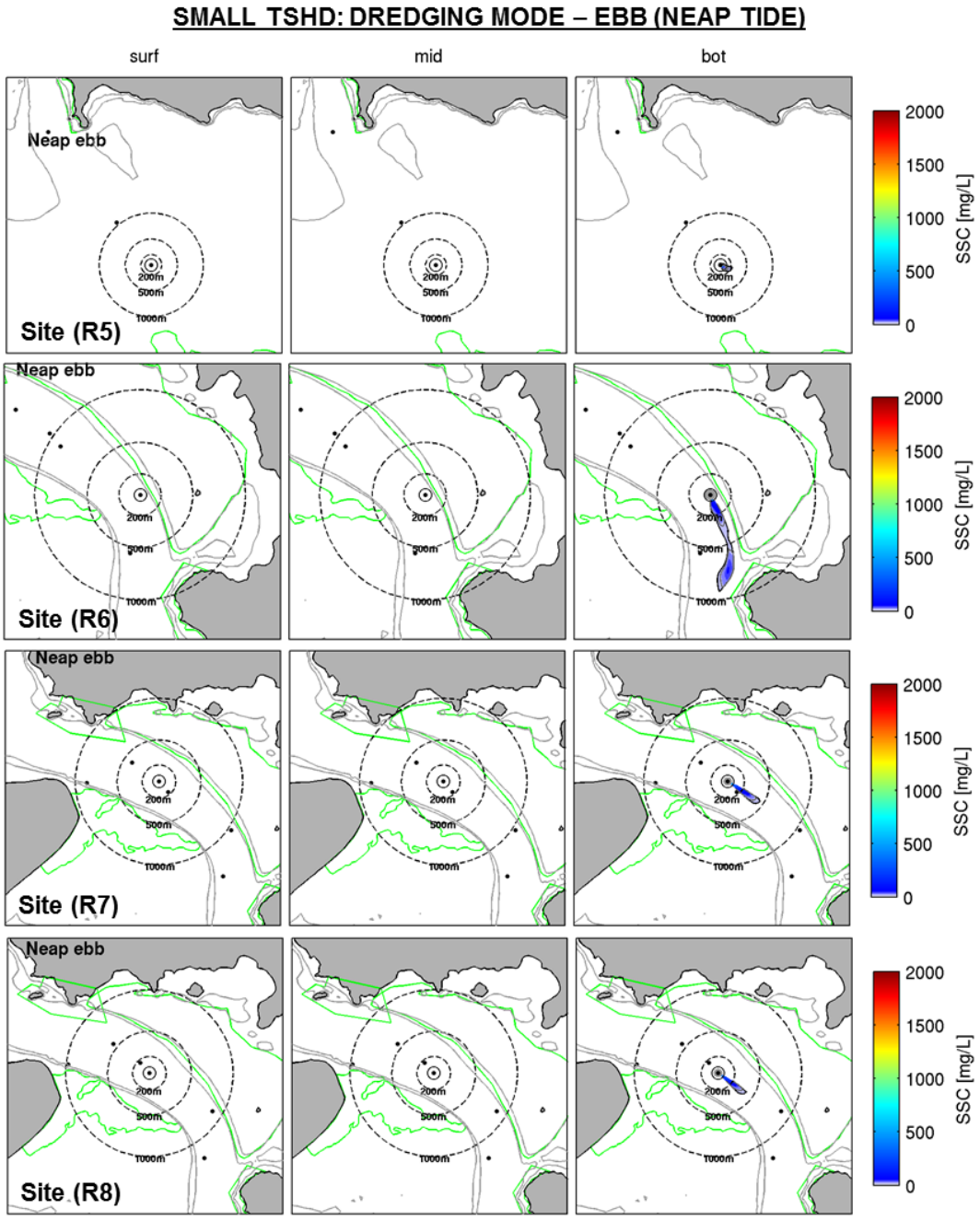

Probabilistic *SSC* plumes at Neap flood tide during dredging phase (large TSHD) at sites R0 to R4 at three levels of the water column considering a 3.0 % production rate for the drag head source.

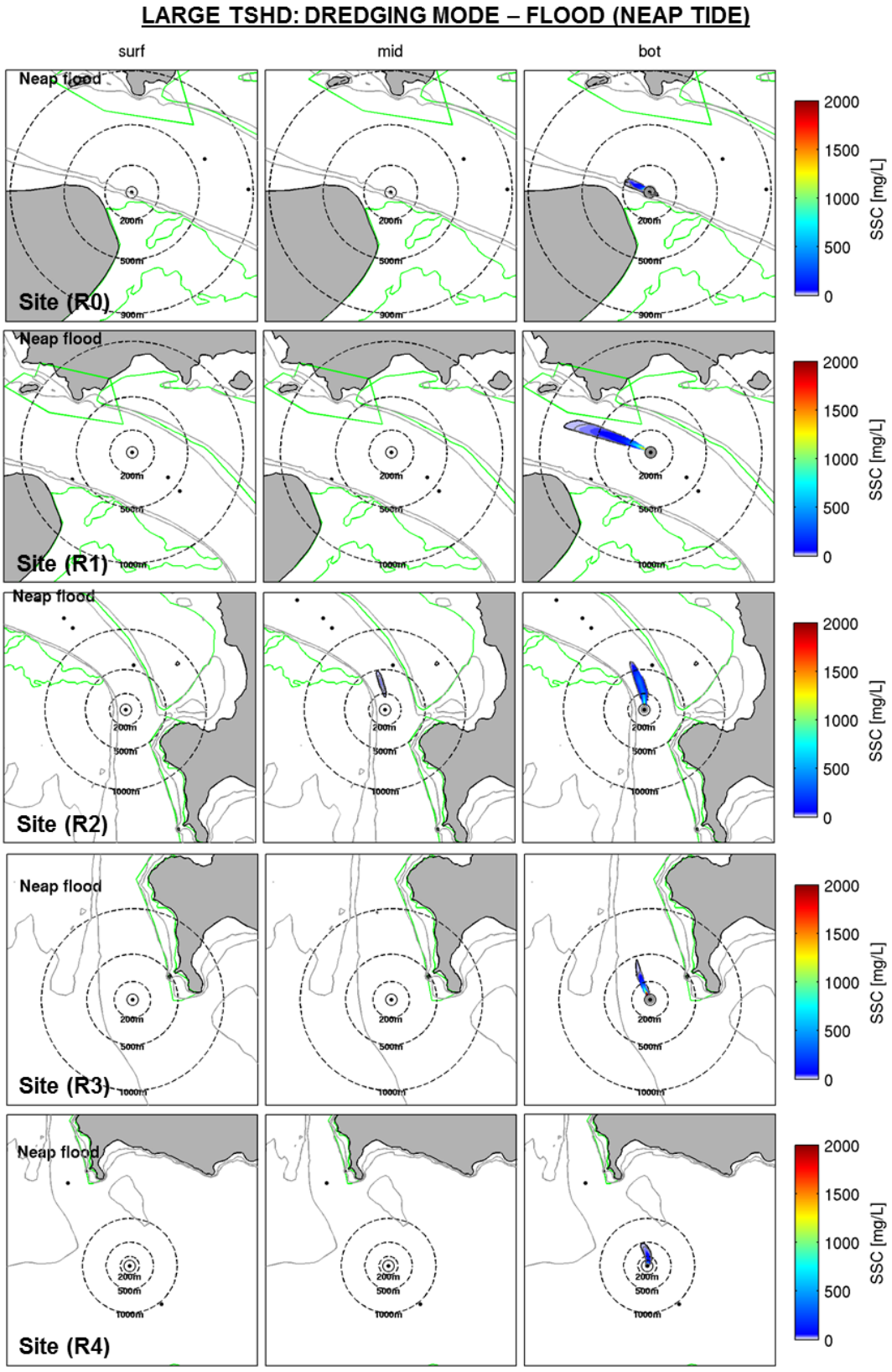

Probabilistic *SSC* plumes at Neap flood tide during dredging phase (large TSHD) at sites R5 to R8 at three levels of the water column considering a 3.0 % production rate for the drag head source.

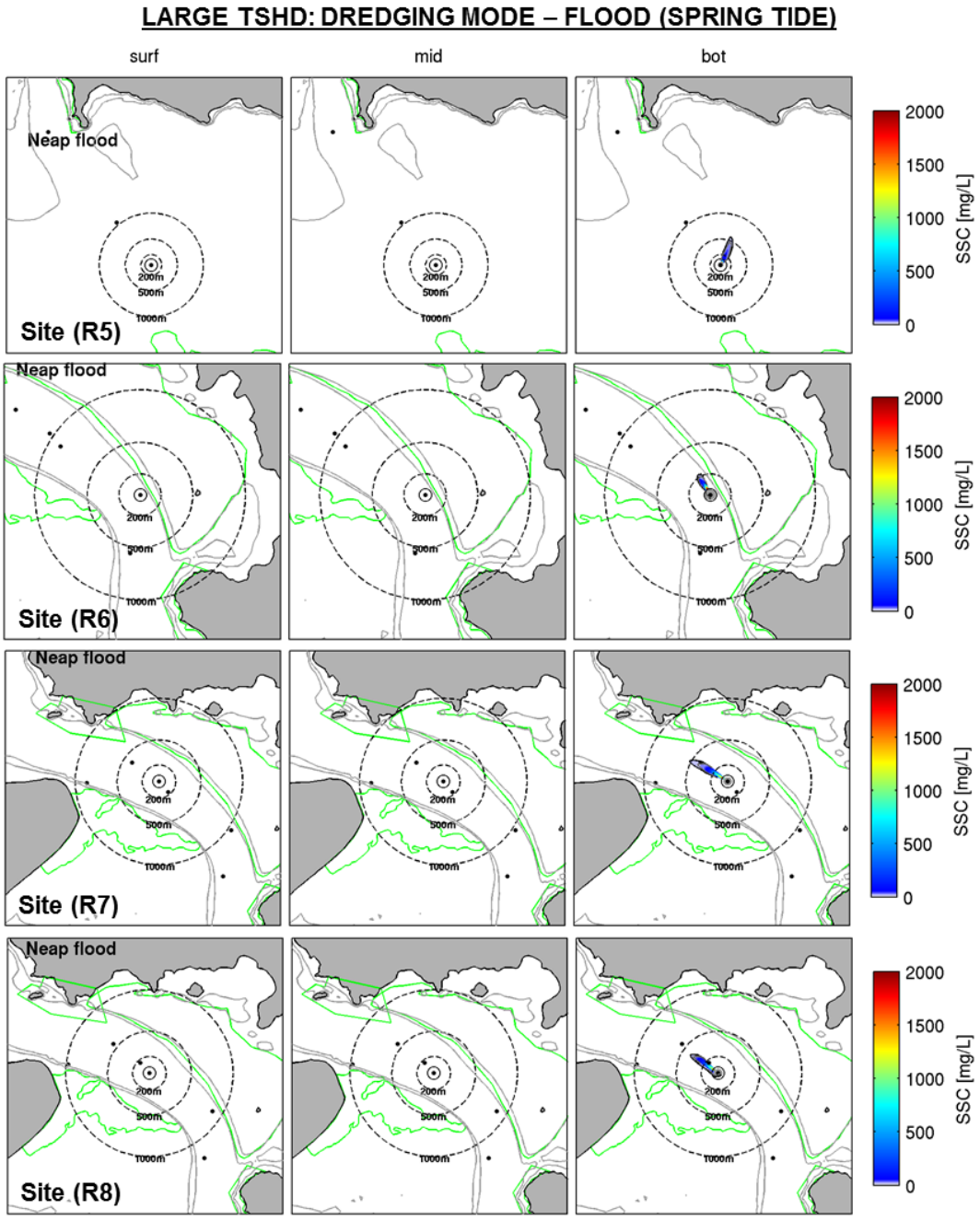

Probabilistic *SSC* plumes at Neap flood tide during dredging phase (small TSHD) at sites R0 to R4 at three levels of the water column considering a 3.0 % production rate for the drag head source.

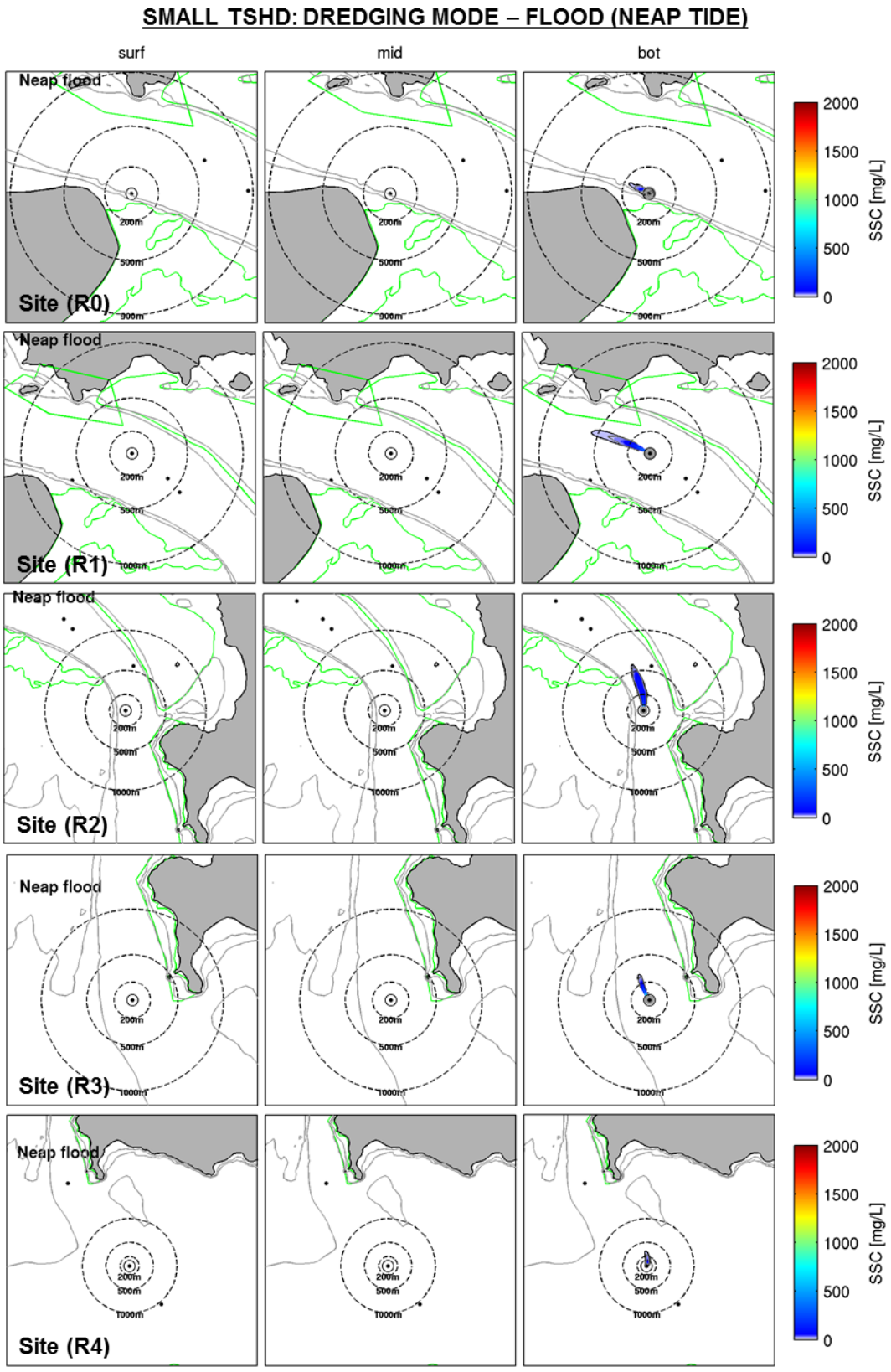

Probabilistic *SSC* plumes at Neap flood tide during dredging phase (large TSHD) at sites R5 to R8 at three levels of the water column considering a 3.0 % production rate for the drag head source.

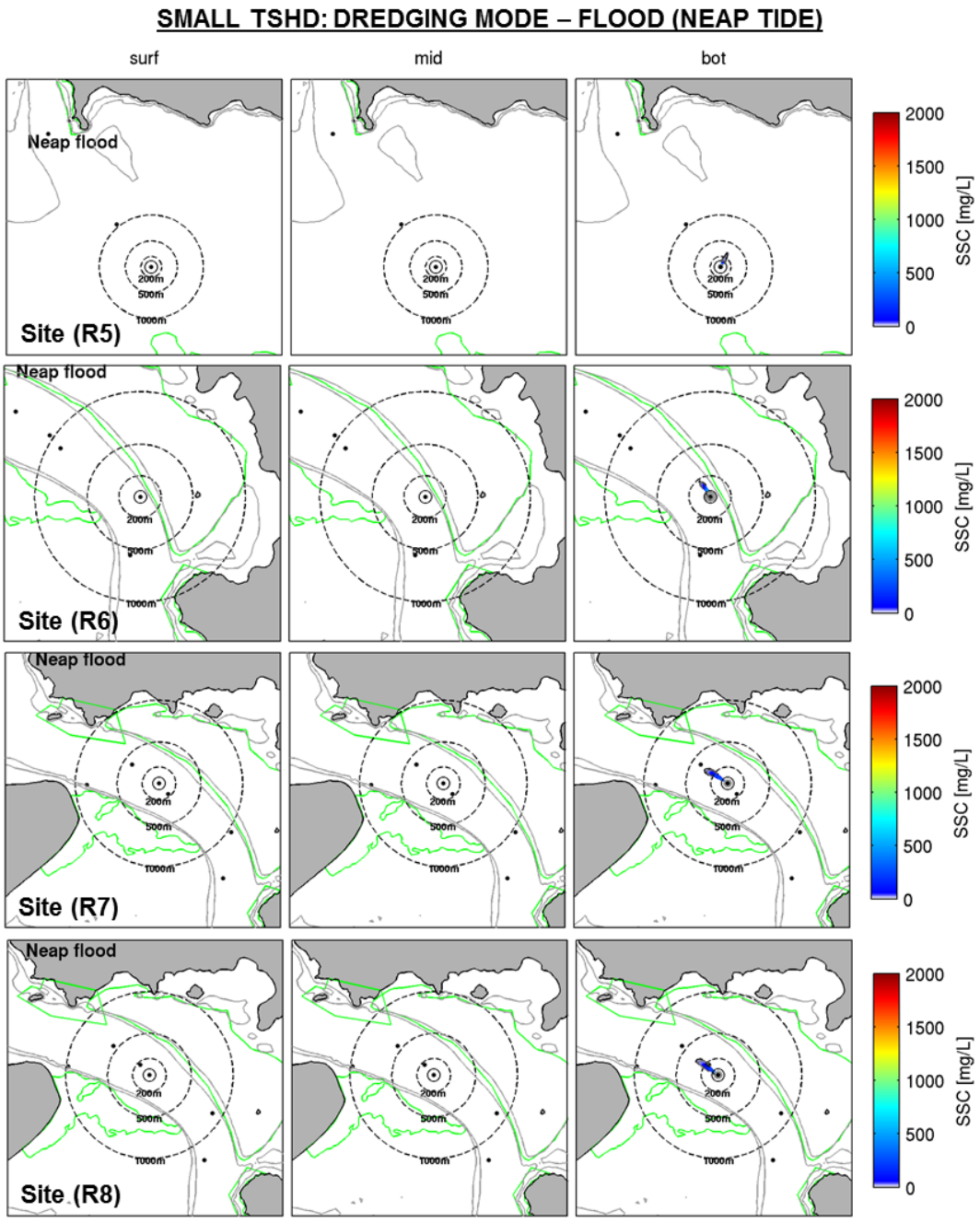

Probabilistic *SSC* plumes at spring ebb tide during dredging phase (large TSHD) at sites R0 to R4 at three levels of the water column considering a 3.0 % production rate for the drag head source.

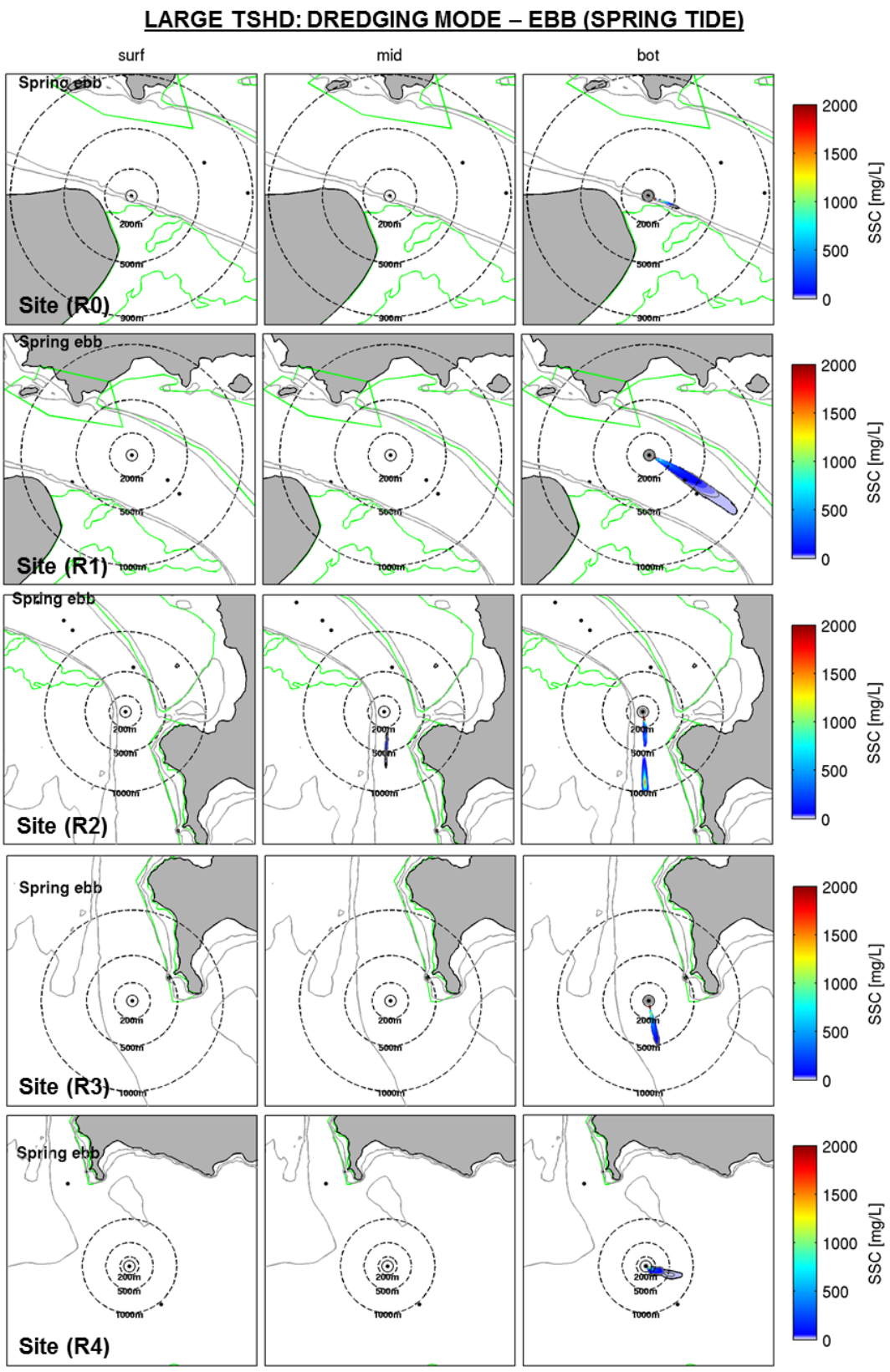

Probabilistic *SSC* plumes at spring ebb tide during dredging phase (large TSHD) at sites R5 to R8 at three levels of the water column considering a 3.0 % production rate for the drag head source.

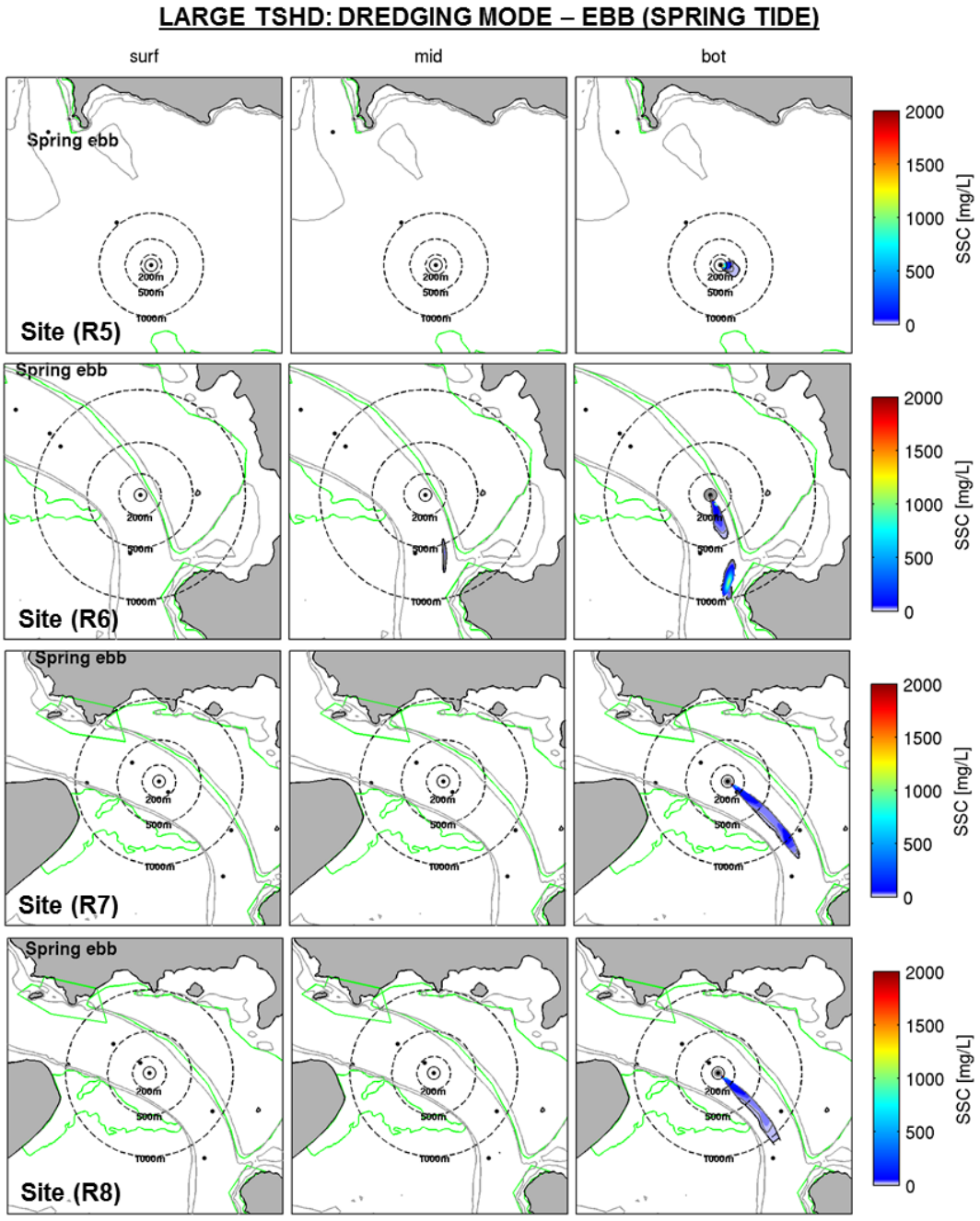

Probabilistic *SSC* plumes at spring ebb tide during dredging phase (small TSHD) at sites R0 to R4 at three levels of the water column considering a 3.0 % production rate for the drag head source.

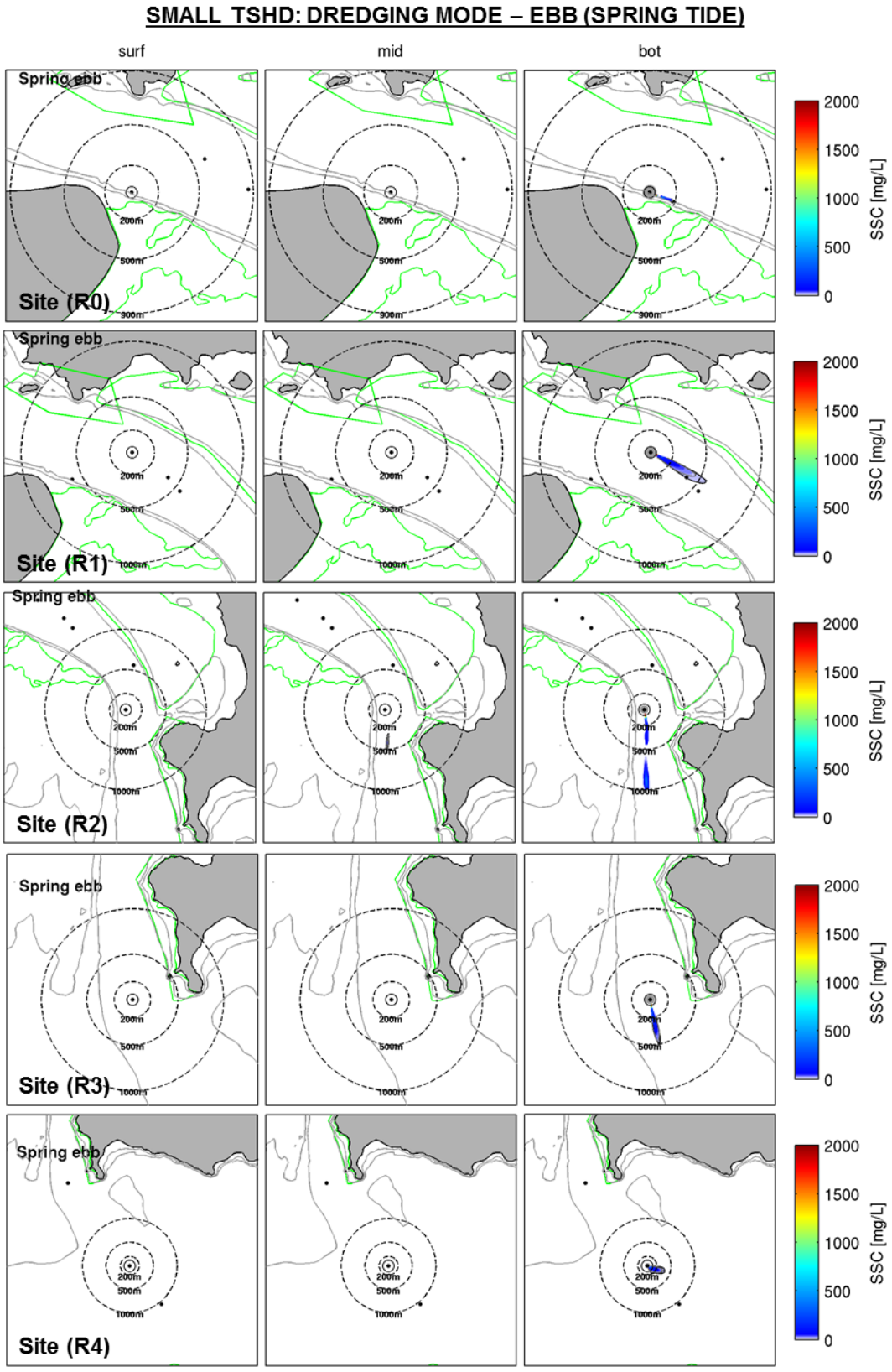

Probabilistic *SSC* plumes at spring ebb tide during dredging phase (small TSHD) at sites R5 to R8 at three levels of the water column considering a 3.0 % production rate for the drag head source.

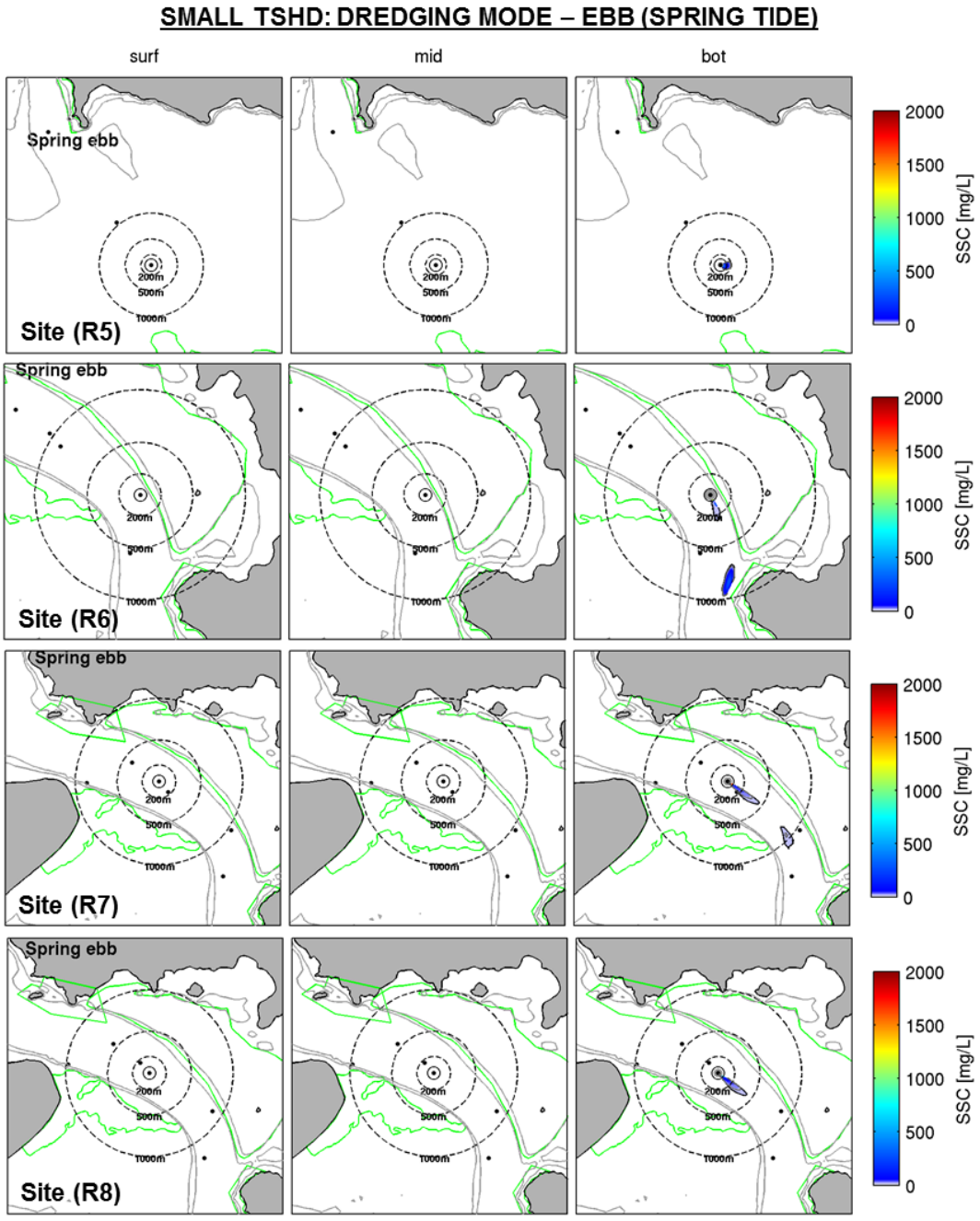

Probabilistic *SSC* plumes at spring flood tide during dredging phase (large TSHD) at sites R0 to R4 at three levels of the water column considering a 3.0 % production rate for the drag head source.

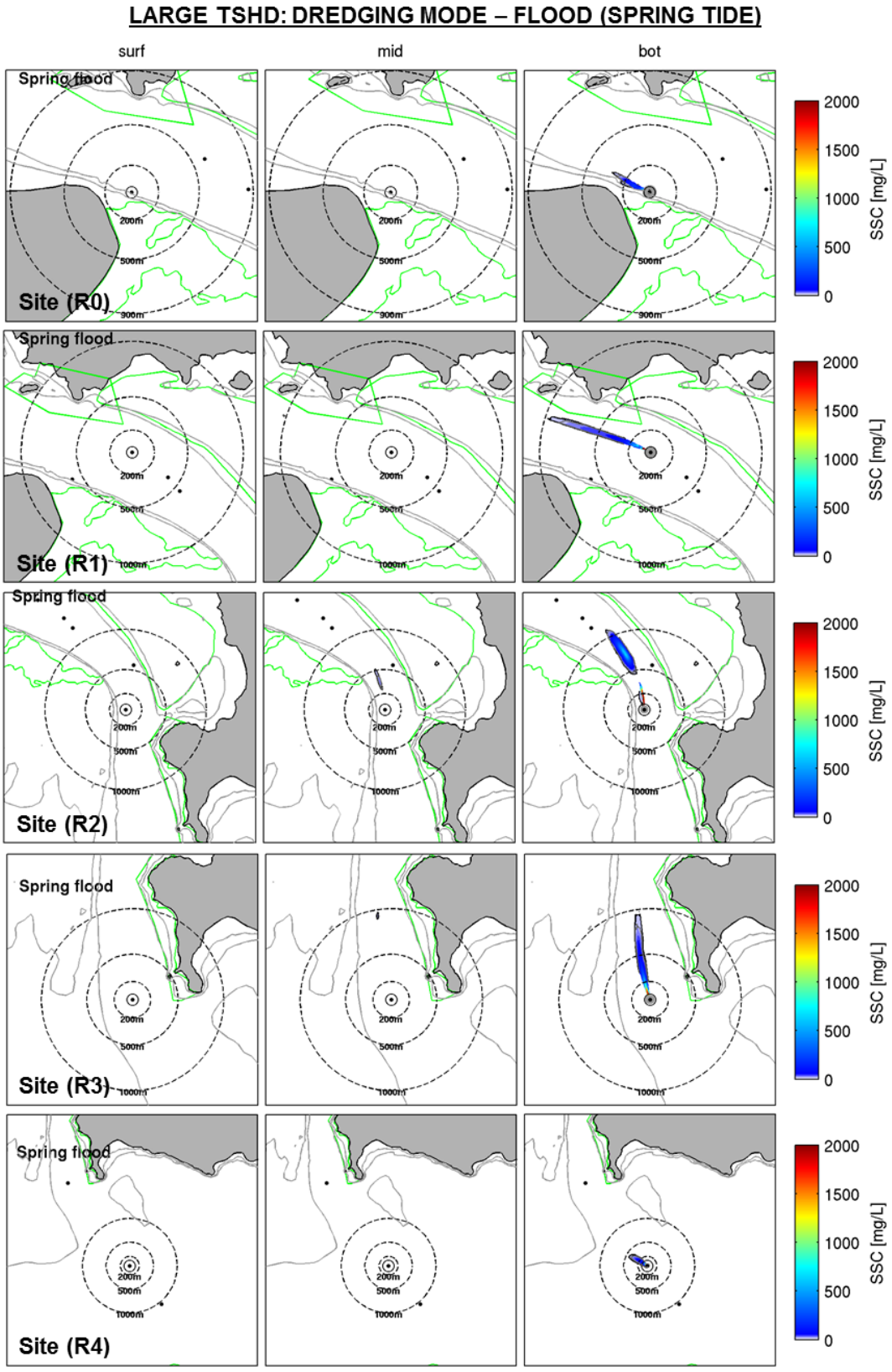

Probabilistic *SSC* plumes at spring flood tide during dredging phase (large TSHD) at sites R5 to R8 at three levels of the water column considering a 3.0 % production rate for the drag head source.

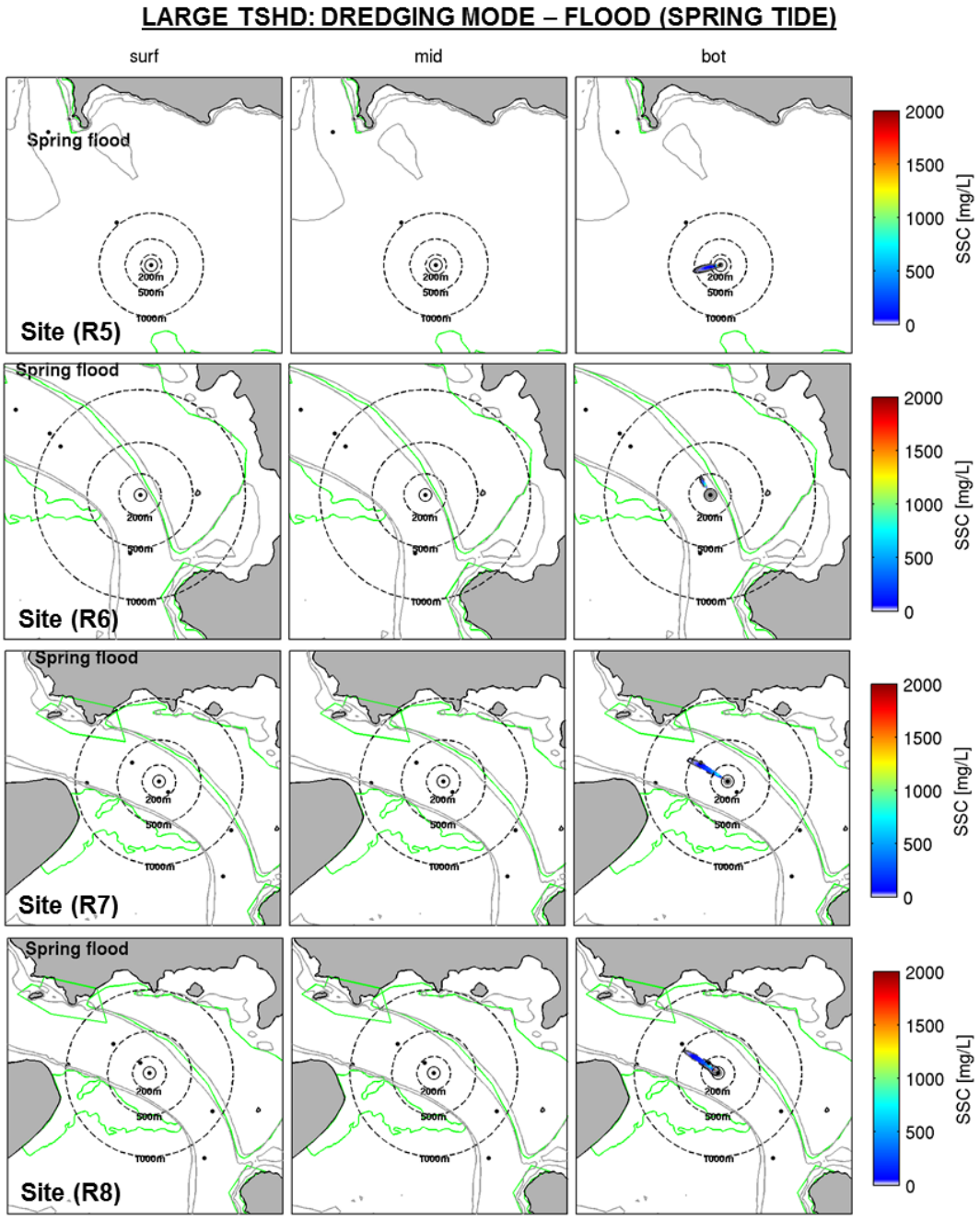

Probabilistic *SSC* plumes at spring flood tide during dredging phase (small TSHD) at sites R0 to R4 at three levels of the water column considering a 3.0 % production rate for the drag head source.

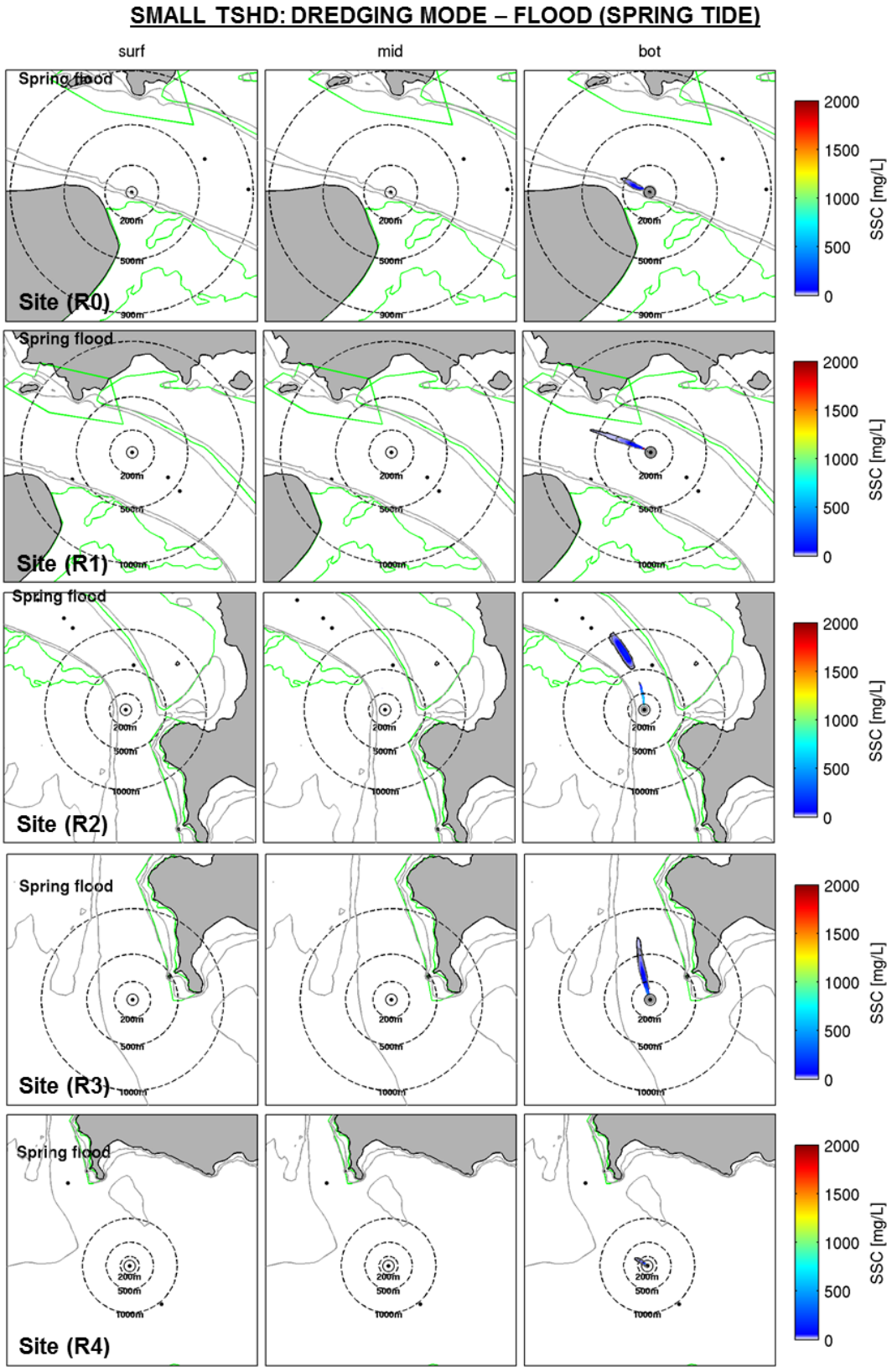

Probabilistic *SSC* plumes at spring flood tide during dredging phase (small TSHD) at sites R5 to R8 at three levels of the water column considering a 3.0 % production rate for the drag head source.

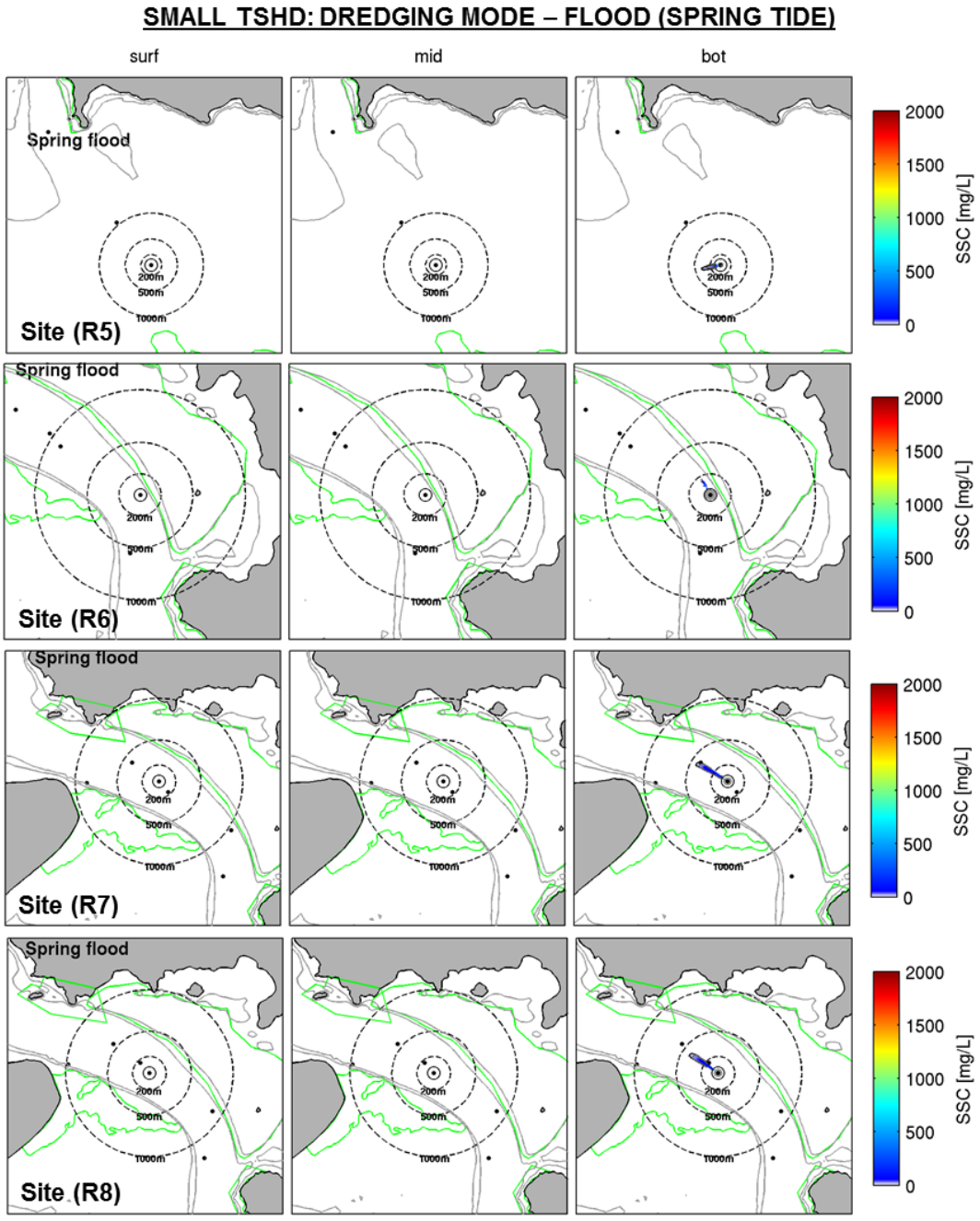

APPENDIX G – OVERFLOW MODE AT DIFFERENT TIDE STAGES

Probabilistic *SSC* plumes at neap ebb tide during the overflow (large TSHD) at sites R0 to R4.

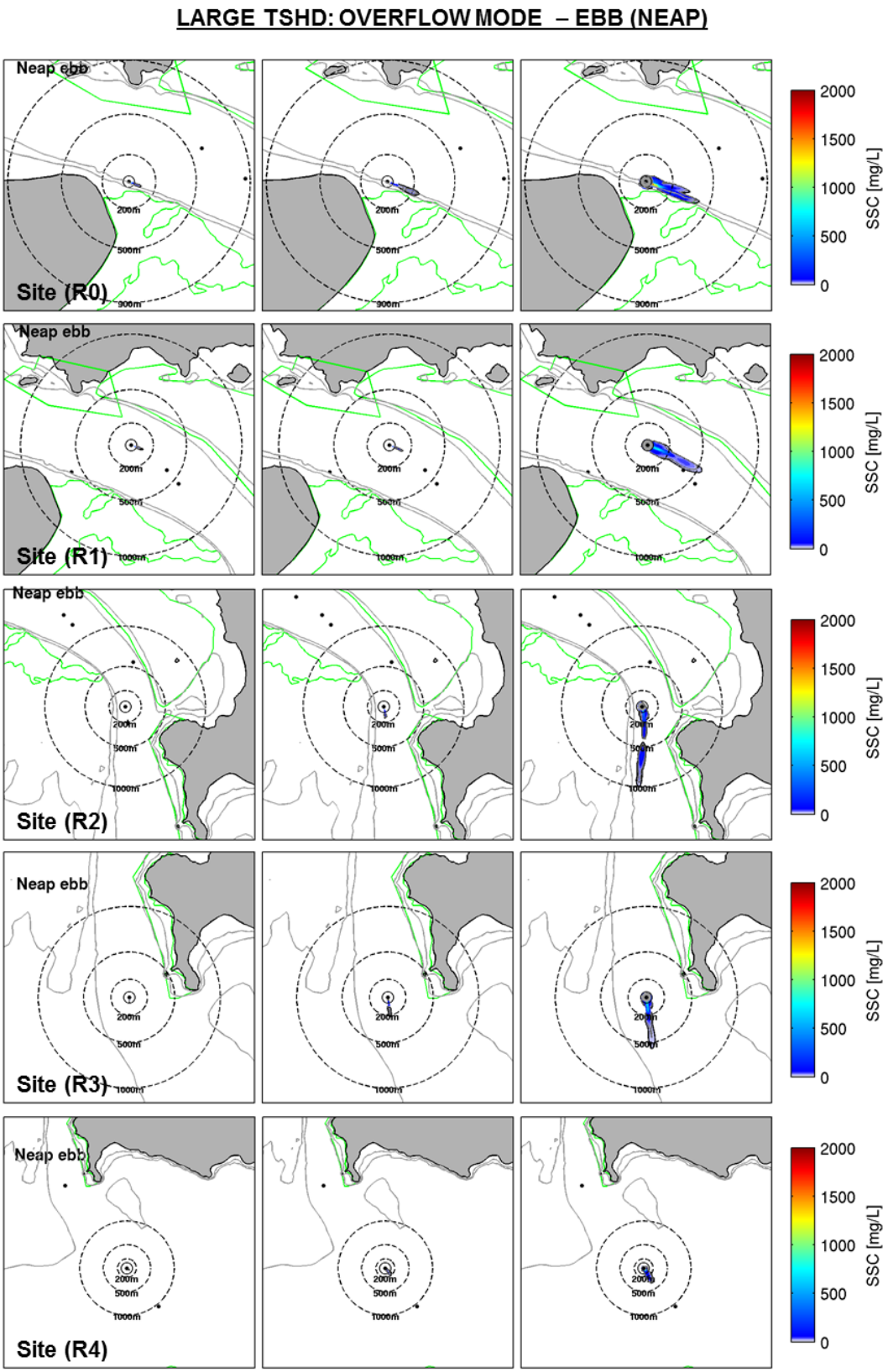

Probabilistic *SSC* plumes at neap ebb tide during the overflow (large TSHD) at sites R5 to R8.

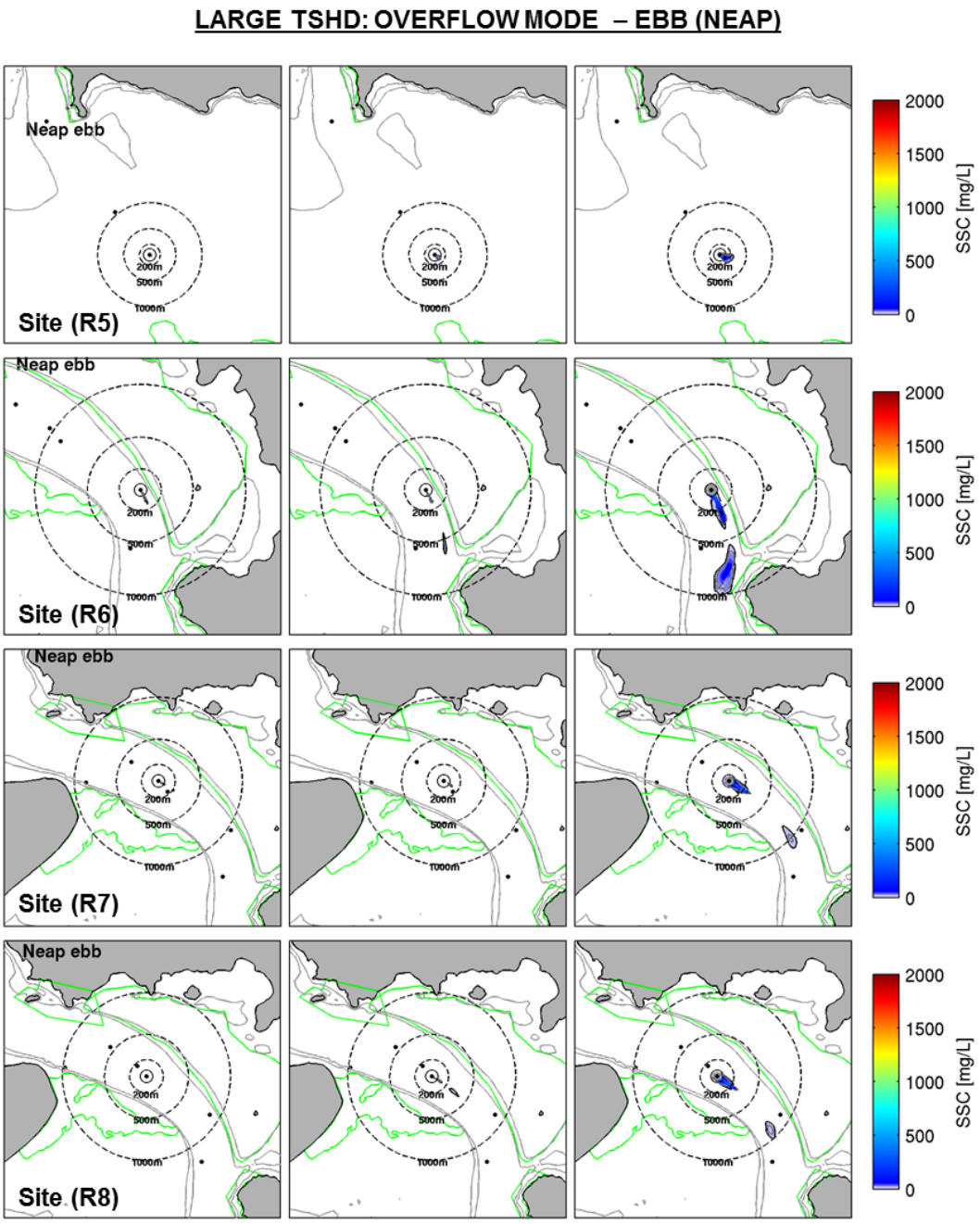

Probabilistic *SSC* plumes at neap ebb tide during the overflow (small TSHD) at sites R0 to R4.

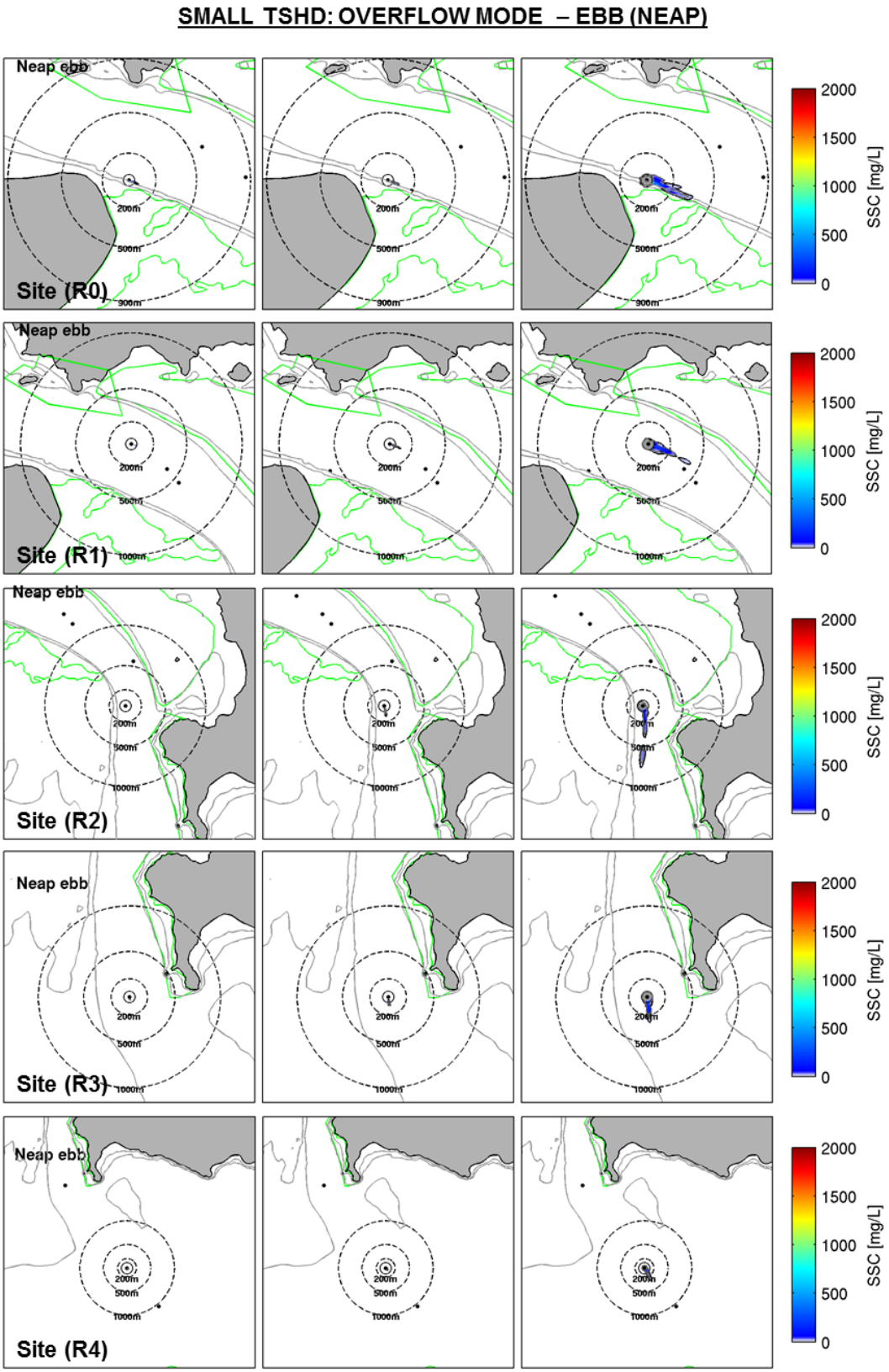

Probabilistic *SSC* plumes at neap ebb tide during the overflow (small TSHD) at sites R5 to R8.

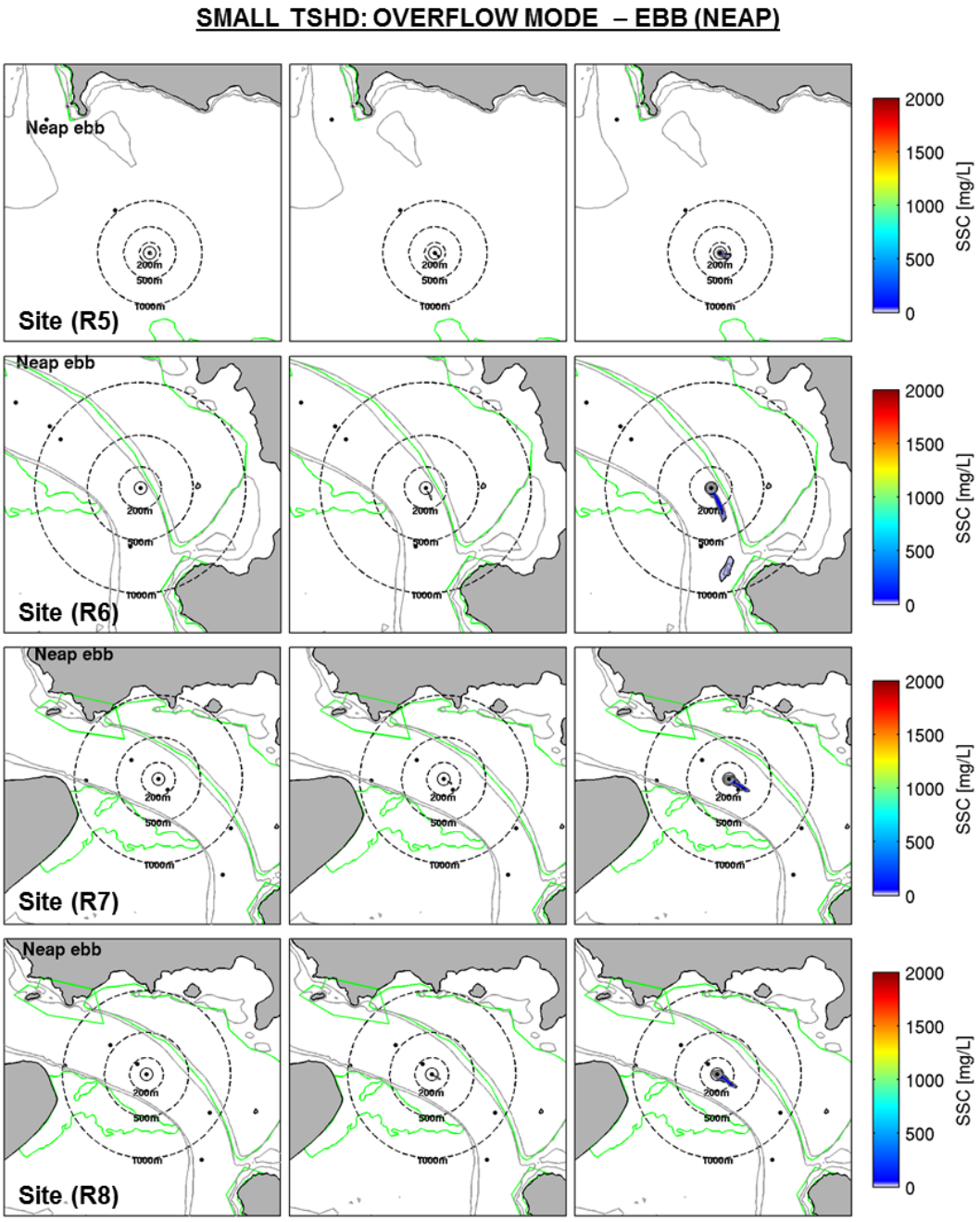

Probabilistic *SSC* plumes at neap flood tide during the overflow (large TSHD) at sites R0 to R4.

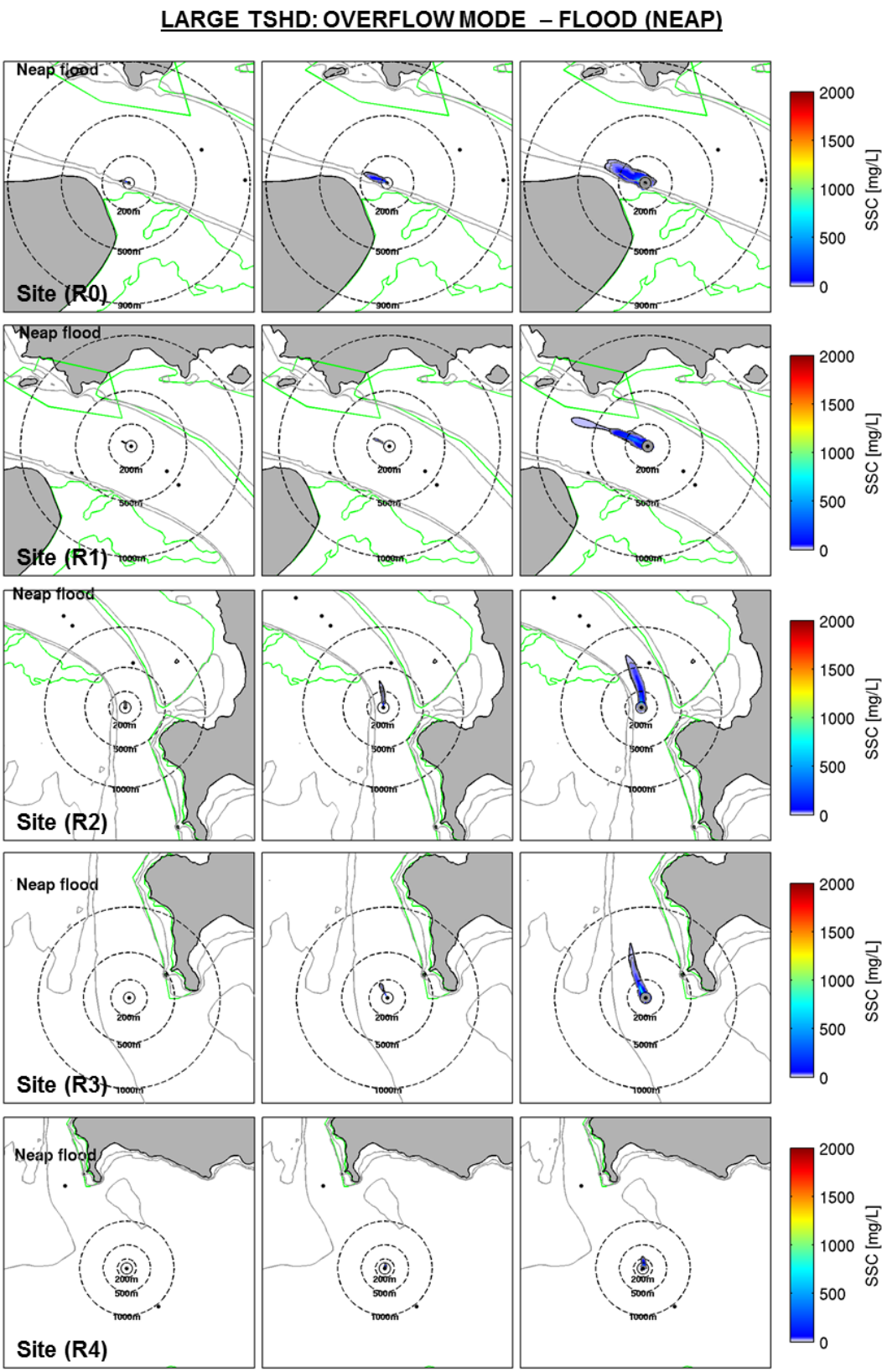

Probabilistic *SSC* plumes at neap flood tide during the overflow (large TSHD) at sites R5 to R8.

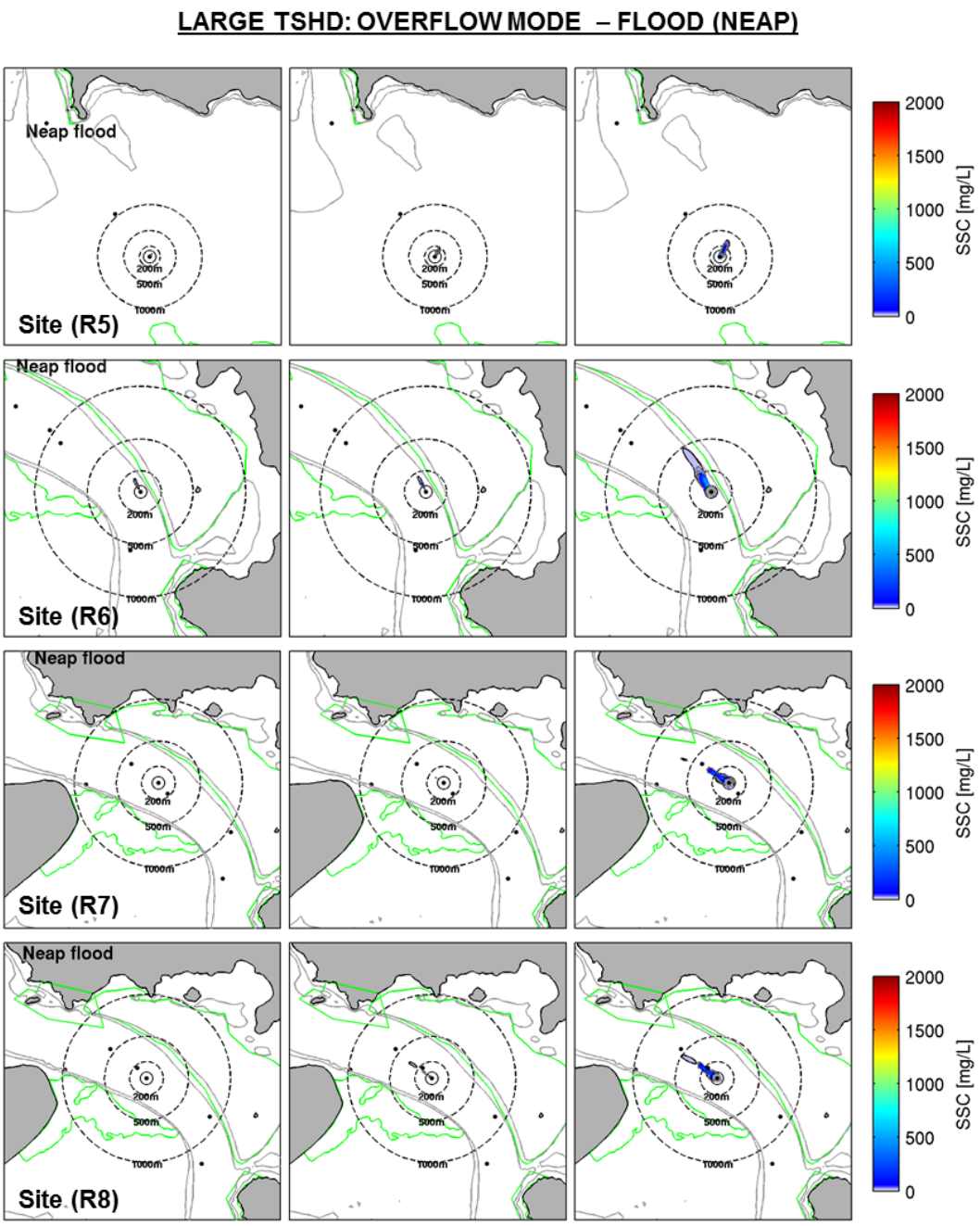

Probabilistic *SSC* plumes at neap flood tide during the overflow (small TSHD) at sites R0 to R4.

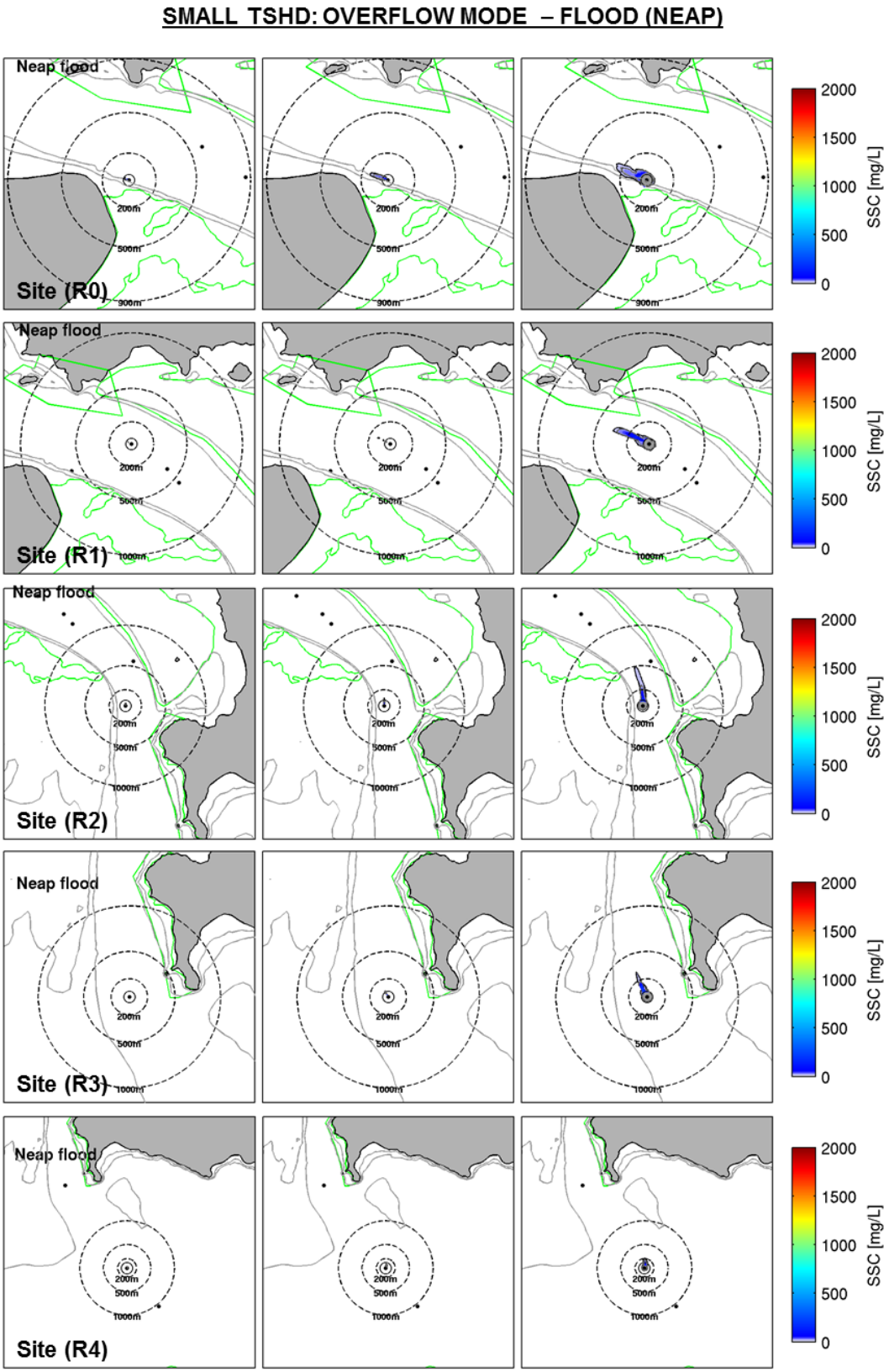

Probabilistic *SSC* plumes at neap flood tide during the overflow (small TSHD) at sites R5 to R8.

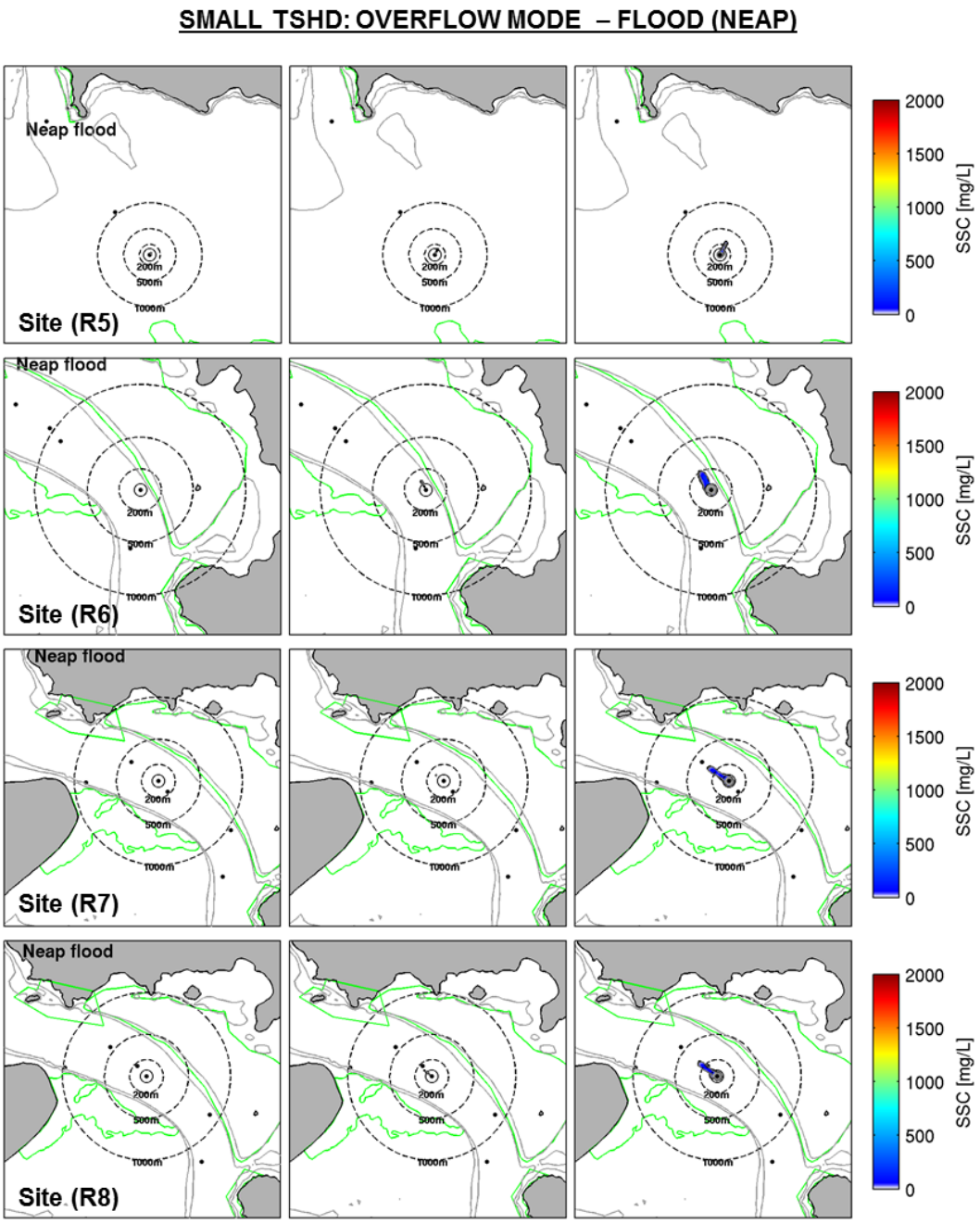

Probabilistic *SSC* plumes at spring flood tide during the overflow (large TSHD) at sites R0 to R4.

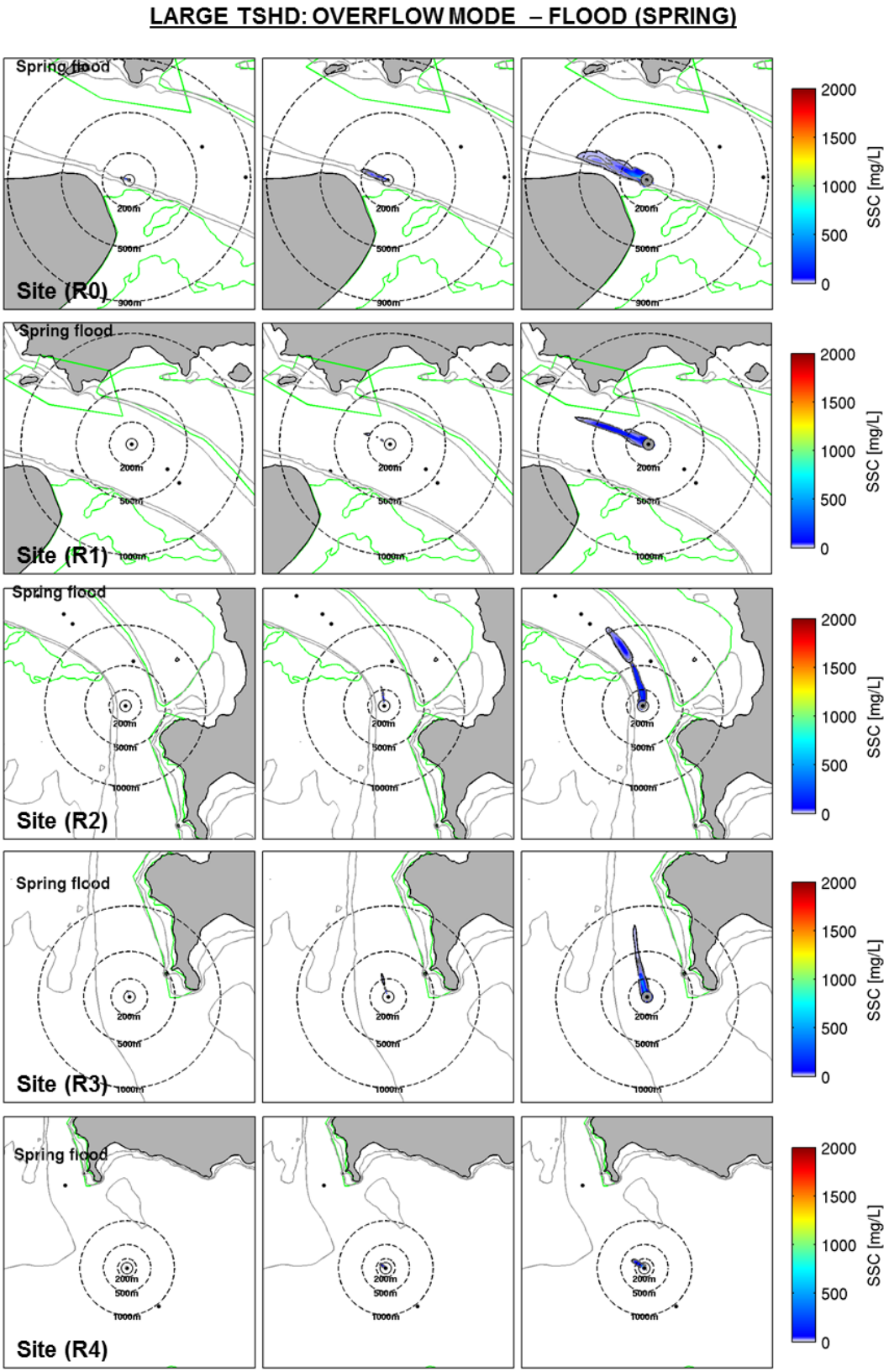

Probabilistic *SSC* plumes at spring flood tide during the overflow (large TSHD) at sites R5 to R8.

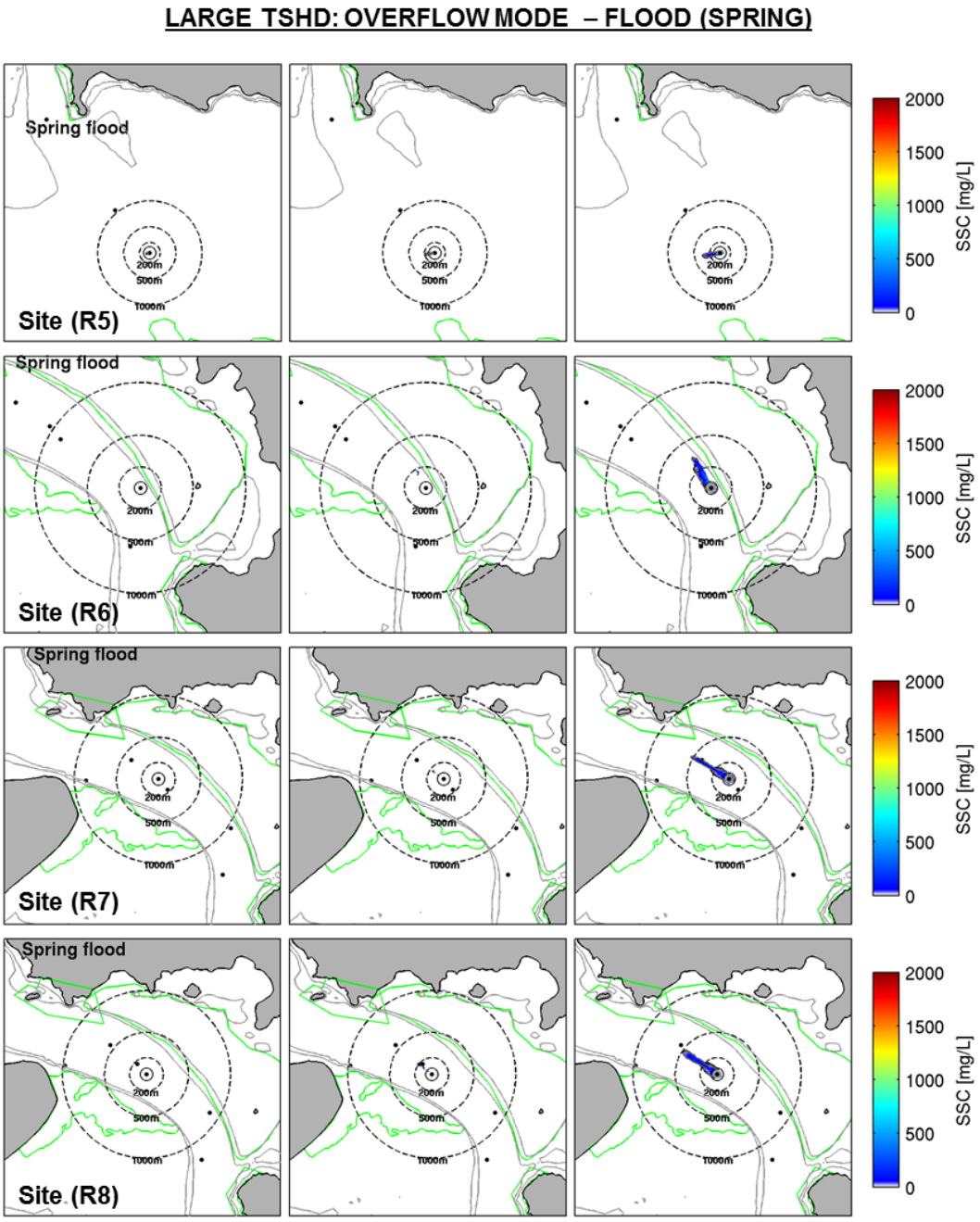

Probabilistic *SSC* plumes at spring flood tide during the overflow (small TSHD) at sites R0 to R4.

SMALL TSHD: OVERFLOW MODE – FLOOD (SPRING)

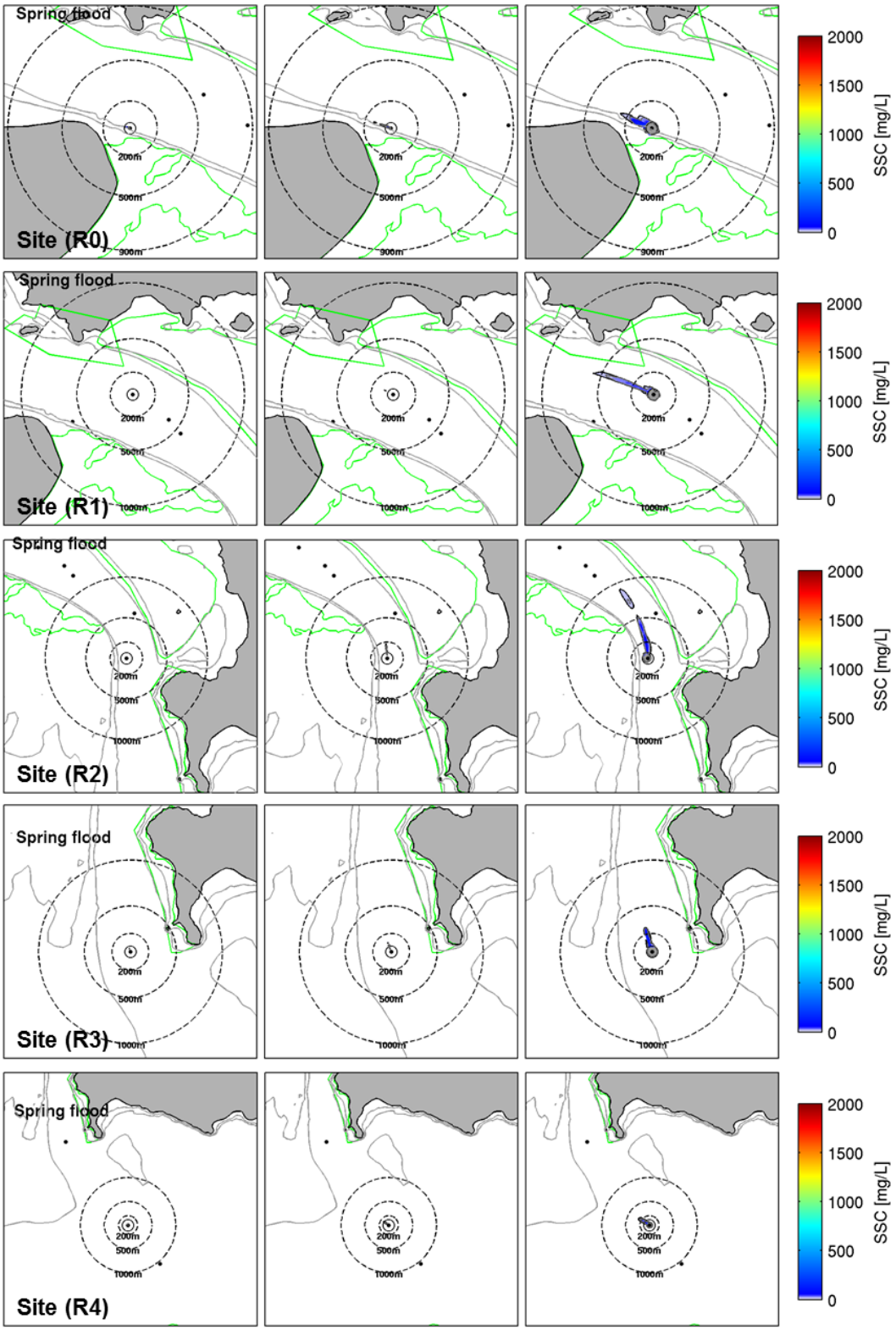

Probabilistic *SSC* plumes at spring flood tide during the overflow (small TSHD) at sites R5 to R8.

SMALL TSHD: OVERFLOW MODE – FLOOD (SPRING)

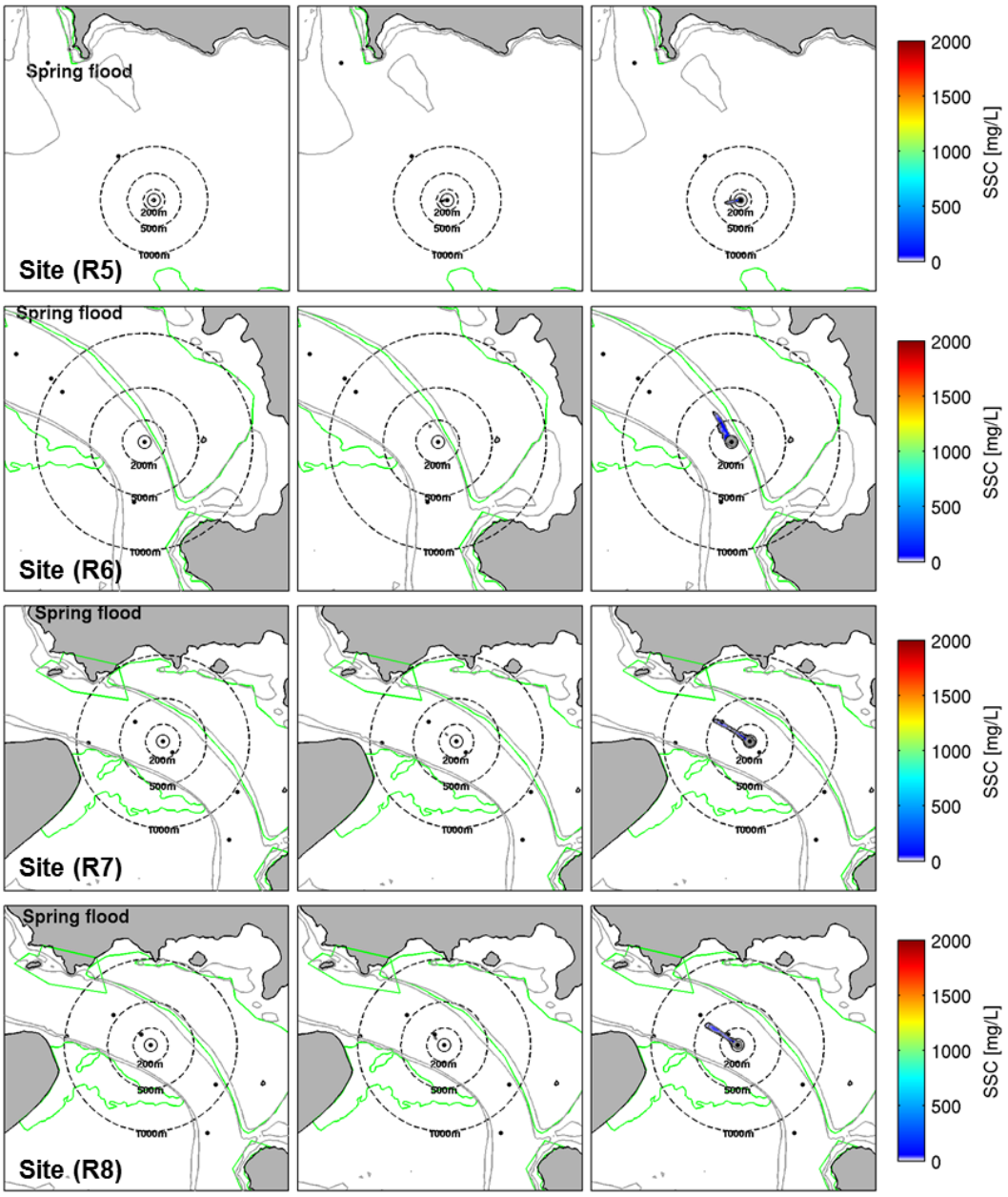

Probabilistic *SSC* plumes at spring ebb tide during the overflow (large TSHD) at sites R0 to R4.

LARGE TSHD: OVERFLOW MODE – EBB (SPRING)

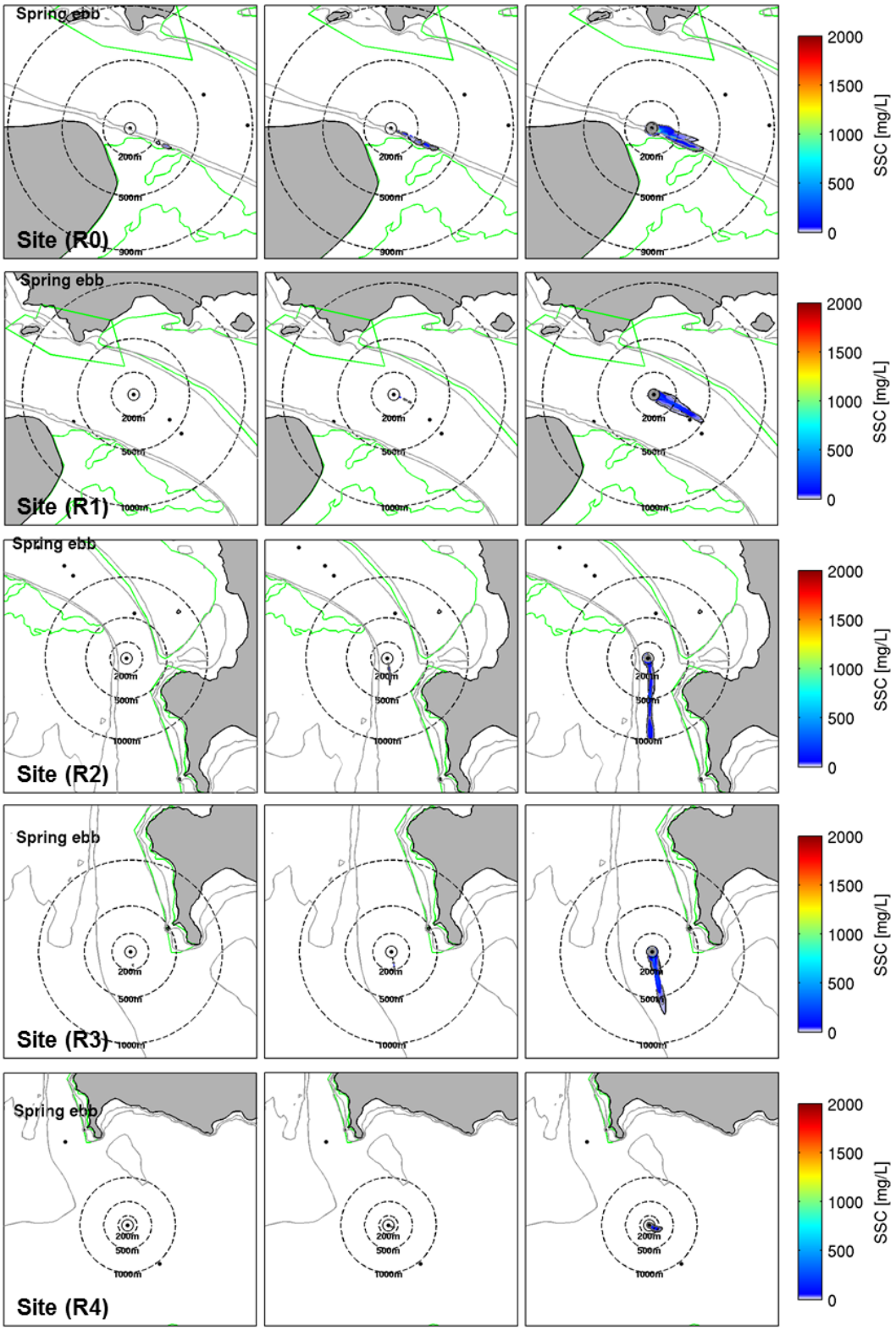

Probabilistic *SSC* plumes at spring ebb tide during the overflow (large TSHD) at sites R5 to R8.

LARGE TSHD: OVERFLOW MODE – EBB (SPRING)

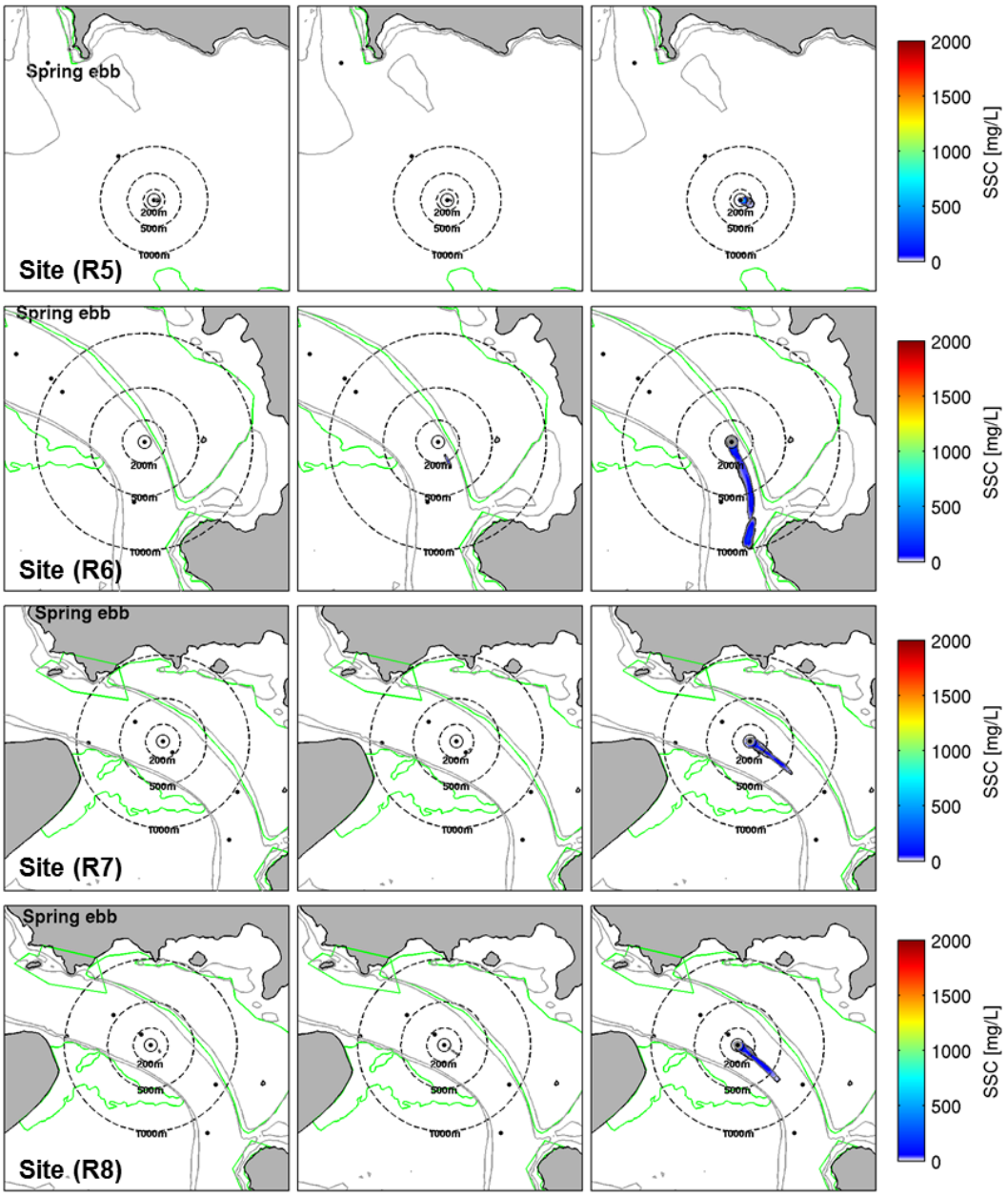

Probabilistic *SSC* plumes at spring ebb tide during the overflow (small TSHD) at sites R0 to R4.

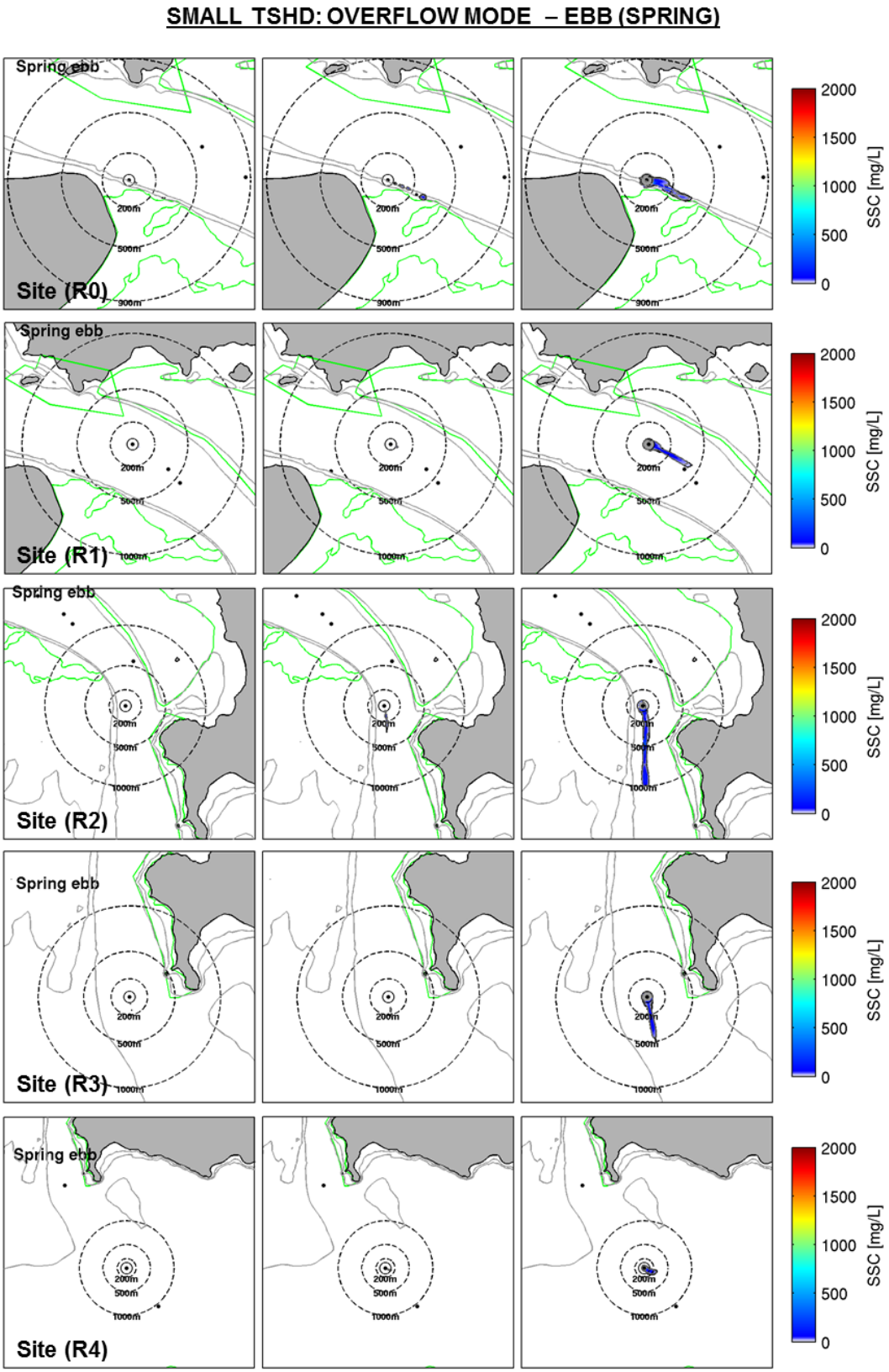

Probabilistic *SSC* plumes at spring ebb tide during the overflow (small TSHD) at sites R5 to R8.

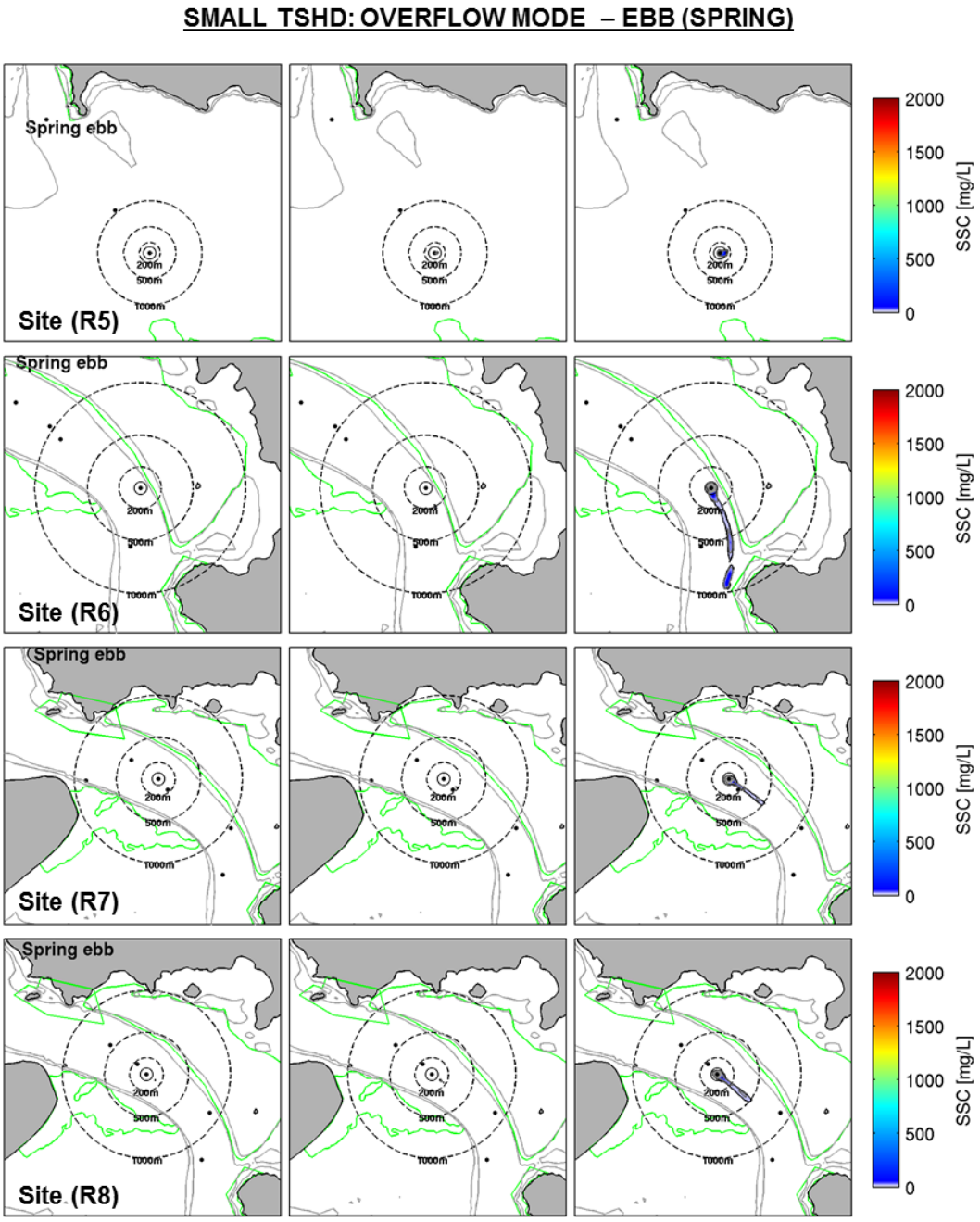

APPENDIX H – SENSITIVITY ANALYSIS OF THE PLUME MODEL

Parameters tested to simulate the plume dispersion during overflow phase (large trailing suction hopper dredger, TSHD) for a period of 79 min.

Cases	Overflow release	Silt fraction in release	Settling velocity (mm/s)
	Cylinder		
a)	2 m High, 60 m radius	5%	1
b)	2 m High, 100 m radius	5%	0.4
c)	4 m High, 60 m radius	5%	0.4
d)	4 m High, 60 m radius	10%	0.4

Probabilistic SSC plumes during overflow phase (large trailing suction hopper dredger, TSHD) at site R0 at three levels of the water column for a 79 min period for four model configurations (a, b, c, d) described in the previous table.

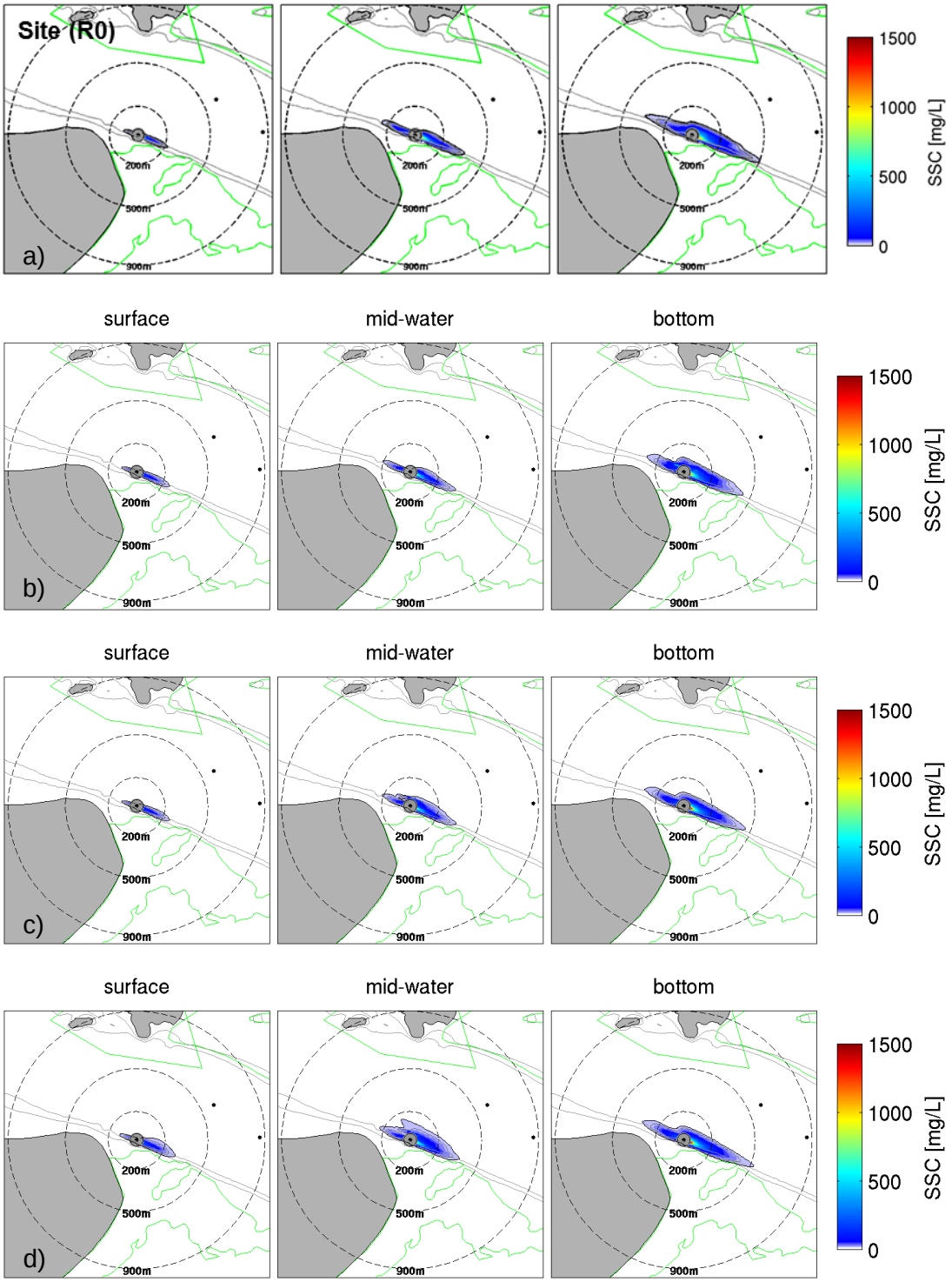

Probabilistic *SSC* plumes during overflow phase (large trailing suction hopper dredger, TSHD) at site R1 at three levels of the water column for a 79 min period for four model configurations (a, b, c, d) described in the previous table.

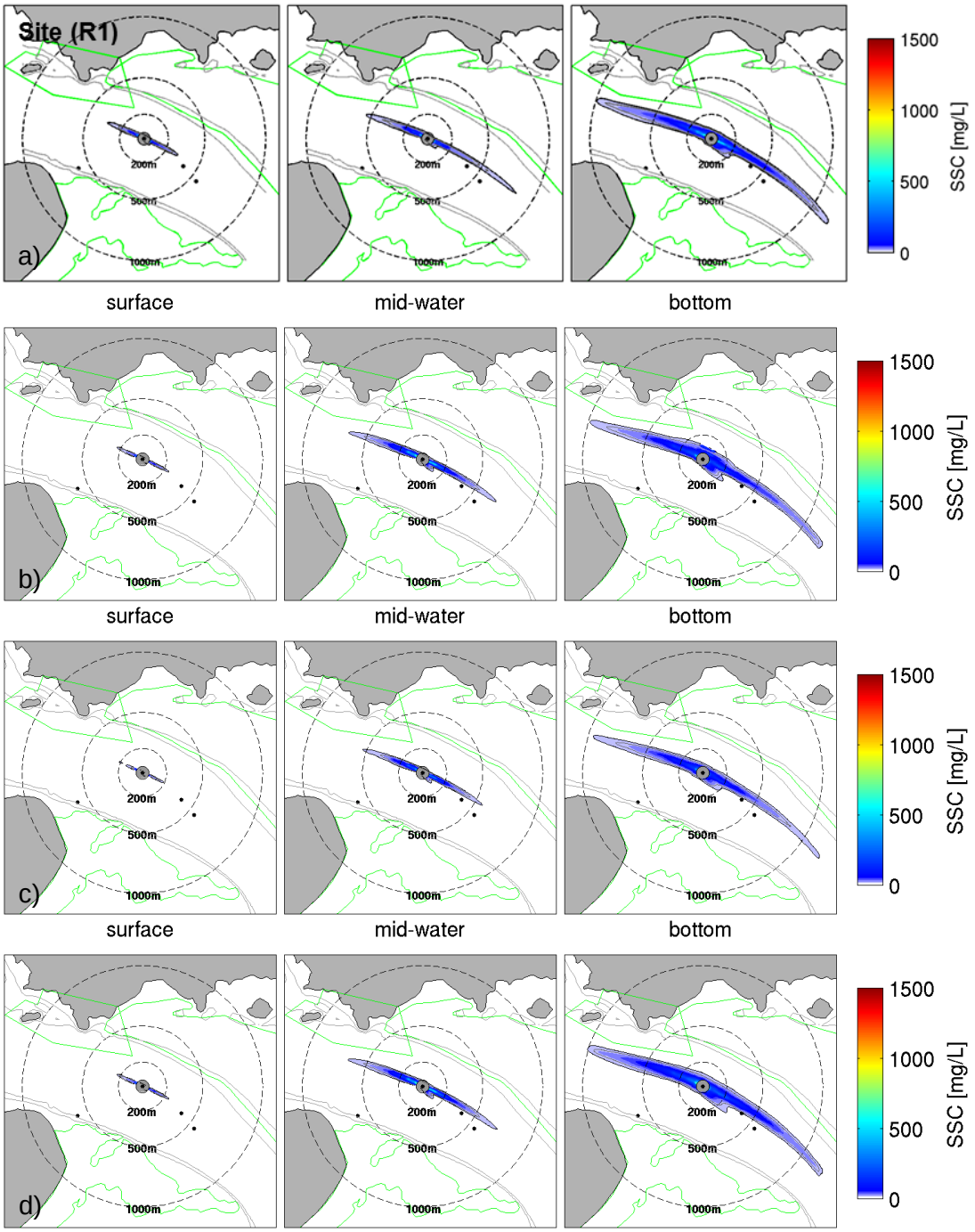

Probabilistic *SSC* plumes during overflow phase (large trailing suction hopper dredger, TSHD) at site R2 at three levels of the water column for a 79 min period for four model configurations (a, b, c, d) described in the previous table.

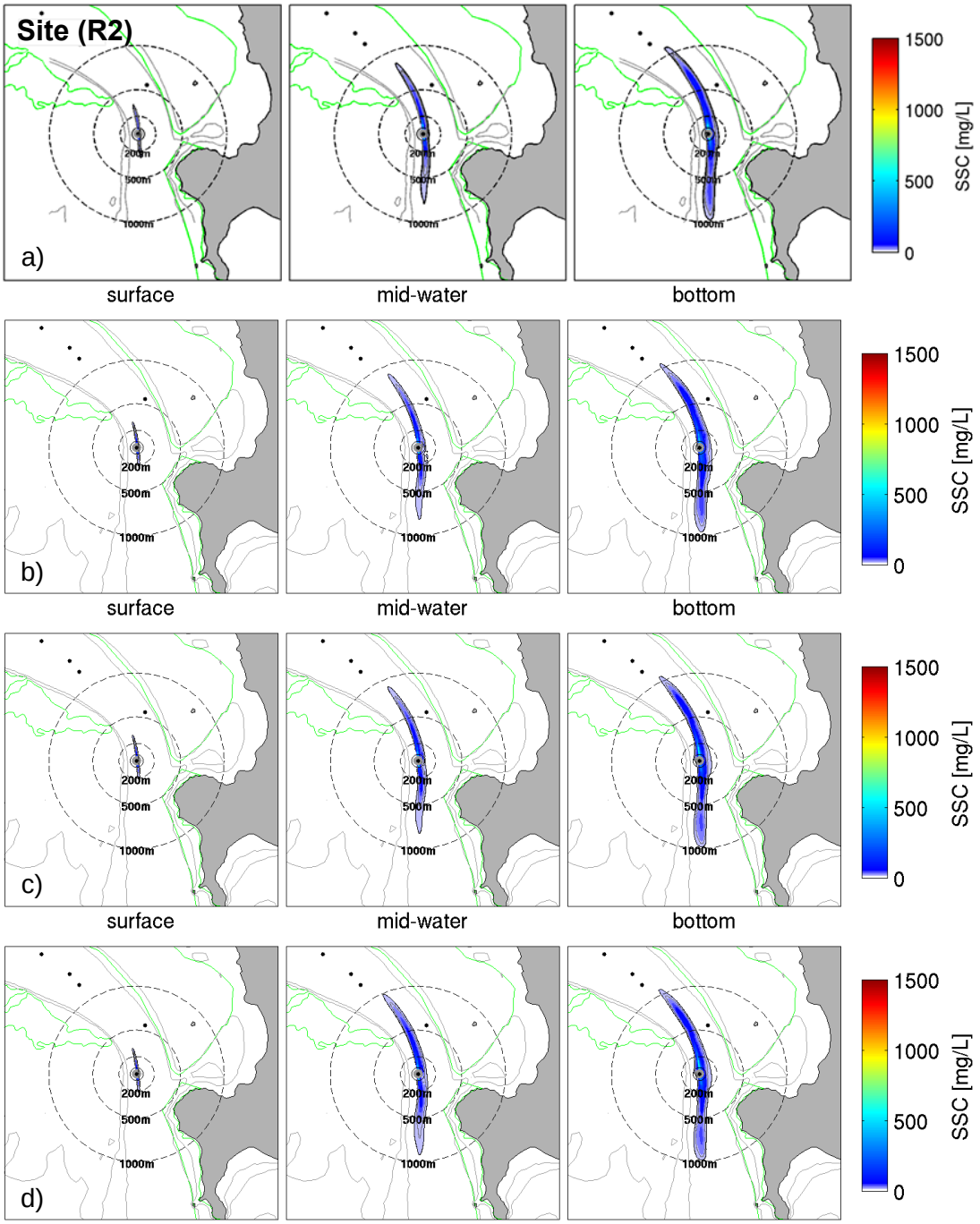

Probabilistic *SSC* plumes during overflow phase (large trailing suction hopper dredger, TSHD) at site R3 at three levels of the water column for a 79 min period for four model configurations (a, b, c, d) described in the previous table.